Structural investigation of complexes involved in endoplasmic-reticulum-associated protein degradation

Dissertation

zur Erlangung des Doktorgrades

der Naturwissenschaften

vorgelegt dem Fachbereich

Biochemie, Chemie und Pharmazie (FB 14)

der Johann Wolfgang Goethe-Universität

in Frankfurt am Main

von

Andreas Kniß

aus Frankfurt am Main

Frankfurt am Main (2018)

(D30)

Vom Fachbereich Biochemie, Chemie und Pharmazie (FB 14) der
Johann Wolfgang Goethe-Universität als Dissertation angenommen.

Dekan:	Prof. Dr. Clemens Glaubitz
Gutachter:	Prof. Dr. Volker Dötsch
	Prof. Dr. Thomas Sommer

Datum der Disputation: 09.05.2018

Eidesstattliche Erklärung

Ich erkläre hiermit an Eides statt, dass ich die vorgelegte Dissertation über „Structural investigation of complexes involved in endoplasmic-reticulum-associated protein degradation“ selbständig angefertigt und mich anderer Hilfsmittel als der in ihr angegebenen nicht bedient habe. Ich erkläre weiterhin, dass Entlehnungen aus Schriften, soweit sie in der Dissertation nicht ausdrücklich als solche bezeichnet sind, nicht stattgefunden haben. Ich habe bisher an keiner anderen Universität ein Gesuch um Zulassung zur Promotion eingereicht oder die vorliegende oder eine andere Arbeit als Dissertation vorgelegt.

Frankfurt am Main, den 12.02.2018

Andreas Kniss

Table of Contents

Table of Contents I

Abbreviations V

Summary 1

Zusammenfassung 3

1. Introduction 9

1.1. Ubiquitin-proteasome-system 10

1.1.1. Ubiquitin and the ubiquitination cascade 10

1.1.2. Cellular functions of ubiquitin signaling 12

1.1.3. Ubiquitin binding domains 13

1.1.4. Structures and conformations of ubiquitin chains 14

1.1.5. Deubiquitinating enzymes 16

1.1.6. SUMO and other ubiquitin-like proteins 16

1.2. Endoplasmic-reticulum-associated protein degradation (ERAD) 17

1.2.1. Protein folding and ER quality control 17

1.2.2. Substrate selection in ERAD 18

1.2.3. ERAD ubiquitin ligases 18

1.2.4. Cytosolic degradation of ERAD substrates 21

2. Objectives 22

3. Materials 23

3.1. Laboratory equipment 23

3.2. Laboratory consumables 23

3.3. Chromatography equipment 23

3.4. Kits 24

3.5. Enzymes 24

3.6. Bacterial strains 24

3.7. Vectors 24

3.8. Oligonucleotides and synthetic genes 25

3.9. Reagents and chemicals 28
3.10. Buffers and media 28
3.10.1. Buffers and media for bacterial cultivation 28
3.10.2. Buffers for agarose gels and SDS PAGE 29
3.10.3. Buffers for protein purification and analysis 29
3.11. Software 30
4. Methods 31
4.1. Microbiological methods 31
4.1.1. Primer design 31
4.1.2. Restriction-based cloning 31
4.1.3. Restriction-free (RF) cloning and site-directed mutagenesis 33
4.2. Protein expression and analysis 34
4.2.1. Preparative protein expression 34
4.3. Protein purification 35
4.3.1. Cell lysis of *E. coli* 35
4.3.2. Solubilization of inclusion bodies 35
4.3.3. Ni-NTA chromatography 35
4.3.4. GST affinity purification 36
4.3.5. Dialysis and buffer exchange 36
4.3.6. *In vitro* protein refolding 36
4.3.7. Cleavage of the purification tag 37
4.3.8. Tag removal by "reversed" affinity chromatography 37
4.3.9. Purification of non-tagged ubiquitin 37
4.3.10. Cation and anion exchange chromatography 37
4.3.11. Analytical size exclusion chromatography (SEC) 38
4.3.12. Preparative size exclusion chromatography (SEC) 38
4.3.13. SDS PAGE and Coomassie Brilliant Blue staining 39
4.3.14. Concentrating of protein containing solutions and determination of protein concentrations 39

4.4. Biochemical methods involving ubiquitination reactions 39
4.4.1. Synthesis of proximally capped diubiquitins 39
4.4.2. Synthesis of proximally capped tri- and tetraubiquitins 40
4.4.3. Synthesis and purification of wild type ubiquitin chains 41
4.4.4. Stable charging of E2 enzymes 42
4.4.5. Fluorescence based analysis of *in vitro* ubiquitin chain elongation 42
4.5. Protein Nuclear Magnetic Resonance (NMR) spectroscopy 43
4.5.1. Experimental conditions and NMR sample preparation 43
4.5.2. Assignment of backbone and side chain resonances 43
4.5.3. NMR structure calculation 44
4.5.4. NMR titration experiments 44
4.5.5. Paramagnetic relaxation enhancement (PRE) experiments 45
4.5.6. HADDOCK modeling 46
4.6. Pulsed electron-electron double resonance (PELDOR) spectroscopy 47
4.6.1. Site-directed spin labeling and sample preparation 47
4.6.2. PELDOR data collection, analysis and structure ensemble generation 47
4.7. Biophysical methods for studying protein-protein interactions 47
4.7.1. Isothermal titration calorimetry (ITC) 47
4.7.2. Surface plasmon resonance (SPR) spectroscopy 48
5. Results 49
5.1. The CUE domain of Cue1 accelerates the ubiquitin chain elongation process in ERAD 49
5.1.1. Analysis of ubiquitin binding by the CUE domain of Cue1 49
5.1.2. Ubiquitin chain elongation kinetics correlates with ubiquitin binding affinity 51
5.1.3. CUE domain binding adjacent to the distal tip of a growing ubiquitin chain promotes chain elongation 52
5.2. Chain assembly and disassembly processes differently affect the conformational space of ubiquitin chains 58
5.2.1. Differently linked diubiquitins show distinct conformational flexibilities 58
5.2.2. Investigation of the conformational space of K48-linked ubiquitin chains 60

5.2.3. Ubiquitin chain elongation is impacted by the presence of binding proteins 64

5.2.4. The CUE domain of Cue1 uses conformational selection to support the chain elongation process 66

5.2.5. Chain recognition during hydrolysis requires remodeling of the conformational distribution 68

5.3. Analysis of interactions involving the E2 enzyme Ubc7 70

5.3.1. Optimization of Hrd1 and Ubc7 constructs for NMR studies 70

5.3.2. Activity and structural differences between Hrd1 and Doa10 RING domains 72

5.3.3. HADDOCK model of the Ubc7-U7BR-Hrd1(RING) complex 77

5.3.4. Investigation of the interaction between the donor ubiquitin and Ubc7 78

5.3.5. Ubc7 catalyzes ubiquitin dimer formation in absence of the CUE domain 80

5.3.6. Ubc7 transiently dimerizes *in vitro* 83

5.4. Structural analysis of glycan recognition by the MRH domain of Yos9 within ERAD 86

5.4.1. Optimization of Yos9 MRH domain constructs for structural studies 86

5.4.2. Glycan binding to the MRH domain of Yos9 results in structural rearrangements of the β-barrel structure 88

5.5. Characterization of high affinity SUMO-based Ubc9 inhibitors by ITC and NMR 93

5.5.1. ITC experiments of the SUMO2–Ubc9 interaction 93

5.5.2. SUMO2-variants bind to the back side of Ubc9 95

6. Discussion 97

6.1. The CUE domain of Cue1 accelerates the ubiquitin chain elongation process in ERAD 98

6.2. Chain assembly and disassembly processes differently affect the conformational space of ubiquitin chains 100

6.3. Analysis of interactions involving the E2 enzyme Ubc7 103

6.4. Structural analysis of glycan recognition by the MRH domain of Yos9 within ERAD 107

6.5. Characterization of high affinity SUMO-based Ubc9 inhibitors by ITC and NMR 109

7. References 111

8. Appendix 125

Abbreviations

3C protease	human rhinovirus 3C protease
AAA-ATPase	ATPases associated with diverse cellular activities
AEBSF	4-(2-Aminoethyl)benzensulfonylfluorid
AMBER	assisted model building and energy refinement
AMFR	autocrine motility factor receptor
AMP	adenosine monophosphate
APC/C	anaphase-promoting complex/cyclosome
ATP	adenosine triphosphate
AU	absorbance units
bp	base pair
CPY	carboxypeptidase Y
CS	cross saturation
CSP	chemical shift perturbation
CUE	coupling of ubiquitin to endoplamic reticulum degradation
Da	dalton
DD	dimerization domain
DMSO	dimethyl sulfoxid
DNA	deoxyribonucleic acid
dNTP	desoxyribonucleic trisphophate
Doa10	degradation of Mat-α2-10
DSS	4,4-dimethyl-4-silapentane-1-sulfonic acid
DTT	dithiothreitol
DUB	deubiquitinating enzyme
E. coli	*Escherichia coli*
E1	ubiquitin-activating enzyme
E2	ubiquitin-conjugating enzyme
E3	ubiquitin protein ligase
EDTA	ethylenediaminetetraacetic acid
EPR	electron paramagnetic resonance
ER	endoplasmic reticulum
ERAD	endoplasmic-reticulum-associated degradation
EtOH	ethanol

FPLC	fast protein liquid chromatography
FRET	fluorescence resonance energy transfer
GB1	B1 domain of protein G
Glc	glucose
GlcNAc	N-acetylglucosamine
GSH	reduced glutathione
GSSG	glutathione disulfide (oxidized)
GST	glutathione S-transferase
h	hour
HADDOCK	High Ambiguity Driven protein-protein DOCKing
HECT	homologous to E6-AP carboxyl terminus
HEPES	4-(2-hydroxyethyl)-1-piperazineethanesulfonic acid
His10	decahistidin-tag
His6	hexahistidine-tag
HMG-CoA	3-hydroxy-3-methylglutaryl-coenzyme A
Hrd1	HMG-CoA reductase degradation protein 1
HSQC	heteronuclear single quantum coherence
IPTG	isopropyl-β-D-thiogalactopyranosid
ITC	isothermal titration calorimetry
Kan^R	kanamycin resistance
K_D	dissociation constant
L	liter
LB	lysogeny broth
M9	minimal medium
Man	mannose
MBP	maltose binding protein
MeOH	methanol
min	minute
MRH	mannose 6-phosphate receptor homology
MTS	S-(2,2,5,5-tetramethyl-2,5-dihydro-1H-pyrrol-3-yl)methyl methanesulfonothioate
MTSL /MTSSL	MTS label / MTS spin label
MWCO	molecular weight cut off
Nedd8	neural precursor cell expressed developmentally down-regulated protein 8
NF-κB	nuclear factor 'kappa-light-chain-enhancer' of activated B-cells
Ni-NTA	nickel-nitrilotriacetic acid
NMR	nuclear magnetic resonance

NOESY	nuclear Overhauser effect spectroscopy
OD	optical density
OTU	ovarian tumor domain containing protein
PAGE	polyacrylamide gel electrophoresis
PBS	phosphate buffered saline
PCR	polymerase chain reaction
PDB	protein data bank
PELDOR	pulsed electron-electron double resonance
PH	pleckstrin-homology
pH	potential of hydrogen
PIC	protease inhibitor cocktail
pK_A	logarithmic acid dissociation constant
PML	promyelocytic leukemia
PPi	pyrophosphate
ppm	parts per million
PRE	paramagnetic relaxation enhancement
RBR	RING between RING
RDC	residual dipolar coupling
RF	restriction-free
RING	really interesting new gene
RMSD	root-mean-square deviation
SANS	small-angle neutron scattering
SAXS	small-angle X-ray scattering
SDS	sodium dodecyl sulfate
SEC	size exclusion chromatographie
SOC	super optimal broth supplemented with 20 mM glucose
SPR	surface plasmon resonance
SUMO	small ubiquitin-like modifier
TALOS	torsion angle likeliness obtained from shift and sequence similiarity
TB	terrific broth
TCEP	tris (2-carboxyethyl)phosphine
TEV	tobacco etch virus
TOCSY	total correlation spectroscopy
Tris	tris(hydroxymethyl)aminomethane
U7BR	Ubc7 interacting region
Ub	ubiquitin

Ubc	ubiquitin-conjugation enzyme
UBD	ubiquitin binding domain
UBL	ubiquitin-like protein
UPR	unfolded protein response
UPS	ubiquitin-proteasome-system
wt	wild type

Amino acids are abbreviated using the common single or three letter codes

Summary

The endoplasmic-reticulum-associated protein degradation pathway ensures quality control of newly synthesized soluble and membrane proteins of the secretory pathway. Proteins failing to fold into their native structure are processed in a multistep process and finally ubiquitinated and degraded by the proteasome in order to protect the cell from proteotoxic stress. My thesis covers structural as well as functional studies of various protein components that constitute the protein complexes that are responsible for this process.

One sub-project addressed the mechanism of glycan recognition by Yos9 as part of the ERAD substrate selection. NMR solution structures of the mannose-6-phosphate homology (MRH) domain of Yos9 both in a free and glycan bound conformation reveal a gripping movement of loop regions upon binding of correctly processed glycan structures.

The main projects focused on revealing the mechanism of efficient ubiquitin chain assembly by the ERAD ubiquitination machinery. This included the investigation of the role of the ERAD components Cue1 and Ubc7 in processive ubiquitin chain formation, how ubiquitin chain conformations change during elongation, how the conformation of a chain is impacted by interacting proteins and finally understand the activity regulation of the ERAD E2 enzyme Ubc7 by its cognate RING E3 ligases.

Nuclear magnetic resonance (NMR) analysis and fluorescence-based ubiquitination assays show that the CUE domain of Cue1 contributes with its proximal binding preference as well as with its position dependent accelerating effect to efficient ubiquitin chain formation. This is required to efficiently drive degradation of substrates. Specific ubiquitin binding events dictate and coordinate the spatial arrangement of the E2 enzyme relative to the distal tip of a chain. This process can be further accelerated by RING E3 ligases that promote Ubc7 activity by more than ~20 fold via inducing allosteric changes around the catalytic cysteine. My results additionally suggest a model where Ubc7 dimerization results in proximity induced activation of the E2. This data ensures rapid diubiquitin formation that is followed by a CUE domain assisted chain elongation mechanism where Cue1 acts in an E4 like fashion.

How ubiquitin binding events can modulate the conformations of a ubiquitin chain were investigated by pulsed electron-electron double resonance (PELDOR) spectroscopy combined with molecular modeling. This shows that K48-linked diubiquitin samples a broad conformational space which can be modulated in distinct ways. The CUE domain of Cue1 uses conformational selection of pre-populated open conformations to support ubiquitin chain elongation. In contrast, deubiquitinating enzymes shift the conformational distribution to weakly or even non-populated conformations to allow cleavage of the isopeptide bond that connects adjacent ubiquitins. Ubiquitin chain elongation increases the sampled conformational space and suggests that this high conformational flexibility might contribute to efficient proteasomal recognition.

Zusammenfassung

Die Qualitätskontrolle von sowohl löslichen als auch membran-gebundenen Proteinen des sekretorischen Weges erfolgt über das Endoplasmatische Retikulum (ER) assoziierte Degradationssystem (ERAD). Proteine deren Faltungsprozess erfolglos verbleibt werden spezifisch in einem mehrstufigen Prozess erkannt, aus dem ER transportiert, ubiquitiniert und letztlich proteasomal abgebaut. Da fehlerhafte Proteine für die Zelle toxisch sind, ist dieser zelluläre Mechanismus grundlegend für die Kontrolle und Aufrechterhaltung der Protein-Homöostase.
Die vorliegende Dissertation umfasst strukturelle und funktionelle Studien zu diversen Proteinkomplexen, welche für den ERAD Prozess verantwortlich sind. Als Modellsystem zum Verständnis dieses Weges, gilt das System der Hefe, da es evolutionär sehr konserviert ist. Daher wurde dieses auch in der vorliegenden Arbeit mechanistisch und strukturell untersucht.
Die ERAD Ubiquitin E3 Ligase Komplexe HRD1 und DOA10 bewerkstelligen die Erkennung fehlgefalteteter Proteine, deren Transport über die ER-Membran und den Prozess der Synthese von K48-verknüpften Ubiquitinketten auf Substratproteinen, um diese für den Abbau durch das Proteasom zu markieren. Erkennung von fehlgefalteten Proteinen im ER erfolgt unter anderem durch das kohlenhydratbindende Protein Yos9, welches über seine Mannose-6-Phosphat-Homologie (MRH) Domäne prozessierte Kohlenhydratstrukturen (N-Glykane) auf diesen fehlgefalteten Proteinen erkennt. Auf der zytosolischen Seite der ER Membran ist das Protein Cue1 zusammen mit dem E2 Enzym Ubc7 ein entscheidender Bestandteil der Ubiquitinierungsmaschinerie.
In dieser Arbeit wurde erforscht, wie die Erkennung von prozessierten Glykanen durch die Yos9 MRH Domäne als Teil des Substratselektionsprozesses in ERAD erfolgt (Kapitel 5.4), wie die Ubiquitin bindende Domäne (CUE Domäne) von Cue1 den Prozess der Ubiquitinkettenbildung unterstützt und beschleunigt (Kapitel 5.1) und wie die Aktivität von Ubc7 durch die RING Domänen der E3 Ligasen moduliert wird (Kapitel 5.3). In einem weiteren Projekt wurde der Konformationsraum von Ubiquitinketten untersucht und wie interagierende Proteine und Kettenverlängerung diese Konformationsverteilung beeinflusst (Kapitel 5.2).

Ich habe mittels Kernspinresonanzspektroskopie (NMR-Spektroskopie) die Struktur der ungefähr 20 kDa großen Yos9 MRH Domäne in zwei distinkten Konformationen gelöst: in einer freien Form, sowie gebunden an ein komplexes Oligosaccharid (3α, 6α-Mannopentaose). Dieser Zucker weist dabei das gleiche terminale α1,6-gebundene Mannose-Strukturmerkmal auf, welches auch auf fehlgefalteten Proteinen im ER-Lumen präsentiert wird, um diese für den ERAD Prozess zu markieren. Die Struktur der MRH Domäne besteht aus einem β-Fass, welches auch schon bereits gelöste homologe MRH

Domänen gezeigt haben. Jedoch ist dieser aus neun β-Strängen bestehenden Struktur an einem Ende eine 20 Aminosäure lange α Helix angelagert. Solch ein helikales Strukturelement wurde bisher noch nicht bei MRH Domänen gezeigt. Bei Yos9 schränkt die Anwesenheit dieser Helix die Anordnung der β-Stränge stark ein, sodass signifikante Unterschiede zu homologen MRH Domänen existieren. Erkennung der richtig prozessierten Glykanstruktur erfolgt an einer Seite des β-Fasses und induziert signifikante Änderungen in der Struktur des Peptidrückgrates, insbesondere in Schleifenregionen der MRH Domäne. Dieses erinnert an eine koordinierte, greifende Bewegung bei Zuckerbindung. Zentrale Komponente der Binderegion ist neben den genannten Schleifenregionen (β1β2, β6β7, β8β9), das FW-Motif in Yos9, welches analog zu dem WW-Motif des homologen Proteins OS-9 angeordnet ist. Eventuell könnten die konformationellen Veränderungen in der MRH Domäne von Yos9 Teil eines Signals sein, welches anschließend fehlgefaltete Proteine an weitere Komponenten des HRD1 Komplexes weiterreicht.

Nach erfolgter Retrotranslokation der ERAD Substrate erfolgt die Polyubiquitinierung auf der zytoplasmatischen Seite der ER-Membran. Dieser Prozess wurde im Rahmen dieser Dissertation intensiv studiert. Das Protein Cue1 ist mittels einer Transmembranhelix in der ER Membran verankert und damit in der Nähe der Komponenten, welche Proteine über die Membran befördern. Cue1 trägt zudem sowohl eine Ubiquitin-bindende CUE Domäne als auch eine Ubc7-aktivierende Region (U7BR), welche Ubc7 damit auch zur ER-Membran rekrutiert. Meine NMR Titrationsstudien zeigen, dass die CUE Domäne präferentiell an das proximale Ubiquitin in K48-verknüpftem Diubiqitin bindet. Das proximale Ubiquitin ist das Ubiquitinmolekül einer Kette welches auf einem Lysinrest eine weitere Ubiquitinmodifikation trägt und damit den Beginn einer Kette darstellt. Obwohl diese Bindungspräferenz nur gering ausgeprägt ist (Dissoziationskonstante ist 80 µM, verglichen mit 150 µM für die distale Einheit) und die Bindung insgesamt nur sehr schwach ist, bewirkt dies eine stärker werdende Bindung mit Zunahme der Anzahl der Bindestellen und einen dynamischen Prozess. Kinetische Studien mittels Fluoreszenz-basierten Ubiquitinierungsassays zeigen, dass die Elongationskinetik mit der Ubiquitin-Affinität korreliert. Dies konnte schon während meiner Diplomarbeit mittels Mutationen in der CUE Domäne gezeigt werden. Dieser Effekt ließ sich auch *in vivo* mit Hilfe eines Cycloheximid-basierten-Abbau Tests zeigen. Die Abbaurate des ERAD Modellsubstrates Ubc6 war bei dysfunktionaler CUE Domäne verlangsamt, welches die Bedeutung von Ubiquitinbindungsprozessen beim effizienten Aufbau von Ubiquitinsignalen verdeutlicht.

In vitro Ubiquitinkettenelongationsexperimente zeigen, dass der Verlängerungsprozess nur dann optimal stattfindet, wenn die CUE Domäne eine Bindestelle direkt benachbart zum distalen Akzeptorubiquitin einnimmt. Dies konnte zum einen mittels CUE-bindungsdefizienten Ubiquitinmutanten (R42A) gezeigt werden, die an spezifischen Stellen innerhalb einer Kette eingebracht wurden. Mutation der proximalen Einheit eines Diubiquitins verlangsamte die Elongationsrate signifikant, während kein signifikanter Effekt für eine Mutation im distalen Ubiquitin

gemessen wurde. Basierend auf meinem Strukturmodell des CUE-Ubiquitin Komplexes wurde dieser Positionierungseffekt auch über chemisch vernetzte CUE-Diubiquitin Komplexe gezeigt. Durch die Positionspräferenz organisiert Cue1 die räumliche Anordnung der enzymatischen Komponenten und beteiligten Moleküle am distalen Ende einer Ubiquitinkette und bewirkt eine effiziente Verlängerung. Die schnelle Bildung von ausreichend langen Ubiquitinketten ist relevant um die Degradation von ERAD Substraten sicherzustellen, da längere Ubiquitinketten ein effektiveres Abbausignal darstellen. Interessanterweise benötigt die CUE Domäne schon eine bereits synthetisierte Diubiquitinkette, um ihren Positionierungseffekt ausspielen zu können. Daher ergibt sich die Frage, wie die Ketteninitiation (Bildung des ersten Diubiquitins) effizient katalysiert wird.

Meine Untersuchungen zu dem ERAD E2 Enzym Ubc7 zeigen, dass die Kettenbildungsaktivität durch RING Domänen weiter moduliert werden kann. Ubc7 kann dabei über eine Schleifenregion, welche benachbart zum aktiven Zentrum des Enzyms liegt, mit den RING Domänen der E3 Ubiquitin Ligasen Doa10 und Hrd1 interagieren. Dies wurde mittels NMR Titrationsexperimenten gezeigt, welche erst durch Generierung eines stabilen kovalent verknüpften Ubc7-U7BR Komplexes und Deuterierung ermöglicht wurde. Aus diesen Daten habe ich ein Strukturmodell eines Komplexes aus Ubc7, der U7BR aus Cue1 und der RING Domäne von Hrd1 mittels HADDOCK-Modellierung berechnet. Hierfür wurde auch die Lösungsmittel-NMR Struktur von der RING Domäne von Hrd1 von mir bestimmt.

Fluoreszenz-basierte Untersuchungen der Ubiquitinierungskinetik zeigen, dass Hrd1 deutlich aktivierender (~28-fache Beschleunigung) als Doa10 (7-fache Beschleunigung eines einzelnen Kettenverlängerungsschrittes) wirkt. Eine strukturelle Interpretation dieser Tatsache könnte darin liegen, dass Hrd1 im Gegensatz zu Doa10 fähig ist allosterische Veränderungen in der Region um das katalytische Cystein von Ubc7 auszulösen. Weiterhin besitzt die Hrd1 RING Domäne einen konservierten Argininrest, welcher bei anderen RING Domänen schon als relevant für das Einnehmen einer geschlossenen Konformation des Donorubiquitins auf dem E2 gezeigt werden konnte. Dieser ist im Strukturmodell in elektrostatischen Interaktionen mit Glutamatresten der sauren Schleife von Ubc7 involviert. In Doa10 ist dieser Argininrest nicht vorhanden.

Durch Bildung einer Isopeptidbindung zwischen einer C89K Mutante von Ubc7 und dem C-terminus von Ubiquitin konnte das reaktionsfreudige Thioester-verknüpfte-Ubiquitin-Intermediat der Ubiquitinierungsreaktion nachgeahmt werden. NMR Experimente zeigen, dass dieses am aktiven Zentrum kovalent verknüpfte Ubiquitin signifikant Ubc7 an sekundären Interaktionsstellen ($\alpha2\alpha3$ Schleife und Helix $\alpha3$) bindet. Eine Mutationsanalyse von Ubc7 zeigt, dass sowohl negativ geladene Reste in der sauren Schleife, als auch R145 in der Helix $\alpha3$ entscheidend für die katalytische Aktivität von Ubc7 sind. Diese Reste sind aller Vorrausicht nach relevant für die exakte Ausrichtung von Akzeptor- und Donorubiquitin im katalytischen Zyklus, um den nukleophilen Angriff zu ermöglichen. Interessanterweise zeigte eine D146R Mutation, welche am Ende der Helix $\alpha3$ lokalisiert ist, ein hyper-aktiviertes Verhalten in Abwesenheit von RING Domänen. Dies könnte auf

eine Modulierung der Donorubiquitin-Interaktion hindeuten, hin zu geschlossenen Konformationen, die den nukleophilen Angriff erleichtern.

Weiterhin zeigen meine Analysen, dass Ubc7 in der Lage ist transient zu dimerisieren. Erste Hinweise für diese Selbstassoziation lieferten Ubiquitinkettenelongationsexperimente in welchem Ubc7 bei geringer E2-Konzentrationen (0.3 µM) deutlich schneller Diubiquitin aus Monoubiquitin (1µM) formt als in zehnfach-höherer Konzentration vorliegende Diubiquitinketten zu verlängern. Da E2 Enzyme in der Zelle hauptsächlich als E2-Ubiquitin-Konjugate vorliegen ergibt sich folgendes Modell:

Die schnelle Bildung von Diubiquitin lässt sich durch die Dimerisierung von mit Ubiquitin-beladenen Ubc7 Molekülen erklären. Dies induziert die Nähe zweier Ubiquitinmoleküle und führt zur Ausbildung einer Isopeptidbindung zwischen den zwei Ubiquitinmolekülen. Dieses Diubiquitin wird im Rahmen des *in vitro* Experimentes vom katalytischen Rest eines Ubc7 Moleküls freigesetzt wird.

NMR Experimente, welche auf paramagnetischer Relaxationsverstärkung basieren, unterstützen das Modell der Bildung von transienten, dimeren Ubc7-Komplexen. Hierfür wurden ^{15}N-markierte Ubc7-U7BR Komplexe mit Ubc7-U7BR Komplexen gemischt, welche an verschieden Stellen mit der Spinsonde MTSSL markiert waren. Dimerisierung von ^{15}N-markierten mit MTSSL-markierten Molekülen induziert auf diese Weise intermolekulare relaxationsverstärkende Effekte auf den ^{15}N-markierten Molekülen, die mittels HSQC Experimenten ausgewertet wurden. Die Stärke dieser Effekte waren zudem salzkonzentrationsabhängig, was auf eine durch elektrostatische Interaktionen getriebene Selbstassoziation hinweist.

Diese Erkenntnisse erweitern das Modell der Ubiquitinierung im ERAD Prozess dahingehend, dass Ubc7-Dimerisierung die Ketteninitiation durch Konjugation eines Diubiquitins auf ein Substrat katalysiert. Anschließend erfolgt CUE Domänen-abhängige und prozessive Kettenelongation über den vorhin beschriebenen Effekt, dass die CUE Domäne während dieses Prozess jeweils benachbart zum distalen Akzeptorubiquitin bindet. Die Fähigkeit, dass Ubc7 Ubiquitinketten auf seinem katalytischen Rest synthetisieren kann wurde bereits in der Literatur beschrieben und als Mechanismus zur Autoregulation der zellulären Ubc7 Konzentration identifiziert. Meine Ergebnisse schlagen vor, dass sowohl diese Autoubiquitinierung sowie die Ketteninitiation auf Substratproteinen durch die Dimerisierung von beladenen Ubc7 Molekülen gefördert wird.

Die im Rahmen des ERAD Prozesses gebildeten Ubiquitinketten weisen vorwiegend K48-Verknüpfungen zwischen den Ubiquitinen auf und dienen als Signal zur proteasomalen Degradation. In der Literatur sind zahlreiche Studien zu finden, welche sich speziell mit der Konformation dieser Kettenart beschäftigen. Jedoch liefern diese Studien nur Schnappschüsse spezifischer Konformationen, die entweder durch Kristallkontakte stabilisiert sind (Kristallstrukturen) oder basierend auf kurzreichweitigen Distanzeinschränkungen bestimmt wurden. Hier wurde mit Hilfe von gepulster Elektronen-Elektronen Doppelresonanz (PELDOR) Spektroskopie der

Konformationsraum von K48-verknüpften Ubiquitinketten untersucht. Hierzu wurden selektiv Nitroxidmarkierungen (MTSSL) an unterschiedlichen Positionen innerhalb von K48-verknüpften Ubiquitinketten eingebracht und die Abstandsverteilung dieser Spinsonden bestimmt, um so auf die Inter-Domänen Orientierungen schließen zu können. Computergestützte Modellierungen auf Basis der bestimmten Abstandsverteilungen lieferten dann das Ergebnis, dass K48-verknüpfte Ketten eine breite Konformationsverteilung einnehmen, welche durch distinkte höher populierte Regionen gekennzeichnet ist. Offene Konformationen, die die Zugänglichkeit zu der L8-I44-V70-hydrophoben Oberfläche von Ubiquitin nicht beeinträchtigen, sind schon im ungebunden Zustand der Ubiquitinkette hoch-populiert. Wie sich nun dieser Konformationsraum bei Anwesenheit von interagierenden Proteinen oder bei Verlängerung der Ubiquitinkette verändert wurde ebenfalls untersucht.

Die CUE Domäne von Cue1 bindet die untersuchte Diubiquitinkette unter konformationeller Selektion von vorher schon hoch-populierten, offenen Konformationen, um die Zugänglichkeit des Lysinrestes des distalen Akzeptorubiquitins sicherzustellen. Geschlossene oder kompakte Konformationen würden einen prozessiven Verlängerungsprozess behindern. Daher scheint die CUE Domäne von Cue1 auch aus konformationeller Sicht optimal geeignet, um Kettenelongationsprozesse zu unterstützen.

Ähnliche konformationelle Anforderungen existieren auch für Prozesse, die den Kettenabbau katalysieren, da hier Zugang zur Isopeptidbindung gewährleistet werden muss. Untersucht wurde dieser Aspekt über die Messung der Konformationsverteilung der Ubiquitinketten in Anwesenheit einer katalytisch inaktiven Mutante des deubiquitinierenden Enzyms OTUB1. Das so bestimmte Konformationsensemble ist zu Gunsten vorher sehr gering oder sogar gar nicht populierten Konformationen verschoben. Dies weist auf einen Mechanismus der konformationellen Umgestaltung hin.

Das zuvor existierende Model für die Konformation von K48-verknüpftem Tetraubiquitin in Lösung basierte maßgeblich auf einer Kristallstruktur, welche eine kompakte Struktur zeigt in der zwei Diubiquitineinheiten in jeweils geschlossener Konformation zusätzlich noch an sekundären Interaktionsstellen miteinander interagieren. Im Gegensatz zeigen die in dieser Arbeit berichteten Daten, dass eine Kettenverlängerung die konformationelle Flexibilität stark erhöht und daher den eingenommen Konformationsraum stark erweitert. Messungen an mit Spinsonden-markierten Diubiquitineinheiten als Teil längerer Ketten, weist zudem daraufhin, dass jede Diubiquitineinheit in gleichförmiger Art und Weise zur Konformationsverteilung längerer Ketten beiträgt, ohne zu einer Stabilisierung zu führen. Interaktionen zwischen direkt benachbarten oder anderen Ubiquitineinheiten einer Kette spielen für den eingenommen Konformationsraum eine untergeordnete Rolle. Dies konnte über Mutationen in der hydrophoben Oberfläche von Ubiquitin oder direkt benachbart dazu gezeigt werde (V70A oder R42A). Diese Mutationen hatten keinen

signifikanten Einfluss auf das PELDOR Signal und die daraus bestimmte Abstandsverteilungen. Dies spricht dafür, dass keine signifikanten Konformationsraum-bestimmenden nichtkovalenten Interaktionen existieren, wie sie beispielsweise die Kristallstruktur vorhersagt.
Die gefundene hohe Flexibilität längerer Ketten scheint notwendig zu sein um beispielsweise die simultane Assoziation mit den proteasomalen Rezeptoren Rpn10 und Rpn13 zu bewerkstelligen, ohne eine weitere strukturelle Umgestaltung der Kette zu benötigen.

In einem letzten Projekt in dieser Arbeit wurde die Interaktion von dem SUMO-spezifischen E2 Enzym Ubc9 und hoch affinen SUMO2 Varianten mittels NMR Spektroskopie und Isothermaler Titrationskalorimetrie (ITC) im Rahmen eines Kooperationsprojektes untersucht. Ich konnte über NMR Titrationsexperimente die Bindestelle der SUMO2 Varianten, welche über die Phagen-Display-Technik generiert wurden, auf die sogenannte Rückseite des E2 Enzyms kartieren. Die Affinität der am höchsten affinen Variante war mit einer Dissoziationskonstante von 16 nM 150-fach höher als die des Wildtyp-Proteins und wurde mittels eines Verdrängungsassays bestimmt. Analyse der Thermodynamik der Interaktion zeigte, dass die Interaktion mit dem Wildtyp-Protein entropiegetrieben ist, während die Interaktion mit der am höchsten affinen SUMO2-Variante ausschließlich enthalpiegetrieben ist.

1. Introduction

The eukaryotic cell has to constantly cope with a variety of cellular stresses and adapt to a changing environment to ensure cell viability. In particular, posttranslational modifications of cellular proteins contribute to the cell's capability to adapt. These modifications for example include phosphorylation, acetylation, methylation and ubiquitination and occur to 50 % of proteins in humans (Hornbeck et al., 2015). Protein ubiquitination controls widespread functions and signaling processes in the cell by altering protein interaction profiles, activity and localization of proteins (Komander and Rape, 2012). Protein degradation is also mediated by conjugation to ubiquitin and is required for selective disposal of defective protein species as well as for regulatory reasons.

The cell has evolved two major protein quality control and degradation systems called the ubiquitin-proteasome system and the autophagy-lysosome system to ensure protein homeostasis. Especially impaired protein degradation and the accumulation of terminally misfolded proteins represent a major threat to the cell and have been connected to numerous human diseases (Bassermann et al., 2014; Chiti and Dobson, 2017; Petrucelli and Dawson, 2004).

Quality control of newly synthesized soluble and membrane bound proteins and assembled protein complexes of the secretory pathway is ensured by a process called endoplasmic-reticulum-associated protein degradation (ERAD) (Werner et al., 1996) and is also based on protein ubiquitination. Proteins failing to fold into their native structure are processed in a multistep process and finally ubiquitinated and degraded by the proteasome in the cytosol.

The experimental work presented here provides new structural and mechanistic insights into ubiquitination and the ERAD pathway. The following introductory paragraph provides an overview of the ubiquitin-proteasome system, the variety of different ubiquitin signals and summarizes the ERAD process in more detail.

1.1. Ubiquitin-proteasome-system

1.1.1. Ubiquitin and the ubiquitination cascade

Cellular proteins can be post-translationally modified with ubiquitin, a highly stable and conserved 76-amino acid protein (Vijay-Kumar et al., 1987) with diverse regulatory and signaling functions in eukaryotic cells. The covalent conjugation of ubiquitin to a substrate protein requires the concerted action of three enzyme classes (Figure 1) called ubiquitin-activating enzymes (E1), ubiquitin-conjugation enzymes (E2) and ubiquitin protein ligases (E3) (Hershko and Ciechanover, 1998). In order to achieve substrate specificity and allow the synthesis of different topological forms of ubiquitin chains the human genome encodes two E1, ~40 E2 and ~600-1000 E3 enzymes (Ye and Rape, 2009). The yeast (*Saccharomyces cerevisiae*) system has a decreased complexity, but still has 13 E2 enzymes and 60-100 putative E3s encoded in its genome (Finley et al., 2012). An overview of the ubiquitination cascade is given in Figure 1.

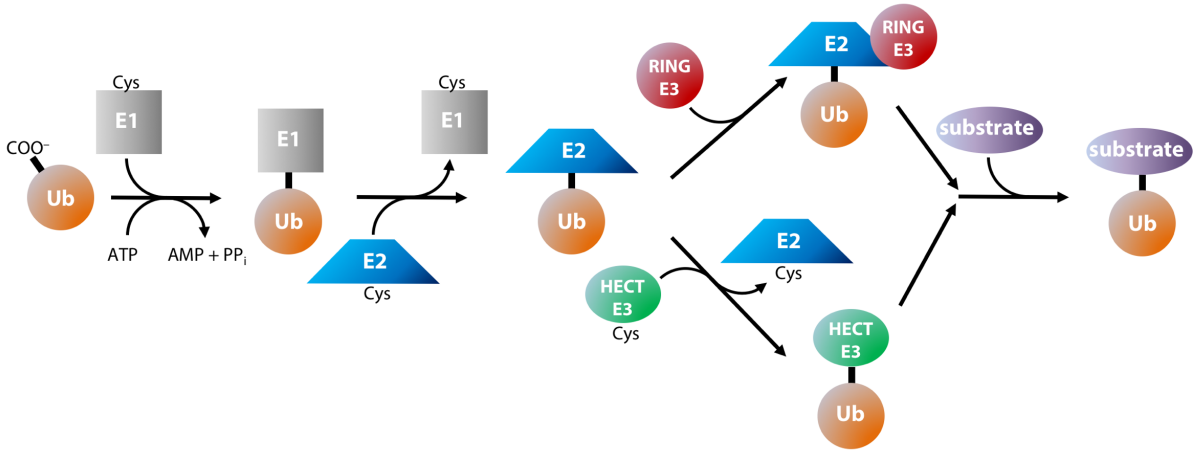

Figure 1: The ubiquitination cascade. Ubiquitin is conjugated via its C-terminal glycine residue to a substrate molecule. The ubiquitination cascade involves ubiquitin activation and charging of an E2 enzyme by an E1 enzyme, followed by ubiquitin transfer to a substrate catalyzed either by RING E3 or HECT E3 ligases. While RING domain E3 ligases bring substrate and E2 enzyme in proximity and activate discharging of the E2 enzyme, HECT domain ligases form a thioester intermediate before ubiquitin transfer to a substrate.

Ubiquitin-activating enzymes (E1) catalyze the formation of a thioester linkage between the C-terminal glycine carboxylate group and the sulfhydryl group of a cysteine residue of the E1 enzyme. This reaction requires the formation of an activated ubiquitin-AMP intermediate (carboxy-terminal adenylation). Subsequently, the E1 enzyme binds to a ubiquitin conjugating enzyme (E2) and catalyzes a thioester transfer reaction. Mechanistically, this is achieved by exposing an E2 binding site after the E1 enzyme is charged with ubiquitin (Lee and Schindelin, 2008). The E2~ubiquitin conjugate can then cooperate with either RING domain E3 ligases or HECT domain E3 ligases. These interactions are usually weak and in the micromolar range and enhance the intrinsic activity of E2 enzymes (Ye and Rape, 2009) by promoting ubiquitin discharge. The rationale behind these weak interactions is that E2 enzymes are interaction platforms and have to consecutively engage with E1

and E3 enzymes which usually have overlapping interacting regions (Eletr et al., 2005). It has been suggested that RING interactions promote closed conformations of the conjugated ubiquitin molecule thereby positioning the C-terminus of ubiquitin for nucleophilic attack by acceptor lysine residues of a substrate molecule (Pruneda et al., 2012). However, counterexamples exist that E2 enzymes significantly populate closed states even in absence of an E3 enzyme as has been shown for Ube2S (Wickliffe et al., 2011). In contrast to this direct ubiquitin transfer of RING E3 ligases, HECT E3 ligases (Scheffner et al., 1995) catalyze the formation of an additional E3~ubiquitin conjugate. Ubiquitin is transferred from the catalytic cysteine of the E2 enzyme to an E3 active site cysteine (Deshaies and Joazeiro, 2009). Here, it has been proposed that open E2~Ub states are active towards these transthiolation reactions (Kamadurai et al., 2009). The so-called RING-Between-RING (RBR) ligases, use a RING-HECT-hybrid mechanism to catalyze ubiquitin transfer. They contain both an E2 binding RING domain and a domain called RING2 which contains an active cysteine residue for formation of a ubiquitin thioester intermediate similar to HECT domain ligases. In each case ubiquitin is finally conjugated to solvent exposed ε-amino groups of lysine residues, but can involve in some cases even the modification of serine or threonine residues (Wang et al., 2007). The final ubiquitin transfer step, either catalyzed by E2 or HECT E3 enzymes, determines substrate and residue specificity of the reaction. Some E2 enzymes are solely responsible for ubiquitin chain initiation on a substrate molecule, whereas other are chain elongation enzymes. Since ubiquitin contains 7 internal lysine residues and a free amino group at its N-terminus sequential rounds of ubiquitin conjugation can lead to the formation of ubiquitin chains. The exact complex composition and spatial organization determines whether a substrate or ubiquitin itself is modified. Chain elongating E2s have evolved several mechanisms to position acceptor lysine residues of a ubiquitin molecule in a way to specifically allow a thioester attack. The K63-linkage specific Ubc13 acts as a heterodimer with an E2-like subunit to position the acceptor K63 side chain (Eddins et al., 2006). Some K48-specific E2s, like Cdc34, feature an acidic loop in proximity to the catalytic site that is involved in aligning the K48 residue with the donor ubiquitin (Chong et al., 2014). It has also been proposed that this loop could additionally lower the pK_A value of the incoming lysine (Ziemba et al., 2013) to transform it into a nucleophile. Further regulation of E2 enzymes is achieved by non-covalent binding events at the back side of the E2 enzyme. This can involve monoubiquitin, ubiquitin as part of another E2 ubiquitin conjugate or E2 interacting regions, like the Ube2g2 binding region G2BR or the Ubc7 interacting region U7BR (Bazirgan and Hampton, 2008; Das et al., 2013; Metzger et al., 2013; Page et al., 2012; Sakata et al., 2010). All these mechanisms have the aim to increase processivity of chain elongation in order to ensure that the signal is correctly transmitted, since ubiquitin signaling is also chain length dependent. The E2 interacting regions are additionally involved in E2 recruitment to large E3 ubiquitin complexes as described in more detail for Ubc7 in chapter 1.2.3. This work addresses,

among other things, the interactions of this E2 enzyme and characterizes how interactions with RING domains, ubiquitin or the cofactor Cue1 affect processivity and activity of Ubc7.

1.1.2. Cellular functions of ubiquitin signaling

Specificity of ubiquitin signaling is achieved by distinct ubiquitination patterns and assembly of different polymeric signals that can both differ in chain length as well as in linkage type. Signaling functions include for example cell cycle progression (Jin et al., 2008), DNA repair (Huang and D'Andrea, 2006), transcriptional activation (Conaway, 2002), endocytosis (Haglund et al., 2003), immune response (Goto et al., 2010) or protein degradation (Thrower, 2000). Figure 2 summarizes the variety of ubiquitination signals that were detected in cells and all convey these specific signals. Target proteins can either be modified by a single ubiquitin (monoubiquitination), multiple ubiquitins or with structurally distinct ubiquitin chains (polyubiquitination). Mass spectrometry studies have revealed that all seven lysine residues can participate in forming ubiquitin linkages *in vivo* (Peng et al., 2003) however, with cell type and cell cycle stage specific abundances (Matsumoto et al., 2010). This underscores the flexibility and versatility of the ubiquitination system.

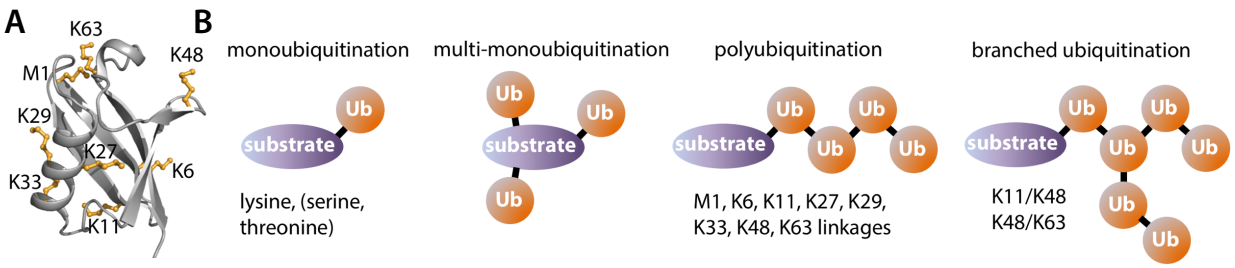

Figure 2: The variety of ubiquitination signals. (A) Cartoon representation of ubiquitin (PDB code: 1UBQ) showing all possible linkage possibilities. (B) Summary of all possible ubiquitin modifications: monoubiquitination, multi-monoubiquitination, polyubiquitination via all 8 different linkages or branched ubiquitination, where a single ubiquitin is linked to two ubiquitins via different lysines. Mixed ubiquitin chains are also possible, but topologically similar to polyubiquitination, but not homogeneously linked and are not shown.

The classical and first described function of ubiquitin chains to promote proteasomal degradation was initially described in 1980 by Hershko and coworkers (Hershko et al., 1980). Further studies have revealed that the assembly of at least four K48-linked ubiquitins target proteins for efficient degradation by the 26S proteasome (Chau et al., 1989; Finley, 2009; Thrower, 2000). Similar proteolytic functions have also been shown for K11-linked ubiquitin chains, that have crucial functions in ERAD (Xu et al., 2009) and cell cycle control (Jin et al., 2008).

Many nonproteolytic functions are conveyed by monoubiquitin, K63 or M1-linked (linear) chains and include the beforehand mentioned regulation of DNA repair or NF-κB activation, a process controlling inflammation, apoptosis and immunity (Chen, 2005; Ikeda et al., 2011).

Complexity of the ubiquitin code is further increased by the possibility to form mixed (Nakasone et al., 2013) and branched ubiquitin chains. Thus far physiological important roles have been ascribed

to K11/K48- and K48/K63-branched ubiquitin chains. The K11/K48-linked branch which is generated by the anaphase-promoting complex (APC/C) has been shown to improve proteasomal degradation thereby driving the turnover of cell cycle regulators (Meyer and Rape, 2014). The most recently identified K48/K63-linked branches have functions in regulating and amplifying NF-κB signaling (Ohtake et al., 2016).

1.1.3. Ubiquitin binding domains

Ubiquitin binding domains (UBDs) are the decoders of ubiquitin signaling (Husnjak and Dikic, 2012). They can distinguish between all different kinds of ubiquitin modifications and transform them into specific cellular functions. Usually UBDs are part of larger modular effector proteins and serve as the recognizing element to guide those proteins to ubiquitinated substrates.

Unlike this classical role of UBDs in interpreting information encoded by the ubiquitin chains, ubiquitin binding events can also be involved in the ubiquitination process itself (Bagola et al., 2013; Choi et al., 2010). Here, UBDs exert regulatory functions in ubiquitination cascades. A prominent example is the protein Cue1 which acts as a regulator of K48-linked chain synthesis. The sequential assembly of ubiquitin chains challenges the ubiquitination machinery to cope with a constantly changing position of the distal tip of a chain relative to the chain elongating E2 enzyme. Here, ubiquitin binding events might be crucial for processive ubiquitin chain formation. This question was addressed in a collaborative research project with the group of Thomas Sommer from the Max-Delbrück-Centrum in Berlin (von Delbrück. et al., 2016).

UBDs are structurally diverse and make up more than 20 different protein families, that can be structurally classified into alpha helical domains (e.g. UBA, CUE), zinc fingers, pleckstrin-homology (PH)-like (e.g. PRU) and ubiquitin-conjugating-like domains as described in the indicated review articles (Dikic et al., 2009; Husnjak and Dikic, 2012).

The present work covers interaction studies with ubiquitin associated (UBA) domains, coupling of ubiquitin to endoplasmic reticulum degradation (CUE) domains and pleckstrin-like receptors for ubiquitin (PRU). Studied CUE domains include the CUE domains of Cue1 (von Delbruck et al., 2016), Cue2 (Kang et al., 2003) and gp78 (Liu et al., 2012).

Ubiquitin receptors play important roles in proteasomal degradation, since they are either stable subunits of the proteasome or can reversibly associate with it (Elsasser et al., 2004). They directly mediate the link between ubiquitination and proteasomal degradation. During this thesis Rpn13 (Husnjak et al., 2008) and the UBA2 domain of the human UV excision repair protein Rad23 (hHR23A) was studied. Rpn13 is a stable subunit of the proteasome, while hHR23A represents a shuttling factor for the 26S proteasome that can associate with the 19S regulatory particle of the proteasome (Schauber et al., 1998).

Ubiquitin chain recognition by UBDs is usually weak with K_D values in the µM range as summarized by Hurley et al. (2006) to ensure reversible binding in dynamic signaling processes. Since different linkage types exclude specific residues from participating in UBD complex formation, unique binding surfaces are created that allow linkage specific recognition. A prominent example is the UBA2 domain of hHR23A that binds in a sandwich like conformation between both ubiquitin moieties in K48-linked diubiquitin (Varadan et al., 2005). Another binding mechanism involves multiple UBDs organized in tandem and utilizes specific spatial distributions of ubiquitin moieties. This mechanism has been termed linkage-specific avidity and is the reason for the observed K63-linkage preference of human Rap80 that bind to K63-linked chains in the course of DNA double strand breaks (Sims and Cohen, 2009). It should be noted that many UBDs termed to be specific can still bind to monoubiquitin or even to other ubiquitin chains and that the subcellular localization as well as the incorporation in complexes also affect their specificity.
The most important interaction surface on ubiquitin, that is used by UBDs, is its famous L8-I44-V70 centered hydrophobic patch, but can also involve the I36 centered patch (Sloper-Mould et al., 2001).

1.1.4. Structures and conformations of ubiquitin chains

The variety of differently linked ubiquitin chains has been the subject of intensive structural studies over the past decade (Alfano et al., 2016). Research dealing with structural investigations on free ubiquitin chains is summarized in Table 1 and covers all possible linkage types for diubiquitin.
In addition, distinct chain conformations have emerged as an additional regulatory layer in ubiquitin signaling (Ye et al., 2012) by for example impacting their recognition by ubiquitin binding domains. How these interacting proteins affect the conformations of ubiquitin chains is part of this thesis and is the key to gain a complete view on ubiquitin signaling. It has already been suggested that they might remodel or select pre-existing conformations (Ye et al., 2012).
The previously employed structural methods to study the conformation of ubiquitin chains range from X-ray crystallography, nuclear magnetic resonance (NMR), small-angle X-ray and neutron scattering (SAXS, SANS), molecular modeling to fluorescence resonance energy transfer (FRET). More specifically, NMR methods included the analysis of chemical shift perturbation (CSP) data, relaxation data, residual dipolar couplings (RDCs), paramagnetic relaxation enhancement (PRE) data and cross saturation (CS) experiments (Table 1). Some studies used NMR data for HADDOCK modeling purposes to calculate structures for certain conformations. However, the large majority of structures was obtained by X-ray crystallography, where crystal packing issues might also influence the obtained ubiquitin orientations in the final structure. This also yielded to inconsistent views on the conformations of certain chain types. For example, analysis of the conformation of K11 diubiquitin produced inconsistent data (Bremm et al., 2010; Castañeda et al., 2013; Matsumoto et al., 2010) concerning the exposure of the hydrophobic patch of ubiquitin.

Table 1: Overview of structural investigations on ubiquitin chains and applied methods. Only studies dealing with conformations of free ubiquitin chains are shown.

ubiquitin chain type	method	PDB	reference
M1-linked diubiquitin	X-ray	2W9N	(Komander et al., 2009a)
M1-linked diubiquitin	X-ray	3AXC	(Rohaim et al., 2012)
M1-linked tetraubiquitin	X-ray	5GO8	(Gao et al., 2016)
K6-linked diubiquitin	X-ray	2XK5	(Virdee et al., 2010)
K6-linked diubiquitin	X-ray	5X3N	to be published by Man, P. et al.
K6-linked diubiquitin	X-ray	5GOB	(Gao et al., 2016)
K11-linked diubiquitin	NMR, SANS	2MBO/2MBQ	(Castañeda et al., 2013)
K11-linked diubiquitin	X-ray	2XEW	(Bremm et al., 2010)
K11-linked diubiquitin	X-ray	3NOB	(Matsumoto et al., 2010)
K11-linked diubiquitin	X-ray	5GOC	(Gao et al., 2016)
K11/K48-branched tetraubiquitin	X-ray	5XDP	to be published by Liang, L. et al.
K27-linked diubiquitin	X-ray	5GOD	(Gao et al., 2016)
K29-linked diubiquitin	X-ray	4S22	(Kristariyanto et al., 2015a)
K29-linked diubiquitin	X-ray	5GOG	(Gao et al., 2016)
K33-linked diubiquitin	X-ray	4XYZ	(Kristariyanto et al., 2015b)
K33-linked diubiquitin	X-ray	5AF4	(Michel et al., 2015)
K33-linked diubiquitin	X-ray	5GOH	(Gao et al., 2016)
K48-linked diubiquitin	X-ray	1AAR	(Cook et al., 1992)
K48-linked diubiquitin	X-ray, NMR (CSP analysis)	3AUL	(Hirano et al., 2011)
K48-linked diubiquitin	X-ray	3M3J	(Trempe et al., 2010)
K48-linked diubiquitin	X-ray	3NS8	(Lai et al., 2012)
K48-linked diubiquitin	X-ray	5GOI	(Gao et al., 2016)
K48-linked diubiquitin	NMR, HADDOCK modeling (CSP analysis, RDCs)	2BGF	(van Dijk et al., 2005)
K48-linked diubiquitin	NMR (relaxation data)	2PE9/2PEA	(Ryabov and Fushman, 2007)
K48-linked diubiquitin	NMR (relaxation analysis)	–	(Ryabov and Fushman, 2006)
K48-linked di- and tetraubiquitin	NMR (CSP analysis, RDCs, relaxation analysis)	–	(Varadan et al., 2002)
K48-linked tetraubiquitin	X-ray	1F9J	(Phillips et al., 2001)
K48-linked tetraubiquitin	X-ray	1TBE	(Cook et al., 1994)
K48-linked tetraubiquitin	X-ray, NMR (PRE analysis)	2O6V	(Eddins et al., 2007)
K63-linked diubiquitin	X-ray	2JF5	(Komander et al., 2009a)
K63-linked diubiquitin	X-ray	3H7P / 3H7S	(Weeks et al., 2009)
K63-linked diubiquitin	X-ray	5GOJ	(Gao et al., 2016)
K63-linked tetraubiquitin	X-ray	3HM3	(Datta et al., 2009)
all diubiquitins	molecular modeling	–	(Fushman and Walker, 2010)
K48-, K63- and Met1-linked diubiquitin	FRET	–	(Ye et al., 2012)
K48-linked and K63-linked di- and tetraubiquitin	SAXS, NMR (CSP analysis, cross-saturation data)	–	(Tenno et al., 2004)

For the most intensively studied K48-linked diubiquitin a compact arrangement of both ubiquitin moieties has been suggested to represent the major conformation in solution (Ryabov and Fushman, 2006). This closed conformation of K48-linked diubiquitin is defined by the relative distance of both I44 centered hydrophobic patches. How chain conformations and dynamics in solution are altered with increasing chain length still remains elusive and is of protruding importance due to the chain length dependence of ubiquitin signaling. This is in particular true for marking substrates for efficient proteasomal degradation (Thrower, 2000). The existing data on chains longer than diubiquitin is still limited (Table 1). X-ray crystallography analysis of K48-linked tetraubiquitin revealed that secondary interactions apart from interactions between the hydrophobic patches, help to stack diubiquitin units onto one another (Eddins et al., 2007) to form a compact arrangement.

This would necessitate protein remodeling for efficient recognition by proteasomal ubiquitin receptors like Rpn10 or Rpn13 (Zhang et al., 2016).
In summary it can be stated, that the previously applied methods are either based on crystallography or mainly sensitive to short-range interactions yielding only snapshots of specific conformations, while the actually sampled conformational remains elusive. This work addresses this question and analyzes the accessible conformational space of ubiquitin by the help of pulsed electron-electron double resonance (PELDOR) spectroscopy. The influence of chain length on conformational flexibility and the impact of binding partners are addressed as well.

1.1.5. Deubiquitinating enzymes

Ubiquitination is reversible, similar to protein phosphorylation, and ubiquitin chains can be hydrolyzed by deubiquitinating enzymes (DUBs) (Komander et al., 2009b). This enables to stop or edit ubiquitin signaling by completely hydrolyzing or distally trimming of the chains. In addition, generation of monoubiquitin from linear ubiquitin fusions (Wiborg et al., 1985), as it is expressed in the cell, and recycling of ubiquitin requires DUB activity.
Thus far, ~100 human DUBs are known and organized in six different DUB families (Abdul Rehman et al., 2016). The thiol proteases of the ovarian tumor (OTU) family are for example involved in the regulation of important signaling cascades. In this work the chain recognition mechanism of two different linkage specific DUBs, OTUD7B (Cezanne) and OTUB1 was analyzed by PELDOR spectroscopy. OTUD7B is specific for K11 linkages (Bremm et al., 2010) and has functions in regulating NF-κB signaling (Hu et al., 2013). OTUB1 has K48-linkage specificity (Edelmann et al., 2009) and participates for example in DNA damage response (Nakada et al., 2010)

1.1.6. SUMO and other ubiquitin-like proteins

Ubiquitin is not the only protein that can modulate protein functions in the cell by covalent attachment to target proteins. In total, 17 ubiquitin-like proteins (UBL) exist and require distinct enzymatic cascades for their conjugation (Schulman and Harper, 2009). Other well-studied UBLs include for example NEDD8, the three SUMO family members (SUMO1, SUMO2 and SUMO3) (Gareau and Lima, 2010) and the autophagy related proteins of the ATG8 and ATG12 families (van der Veen and Ploegh, 2012).
SUMOylation has been shown to regulate for example genome integrity, gene expression and ribosome biogenesis (Flotho and Melchior, 2013; Raman et al., 2013). Only a single E1 (heterodimer of SAE1/SAE2) and E2 (Ubc9) pair is mediating SUMO conjugation to substrates. This process can be facilitated by E3 enzymes, but is not strictly dependent on their presence (Streich and Lima, 2014). SUMO2 and SUMO3 are able to form poly-SUMO chains via an internal lysine residue, while SUMO1 is predominantly involved in mono-SUMOylation (Matic et al., 2008).

SUMO chains have already been identified to form as a stress response mechanism for degradation or as a reaction to DNA damage (Nie and Boddy, 2016) and provide docking sites for cellular proteins that harbor SUMO interaction motifs organized in tandem. The well-studied group of SUMO-targeted E3 ubiquitin ligases (StUBLs) (Sriramachandran and Dohmen, 2014) for example provides a link to the ubiquitin-proteasome system. A famous example of poly-SUMO-dependent ubiquitination of substrate proteins is the degradation of promyelocytic leukemia (PML) protein (Lallemand-Breitenbach et al., 2008) by RNF4 which is induced by arsenic trioxide treatment in acute promyelocytic leukemia (Tatham et al., 2008). In addition RNF4 has also been shown to promote DNA double-strand repair by targeting the DNA damage checkpoint 1 protein (MDC) (Galanty et al., 2012). The E2 enzyme Ubc9 is the predominant determinant of substrate specificity in the SUMO system since it features a preference for a consensus motif for SUMOylation of substrates (Rodriguez et al., 2001). It can interact with SUMO covalently via thioester bond formation as well as via noncovalent binding to the back side of the E2 enzyme (Knipscheer et al., 2007) which is critical for poly-SUMO chain formation by SUMO E3 ligases (Eisenhardt et al., 2015). Thus, interfering with this back side binding is a target for selectively interfering with poly-SUMO formation, while leaving mono-SUMOylation unaffected. This approach was pursued by Wiechmann et al. (2017) by generating SUMO2-based Ubc9 inhibitors using protein engineering and phage display methods. In the present work SUMO2 binding to Ubc9 was studied. The interaction with high affinity SUMO2 variants was biophysically characterized using isothermal titration calorimetry (ITC) and nuclear magnetic resonance (NMR).

1.2. Endoplasmic-reticulum-associated protein degradation (ERAD)

1.2.1. Protein folding and ER quality control

The endoplasmic reticulum (ER) is the main folding compartment of the eukaryotic cell. All proteins of the secretory pathway, about one third of all synthesized polypeptides (Lander et al., 2001), pass the ER quality control system. Here, they experience maturation guidance before they are shuttled to their final destinations in the cell, like membranes or other cellular compartments. This error prone process of protein biogenesis necessitates that defective proteins that are unable to fold properly are rapidly and specifically degraded (Schubert et al., 2000). Possible sources of error include transcriptional and translational errors, genetic mutations, failed formation of multi-protein complexes or even environmental stresses (Hirsch et al., 2009).

Since the ERAD system is conserved among all eukaryotes and the *Saccharomyces cerevisiae* is the best studied system it provides a guideline for understanding the more differentiated human system. In the following, only protein components of the yeast system are described in more detail.

Protein translocation across the ER membrane happens cotranslationally and requires the heterotrimeric Sec61 translocon (Becker et al., 2009; Matlack et al., 1998). The nascent polypeptide is modified with preassembled asparagine linked oligosaccharides called N-glycans that are composed of a glucose$_3$-mannose$_9$-N-acetylglucosamine$_2$ carbohydrate ($Glc_3Man_9GlcNAc_2$) (Xu and Ng, 2015). These glycans both guide cotranslational folding of polypeptides (Daniels et al., 2003) and serve as a marker and timer during protein folding. Glucosidases sequentially remove two glucose residues and initiate the folding process mediated by ER chaperones. Further processing of the glycan structure involves removal of the last glucose residue after successful folding. By contrast, the mammalian system has a cycle of glucose trimming and reglucosylation to allow several folding attempts (Hebert et al., 1995).

Glycans on proteins that are unable to attain their native structure in a certain time frame are further trimmed by the mannosidases Mns1 (Camirand et al., 1991) and Htm1 (Clerc et al., 2009) in yeast. This trimming marks substrate proteins for ERAD.

1.2.2. Substrate selection in ERAD

Luminal ERAD substrates are identified by a unique mannose$_7$-N-acetylglucoseamine$_2$ carbohydrate structure that displays a terminal α-1,6-linked mannose residue (Quan et al., 2008). But, studies using the ERAD model substrate CPY*, a mutated version of Carboxypeptidase Y, revealed that the actual signal seems to be bipartite and is also dependent on the surrounding peptide (Smith et al., 2014). Detailed mechanistic insights of this recognition mechanism are still missing and one aim of a sub-project of this thesis was to investigate glycan recognition by the quality control lectin Yos9 (yeast osteosarcoma 9). Yos9 is a luminal part of the HRD1 E3 ligase complex and is involved in selection of misfolded glycoproteins for ERAD (Gauss et al., 2006) by having the greatest affinity for terminal α-1,6-linked mannose residues.

1.2.3. ERAD ubiquitin ligases

In order to target a large variety of substrate proteins carrying defects in cytosolic, luminal or transmembrane parts, distinct converging sub-branches of the ERAD pathway have evolved (Carvalho et al., 2006). The luminal ERAD pathway (ERAD-L) is conducted by the HRD1 complex (HMG-CoA reducatase degradation 1) and processes luminal proteins. In contrast, proteins with defects in their cytosolic domains are substrates of the DOA10 E3 ligase complex (degradation of Mat-α2-10). It has been shown that both ligases have the capability to recognize defective transmembrane regions (ERAD-M) (Habeck et al., 2015; Nakatsukasa et al., 2008).

These large membrane embedded E3 ubiquitin ligase complexes are described in more detail in the following sections.

HRD1 E3 ligase complex

The central component of the HRD1 E3 ligase complex is the multi-spanning transmembrane ubiquitin E3 ligase Hrd1 that has a RING domain located in the cytosol (Bays et al., 2001). The structure of the dimeric transmembrane part of Hrd1 in complex with its luminal binding partner Hrd3 has recently been solved by cryo-electron microscopy (Schoebel et al., 2017). This work also describes an aqueous cavity formed by the Hrd1 dimer and suggests that Hrd1 forms a retro-translocation channel for the movement of misfolded polypeptides across the ER membrane for cytosolic polyubiquitination. Hrd1 additionally interacts with the transmembrane protein Usa1 (U1-SNp1 asociating-1) (Carvalho et al., 2006) which mediates Der1 (degradation in the ER-1) recruitment (Knop et al., 1996). Der1 has also been reported to oligomerize and proposed to be involved in the export of misfolded proteins (Mehnert et al., 2014).

On the luminal side of the complex Hrd3 interacts with the lectin Yos9. Both proteins act as substrate recognition factors. Hrd3 binds unfolded membrane or luminal proteins independent of glycosylation (Gauss et al., 2006), whereas Yos9 recognizes glycans marked for ERAD. The exact process of substrate recognition and the interplay of both receptors is still not known.

It has been proposed that Yos9 interacts with Hrd3 via its N-terminally located mannose 6-phosphate receptor homology (MRH) domain, but thus far structural studies were only limited to the dimerization domain (DD) of Yos9 (Hanna et al., 2012). In this work the solution structure of the MRH domain (~20 kDa) of Yos9 was solved by NMR in two states. This allowed the analysis and comparison of the free and glycan bound conformations of Yos9 to study the conformational changes induced by glycan recognition.

The ubiquitination machinery is located on the cytosolic side of the complex. After retrotranslocation of terminally misfolded substrates K48-linked ubiquitination is executed by the E2 enzyme Ubc7 that is recruited to the ER membrane via its membrane anchored cofactor Cue1 (Bazirgan and Hampton, 2008; Biederer et al., 1997; Kostova et al., 2009).

Cue1 is a multi-domain protein comprised of a N-terminal transmembrane helix, a ubiquitin binding CUE domain and a Ubc7-interacting region (U7BR) at the C-terminus. Under Cue1-limiting conditions Ubc7 is autoubiquitinated and degraded which further supports the fact that Cue1 and Ubc7 act together (Ravid and Hochstrasser, 2007). Next to these roles in controlling localization and stability of Ubc7, the U7BR of Cue1 activates Ubc7 via enhancing RING domain interactions and increasing the accessibility of the catalytic cysteine (Metzger et al., 2013). The structure of Ubc7 in complex with the U7BR was solved by X-ray crystallography (Metzger et al., 2013). The CUE domain of Cue1 has been shown to bind ubiquitin chains and enhances degradation of certain ERAD substrates as Hmg2p and Ubc6 (Bagola et al., 2013). The solution NMR structure of the CUE domain of Cue1 was solved during my diploma thesis. The work described here, expands this research project in form of

a collaboration with Maximilian von Delbrück from the group of Thomas Sommer and studies the CUE domain assisted ubiquitin elongation mechanism by Cue1 and Ubc7.

Ubiquitination also involves the RING domain of the Hrd1 protein as the E3 ligase. This thesis also includes interactional studies of the Ubc7-U7BR-RING complex. I solved the NMR solution structure of the HRD1 RING domain as well as calculated a structural model of the trimeric ubiquitination complex Ubc7-U7BR-Hrd1(RING).

Further components required for functioning of the HRD1 complex are the membrane protein Ubx2 (ubiquitin regulatory X domain containing 2) which interacts with a complex comprising the AAA-ATPase Cdc48, Ufd1 (ubiquitin fusion degradation1) and Npl4 (nuclear protein localization 4) (Neuber et al., 2005; Schuberth and Buchberger, 2005). It has been proposed that these proteins provide the driving force for retrotranslocation as well as extraction of polyubiquitinated proteins from the membrane (Ye et al., 2001).

The basic components of the HRD1 complex are illustrated and summarized in Figure 3.

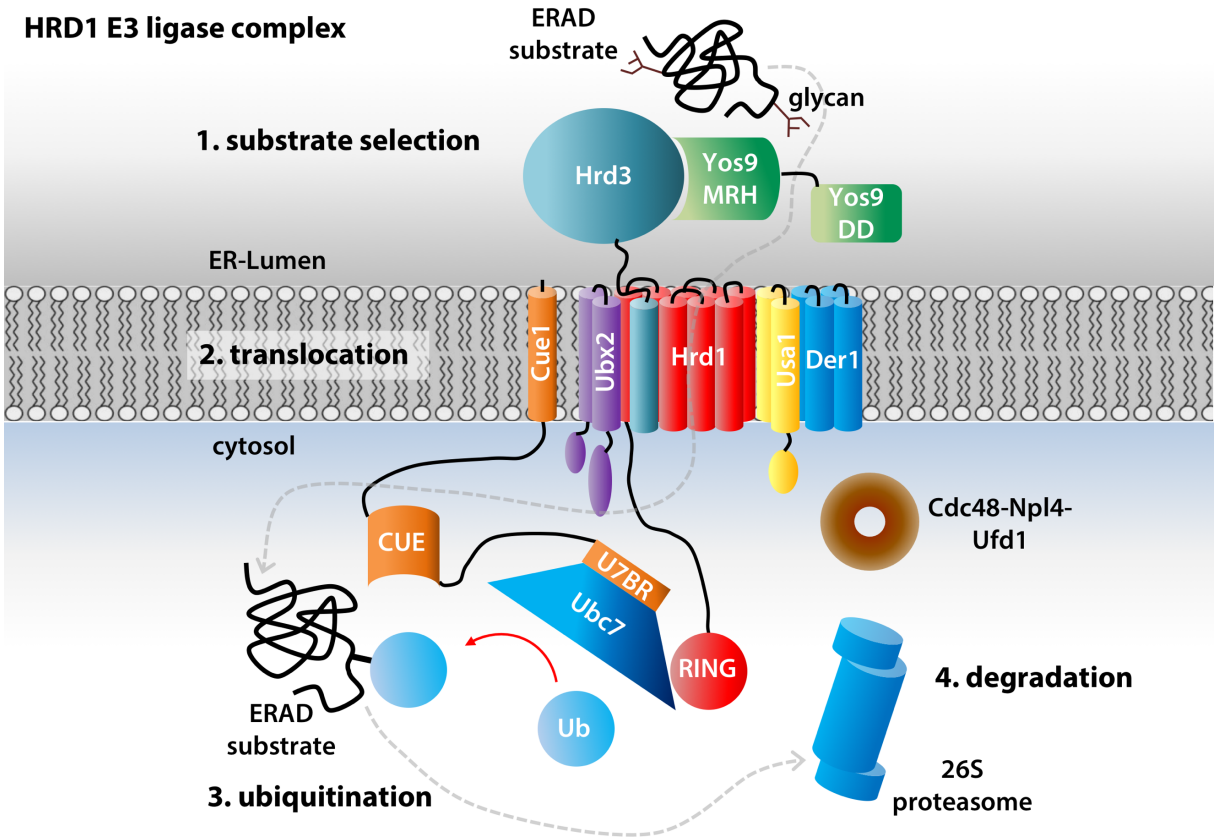

Figure 3: Schematic depiction of the HRD1 E3 ligase complex. The ERAD-L pathway that targets glycosylated proteins is composed of 4 major steps: substrate selection in the ER lumen which requires Hrd3 and Yos9 (step 1), retrotranslocation by membrane components like Hrd1 (step 2), cytosolic ubiquitination by a complex involving the E2 enzyme Ubc7, the cofactor Cue1 and the RING domain of the E3 ligase Hrd1 (step 3) and extraction from the membrane by Cdc48-Npl4-Ufd1 followed by proteasomal degradation (step 4). Further necessary components are Usa1, Der1 and Ubx2. A more detailed description is found in the text.

DOA10 E3 ligase complex

Since the DOA10 E3 ligase complex mainly processes target proteins with defects in their cytosolic domains (ERAD-C), it also features a different modular composition. The central component Doa10 has a N-terminal RING domain (Kreft et al., 2006) and 14 transmembrane segments compared to eight in Hrd1 (Schoebel et al., 2017). Other components are also found in the HRD1 complex and include the Ubc7-Cue1 complex for ubiquitin chain formation and the AAA-ATPase containing complex of Cdc48-Npl4-Ufd1 that is recruited to the membrane via Ubx2 (Figure 4). Another possible E2 enzyme that works in conjunction with Doa10 is the membrane anchored Ubc6 (Kreft and Hochstrasser, 2011).

In this thesis the interaction of the Doa10 RING domain and the Ubc7-U7BR complex is studied.

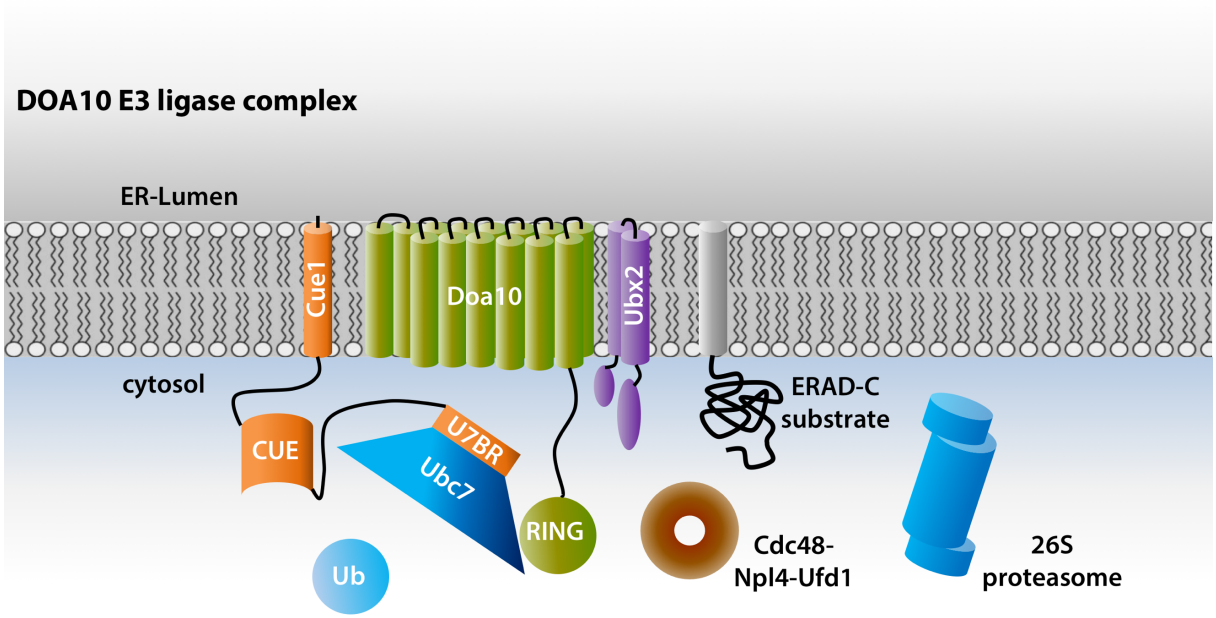

Figure 4: Schematic depiction of the DOA10 E3 ligase complex: The DOA10 E3 ligase complex is involved in processing of ERAD-C substrates. ERAD-C substrates contain misfolded structures in their cytosolic parts. The basic composition of the DOA10 E3 ligase complex includes Doa10, Cue1-Ubc7, Ubx2 and the Cdc48-Npl4-Ufd1 complex. The pathway also leads to proteasomal degradation.

1.2.4. Cytosolic degradation of ERAD substrates

After extraction of polyubiquitinated proteins from the ER membrane they are shuttled to the 26S proteasome. This is achieved by the UBD containing proteins Rad23 or Dsk2 in yeast (Medicherla et al., 2004). It has also been reported that initial ubiquitin chains generated by the E1-E2-E3 cascade can be further elongated by E4 enzymes like Ufd2 (Koegl et al., 1999).

The proteasomal ubiquitin receptors Rpn10 and Rpn13 as part of the 19S regulatory particles of the proteasome recognize K48-linked ubiquitin modifications (Elsasser et al., 2004; Husnjak et al., 2008). In addition, proteasome associated deubiquitinating enzymes remove the ubiquitin modifications (Hu et al., 2005) which is required for entry of the polypeptide chain into the catalytically active 20S core of the proteasome (Voges et al., 1999).

2. Objectives

- **Elucidate the role of Cue1 in ubiquitin chain formation as part of the ERAD process.**
- **Investigate ubiquitin chain conformations and how they are impacted by interacting proteins.**
- **Understand the activity regulation of the ERAD E2 enzyme Ubc7 by RING domains.**
- **Understand glycan recognition by Yos9 as part of the ERAD substrate selection.**

3. Materials

3.1. Laboratory equipment

Product	Manufacturer
Agarose gel electrophoresis system	PEQLAB Biotechnologie
ÄKTApurifier FPLC system	GE Healthcare
ÄKTAprime plus	GE Healthcare
Autoclave	Getinge AB
NanoDrop 1000 UV-/Vis Spectrophotometer	PEQLAB Biotechnologie
PCR Gradient cycler peqSTAR	PEQLAB Biotechnologie
pH-meter PHM210	Radiometer Analytical SAS
Sonicator Labsonic U	B. Braun Biotech International
NMR spectrometers (600 MHz, 700 MHz, 800 MHz, 950 MHz)	Bruker
MicroCal VP-ITC calorimeter	Malvern Instruments Ltd
Biacore X100	GE Healthcare
Pipettes, Eppendorf Research® plus	Eppendorf AG
Incubation shaker Innova 4330	New Brunswick Scientific
Incubation shaker Multitron	Infors-HT
Mini-Protean Tetra Cell gel electrophoresis system	Bio-Rad Laboratories
Centrifuge 5810 R	Eppendorf AG
Centrifuge Sorvall RC-5B	Sorvall Instruments
Centrifuge RC 12BP+	Thermo Fisher Scientific
Centrifuge rotor GSA	Sorvall Instruments
Centrifuge rotor SS-34	Sorvall Instruments
Centrifuge rotor H-12000	Thermo Fisher Scientific
Fixed-angle rotor F34-6-38	Eppendorf AG
Swing-bucket rotor A-4-62	Eppendorf AG
ELEXSYS E580 EPR spectrometer	Bruker

3.2. Laboratory consumables

Product	Manufacturer
Amicon Ultra-15 centrifugal filter units (3, 10, 30 and 50 kDa)	Merck Millipore
Amicon Ultra-4 centrifugal filter units (3, 10, 30 kDa)	Merck Millipore
Amicon Ultra-0.5 mL centrifugal filters	Merck Millipore
Spectra/Por® RC dialysis membrane (MWCO 3.5 kDa)	SPECTRUM labs
Spectra/Por® RC dialysis membrane (MWCO 6-8 kDa)	SPECTRUM labs
Syringe filter 0.22 µm polyethersulfone	Carl Roth
4–20% Mini-PROTEAN® TGX™ Precast Protein Gels, 15-well, 15 µl	Bio-Rad Laboratories
Sensor chip SA for Biacore	GE Healthcare

3.3. Chromatography equipment

Chromatography column	application	Manufacturer
HisTrap FF, 5 mL	Ni-NTA affinity purification	GE Healthcare
HisTrap HP, 5 mL	Ni-NTA affinity purification	GE Healthcare
HisTrap HP, 1 mL	Ni-NTA affinity purification	GE Healthcare
GSTrap FF, 5 mL	GST affinity purification	GE Healthcare
Superdex 75 10/300 GL	Size exclusion chromatography (SEC)	GE Healthcare
HiLoad 16/600 Superdex 75 pg	Size exclusion chromatography (SEC)	GE Healthcare
HiLoad 16/600 Superdex 200 pg	Size exclusion chromatography (SEC)	GE Healthcare
HiLoad 26/600 Superdex 75 pg	Size exclusion chromatography (SEC)	GE Healthcare
HiTrap Q HP, 5 mL	Anion exchange chromatography (AEX)	GE Healthcare
HiTrap SP HP, 5 mL	Cation exchange chromatography (CEX)	GE Healthcare
Mono S 5/50 GL	Cation exchange chromatography (CEX)	GE Healthcare

3.4. Kits

Kit	Manufacturer
Gel Filtration LMW Calibration Kit	GE Healthcare
QIAprep Spin Miniprep Kit	Qiagen
QIAquick Gel Extraction Kit	Qiagen
QIAquick PCR Purification Kit	Qiagen

3.5. Enzymes

Enzyme		Source
PfuUltra High-Fidelity	DNA Polymerase	Agilent Technologies
Phusion® High-Fidelity	DNA Polymerase	New England BioLabs
DpnI	Restriction endonuclease	New England BioLabs
T4 DNA Ligase	Ligase	New England BioLabs
TEV protease	Protease	self made
HRV 3C protease	Protease	self made
Antarctic Phosphatase	Phosphatase	New England BioLabs
BamHI-HF®	Restriction endonuclease	New England BioLabs
NcoI-HF®	Restriction endonuclease	New England BioLabs
DNAse I from bovine pancreas	Endonuclease	Sigma-Aldrich (Merck)
Lysozyme from chicken egg white	Hydrolase	Sigma-Aldrich (Merck)
GST-tagged 3C protease	Protease	self made
Human E1 enzyme Ube1	Ubiquitin activating enzyme	self made according to (Berndsen and Wolberger, 2011)
Cdc34	Ubiquitin conjugating enzyme	self made
Ubc13/Uev1a heterodimer	Ubiquitin conjugating enzyme	self made
Ube2SΔC (aa 1-156) with C-terminal TEV cleavable His6 tag	Ubiquitin conjugating enzyme	self made
OTUB1 (full-length, aa 1-271)	Deubiquitinating enzyme	self made according to (Mevissen et al., 2013)
Cezanne (OTUD7B; aa 53-446)	Deubiquitinating enzyme	self made according to (Mevissen et al., 2013)

3.6. Bacterial strains

Strain	Manufacturer
DH5α Competent *E. coli* (High Efficiency)	New England BioLabs
T7 Express Competent *E. coli* (High Efficiency)	New England BioLabs
SHuffle® T7 Express Competent *E. coli*	New England BioLabs

3.7. Vectors

Vector	origin
pET39_Ub19 vector (Kan^R)	modified version of pET39b(+), (Rogov et al., 2012)
pETGB1 (Kan^R)	gift from Haribabu Arthanari, Harvard Medical School
pETMBP (Kan^R)	gift from Haribabu Arthanari, Harvard Medical School
pETM-60 (Kan^R)	the vector was initially constructed by G. Stier (EMBL)

3.8. Oligonucleotides and synthetic genes

All primers used for cloning, site-directed mutagenesis and sequencing were obtained from Eurofins Genomics. Codon optimized synthetic genes were purchased from GenScript USA Inc. and smaller synthetic fragments (up to a length of 600 bp) were ordered as uncloned, double-stranded DNA from ThermoFisher Scientific.

Mutagenesis primer

Primer		sequence	
Hrd1_K407stop_for	5'-	GATTGCCTGTCTTTGATGAATAAGGTAATGTTGTGCAAACG	-3'
Hrd1_K407stop_rev	5'-	CGTTTGCACAACATTACCTTATTCATCAAAGACAGGCAATC	-3'
Hrd1_T413stop_for	5'-	GAAAAAGGTAATGTTGTGCAATAAACTTTCACTTCCAATAGTGATATC	-3'
Hrd1_T413stop_rev	5'-	GATATCACTATTGGAAGTGAAAGTTTATTGCACAACATTACCTTTTTC	-3'
Hrd1_325-336del_for	5'-	GTATTTTCAGGGCGCCATGGGCGAACAGCTACAAAATTCTGCAAATG	-3'
Hrd1_325-336del_rev	5'-	CATTTGCAGAATTTTGTAGCTGTTCGCCCATGGCGCCCTGAAAATAC	-3'
Hrd1_Q437stop_for	5'-	CACTGGGATAGCGACAGATTAACAAGGTTTCGCAAACGAAG	-3'
Hrd1_Q437stop_rev	5'-	CTTCGTTTGCGAAACCTTGTTAATCTGTCGCTATCCCAGTG	-3'
Hrd1_T466stop_for	5'-	GTGCCTACTCAAAATATAGACTAATTAGCAATGAGAACAAGGTCAACC	-3'
Hrd1_T466stop_rev	5'-	GGTTGACCTTGTTCTCATTGCTAATTAGTCTATATTTTGAGTAGGCAC	-3'
Doa10_19start_for	5'-	GGTGAGAATCTGTATTTTCAGGGCGTTGCAAATGAAGAAACCGATACC	-3'
Doa10_19start_rev	5'-	GGTATCGGTTTCTTCATTTGCAACGCCCTGAAAATACAGATTCTCACC	-3'
Doa10_I102stop_for	5'-	CGATCCAGTTTAAAACCTAATATGCCGAAAATATGCC	-3'
Doa10_I102stop_rev	5'-	GGCATATTTTCGGCATATTAGGTTTTAAACTGGATCG	-3'
Ubc7_D46R_for	5'-	CCTGATTCAGGGTCCGCCGCGCACCCCGTATGCAGACGG	-3'
Ubc7_D46R_rev	5'-	CCGTCTGCATACGGGGTGCGCGGCGGACCCTGAATCAGG	-3'
Ubc7_D46A_for	5'-	CCTGATTCAGGGTCCGCCGGCGACCCCGTATGCAGACGG	-3'
Ubc7_D46A_rev	5'-	CCGTCTGCATACGGGGTCGCCGGCGGACCCTGAATCAGG	-3'
Ubc7_D9899R_for	5'-	GATCCTGCACAGCCCGGGCCGCCGTCCGAACATGTACGAACTG	-3'
Ubc7_D9899R_rev	5'-	CAGTTCGTACATGTTCGGACGGCGGCCCGGGCTGTGCAGGATC	-3'
Ubc7_D9899A_for	5'-	GATCCTGCACAGCCCGGGCGCGGCACCGAACATGTACGAACTG	-3'
Ubc7_D9899A_rev	5'-	CAGTTCGTACATGTTCGGTGCCGCGCCCGGGCTGTGCAGGATC	-3'
Ubc7_E104R_for	5'-	CGATGACCCGAACATGTACCGCCTGGCGGAAGAACGTTGG	-3'
Ubc7_E104R_rev	5'-	CCAACGTTCTTCCGCCAGGCGGTACATGTTCGGGTCATCG	-3'
Ubc7_E104A_for	5'-	CGATGACCCGAACATGTACGCGCTGGCGGAAGAACGTTGG	-3'
Ubc7_E104A_rev	5'-	CCAACGTTCTTCCGCCAGCGCGTACATGTTCGGGTCATCG	-3'
Ubc7_E107108R_for	5'-	GAACATGTACGAACTGGCGCGCCGTCGTTGGTCTCCGGTTCAG	-3'
Ubc7_E107108R_rev	5'-	CTGAACCGGAGACCAACGACGGCGCGCCAGTTCGTACATGTTC	-3'
Ubc7_E107108A_for	5'-	GAACATGTACGAACTGGCGGCGGCACGTTGGTCTCCGGTTCAG	-3'
Ubc7_E107108A_rev	5'-	CTGAACCGGAGACCAACGTGCCGCCGCCAGTTCGTACATGTTC	-3'
Ubc7_R109E_for	5'-	GTACGAACTGGCGGAAGAAGAATGGTCTCCGGTTCAGAG	-3'
Ubc7_R109E_rev	5'-	CTCTGAACCGGAGACCATTCTTCTTCCGCCAGTTCGTAC	-3'
Ubc7_R109A_for	5'-	GTACGAACTGGCGGAAGAAGCGTGGTCTCCGGTTCAGAG	-3'
Ubc7_R109A_rev	5'-	CTCTGAACCGGAGACCACGCTTCTTCCGCCAGTTCGTAC	-3'
Ubc7_E129R_for	5'-	GTTATGTCCATGCTGTCACGCCCGAATATCGAATCTGGTG	-3'
Ubc7_E129R_rev	5'-	CACCAGATTCGATATTCGGGCGTGACAGCATGGACATAAC	-3'
Ubc7_E129A_for	5'-	GTTATGTCCATGCTGTCAGCGCCGAATATCGAATCTGGTG	-3'
Ubc7_E129A_rev	5'-	CACCAGATTCGATATTCGGCGCTGACAGCATGGACATAAC	-3'
Ubc7_E133R_for	5'-	GCTGTCAGAACCGAATATCCGCTCTGGTGCGAACATTGATG	-3'
Ubc7_E133R_rev	5'-	CATCAATGTTCGCACCAGAGCGGATATTCGGTTCTGACAGC	-3'
Ubc7_E133A_for	5'-	GCTGTCAGAACCGAATATCGCGTCTGGTGCGAACATTGATG	-3'
Ubc7_E133A_rev	5'-	CATCAATGTTCGCACCAGACGCGATATTCGGTTCTGACAGC	-3'
Ubc7_R145E_for	5'-	GATGCCTGTATCCTGTGGGAAGACAATCGCCCGGAATTTG	-3'
Ubc7_R145E_rev	5'-	CAAATTCCGGGCGATTGTCTTCCCACAGGATACAGGCATC	-3'
Ubc7_R145A_for	5'-	GATGCCTGTATCCTGTGGGCGGACAATCGCCCGGAATTTG	-3'
Ubc7_R145A_rev	5'-	CAAATTCCGGGCGATTGTCCGCCCACAGGATACAGGCATC	-3'
Ubc7_D146R_for	5'-	GCCTGTATCCTGTGGCGTCGCAATCGCCCGGAATTTGAAC	-3'
Ubc7_D146R_rev	5'-	GTTCAAATTCCGGGCGATTGCGACGCCACAGGATACAGGC	-3'
Ubc7_D146A_for	5'-	GCCTGTATCCTGTGGCGTGCGAATCGCCCGGAATTTGAAC	-3'
Ubc7_D146A_rev	5'-	GTTCAAATTCCGGGCGATTCGCACGCCACAGGATACAGGC	-3'

Ubc7_R148E_for	5′-	GTATCCTGTGGCGTGACAATGAACCGGAATTTGAACGCCAAG	-3′
Ubc7_R148E_rev	5′-	CTTGGCGTTCAAATTCCGGTTCATTGTCACGCCACAGGATAC	-3′
Ubc7_R148A_for	5′-	GTATCCTGTGGCGTGACAATGCGCCGGAATTTGAACGCCAAG	-3′
Ubc7_R148A_rev	5′-	CTTGGCGTTCAAATTCCGGCGCATTGTCACGCCACAGGATAC	-3′
Ubc7_E152R_for	5′-	GACAATCGCCCGGAATTTCGCCGCCAAGTCAAACTGTCC	-3′
Ubc7_E152R_rev	5′-	GGACAGTTTGACTTGGCGGCGAAATTCCGGGCGATTGTC	-3′
Ubc7_E152A_for	5′-	GACAATCGCCCGGAATTTGCGCGCCAAGTCAAACTGTCC	-3′
Ubc7_E152A_rev	5′-	GGACAGTTTGACTTGGCGCGCAAATTCCGGGCGATTGTC	-3′
Ubc7_S30C_for	5′-	GTATCGTCGCAGGTCCGAAATGCGAAAACAATATTTTTATC	-3′
Ubc7_S30C_rev	5′-	GATAAAAATATTGTTTTCGCATTTCGGACCTGCGACGATAC	-3′
Ubc7_A106C_for	5′-	CCGAACATGTACGAACTGTGCGAAGAACGTTGGTCTCCG	-3′
Ubc7_A106C_rev	5′-	CGGAGACCAACGTTCTTCGCACAGTTCGTACATGTTCGG	-3′
Ubc7_S128C_for	5′-	GAGTGTTATGTCCATGCTGTGCGAACCGAATATCGAATCTG	-3′
Ubc7_S128C_rev	5′-	CAGATTCGATATTCGGTTCGCACAGCATGGACATAACACTC	-3′
Ubc7_S158C_for	5′-	GAACGCCAAGTCAAACTGTGCATTCTGAAATCACTGGG	-3′
Ubc7_S158C_rev	5′-	CCCAGTGATTTCAGAATGCACAGTTTGACTTGGCGTTC	-3′
Ubc7_C89K_for	5′-	CTATCCGAATGGTGAAGTTAAAATTTCGATCCTGCACAGCCC	-3′
Ubc7_C89K_rev	5′-	GGGCTGTGCAGGATCGAAATTTTAACTTCACCATTCGGATAG	-3′
Ubc7_S39C_for	5′-	CAATATTTTTATCTGGGACTGCCTGATTCAGGGTCCGC	-3′
Ubc7_S39C_rev	5′-	GCGGACCCTGAATCAGGCAGTCCCAGATAAAAATATTG	-3′
Ubc7_S141C_for	5′-	GGTGCGAACATTGATGCCTGTATCCTGTGGCGTGACAATC	-3′
Ubc7_S141C_rev	5′-	GATTGTCACGCCACAGGATACAGGCATCAATGTTCGCACC	-3′
Ub_T9C_for	5′-	GATTTTCGTGAAAACCCTTTGCGGGAAGACCATCACCCTC	-3′
Ub_T9C_rev	5′-	GAGGGTGATGGTCTTCCCGCAAAGGGTTTTCACGAAAATC	-3′
Ub_T22C_for	5′-	CTCGAAGTTGAACCCTCGGATTGCATAGAAAATGTAAAGGCC	-3′
Ub_T22C_rev	5′-	GGCCTTTACATTTTCTATGCAATCCGAGGGTTCAACTTCGAG	-3′
Ub_E24C_for	5′-	GAACCCTCGGATACGATATGCAATGTAAAGGCCAAGATCC	-3′
Ub_E24C_rev	5′-	GGATCTTGGCCTTTACATTGCATATCGTATCCGAGGGTTC	-3′
Ub_N25C_for	5′-	CCTCGGATACGATAGAATGCGTAAAGGCCAAGATCCAG	-3′
Ub_N25C_rev	5′-	CTGGATCTTGGCCTTTACGCATTCTATCGTATCCGAGG	-3′
Ub_A28C_for	5′-	GGATACGATAGAAAATGTAAAGTGCAAGATCCAGGATAAGGAAGG	-3′
Ub_A28C_rev	5′-	CCTTCCTTATCCTGGATCTTGCACTTTACATTTTCTATCGTATCC	-3′
Ub_E34C_for	5′-	CCAAGATCCAGGATAAGTGCGGAATACCTCCTGATCAG	-3′
Ub_E34C_rev	5′-	CTGATCAGGAGGTATTCCGCACTTATCCTGGATCTTGG	-3′
Ub_R42A_for	5′-	CTCCTGATCAGCAGGCACTGATCTTTGCTGGC	-3′
Ub_R42A_rev	5′-	GCCAGCAAAGATCAGTGCCTGCTGATCAGGAG	-3′
Ub_V70A_for	5′-	GAGTCTACTCTTCATCTTGCCTTGAGACTTCGTGGTGG	-3′
Ub_V70A_rev	5′-	CCACCACGAAGTCTCAAGGCAAGATGAAGAGTAGACTC	-3′
Ube2S_156del_for	5′-	CTGCTCACAGAGATCCACGGGCACCACCACCACCACCACTG	-3′
Ube2S_156del_rev	5′-	CAGTGGTGGTGGTGGTGGTGCCCGTGGATCTCTGTGAGCAG	-3′
Ube2S-TEV_for	5′-	CTGCTCACAGAGATCCACGGGGGCTCCGAAAACCTGTATTTCCAGGGCTCCCAC CACCACCACCACCACTG	-3′
Ube2S-TEV_rev	5′-	CAGTGGTGGTGGTGGTGGTGGGAGCCCTGGAAATACAGGTTTTCGGAGCCCCCG TGGATCTCTGTGAGCAG	-3′
OTUB1_C91A_for	5′-	CCAGGCCTGACGGCAACGCCTTCTATCGGGCTTTCGG	-3′
OTUB1_C91A_rev	5′-	CCGAAAGCCCGATAGAAGGCGTTGCCGTCAGGCCTGG	-3′
OTUD7B_C194S_for	5′-	CAACTACTGGAGATGGGAACAGCCTCCTGCATGCAGCCTCCC	-3′
OTUD7B_C194S_rev	5′-	GGGAGGCTGCATGCAGGAGGCTGTTCCCATCTCCAGTAGTTG	-3′
Cue1_T66C_for	5′-	GCGGTCATCCCGTTTGCACCCAGATGGTCGAAAC	-3′
Cue1_T66C_rev	5′-	GTTTCGACCATCTGGGTGCAAACGGGATGACCGC	-3′
Cue1_biotin59-115_for	5′-	GTATTTTCAGGGCGCCATGGGCCTGAACGACATCTTCGAGGCTCAGAAAATCG AATGGCACGAAGTTAATGGCGGTCATCCCGTTACC	-3′
Cue1_biotin59-115_rev	5′-	GGTAACGGGATGACCGCCATTAACTTCGTGCCATTCGATTTTCTGAGCCTCGAA GATGTCGTTCAGGCCCATGGCGCCCTGAAAATAC	-3′

Cloning primer

Doa10_2-112_for	5'-	CCCCCATGGATGTGGATAGTGATGTTAATGTTAG	-3'
Doa10_2-112_rev	5'-	CGAAAATATGCCGGAAAAAATTCCGTAACTCGAGCGG	-3'
Cue2CUE1_for	5'-	CCCCCATGGGCAACGATGATCACGAAAGCAAACTGAG	-3'
Cue2CUE1_rev	5'-	GGGGGATCCTTAGCTTTTGTCATCATTTTCTTTCAGCAGC	-3'
gp78CUE_for	5'-	CCCCCATGGGCAGCAATAGCCAGCTGAATGCAATGG	-3'
gp78CUE_rev	5'-	GGGGGATCCTTAGGTCGGAAACGGCACCTGAATAC	-3'
hHR23A_UBA2_for	5'-	CCCCCATGGGCCAGGTTACACCGCAAGAAAAAGAAG	-3'
hHR23A_UBA2_rev	5'-	GCTGAGCCAGAACTTTGATGATGAATAAGGATCCCCC	-3'
RF _Ubc9_for	5'-	GAATCTGTATTTTCAGGGCGCCATGTCGGGGATCGCCCTC	-3'
RF _Ubc9_rev	5'-	GACGGAGCTCGAATTCTTAGGATCCTTATGAGGGCGCAAACTTCTTGG	-3'
RF_Ubc7U7BR_for	5'-	GTCCATTCTGAAATCACTGGGTTTTGGCGGCTCAGCAGAAAACCTGCTGGATA AATTTC	-3'
RF_Ubc7U7BR_rev	5'-	GACGGAGCTCGAATTCTTAGGATCCTTAGGTCAGCAGGCTTTGCAGGTC	-3'
Hrd1_341-401_for	5'-	CAGGGCGCCATGGGCAATTCTGCAAATGATGACAATATTTGTATCATTTG	-3'
Hrd1_341-401_rev	5'-	GACGGAGCTCGAATTCTTAGGATCCTTACAATCTACAAATAGGACAAGTCTGA GAACG	-3'
Hrd1_325-412_for	5'-	GTATTTTCAGGGCGCCATGGGCAAACAGCTCGACGACACTCTTGTC	-3'
Hrd1_325-412_rev	5'-	GACGGAGCTCGAATTCTTAGGATCCCTAGATATGCTGGATAAATTTATCTGGTA TGAC	-3'
Hrd1_325-551_for	5'-	GTATTTTCAGGGCGCCATGGGCAAACAGCTCGACGACACTCTTGTC	-3'
Hrd1_325-551_rev	5'-	GACGGAGCTCGAATTCTTAGGATCCCTAGATATGCTGGATAAATTTATCTGGTA TGAC	-3'
Cue1_25-203_for	5'-	GGAGCCTGGCAGCGCCGCTGGTAGCAGCGATACGATCG	-3'
Cue1_25-203_rev (+His6)	5'-	CGGAGCTCGAATTCTTAGGATCCTTAGTGATGGTGATGATGATGGCCGCCGG TCAGCAGGCTTTGCAGGTC	-3'
MBP-Hrd1_337_for	5'-	GAGAATCTTTATTTTCAGGGCGCCGAACAGCTACAAAATTCTGCAAATGATG	-3'
MBP-Hrd1_412_rev	5'-	CTCGAATTCGGATCCGGTACCTTATTGCACAACATTACCTTTTTCATCAAAG	-3'
MBP-Hrd1_420_rev	5'-	CTCGAATTCGGATCCGGTACCTTAATCACTATTGGAAGTGAAAGTCGTTTGC	-3'
GB1-Yos9_90_for	5'-	GAGAATCTTTATTTTCAGGGCGCCAGCAATAGTGAAAAGACAGCATTATTAAC TAAAACC	-3'
GB1-Yos9_105_for	5'-	GAGAATCTTTATTTTCAGGGCGCCGGTGTTAAGACAATTTTCGATAAATTAAAT GAACG	-3'
GB1-Yos9_115_for	5'-	GAGAATCTTTATTTTCAGGGCGCCGAACGGTGCATCTTCTACCAAGCC	-3'
GB1-Yos9_242_rev	5'-	CTCGAATTCGGATCCGGTACCTTATTCTAAATTGCACAATTCAGGTATGGTAAC TTG	-3'
GB1-Yos9_249_rev	5'-	CTCGAATTCGGATCCGGTACCTTAGTCTTCATTTTTGGCTAGTAATTCTAAATTGC	-3'
GB1-Yos9_262_rev	5'-	CTCGAATTCGGATCCGGTACCTTATGCGGGCATCCTGCAAAGTATAG	-3'
GB1-Yos9_32_for	5'-	GAGAATCTTTATTTTCAGGGCGCCTCGAATAAGTACCTCATATCTTACATCGATG	-3'

Sequencing primer

T7_Promoter	5'-	TAATACGACTCACTATAGGG	-3'
T7_Terminator	5'-	GCTAGTTATTGCTCAGCGG	-3'
pOPINS_forward	5'-	CGGAAGACCTGGATATGGAAGAC	-3'
pETG_forward	5'-	CTGGCAAGCCACGTTTGG	-3'

Synthetic genes and DNA fragments

hHR23A UBA2 (315-363)	codon optimized (*E. Coli*), with NcoI and BamHI restriction sites, ordered as fragment
Doa10 RING (2-112)	codon optimized (*E. Coli*), with NcoI and BamHI restriction sites, ordered as fragment
Hrd1 RING (337-406)	codon optimized (*E. Coli*), with NcoI and BamHI restriction sites, ordered as fragment
Cue1 (25-203), C147S	codon optimized (*E. Coli*), with NcoI and BamHI restriction sites, ordered as gene
Ubc7 (1-165)	codon optimized (*E. Coli*), with NcoI and BamHI restriction sites ordered as gene
gp78CUE (453-503)	codon optimized (*E. Coli*), with NcoI and BamHI restriction sites, ordered as fragment
Cue2CUE1 (6-54)	codon optimized (*E. Coli*), with NcoI and BamHI restriction sites, ordered as fragment
Cue1CUE (45-115)	codon optimized (*E. Coli*), with NcoI and BamHI restriction sites ordered as gene

3.9. Reagents and chemicals

All chemicals were purchased from either Carl Roth GmbH or Sigma-Aldrich (Merck). Some specific reagents used for fluorescent labeling, spin labeling, cross-linking or used as interaction partners are summarized in the following table.

Product	Manufacturer
Alexa Fluor! 488 C_5 Maleimide	ThermoFisher Scientific
(1-Oxyl-2,2,5,5-tetramethylpyrroline-3-methyl) methanethiosulfonate (MTS) spin label (MTSSL)	Santa Cruz Biotechnology
BM(PEG)2 (1,8-bismaleimido-diethyleneglycol)	ThermoFisher Scientific
2α-Mannobiose	Sigma-Aldrich (Merck)
3α,6α-Mannopentaose	Sigma-Aldrich (Merck)

3.10. Buffers and media

All buffers and solutions were prepared with MilliQ water. Media and stock solutions for bacterial cultivation were autoclaved if applicable or sterilized by filtration through 0.22 µM filters.

3.10.1. Buffers and media for bacterial cultivation

Medium, stock solution	composition
Ampicillin (1000 x)	100 mg/mL ampicillin (sodium salt) in 50% EtOH
Kanamycin (1000 x)	50 mg/mL kanamycin sulfate in H_2O
IPTG (isopropyl-β-D-1-thiogalactopyranoside)	1M, 11.91 g in 50 mL H_2O
LB medium	10 g/L tryptone. 5 g/L yeast extract, 10 g/L NaCl
TB medium	12 g/L tryptone, 24 g/L yeast extract, 4 mL glycerol, 12.54 g/L K_2HPO_4, 2.31 g KH_2PO_4
M9 medium	7.5 g/L Na_2HPO_4, 3 g/L KH_2PO_4, 0.5 g/L NaCl, 2 mM $MgSO_4$, 0.1 mM $CaCl_2$, 10 µM $FeSO_4$, 4 g/L glucose (2 g/L for ^{13}C-glucose), 1 g/L NH_4Cl or $^{15}NH_4Cl$, vitamin mix (1 x), trace elements mix (1 x), 100 µM $ZnCl_2$ (only if zinc binding proteins are expressed)
M9 medium (deuterated)	Analogous to H_2O based M9 medium with the following adaptations: All solutions were prepared in D_2O and 2g/L ^{2}H,^{13}C-glucose (or ^{2}H-glucose for ^{2}H, ^{15}N labeling) and 1.5 g/L $^{15}NH_4Cl$ were added. (Medium is sterile filtrated)
Vitamin mix (1000 x)	1 g/L D-biotin, 500 mg/L choline chloride, 500 mg/L folic acid, 1 g/L myoinositol, 500 mg/L nicotinamide, 500 mg/L pantothenic acid, 500 mg/L pyridoxal hydrochloride, 50 mg/L riboflavin, 500 mg/L thiamine hydrochloride, pH adjusted to 7.5
Trace Elements mix (100 x)	5g/L EDTA (dissolved and pH adjusted to 7.5) subsequently the following was added: 0.83 g/L $FeCl_3$ x $6H_2O$, 84 mg/L $ZnCl_2$, 13 mg/L $CuCl_2$ x $2H_2O$, 10 mg/L $CoCl_2$ x $6H_2O$, 10 mg/L H_3BO_3, 1.6 mg/L $MnCl_2$ x 6 H_2O.
SOC medium	20 g/L tryptone, 5 g/L yeast extract, 0.5 g/L NaCl, pH 7.0, 25 mM KCl, 10 mM $MgCl_2$, 20 mM glucose
LB agar plates	10 g/L tryptone. 5 g/L yeast extract, 10 g/L NaCl, 15 g/L agar

3.10.2. Buffers for agarose gels and SDS PAGE

Buffer, stock solution	composition
Agarose for electrophoresis	1.5 % agarose in 1x TAE buffer
TAE buffer (50 x)	2M Tris, 5.7 % (v/v) acetic acid, 50 mM EDTA, pH 8.0
Sample buffer (DNA) for agarose gel electrophoresis (6 x)	40 % (w/v) sucrose, 0.25 % (w/v) bromophenol blue, 0.25 % (w/v) xylene cyanol in H_2O
SDS loading buffer (5 x)	250 mM Tris-HCl. pH 6.8, 10 % (w/v) SDS, 30 % (v/v) glycerol, 5 % (v/v) β-mercaptoethanol, 0.02 % (w/v) bromophenol blue
Coomassie staining solution	40% (v/v) MeOH, 10% (v/v) acetic acid, 0.1 % (w/v) Coomassie Brilliant Blue G-250 or R-250 in H_2O
Coomassie destaining solution	40% (v/v) MeOH, 10% (v/v) acetic acid in H_2O
Tris-Glycine SDS PAGE buffer	25 mM Tris, pH 8.3, 192 mM glycine, 0.1 % (w/v) SDS

3.10.3. Buffers for protein purification and analysis

Buffers for lysis, Ni-NTA chromatography, GST affinity purification and refolding

Buffer	Composition
Lysis Buffer	50 mM Tris, 250 mM NaCl, pH 7.8, 5 % glycerol, 1x PIC (0.1 mM AEBSF, 0.3 µM Aprotinin, 1 µM Bestatin, 1 µM E-64, 0.1 mM Leupeptin, 1 µM Pepstatin A)
Ni-NTA Wash	50 mM Tris, 250 mM NaCl, pH 7.8, 1 % glycerol, 20 mM imidazole
Ni-NTA Elution	50 mM Tris, 250 mM NaCl, pH 7.8, 1 % glycerol, 400 mM imidazole
TEV/3C buffer	50 mM Tris, 250 mM NaCl, pH 7.8
Ni-NTA Wash + urea	50 mM Tris, 250 mM NaCl, pH 7.8, 1 % glycerol, 20 mM imidazole, 6 M urea
Ni-NTA Elution + urea	50 mM Tris, 250 mM NaCl, pH 7.8, 1 % glycerol, 400 mM imidazole, 6 M urea
GST Binding buffer	PBS, pH 7.5 (140 mM NaCl, 2.7 mM KCl, 12 mM phosphate)
GST Elution buffer	50 mM Tris, pH 8.0, 20 mM reduced glutathione (GSH)
Yos9 Refolding buffer	100 mM Tris, 150 mM NaCl, 1 mM $CaCl_2$, 0.5 M arginine, 5 mM GSH, 0.5 mM GSSG, pH 8.5
Yos9 Denaturing buffer	100 mM Tris, 150 mM NaCl, 7M urea, pH 8.5
Ubc7 Refolding buffer	50 mM Tris, 200 mM NaCl, pH 7.0, 50 mM arginine, 2mM TCEP

Buffers for ion exchange chromatography (IEX)

Buffer	composition
AEX A buffer	50 mM Tris, pH 8.5
AEX B buffer	50 mM Tris, ph 8.5, 1 M NaCl
CEX A buffer	50 mM ammonium acetate, pH 4.5
CEX B buffer	50 mM ammonium acetate, pH 4.5, 1 M NaCl

Buffers for size exclusion chromatography (SEC) and NMR/EPR spectroscopy

Buffer	composition
E1 buffer	20 mM Tris, pH 7.8, 100 mM NaCl, 7.5 mM β-mercaptoethanol
Ub SEC buffer	50 mM Tris, pH 8.0
Yos9 NMR buffer	25 mM HEPES/NaOH, 50 mM NaCl, pH 7.0, 0.03 % NaN_3, 0.15 mM DSS, PIC, 5 % D_2O
NMR buffer (Hrd1, Doa10, Ubc7, Ubc9)	25 mM HEPES/NaOH, 150 mM NaCl, pH 7.0, 2 mM TCEP, 0.03 % NaN_3, 0.15 mM DSS, PIC, 5 % D_2O
SEC Buffer 50	25 mM HEPES/NaOH, 50 mM NaCl, pH 7.0
SEC Buffer 150	25 mM HEPES/NaOH, 150 mM NaCl, pH 7.0
SPR buffer	10 mM HEPES (pH 7.4), 150 mM NaCl, 3 mM EDTA, 0.05 % Tween 20.
EPR buffer (deuterated)	12 mM phosphate, 140 mM NaCl, 2.7 mM KCl, 20 % d8-glycerol, pD = 7.2
Protease inhibitor cocktail (PIC) (100 x)	10 mM AEBSF, 30 µM Aprotinin, 100 µM Bestatin, 100 µM E-64, 1 mM Leupeptin, 100 µM Pepstatin A

3.11. Software

Software	Manufacturer
Adobe Illustrator CS6	Adobe Systems
Adobe Photoshop CS6	Adobe Systems
PyMOL v.1.8.6.0	Schrödinger, LLC
Office 365	Microsoft
OriginPro 9.1	OriginLab Corporation
UNICORN 5.11	GE Healthcare
CYANA 3.9	(Guntert and Buchner, 2015; Guntert et al., 1997)
SPARKY 3.13 (NMRFAM-SPARKY)	T. D. Goddard and D. G. Kneller, UCSF and (Lee et al., 2015)
TopSpin 4.0.1.	Bruker
EndNote X8.1	Clarivate Analytics

4. Methods

4.1. Microbiological methods

4.1.1. Primer design

Primers were designed by taking the following principles into account: GC content in the range of 40–60 %, annealing temperature higher than 62°C and at least a single G or C at the beginning of the primer sequence. Annealing temperatures (salt adjusted) were determined using the online tool Oligo Calc (http://biotools.nubic.northwestern.edu/OligoCalc.html). Reverse complement primer sequences were determined using the online tool rev_comp.html (https://www.bioinformatics.org/sms/rev_comp.html).

In case of primers for site-directed mutagenesis, the mismatches were placed in the central region of the primer.

To allow in frame cloning of inserts into pET39_Ub19 vector using NcoI and BamHI restriction sites the following sequence was added to the 5'-end of the forward primer: CCC CCATGG GC. The reverse primer required the addition of TAA GGATCC CCC to the 3'-end before calculating the reverse complement.

Primers for restriction-free (RF) cloning purposes contain both regions able to anneal with the target vector and regions annealing with a desired insert sequence encoded on another plasmid.

Forward primers for RF cloning into pET-MBP and pET-GB1 vectors were designed by adding a target vector sequence (GAGAATCTTTATTTTCAGGGCGCC) to the 5'-end of the primer with the sequence of the insert. Reverse primers for RF cloning were created by calculating the reverse complement of the insert sequence followed by the stop codon TAA and a sequence of the target vector (GGTACCGGATCCGAATTCGAG).

Lyophilized primers were obtained from Eurofins Genomics and diluted to a concentration of 100 µM with H_2O. Primers were further diluted to 10 µM for usage in polymerase chain reactions (PCR).

4.1.2. Restriction-based cloning

Vector preparation

2.5 µg pET39_Ub19 plasmid was digested in a reaction volume of 50 µL containing 20 units NcoI-HF® and 20 units BamHI-HF® and 1 x CutSmart® buffer (NEB) for 4 h at 37°C. After addition of sample buffer, the reaction was loaded on a 1.5 % TAE-agarose gel and separated in the electric field (120 V) for 0.5–1.0 h. DNA was extracted from the gel using the QIAquick Gel Extraction Kit. The purified, linearized vector was dephosphorylated using Antarctic Phosphatase for 1 h at 37°C. Phosphatase was heat inactivated at 80°C for 2 min.

PCR and insert preparation

Polymerase chain reactions (PCR) were performed to amplify the inserts. A 100 µL reaction contained 20 µL of 5 x Phusion GC buffer (NEB), 2 µL dNTP's (10 mM stock), 4 µL of forward and reverse primers (10 µM stocks), 50 ng template DNA, 3 % DMSO and 0,5 µL (1U) Phusion® HF polymerase. The PCR reaction was carried out on a PCR Gradient cycler peqSTAR. The cycling conditions covered the following steps: 60 s at 98°C (initialization), 35 repetitions of denaturation, annealing and elongation (30 s at 98°C, 30 s at 58°C, 30 s per kb of expected product at 72°C) followed by a final elongation step of 240 s at 72°C. PCR products were purified using the QIAquick PCR Purification Kit.
5 µL of 10 x CutSmart® buffer was added to 40 µL of purified PCR products and subsequently digested using 20 units NcoI-HF® and 20 units BamHI-HF® for 4h at 37°C. After incubation, reactions were loaded on a 1.5 % TAE-agarose gel and separated in the electric field (120 V) for 0.5–1.0 h. DNA was extracted as described above.

Ligation

Ligation reactions were performed using T4 DNA ligase in a reaction volume of 20 µL. 40 ng of vector DNA were incubated with a five-fold molar excess of insert and 1 µL (400 U) T4 DNA ligase in 1x T4 DNA Ligase reaction buffer (NEB). The reactions were incubated at 16°C overnight before transformation into *E. Coli*.

Transformation

Transformation of chemically competent *E. coli* cells (DH5α or T7 Express Competent *E. coli*) was achieved using a heat shock protocol. 5 µL of a ligation or site-directed mutagenesis reaction was added to 50 µL of cells and incubated on ice for 30 min. Subsequently the cells were incubated for 40 s at 42°C, placed back on ice and 450 µL of SOC medium was added. After an additional 1 h of incubation at 37°C, the cells were spread on LB agar plates supplemented with kanamycin or ampicillin and incubated at 37°C overnight.

Isolation of plasmid DNA and concentration determination

5 mL of LB medium containing the appropriate antibiotic for selection were inoculated with a single colony of bacteria. The cultures were incubated at 37°C under shaking overnight to reach saturation. Plasmid DNA was isolated using the QIAprep Spin Miniprep Kit according to the provided protocol except for the elution. The DNA was eluted in 40 µL using MilliQ H_2O. DNA concentration was determined from the absorption at 260 nm using the NanoDrop 1000 UV-/Vis Spectrophotometer. The purity of the preparation can be assessed by the ratio of absorption at 260 and 280 nm.

Sequencing

Every generated plasmid in this work was sequenced to confirm the sequence of all constructs and preclude undesired mutations. Sequencing reactions contained 12 µL of plasmid DNA (400–1200 ng) and 3 µL of a sequencing primer (10 µM). Sequencing was performed by Microsynth AG overnight and plasmids were stored at -20°C until usage.

4.1.3. Restriction-free (RF) cloning and site-directed mutagenesis

RF cloning is a universally applicable method for inserting a DNA fragment into any location independent of the usage of restriction enzymes (van den Ent and Lowe, 2006).

First PCR for RF cloning

The first PCR for RF cloning resembles the PCR protocol described in section 4.1.2. and amplifies the sequence of the insert. The main difference is that the primers contain overhangs that are complementary to the target vector. The insert is purified as described above.

Second PCR for RF cloning and site-directed mutagenesis

The second PCR involves linear amplification using the product of the first PCR as primers for the target vector as template. This PCR is carried out in a volume of 25 µL containing 2.5 µL 10 x PfuUltra buffer, 1 µL dNTP's (10 mM stock), PCR product (30-60-fold molar excess relative to the template plasmid), 30 ng template DNA and 0,5 µL (1.25 U) PfuUltra polymerase. The result is a plasmid containing the new insert.

In case of site-directed mutagenesis reactions the primers contain the desired mutations. The reactions contained 15.5 µL H_2O, 2.5 µL 10 x PfuUltra buffer, 1 µL dNTP's (10 mM stock), 1 µL of forward and reverse primers (10 µM stocks), 30 ng template DNA and 0,5 µL (1.25 U) PfuUltra polymerase.

The cycling conditions for these linear amplification PCRs covered the following steps: 120 s at 95°C (initialization), 25 cycles of denaturation, annealing and elongation (30 s at 95°C, 30 s at 58°C, 120 s per kb at 68°C) followed by a final elongation step of 300 s at 68°C. Subsequently, 1 µL (20 U) DpnI was added to each reaction mixture and incubated at 37°C for 1h in order to digest the parental, methylated template plasmid. 5 µL of each reaction was transformed into DH5α *E. coli* cells and processed as described above.

4.2. Protein expression and analysis

4.2.1. Preparative protein expression

Transformation procedure for protein expressions and precultures

For preparative protein expressions only freshly transformed cells were used. Up to 100 ng of sequenced plasmid DNA was added to 50 µL of T7 Express Competent *E. coli* cells and incubated on ice for 15 min, followed by a heat shock for 40s at 42°C. 450 µL of SOC medium (without antibiotic selection) was added and incubated for 45 min at 37°C before plating on LB agar plates containing the appropriate antibiotic. Several bacterial colonies were picked from the plates and used to inoculate LB, TB or M9 precultures. Different media were prepared according to section 3.10.1. of this thesis. Usually 25 mL of preculture was prepared per liter of the final, total culture size. The cultures were grown overnight at 37°C.

Protein expression in LB, TB and M9 medium

The final cultures (1L medium in 2L flasks) were inoculated with 20 mL of preculture and incubated at 37°C until an optical density (measured at 600 nm) of 0.6–1.0 was reached. Subsequently, the cultures were cooled to their respective induction temperature (15–24°C) and induced with isopropyl-β-D-1-thiogalactopyranoside (IPTG) (0.2–0.5 mM) for approximately 20 h. Ubiquitin and all its variants were expressed at 37°C and induced for 4h with 1 mM IPTG. After expression, the cells were centrifuged at 4500–6000 rpm for 20 min at 4° and the cell pellets resuspended in lysis buffer containing a protease inhibitor cocktail.

Table 2 summarizes the expression conditions for the most important protein constructs expressed in this work. Table 6 in the appendix gives an overview of all successfully expressed protein constructs.

Isotopic labeling was achieved using M9 medium where isotopically enriched ^{15}N-ammonium chloride and ^{13}C-glucose represent the sole nitrogen and carbon sources, respectively.

Deuteration was required for NMR studies on the single chain construct comprising full length Ubc7 and the Ubc7 activating region of Cue1 (147-203, U7BR), called Ubc7-U7BR. H_2O-based M9 precultures were used to inoculate D_2O based precultures. These precultures were grown until an optical density of 1.0 was reached and used to inoculate the main cultures. Otherwise the cultures were processed as described above.

Table 2: Summary of expression conditions of expressed proteins

proteins	induction conditions	isotopic labeling
Cdc34, Ubc13, Uev1a	16°C, 0.5 mM IPTG, 20 h (Bagola et al., 2013)	unlabeled
Cue1 constructs	18°C, 0.2 mM IPTG, 20 h	unlabeled; ^{13}C,^{15}N
Doa10 RING constructs and Hrd1 (325-412)	24°C, 0.5 mM IPTG and 100 µM $ZnCl_2$	unlabeled; ^{13}C,^{15}N
DUBs (OTUB1, OTUD7B)	20°C, 1 mM IPTG, 20 h (Mevissen et al., 2013)	unlabeled
E1 (Ube1)	16°C, 0.2 mM IPTG, 20 h	unlabeled
Hrd1 RING constructs (except for 325-412)	15°C, 0.5 mM IPTG and 100 µM $ZnCl_2$	unlabeled; ^{13}C,^{15}N; ^{15}N
SUMO2 variants	16°C, 0.5 mM IPTG, 20 h	unlabeled
Ubc7-U7BR (and variants)	24°C, 0.5 mM IPTG, 20 h	unlabeled; ^{13}C,^{15}N; ^{2}H,^{15}N; ^{2}H,^{13}C,^{15}N
Ubc9	18°C, 0.2 mM IPTG, 20 h	unlabeled; ^{15}N
UBDs (Cue2, UBA2, gp78CUE, Rpn13)	18°C, 0.5 mM IPTG, 20 h	unlabeled
Ube2SΔC	18°C, 0.5 mM IPTG, 20 h	unlabeled
Ubiquitin (and variants)	37°C, 1 mM IPTG, 4 h	unlabeled; ^{15}N
Yos9 MRH constructs	24°C, 0.5 mM IPTG, 20 h	unlabeled; ^{13}C,^{15}N

4.3. Protein purification

4.3.1. Cell lysis of *E. coli*

The thawed bacterial cell suspension was cooled in ice water and sonicated to lyse the cells. For volumes of up to 40 mL four cycles of 45 seconds duration (with 1 pulse per second) were used. For volumes of up to 200 mL four cycles of 2.5 min were used with longer pauses in between for cooling. Efficiency of cell lysis can be increased by using lysozyme and DNAseI. Cell debris and aggregated proteins in form of inclusion bodies were separated from the lysate by centrifugation at 17.000 rpm for 30 min at 4°C. In case the protein was expected to express in a soluble form the clarified lysate was decanted and the pellet discarded.

4.3.2. Solubilization of inclusion bodies

For Yos9 constructs the obtained clarified cell lysate was discarded and the pellet solubilized in Ni-NTA Wash + urea buffer containing 6M urea. 20 mM β-mercaptoethanol was added and the solution centrifuged again at 17.000 rpm for 30 min to separate solubilized Yos9 protein from cell debris.

4.3.3. Ni-NTA chromatography

Immobilized metal affinity chromatography, also called Ni-NTA chromatography, was generally used for purification of recombinant polyhistidine tagged (His10 or His6) tagged proteins. This method was also employed for purification of ubiquitin tagged (Ub19-tag, containing an internal His10 tag, (Rogov et al., 2012)), His6-GST (glutathione S-transferase), His6-GB1 (B1 domain of protein G) and His6-MBP (maltose binding protein) tagged proteins. The clarified cell lysate containing the desired protein was loaded on one or multiple equilibrated HisTrap FF (5 mL) columns using syringes or a

peristaltic pump. Subsequently, the columns were connected to an ÄKTA FPLC system and washed with 5–15 column volumes Ni-NTA Wash buffer containing 20 mM imidazole. His-tagged proteins were eluted using a one-step gradient with Ni-NTA Elution Buffer (400 mM imidazole). The elution was monitored by measuring the absorption at 280 nm. Peak fractions were collected and pooled. Ni-NTA purification under denaturing conditions (performed for Yos9 constructs) required the use of 6M urea in all Ni-NTA buffers. Purification of deuterated Ubc7-U7BR was also performed under denaturing conditions in order to ensure complete exchange of backbone amide hydrogens.

4.3.4. GST affinity purification

GST-fusion proteins were purified using columns with immobilized glutathione (GSH). The clarified lysate was loaded on a GSTrap FF (5 mL) column preequilibrated with GST Binding buffer, washed with 5–10 column volumes of GST Binding buffer and eluted using GST Elution Buffer containing 20 mM GSH.

4.3.5. Dialysis and buffer exchange

Ni-NTA purified proteins were either dialyzed against TEV/3C Buffer (no imidazole) using Spectra/Por® RC dialysis membranes with the appropriate molecular weight cut off (MWCO) or by multiple cycles of concentrating and diluting using Amicon Ultra-15 centrifugal filter units. This procedure ensures that a second Ni-NTA chromatography purification step can be directly performed after tag cleavage.

4.3.6. *In vitro* protein refolding

Refolding by rapid dilution (performed for Ubc7-U7BR)

Ni-NTA purified ^{2}H, ^{13}C, ^{15}N and ^{2}H, ^{15}N labeled Ub19(His10)-Ubc7-U7BR fusion proteins were concentrated to 2 mL in buffer containing 6M urea. The solution was pipetted drop by drop under continuous mixing into 50 mL of buffer containing 50 mM Tris (pH 7.0), 200 mM NaCl, 50 mM arginine and 2mM TCEP. Here, rapid dilution of urea (final concentration of 240 mM) prevents the proteins from forming aggregates.

Refolding by dialysis (performed for Yos9 MRH)

Ni-NTA purified His6-GB1-Yos9 MRH fusion proteins were diluted to 0.5 mg/mL using buffer containing 100 mM Tris (pH 8.5), 150 mM NaCl, 7 M urea. The protein solutions were transferred into Spectra/Por® RC dialysis membranes (MWCO 6-8 kDa) and dialyzed against Yos9 Refolding buffer (25-fold higher volume) at 4°C overnight. In order to enable correct formation of all three disulfide bonds in Yos9 this buffer contained a redox system (5 mM reduced glutathione and 0.5 mM oxidized

glutathione) and a relatively high pH of 8.5 that favors the formation of cystines. Successful refolding was checked by analytical size exclusion (section 4.3.11.) chromatography.

4.3.7. Cleavage of the purification tag

The purification tags (His6-GB1, His6-GST, Ub19(His10), His6 or His10) were removed from purified proteins containing tobacco etch virus (TEV) or human rhinovirus (HRV) 3C protease cleavage sites. The cleavage reaction was performed in TEV/3C buffer at 16°C overnight using either a His6-tagged version of TEV protease, His6-tagged 3C protease or a GST-tagged version of 3C protease depending on the removed purification tag and cleavage site. Usually 20 µg of TEV/3C protease was used per mg of substrate protein.

4.3.8. Tag removal by "reversed" affinity chromatography

After successful protease cleavage, the purification tag as well as the protease were removed by a "reversed" affinity chromatography step. It was performed as described in section 4.3.3. Briefly, the protein solution was applied onto the column using a syringe or peristaltic pump, washed with 5 column volumes of Ni-NTA Wash buffer and the flow through collected. The target protein is not able to bind to the Ni-NTA resin, whereas non-cleaved fusion proteins, the tagged protease and the cleaved purification tags bind. Consequently, the target protein is found in the flow through, which is subsequently concentrated to less than 4 mL.

4.3.9. Purification of non-tagged ubiquitin

Purification of non-tagged human ubiquitin was achieved by taking advantage of the solubility and stability of ubiquitin at low pH by addition of perchloric acid (Raasi and Pickart, 2005). The clarified lysate containing ubiquitin was slowly titrated with perchloric acid (70%) up to a final concentration of 0.7% while stirring on ice. Precipitated proteins were removed by centrifugation (17.000 rpm, 20 min) and the pH of the supernatant adjusted with NaOH to pH 7. Subsequently, the buffer was exchanged to 50 mM ammonium acetate pH 4.5 and a cation exchange chromatography step performed (4.3.10.) followed by size exclusion chromatography (4.3.12.).

4.3.10. Cation and anion exchange chromatography

A HisTrap SP HP column was used for the purification of non-tagged ubiquitin and its variants by cation exchange chromatography. The column was equilibrated with cation exchange (CEX) buffer A (50 mM ammonium acetate, pH 4.5) and the protein solutions applied using a syringe. The column was connected to an ÄKTA FPLC system, washed with two column volumes buffer A, followed by a

gradient protocol (over 18 column volumes) with a target concentration of 50% buffer B (50 mM ammonium acetate, pH 4.5, 1 M NaCl). Peak fractions were collected and pooled.
The purification of wild type K48-linked ubiquitin chains also involved cation exchange chromatography. The procedure is described in more detail in section 4.4.3.

Anion exchange chromatography was used in some cases (e.g. Ubc7-U7BR) as an additional purification step after protease cleavage. Protein solutions containing less than 20 mM salt were loaded on a HisTrap Q HP column, washed with two column volumes of anion exchange (AEX) buffer A and proteins eluted using a salt gradient with a target concentration of 0.5 M NaCl. Protein containing fractions were concentrated to a volume of less than 4 mL for the final size exclusion chromatography purification.

4.3.11. Analytical size exclusion chromatography (SEC)

Analytical size exclusion chromatography was used to prove the integrity of protein samples, inspect *in vitro* refolding efficiency, or to determine and compare experimental molecular weights and protein sizes. A Superdex 75 10/300 GL column was calibrated using the Gel Filtration LMW Calibration Kit. Molecular weight determination is carried out by plotting an elution volume parameter (e.g. the gel phase distribution coefficient) of a series of standard globular proteins against the log of their molecular weight in Dalton (Andrews, 1970). The data is fitted using linear regression and the obtained relationship used to calculate apparent molecular weights using the experimentally determined elution volumes of proteins of interest.

4.3.12. Preparative size exclusion chromatography (SEC)

Size exclusion chromatography, also called gel filtration, is the final purification step and additionally served as a quality assessment for sample homogeneity. Depending on the size of the protein of interest and sample amount an appropriate column was selected. A HiLoad 16/600 Superdex 75 pg column was usually used, except for the purification of human Ube1 (E1 enyzme) where a HiLoad 16/600 Superdex 200 pg was used. In addition, ubiquitin and its variants were loaded on a HiLoad 26/600 Superdex 75 pg to have an increased loading capacity. In each case the column was equilibrated with the appropriate buffer, that can be found in the Materials chapter of this thesis.
Since the resolution of a column is dependent on flow rate, sample volume and viscosity, the actual running parameters depend on the specific application. Usually a flow rate of 1.0-1.5 mL/min for the 16/600 and 2.5 mL/min for the 26/600 column was used. In cases were separation of two or more components was required, such as ubiquitin chains of different sizes, the flow rate was lowered to 0.3 mL/min for the 16/600 column for increased resolution.

4.3.13. SDS PAGE and Coomassie Brilliant Blue staining

Purified proteins were analyzed by sodium dodecylsulfate-polyacrylamide gel electrophoreses (SDS-PAGE) (Laemmli, 1970) using the Mini-Protean Tetra Cell gel electrophoresis system. Protein solutions were mixed with SDS loading buffer (5 x) and in case the protein concentration was known further diluted with H_2O to reach a protein concentration of approximately 0.5 µg/µL in the final sample. The samples were incubated at 95°C for 5 min and 1–4 µg of protein loaded on 4–20% Mini-PROTEAN® TGX™ Precast Protein Gels (15-well, 15 µl). The gel electrophoresis system was filled with Tris-Glycine SDS PAGE buffer and a voltage of 300 V applied for 20 min.
For the analysis of ubiquitination reactions, purified ubiquitin and ubiquitin conjugates heating of the samples was omitted to reduce gel artifacts as previously described by Dong et al. (2011).
The gels were stained with a Coomassie staining solution (containing 0.1 % Coomassie Brilliant Blue G/R-250) for at least 30 min, followed by gel destaining using Coomassie destaining solution.

4.3.14. Concentrating of protein containing solutions and determination of protein concentrations

Protein solutions were concentrated using Amicon Ultra centrifugal filter units. Samples were centrifuged at 3200 g and 4°C in a swing-bucket rotor (A-4-62) until the target volume was reached. Notably, N-term. His-Ub had to be concentrated at room temperature to prevent precipitation in the cold and thus clogging of the membrane of the centrifugal filters.
Protein concentrations were determined by measuring the absorption at 280 nm using the NanoDrop 1000 UV-/Vis Spectrophotometer. Proteins containing tyrosine and tryptophan residues significantly absorb UV light at a wavelength of 280 nm. The molar extinction coefficient is calculated by summing up the individual contributions for each tryptophan (5500 M^{-1} cm^{-1}), tyrosine (1490 M^{-1} cm^{-1} and formed cystine (125 M^{-1} cm^{-1}) within the protein of interest (Gill and von Hippel, 1989).

4.4. Biochemical methods involving ubiquitination reactions

4.4.1. Synthesis of proximally capped diubiquitins

Synthesis of ubiquitin chains was generally carried out using proximally blocked monoubiquitins (Ub) to allow the synthesis of distinct cysteine carrying ubiquitin chains as well as proximally or distally ^{15}N- labeled diubiquitin. The proximal ubiquitin carried a hexahistidine (His6) tag at its C-terminus (von Delbruck et al., 2016) thereby preventing charging onto E2 enzymes. In this way Ub 6His can only function as an acceptor in ubiquitination reactions, while a non-capped ubiquitin can function both as an acceptor and donor ubiquitin. Some reactions contained a mutant ubiquitin carrying an appropriate K to R mutation in order to prevent functioning as acceptor ubiquitin (Raasi

and Pickart, 2005). This further drove the reaction to the desired diubiquitin product since it left only a single option to react.

Linkage specificity was ensured by using different E2 enzymes as shown in Figure 5. Cdc34 was used to generate K48-linkages, K63-linked chains were produced by using a Ubc13/Uev1a heterodimer and K11 linkages were introduced using Ube2SΔC (Dong et al., 2011). To avoid potential contaminating K63 linkages (Bremm et al., 2010) generated by Ube2SΔC during K11 chain synthesis all cysteine containing ubiquitin variants additionally contained a K63R mutation.

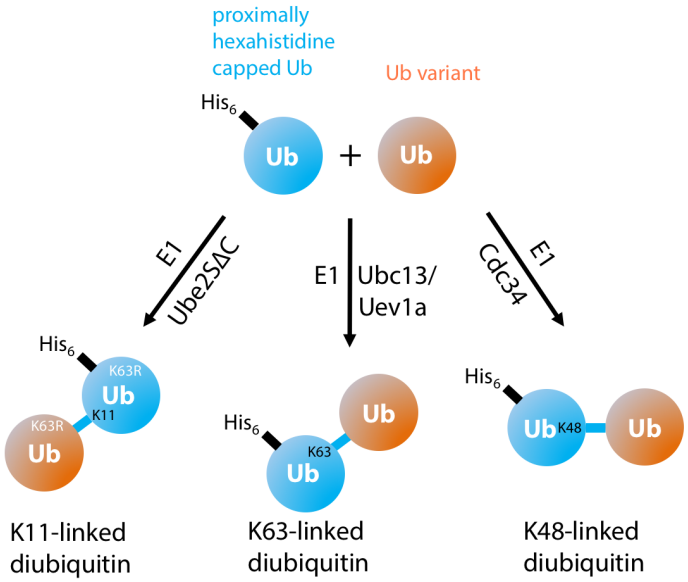

Figure 5. Synthesis strategies for K11, K48 and K63-linked diubiquitin. A proximally hexahistidine capped ubiquitin is mixed with another ubiquitin variant and incubated with E1 and E2 enzymes to generate diubiquitin.

Distinct diubiquitins were synthesized by incubating 750 µM Ub 6His (variant 1) and 750 µM Ub (variant 2) with 0.5 µM E1 (Ube1) and either 3 µM Ubc13/Uev1a, 5 µM Cdc34 or 10 µM Ube2SΔC at 37°C overnight. All preparative ubiquitination reactions were performed in Ub reaction buffer containing 50 mM Tris (pH 8.0), 0.9 mM DTT, 10 mM $MgCl_2$ and 20 mM ATP. The reaction mixture was diluted 10-fold with Ni-NTA Wash buffer and the His6-tagged ubiquitin chains purified by Ni-NTA chromatography (4.3.3.) using HisTrap HP columns. His6-tagged products were further separated and purified by size exclusion chromatography (4.3.12.).

4.4.2. Synthesis of proximally capped tri- and tetraubiquitins

The assembly of distinct K48-linked tri- and tetraubiquitin for pulsed electron-electron double resonance (PELDOR) experiments was performed using an iterative synthesis scheme as depicted in Figure 6. After diubiquitin assembly and purification of the desired His6-tagged product by Ni-NTA purification and gel filtration, this diubiquitin was further incubated with another ubiquitin variant and enzymes. The triubiquitin product was either purified or purified and reemployed in another

reaction using a fourth ubiquitin variant to generate tetraubiquitin. A ubiquitin variant containing a K48R mutation was used in the final elongation round to increase the yield of this single step reaction.

Diubiquitin elongations were performed using 300 µM preassembled His6-tagged diubiquitin and 800 µM monoubiquitin or using only a slight excess in case of K48R containing monoubiquitin. 100 µM triubiquitin was elongated to tetraubiquitin using 150 µM monoubiquitin (K48R).

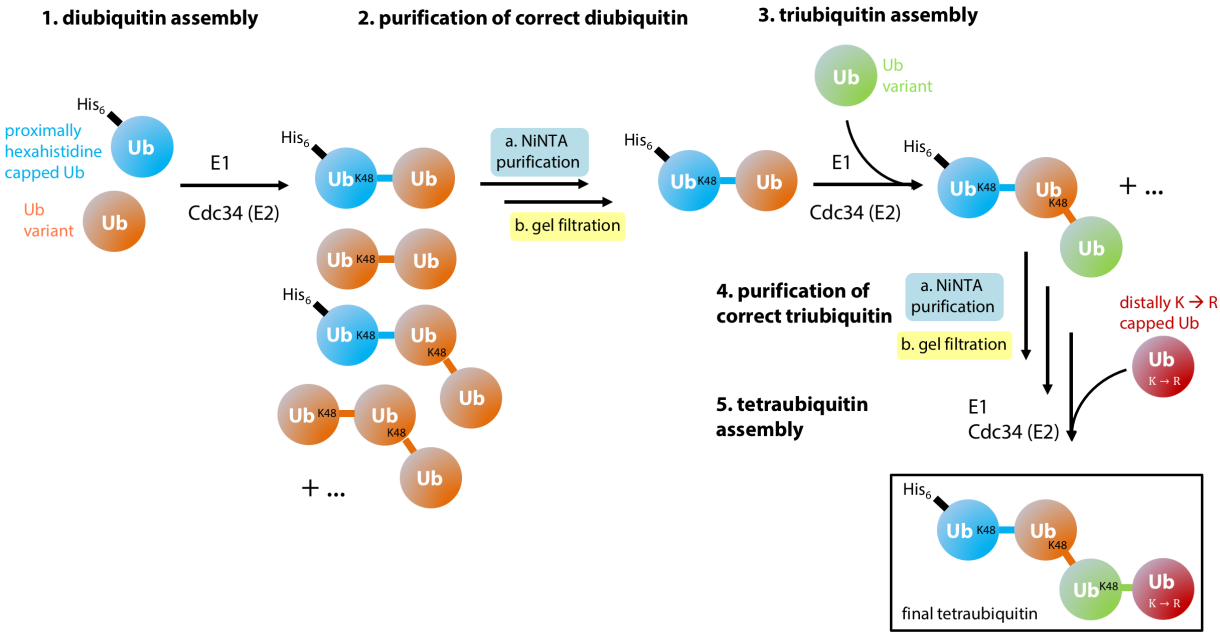

Figure 6. Iterative chain synthesis strategy for the assembly of a distinct K48-linked tetraubiquitin chain. Distinct tri- or tetraubiquitin chains can be assembled using multiple consecutive steps of purification and elongation by a single ubiquitin.

4.4.3. Synthesis and purification of wild type ubiquitin chains

Wild type K48-linked ubiquitin chains for analytical size exclusion experiments were assembled in a 20 mL reaction using 1 µM E1, 10 µM Cdc34, 1500 µM wild type human ubiquitin in buffer containing 50 mM Tris (pH 7.8), 20 mM ATP, 0.9 mM DTT, 9 mM $MgCl_2$ at 37°C overnight (Kniss et al., 2018). The reaction mixture was diluted with CEX buffer A (pH 4.5), precipitated enzymes removed by filtering through a 0.22 µM syringe filter and the protein solution applied onto a 1 mL MonoS 5/50 GL column. Ubiquitin chains were separated in a length dependent manner using a salt gradient protocol over 45 column volumes and a target concentration of 0.5 M NaCl. To obtain pure K48-linked ubiquitin chains of defined length up to K48-linked hexaubiquitin, peak fractions were subjected to multiple size exclusion chromatography runs at low flow rates of 0.3 mL/min on a HiLoad 16/600 Superdex 75 pg column.

4.4.4. Stable charging of E2 enzymes

A stable Ubc7-ubiquitin conjugate was formed enzymatically to study the interaction of an active site linked ubiquitin with its E2 enzyme. Formation of an isopeptide bond linkage between an introduced lysine residue (at the active site) and the C-terminal glycine of ubiquitin to mimic the thioester linked ubiquitin conjugate was first described by Plechanovova et al. (2012).
Purified unlabeled or ^{15}N-labeled Ubc7-U7BR C89K (100 µM) was incubated with 100 µM N-term. His Ub (either ^{15}N-labeled or unlabeled) and E1 (0.5 µM) at 37°C overnight in buffer containing 3 mM ATP, 5 mM $MgCl_2$, 50 mM Tris (pH 10.0), 150 mM NaCl and 1 mM TCEP. The reaction conditions were adapted from Plechanovova et al. (2012) with slight variations. Purification of the E2-Ub conjugate was achieved by Ni-NTA chromatography (4.3.3.), His-tag removal by TEV protease cleavage (4.3.7.), reversed Ni-NTA chromatography (4.3.8) and SEC (4.3.12.) as described earlier.

4.4.5. Fluorescence based analysis of *in vitro* ubiquitin chain elongation

Analysis of ubiquitin chain elongation kinetics was performed using time course experiments. Reactions usually contained 1 µM Alexa Fluor 488 labeled Ub, 10 µM preassembled ubiquitin chains, 0.1–0.2 µM E1, 0.3–2 µM Ubc7 or Ubc7-U7BR and 0.3–3 µM Cue1 (25-203) depending on the specific reaction requirements and experimental design. The reactions were carried out in triplicates at 30°C in 50 mM Tris (pH 7.5), 2.5 mM $MgCl_2$, 4 mM ATP and 0.5 mM DTT.
Optionally Hrd1 or Doa10 RING domain constructs were present at a concentration of 0.5–5.0 µM. For comparing elongation kinetics in presence of ubiquitin binding domains (UBDs), various UBDs were included in the reaction mixture at a concentration of 20 µM (for diubiquitin) and 40 µM (for tetraubiquitin) elongations (Kniss et al., 2018).
In a special set of experiments described in von Delbruck et al. (2016) Cue1 25-203 was crosslinked using BM(PEG)2 (1,8-bismaleimido-diethyleneglycol) as a cysteine reactive cross linker. Reactions included 0.15 µM E1, 2 µM Ubc7, 1.2 µM Cue1 (25-203; T66C, C147S) crosslinked to Ub T9C as the proximal or distal moiety of diubiquitin.
All reactions were stopped at different time points by adding SDS sample buffer, products analyzed by SDS PAGE and fluorescence scanning using the emission filter LBP (510LP) after excitation at 473 nm.
All fluorescence-based ubiquitination assays were performed in the lab of Thomas Sommer (Max-Delbrück-Centrum, Berlin). Maximilian von Delbrück performed ubiquitination assays for the von Delbrück et al. publication, Lukas and I performed ubiquitination assays for the Kniss et al. publication and for the Ubc7 project.

4.5. Protein Nuclear Magnetic Resonance (NMR) spectroscopy

NMR spectra were acquired on Bruker Avance spectrometers operating at proton frequencies ranging from 500 MHz to 950 MHz equipped with 5-mm triple-resonance cryogenic z-axis gradient probes.

4.5.1. Experimental conditions and NMR sample preparation

Uniformly [^{2}H,^{13}C,^{15}N], [^{2}H,^{15}N], [^{13}C,^{15}N], [^{15}N]-labeled protein samples were measured at concentrations between 0.1 and 1.2 mM in a total volume of 300-400 µL in a standard Shigemi tube (for samples with 50 mM NaCl) or in salt tolerant NMR tubes (for samples with 150 mM NaCl). 4, 4-dimethyl-4-silapentane-1-sulphonate (DSS) was used as a NMR standard for chemical shift referencing. Exact experimental conditions for double and triple labeled NMR samples used for backbone assignments and or complete structure determinations are given in Table 3.

Table 3: Summary of experimental conditions for double or triple labeled NMR samples

protein	buffer	temp.
^{2}H,^{13}C,^{15}N Ubc7-U7BR (0.8 mM)	25 mM HEPES/NaOH, 150 mM NaCl, pH 7.0, 2 mM TCEP, 0.03 % NaN_3, 0.15 mM DSS, 1 x PIC, 5 % D_2O	303 K
^{13}C,^{15}N Yos9 (90-249) (0.6 – 1.2 mM)	25 mM HEPES/NaOH, 50 mM NaCl, pH 7.0, 0.03 % NaN_3, 0.15 mM DSS, 1 x PIC, 5 % D_2O	303 K
^{13}C,^{15}N Yos9 (90-249) (0.55 – 1.0 mM) bound to 3α, 6α-Mannopentaose (Man5)	25 mM HEPES/NaOH, 50 mM NaCl, pH 7.0, 0.03 % NaN_3, 0.15 mM DSS, 1 x PIC, 5 % D_2O, 8.25 – 15 mM Man5	303 K
^{13}C,^{15}N Hrd1 (337-412) (0.55 – 0.8 mM)	25 mM HEPES/NaOH, 150 mM NaCl, pH 7.0, 2 mM TCEP, 0.03 % NaN_3, 0.15 mM DSS, 1 x PIC, 5 % D_2O	303 K
^{13}C,^{15}N Doa10 (19-101) (1.0 mM)	25 mM HEPES/NaOH, 150 mM NaCl, pH 7.0, 2 mM TCEP, 0.03 % NaN_3, 0.15 mM DSS, 1 x PIC, 5 % D_2O	303 K

Spectra were processed using the TopSpin software provided by Bruker and analyzed using SPARKY 3.13 software or NMRFAM-SPARKY (Lee et al., 2015).
Screening of appropriate protein constructs and NMR conditions was performed by measuring ^{15}N-HSQC spectra in buffers of different pH (6.0 – 7.0) and NaCl (0 – 150 mM) concentration.

4.5.2. Assignment of backbone and side chain resonances

3D NMR spectra for assignment purposes were recorded by Frank Löhr from the group of Volker Dötsch (Goethe-University Frankfurt). Backbone resonance assignments for Hrd1 RING, Doa10 RING, Ubc7-U7BR and Yos9 MRH were obtained using standard TROSY-based HNCACB, HN(CO)CACB, HN(CA)CO and HNCO experiments (Salzmann et al., 1998, 1999). Backbone resonance assignment for human Ubc9 was adopted from (Liu et al., 1999).
Aliphatic side chain resonances (for Hrd1 RING and Yos9 MRH) were assigned using [^{15}N, ^{1}H]-TROSY-based versions of H(CCCO)NH-TOCSY (Montelione et al., 1992) and (H)C(CCO)NH-TOCSY (Grzesiek et al., 1993) and HCCH-TOCSY experiments (Bax et al., 1990). Assignments for aromatic side chain

resonances were obtained by a standard set of aromatic NMR experiments (Lohr et al., 2007; Yamazaki et al., 1993). Assignments were completed using 3D NOESY-HSQC experiments (Marion et al., 2002). All shifts were manually assigned with the help of the program NMRFAM-SPARKY.

4.5.3. NMR structure calculation

3D ^{15}N-edited NOESY-HSQC and 3D ^{13}C-edited NOESY-HSQC spectra on the aliphatic and aromatic regions, respectively, were recorded with a mixing time of 70 ms by Frank Löhr. Peaks were manually picked and the obtained peak lists used as input in structure calculations. The calculations using the program CYANA 3.9. (Guntert and Buchner, 2015; Guntert et al., 1997) were performed by Sina Kazemi from the group of Prof. Dr. Güntert (Goethe-University Frankfurt). CYANA automatically assigns NOESY peak and generates restraints based on the provided chemical shift lists for calculation of structures. In addition to these distance restraints, dihedral angle restraints obtained by TALOS+ software (Shen et al., 2009) (Torsion angle Likeliness Obtained from Shift and Sequence Similiarity) were used in calculations. The 20 best structures according to their CYANA target function from the final cycle were selected for representation. Tetrahedral coordination of zinc ions in the Hrd1 RING domain was achieved by generating additional restraints for zinc coordination. Energy refinement was carried out using OPALp (Koradi et al., 2000) and was based on the AMBER 94 force field (Ponder and Case, 2003). Structures were deposited in the Protein Data Bank (PDB) under the accession codes 6F98 (Hrd1 RING), 6F99 (Yos9 MRH) and 6F9A (Yos9 MRH complex with 3α, 6α-Mannopentaose). Structural statistics can be found in the appendix Tables 7, 8 and 9.

4.5.4. NMR titration experiments

NMR titration experiments enable both mapping of interaction surfaces (Zuiderweg, 2002) and determination of dissociation constants (Fielding, 2003). Various biomolecular interactions between a labeled and another unlabeled binding partner were investigated in this work. Table 4 gives an overview of performed titration experiments.

Table 4: Summary of NMR titration experiments

labeled protein	unlabeled protein (conc. range)	temp.
^{2}H,^{15}N Ubc7-U7BR (0.2 mM)	Hrd1 (325-412) (0–1.6 mM)	303 K
^{2}H,^{15}N Ubc7-U7BR (0.2 mM)	Doa10 (19-101) (0–4.0 mM)	303 K
^{15}N-proximal K48-linked diubiquitin (0.2 mM)	Cue1 (45-115) (0–1.6 mM)	298 K
^{15}N-distal K48-linked diubiquitin (0.2 mM)	Cue1 (45-115) (0–1.6 mM)	298 K
^{15}N-Cue1 (25-203) (0.2 mM)	Ubiquitin (0–1.6 mM)	298 K
^{13}C,^{15}N Hrd1 (337-412) (0.1 mM)	Ubc7-U7BR (0–0.8 mM)	303 K
^{13}C,^{15}N Doa10 (19-101) (0.1 mM)	Ubc7-U7BR (0–2.0 mM)	303 K
^{13}C,^{15}N Yos9 (90-249) (0.1 mM)	2α-Mannobiose (0–10 mM)	303 K
^{13}C,^{15}N Yos9 (90-249) (0.1 mM)	3α, 6α-Mannopentaose (0–3 mM)	303 K
^{15}N Ubc9 (0.2 mM)	SUMO2 wtΔGG (0–0.8 mM)	303 K
^{15}N Ubc9 (0.2 mM)	SUMO2 variant (E08) (0–0.8 mM)	303 K
^{15}N Ubc9 (0.2 mM)	SUMO2variant (A09) (0–0.8 mM)	303 K

Series of two dimensional ^{15}N, ^{1}H HSQC spectra were recorded and chemical shift perturbations (CSP) analyzed. How exactly the chemical shifts of the labeled binding partner are affected by the presence of the unlabeled protein is determined by the exchange regime of the interaction. CSPs were calculated using the following equation:

$$\mathrm{CSP} = \sqrt{\Delta\delta(\ ^{1}\mathrm{H})^2 + (0.17 \cdot \Delta\delta(^{15}\mathrm{N}))^2} \quad (1)$$

Here, $\Delta\delta(^{1}H)$ is the proton chemical shift difference between the compared spectra and $\Delta\delta(^{15}N)$ the respective nitrogen chemical shift difference.

Dissociation constants (K_D) can be obtained by quantitatively analyzing the chemical shift perturbations (Williamson, 2013) as a function of the molar ratio x of the ligand and the labeled protein.

$$\mathrm{CSP(x)} = \frac{\mathrm{CSP_{max}}\left[[\mathrm{P}]_0\,\mathrm{x} + [\mathrm{P}]_0\ + \mathrm{K_d} - \sqrt{([\mathrm{P}]_0\,\mathrm{x} + [\mathrm{P}]_0\ + \mathrm{K_d})^2 - 4[\mathrm{P}]_0^2\mathrm{x}}\right]}{2[\mathrm{P}]_0} \quad (2)$$

Here, $[P]_0$ represents the concentration of the labeled protein, which is kept constant during the series of HSQC spectra. Thus, the ligand concentration is the molar ratio $x \cdot [P]_0$. CSP_{max} and K_D are obtained by non-linear regression. This equation is only valid for a single binding site.

In order to determine K_D values for proximal and distal ubiquitin moieties in diubiquitin individually, the CSPs upon titration with the CUE domain of Cue1 were analyzed assuming a fitting model for two independent binding sites with different affinities (von Delbruck et al., 2016; Varadan et al., 2005; Wang and Jiang, 1996). The following equations were adapted from Varadan et al. (2005). The CSP ($\Delta\delta$) in the distal ubiquitin can be described as follows:

$$\Delta\delta = \Delta\delta_{\mathrm{max}} \cdot [\mathrm{L}]/([\mathrm{L}] + K_D^d\} \quad (3)$$

where K_D^d is the dissociation for the distal (d) unit of diubiquitin. [L] is the free ligand concentration and $\Delta\delta_{max}$ is the maximal chemical shift perturbation measured. Due to the presence of a second binding site, the free ligand concentration must satisfy, according to Varadan et al (2005), the following equation:

$$[L]^3\ + (2[P]_t\ - [L]_t\ + K_D^d + K_D^p) \cdot [L]^2\ + \{\left([P]_t\ - [L]_t\ \right)\left(K_D^d + K_D^p\right) + K_D^d \cdot K_D^p\} \cdot [\mathrm{L}] - [L]_t\ \cdot K_D^d \cdot K_D^p = 0 \quad (4)$$

Data fitting was performed using OriginPro 9.1 and yielded dissociation constants for proximal and distal ubiquitin moieties.

4.5.5. Paramagnetic relaxation enhancement (PRE) experiments

Sample preparation for intermolecular paramagnetic relaxation enhancement (PRE) experiments required spin labeling of single cysteine containing Ubc7-U7BR mutants with (1-Oxyl-2,2,5,5-

tetramethylpyrroline-3-methyl) methanethiosulfonate spin label (MTSSL). Labeling was performed using 20-fold excess of MTSSL. The procedure is described in more detail in section 4.6.1. Successful labeling was analyzed by continuous wave electron paramagnetic resonance (CW-EPR) experiments indicating labeling efficiencies between 70% and 90%. CW-EPR experiments were performed by Alberto Collauto from the group of Thomas Prisner (Goethe-University Frankfurt).

PRE samples contained 400 µM of spin labeled Ubc7-U7BR variants (S30C, A106C, S128C, S158C), 200 µM ^{15}N-labeled Ubc7-U7BR in 25 mM HEPES, 150 mM NaCl, pH 7.0, 0.03 % NaN_3, DSS, PIC and 5 % D_2O. The diamagnetic reference sample contained 400 µM unlabeled Ubc7-U7BR and 200 µM ^{15}N-labeled Ubc7-U7BR. The same set of samples was prepared under low salt conditions in buffer containing only 50 mM NaCl. NMR spectra were recorded by Frank Löhr and analyzed by me.

Intermolecular paramagnetic relaxation enhancement effects observed on ^{15}N-labeled Ubc7-U7BR were quantitatively analyzed using the two-time-point method (Iwahara et al., 2007) employing the following equation. T_a and T_b represent the two delays in the pulse sequence that are changed for the relaxation measurement.

$$\Gamma_2 = \frac{1}{\mathrm{T_b} - \mathrm{T_a}} \cdot ln\left(\frac{I_{\mathrm{dia}}(\mathrm{T_b}) \cdot I_{\mathrm{para}}(\mathrm{T_a})}{I_{\mathrm{dia}}(\mathrm{T_a}) \cdot I_{\mathrm{para}}(\mathrm{T_b})}\right) \quad (5)$$

Here, Γ_2 is the PRE ^{1}H transverse relaxation rate, I_{dia} the peak intensity observed in the diamagnetic state and I_{para} the peak intensity for the paramagnetic state (Iwahara et al., 2007).

4.5.6. HADDOCK modeling

The HADDOCK (High Ambiguity Driven protein-protein DOCKing) docking protocol is a data driven docking protocol which involves rigid-body docking, semi-flexible refinement and a final water refinement step (de Vries et al., 2010; van Zundert et al., 2016). HADDOCK calculations were successfully performed for the CUE-ubiquitin and the Ubc7-U7BR-Hrd1(RING) complexes using the webserver of HADDOCK. Ambiguous interaction restraints (AIR) were derived from NMR titration experiments which were performed in both possible orientations as described in section 4.5.4. Titration data for the CUE-Ub complex was already obtained during my diploma thesis, while titration data for Ubc7-U7BR and the Hrd1 RING domain were collected in this work. The residues showing the most pronounced CSPs were filtered by solvent accessibility and defined as active residues in HADDOCK. Passive residues were automatically defined as surrounding active residues. For the Ubc7-U7BR-Hrd1 complex a contiguous interaction surface on Ubc7-U7BR was only obtained by excluding CSPs at the interface of Ubc7 and the U7BR and CSPs directly adjacent to catalytic residue C89. In this case the remaining residue showing high CSPs were defined as active in HADDOCK.

4.6. Pulsed electron-electron double resonance (PELDOR) spectroscopy

Pulsed electron-electron double resonance (PELDOR) spectroscopy, also called DEER, is a method which allows the measurement of distance distributions in spin labeled macromolecules in the range of 1.5–8 nm (Jeschke, 2012).

4.6.1. Site-directed spin labeling and sample preparation

Spin labeling with MTSSL (20-fold excess) was performed in PBS buffer and included 100 µM cysteine containing ubiquitin chains. Reactions were incubated for 1 h at room temperature. Removal of excess spin label and buffer exchange was achieved by concentrating and diluting with deuterated PBS buffer (pD 7.2) on Amicon Ultra-0.5 mL centrifugal filters. Prior to flash freezing in liquid nitrogen, 20% d8-glycerol was added as a cryoprotectant.

4.6.2. PELDOR data collection, analysis and structure ensemble generation

4-pulse (Pannier et al., 2000) and 7-pulse Carr-Purcell (CP)-PELDOR sequences (Spindler et al., 2015) were used to measure pulsed EPR data on doubly spin labeled ubiquitin chains. All PELDOR measurements were performed by Denise Schütz from the group of Thomas Prisner (Goethe-University Frankfurt). A detailed description of all experiments and how the data was analyzed can be found in the dissertation of Denise Schütz as well as in our joint publication(Kniss et al., 2018).
Various ubiquitin structures were spin labeled *in silico* in order to identify appropriate labeling sites and for comparison with experimental data. This was also performed by Denise Schütz using a rotamer library approach using the MMM 2015.2 software package in 298 K mode (Polyhach et al., 2011).
Structure ensembles were generated by CYANA 3.9 (Guntert and Buchner, 2015; Guntert et al., 1997) and the ensemble distributions visualized by probability hyper-surfaces as already published (Kniss et al., 2018). PELDOR data based calculations and visualization of the spatial distribution of the distal ubiquitin moiety in respect to the proximal ubiquitin position was conducted by Sina Kazemi from the Peter Güntert group (Goethe-University Frankfurt).

4.7. Biophysical methods for studying protein-protein interactions

4.7.1. Isothermal titration calorimetry (ITC)

For biophysical characterization and determination of thermodynamic parameters of the SUMO2-Ubc9 interaction isothermal titration calorimetry (ITC) experiments were used.
Experiments were performed at 37°C in 25 mM HEPES/NaOH, pH 7.0 and 150 mM NaCl using a MicroCal VP-ITC calorimeter since titrations at 25°C revealed only a small enthalpy binding

contribution for SUMO2 wild type (wt). SUMO2 wt (550 µM) was titrated into Ubc9 (40 µM) using 20 injections of 12.5 µL. High affinity SUMO2 variants, SUMO2-E08 (150 µM) and SUMO2-A09ΔGG (150 µM), generated by phage display (Wiechmann et al., 2017), were titrated into a solution of 10 µM Ubc9. ITC data was analyzed assuming a one-site binding model. Since the interaction with the SUMO2-E08 variant resulted in a rectangular shaped binding isotherm a displacement binding assay was conducted. To this end Ubc9 (20 µM) was pre-saturated with SUMO2 wt (160 µM) and SUMO2 wt molecule displaced by SUMO2-E08 (300 µM) during titration. This data was analyzed using a competition binding model (Velazquez-Campoy and Freire, 2006), where the predetermined interaction parameters for the SUMO2 wt interactions were used.

4.7.2. Surface plasmon resonance (SPR) spectroscopy

Surface plasmon resonance (EPR) spectroscopy experiments were performed to characterize binding of differently linked ubiquitin chains to the CUE domain of Cue1 (von Delbruck et al., 2016). Cue1 (59-115) was biotinylated *in vitro* in 50 mM bicine (pH 8.3), 10 mM ATP, 10 mM MgOAc and 50 µM biotin using BirA. The reaction mixture was incubated for 1h at 30°C. The CUE domain was subsequently immobilized on a streptavidin-coated sensor chip (approximately 100 response units). Ubiquitin was injected at concentrations ranging from 0–800 µM at a flow rate of 50 µL/min for 100 s. For ubiquitin chains the injected concentrations were reduced by a factor equal to the chain length. K_D values were calculated from steady-state response units assuming that all binding sites are equal.

5. Results

5.1. The CUE domain of Cue1 accelerates the ubiquitin chain elongation process in ERAD

This work includes some experiments that were initially conducted during my diploma thesis. This is indicated in the text and figures. The project was continued during this PhD thesis as a collaborative project with the group of Thomas Sommer from the Max-Delbrück-Centrum in Berlin and is published in Molecular Cell with Maximilian von Delbrück and me being co-first authors (von Delbruck et al., 2016).

5.1.1. Analysis of ubiquitin binding by the CUE domain of Cue1

Interaction studies involving the CUE domain of Cue1 and ubiquitin chains was initially established during my diploma thesis, which included optimization of the NMR construct (Cue1 45-115) by NMR and CD spectroscopy, structure calculation and NMR titration experiments using monoubiquitin and differently linked ubiquitin chains. This work had revealed that CUE interacts via α helices 1 and 3 and its LAP (76-78) motif with the famous hydrophobic patch of ubiquitin centered around L8-I44-V70. Significant chemical shift perturbations were also observed for R42, G47 and L71 on ubiquitin. Unlike canonical CUE domain the NMR structure showed that the CUE domain bears a structurally important C-terminal extension that bears several phenylalanine residues.

To preclude that further regions in Cue1 significantly contribute to ubiquitin binding a complete cytosolic fragment covering residues 25-203 (only lacking the N-terminal transmembrane helix) was expressed in minimal medium. The [^{15}N, ^{1}H]-TROSY HSQC spectrum of Cue1 25-203 shows a largely unstructured protein. By contrast, the CUE domain (Cue1 45-115) shows well dispersed signals that represent a subset of the signals found in the spectrum of the entire cytosolic fragment (Figure 7A) suggesting that Cue1 contains a single well folded domain in absence of Ubc7. The presence of unstructured regions was found to do not impact ubiquitin binding activity (Figure 7B) and was similar to the CUE domain construct (Figure 7C).
Based on the previously obtained titration data a structural model of the CUE-Ub complex was calculated using HADDOCK (de Vries et al., 2010). Interestingly, this model supports the contribution of the R42 side chain of ubiquitin in complex formation with the CUE domain by interacting with E100 in CUE (Figure 7D). SPR experiments revealed a K_D of around ~700 µM for a R42A mutant ubiquitin compared to 170 µM obtained for the wild type interaction (data not shown). Comparison of the Cue1-Ub complex with a previously determined complex of the first CUE domain of Cue2 (termed CUE2-1) shows that the site of ubiquitin chain elongation (K48) is freely accessible in the Cue1 complex even though CUE binds in close proximity (Figure 7E). Instead CUE2-1 directly involves

K48 in complex formation (Kang et al., 2003), at least in the structural model, suggesting that polyubiquitination might be partially excluded (Kang et al., 2003).

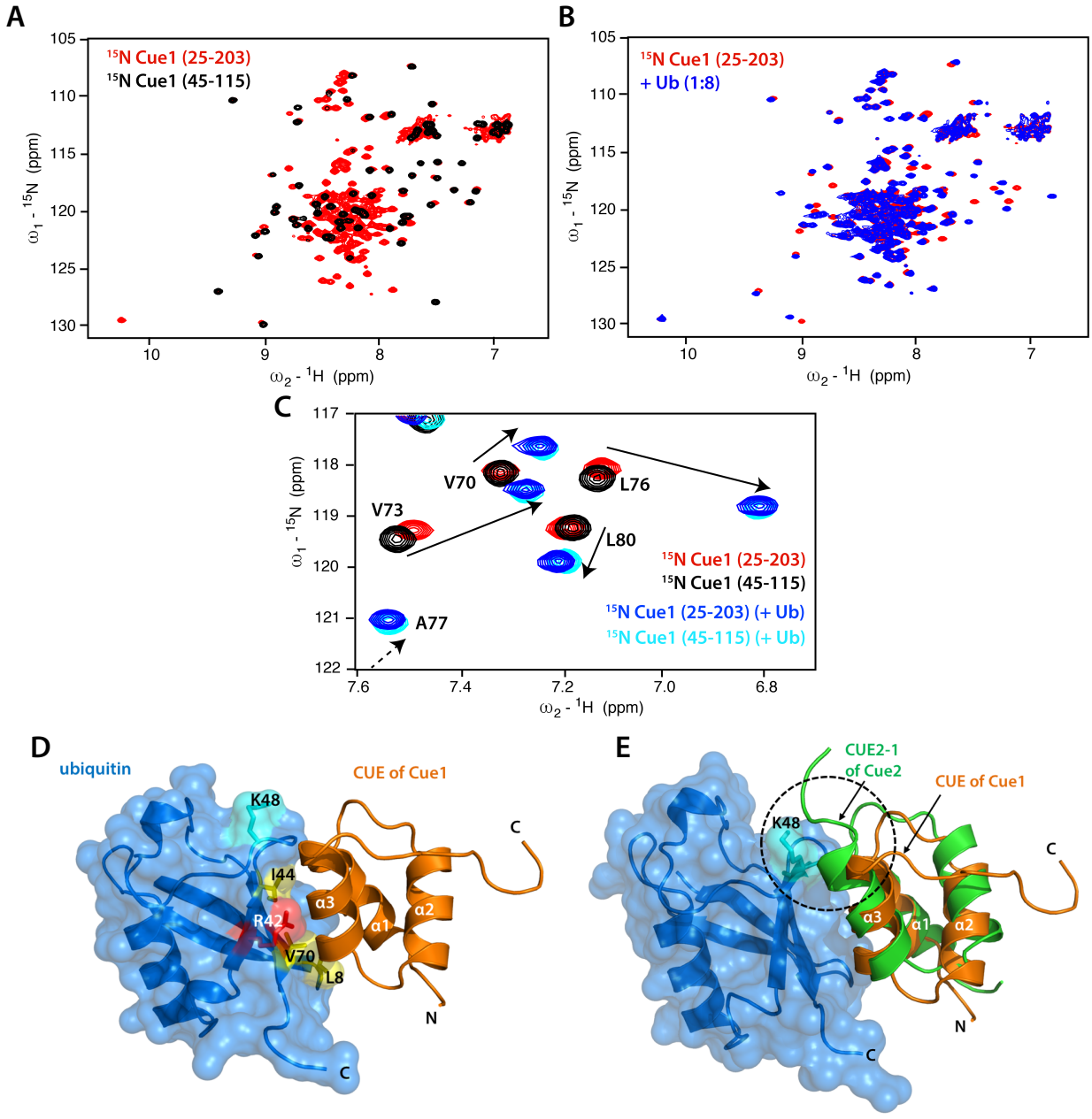

Figure 7: Analysis of ubiquitin binding by the CUE domain of Cue1. (A) Overlay of ^{15}N,^{1}H HSQC spectra of the entire cytosolic fragment of Cue1 (red) and the CUE domain (45-115) construct (black). (B) Titration of ^{15}N Cue1 (25-203) with unlabeled ubiquitin. The spectrum of the free protein (red) is overlaid with the bound form (blue) that was recorded with eight-fold molar excess of ubiquitin. (C) Representative section of HSQC spectra of ^{15}N-labeled cytosolic fragment of Cue1 and CUE domain of Cue1 in absence of ubiquitin (red and black) and under saturating conditions with ubiquitin (blue and cyan). (D) Highest-scored HADDOCK model of the CUE-Ub complex. The structure shows the freely accessible K48 residue and the involvement of R42 of ubiquitin in complex formation. (E) Comparison of CUE2-1 of Cue2 (green) and CUE of Cue1 (orange). Ubiquitin molecules within both complexes were superimposed to compare CUE domain orientations. PDB codes used to generate the figure were: 2MYX (Cue1) and 1OTR (Cue2). Parts of the figure were adapted from von Delbrück et al. 2016.

5.1.2. Ubiquitin chain elongation kinetics correlates with ubiquitin binding affinity

To reveal how ubiquitin binding and ubiquitin chain elongation by Ubc7 are connected and address the impact of ubiquitin binding on the elongation reaction kinetics, a fluorescence-based elongation assay was developed (performed by Maximilian von Delbrück) and different CUE domain mutants tested (Figure 8A). The assay was performed either by measuring fluorescence anisotropy or quantifying fluorescence signals of products at different time points by fluorescent scanning of SDS-PAGE separate chains. Elongation reactions contained ATP, an E1 enzyme, Ubc7 and cytosolic fragments of Cue1 (25-203) and Hrd1 (325-551) (Figure 8B).

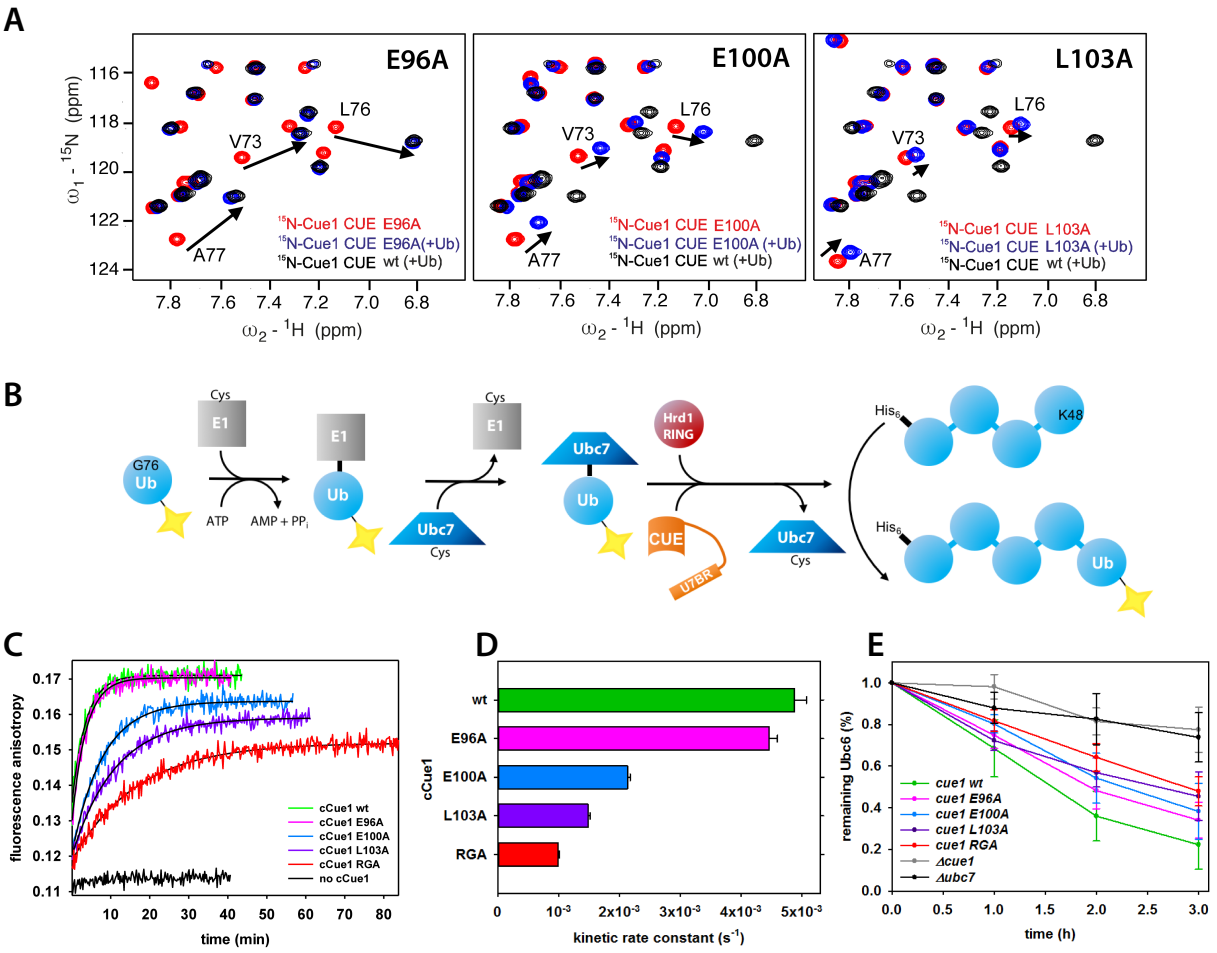

Figure 8: Ubiquitin binding affinity of the CUE domain correlates with chain elongation kinetics *in vitro* and degradation of the ERAD substrate Ubc6 *in vivo*. (A) Superposition of a section of $^{15}N,^{1}H$ HSQC spectra recorded for the CUE domain mutants E96A, E100A and L103A in a free form (red) and recorded with ubiquitin excess (eight-fold, blue). For comparison the spectrum of wild type CUE in presence of ubiquitin is shown in black and indicates differential binding activity of the three mutants. The data was obtained during my diploma thesis. (B) Principle of the fluorescence-based ubiquitin chain elongation assay. The assay includes E1 for ATP-dependent Ub activation, the E2 enzyme Ubc7, cytosolic fragments of Cue1 and Hrd1. C-terminally His6-tagged chains are elongated by a single fluorescently labeled ubiquitin. The assay was designed by Maximilian von Delbrück. (C) Fluorescence anisotropy measurements of elongation reactions employing different CUE domain mutants. Cue1 RGA represents an unfolded CUE domain incapable of binding to ubiquitin as shown by my NMR experiments (not shown here). The assay was performed by Maximilian von Delbrück. (D) Quantification of the assay in C. (E) Quantification of a cycloheximide-based decay assay of Ubc6 as a ERAD model substrate. Δcue1 and Δubc7 strains provide a baseline. The experiment was performed in the group of Thomas Sommer. Raw data can be found published (von Delbruck et al., 2016). The figure was adapted from von Delbrück et al. 2016.

Increasing anisotropy signals originated from the incorporation of the fluorescently labeled monoubiquitins into the chains due to slower tumbling of the reaction product compared to monoubiquitin. The reaction trace without the addition of Cue1 (Figure 8B, black) indicates the absence of U7BR mediated activation of the E2 enzyme and did not lead to product accumulation and is in agreement with previously published data (Metzger et al., 2013). For assessing the influence of the UBD (CUE domain) for chain elongation, a set of CUE mutants with different ubiquitin binding activities (E96A, E100A, L103A, and LAP 76-78 to RGA) was generated and investigated by NMR as well as by the kinetic assay (Figure 8). The RGA mutant is unfolded (as proven by NMR experiments during my diploma thesis) and allows to dissect contributions to elongation arising from U7BR activation and UBD stimulation. Affinity correlated well with elongation kinetics (Figure 8D) indicating that UBD binding assists in ubiquitin chain elongation and accelerates a single turnover by approximately five-fold. This should in principle yield to markedly slower ubiquitin chain formation within the E3 ligase complexes in yeast. To test this idea, a cycloheximide decay assay was performed in the lab of Thomas Sommer. Cue1 containing mutations in the CUE domain delayed the degradation of the Doa10-dependent ERAD model substrate Ubc6 (Figure 8E) although not dramatically. Strains lacking Cue1 (Δcue1) or Ubc7 (Δubc7) and a wild type strain served as controls. A possible explanation for the small effects could be potential rescuing effects by chain elongating E4 enzymes (Koegl et al., 1999) in yeast that support the formation of sufficiently long chains for subsequent proteasomal degradation. However, the final degradation efficiency was still dependent on ubiquitin binding affinity.

In conclusion, efficient ubiquitin chain formation and degradation in ERAD is a UBD dependent process and requires distinct ubiquitin binding events.

In addition to the presented data, Maximilian von Delbrück could show that chain elongation is dependent on the linkage type and chain length (von Delbrück et al., 2016) with K48-linked tetraubiquitin being the most preferred elongation substrate. The CUE domain seems to lead to a progressively accelerated chain elongation with increasing chain length. Without a functional CUE domain ubiquitin chain elongation slowed down with increasing chain length.

5.1.3. CUE domain binding adjacent to the distal tip of a growing ubiquitin chain promotes chain elongation

To understand the linkage preference and get insights into how the CUE domain promotes elongation, either proximally or distally ^{15}N-labeled K48- and K63-linked diubiquitins were synthesized (Figure 9A-B). This allowed to observe binding events at proximal and distal ubiquitin moieties independently. Binding interfaces as deduced form chemical shift perturbation (CSP) analysis were largely similar on proximal and distal ubiquitins in both chain types (Figure 9A-B).

However, in case of K48-linked chains G75 of the distal ubiquitin was significantly affected upon binding suggesting an involvement in the interaction.

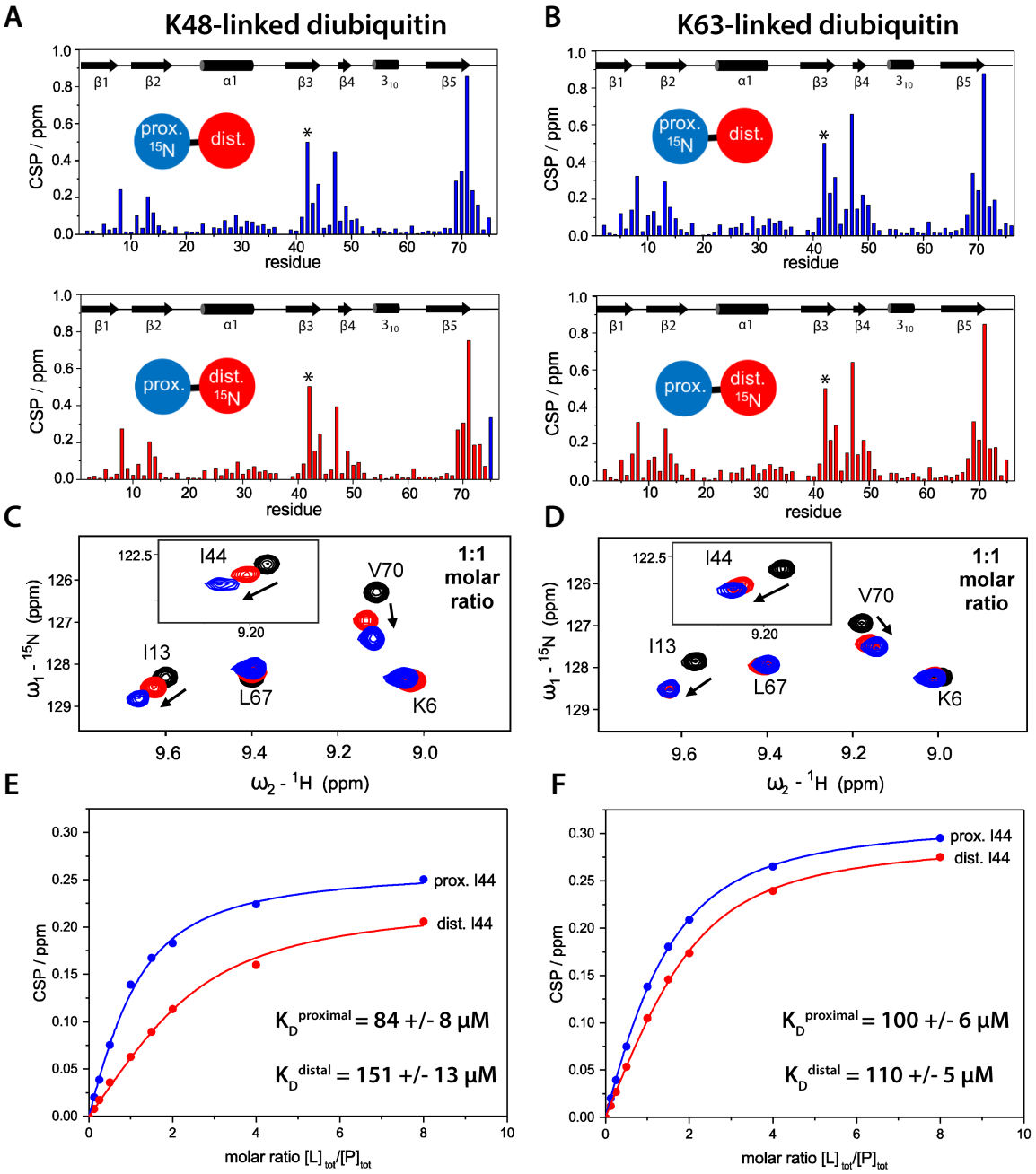

Figure 9: The CUE domain preferentially binds the proximal moiety in K48-linked diubiquitin. (A) Chemical shift perturbation data of backbone amides in the proximal or distal moiety of K48-linked diubiquitin obtained for the interaction with the CUE domain of Cue1. CSPs arising from binding to proximal ubiquitin moieties are colored in blue, while CSPs due to distal binding are colored red. G75 of the distal Ub is engaged in the interaction with proximally bound CUE and enlarges the interaction surface. The asterisk indicates R42 which disappears upon titration. Its CSP value was set to 0.5. (B) Data as in A but for K63-linked diubiquitin. (C) ^{15}N,^{1}H HSQC spectra of free proximal or distal ubiquitin (black) and spectra recorded at equimolar concentrations of CUE and proximally (blue) or distally (red) labeled K48-linked diubiquitin are shown as an overlay. At this CUE concentration the population of proximally bound complexes is significantly higher than distally bound complexes. (D) The same data as in C showing that proximal and distal interactions are similar for K63-linked chains. (E and F) K_D determination from NMR titration experiments using a binding model with two independent binding sites with different affinities. The CSPs of I44 were analyzed in each case. Affinity for K48-linked proximal ubiquitins is approximately two-fold higher compared to the distal moiety. The figure was adapted from von Delbrück et al. 2016.

Since the HADDOCK model had revealed that CUE binding would be directly adjacent to the linkage site in K48-linked chains, this effect results from proximal binding of CUE that additionally affects the C-terminus of the distal ubiquitin. This additional interaction enlarges the surface and distinguishes the proximal from the distal ubiquitin in K48-linked chains thereby increasing the affinity two-fold. Analysis of the peak positions as a function of the CUE : diubiquitin molar ratio and assuming a binding model with two different binding sites (proximal and distal) yielded a dissociation constant of 84 ± 8 µM for the proximal and 151 ± 13 µM for the distal moiety, respectively (Figure 9C-F). The preference for binding the proximal ubiquitin in K48-linked chains is also evident from a larger chemical shift perturbation in the titration experiments compared to the same shifts for the distal ubiquitin (Figure 9C). For K63-linked chains the chemical shift perturbation pattern of the distal and the proximal ubiquitin do not show a significant difference (Figure 9D). Furthermore, NMR titration curves for the distal ubiquitin in K48-linked chains experience a lag phase that originates from preferential binding to the proximal moiety at low molar ratios before the binding sites become more and more saturated (Figure 10).

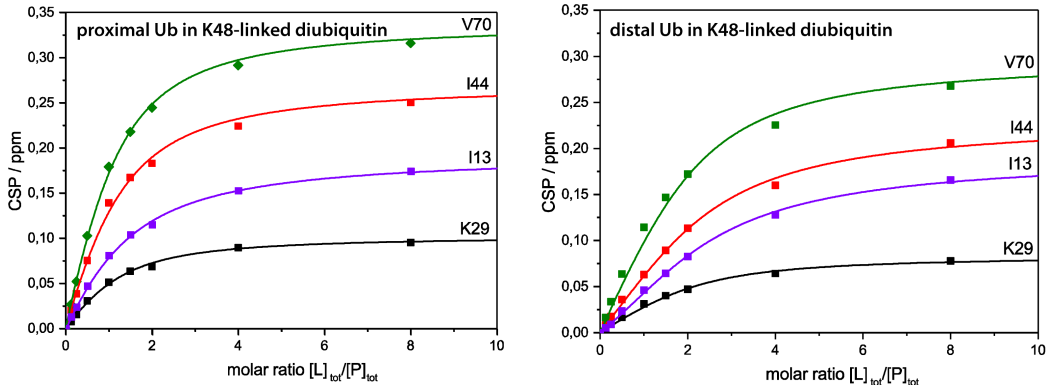

Figure 10: Analysis of chemical shift perturbations in proximal and distal moieties of K48-linked diubiquitin. CSPs of four representative residues were analyzed and fitted. Titration curves for residues in the distal ubiquitin (right) show a slight lag phase compared to the curves obtained for the proximal ubiquitin indicating that both moieties experience distinct interactions. The proximal ubiquitin is preferentially bound. The figure was adapted from von Delbrück et al. 2016.

Notably, similar analyses involving the CUE domain of the mammalian E3 ligase gp78 have shown promiscuous binding with a small preference for the distal moiety (Liu et al., 2012). These differences might be an adaptation to conformational restrictions in assisting ubiquitination in differently organized E3 ligase complexes. Here, the gp78CUE domain is located on the same molecule as the E3 ligase and therefore is positioned differently relative to its cognate E2 enzyme Ube2g2 than Cue1 CUE is positioned relative to Ubc7.

Since binding seemed to be position dependent, ubiquitin chain elongation of monoubiquitin and diubiquitin was measured and compared. The CUE domain was unable to stimulate monoubiquitin elongation compared to diubiquitin elongation (Figure 11A) suggesting that CUE domain binding to the acceptor ubiquitin might be unfavorable for the elongation process. In turn, this raised the

idea of an involvement of proximal binding, as seen in the NMR titration experiments, for productive chain elongation reactions.

Thus, Maximilian von Delbrück measured chain elongation by employing ubiquitin chains carrying a R42A mutation thereby specifically reducing the affinity for either proximal or distal ubiquitins. As expected, ubiquitin elongation of R42A at a proximal position significantly delayed the elongation reaction (Figure 11B). In contrast chain elongation of a distally mutated diubiquitin resembled the wild type chain which further supports that favorable and unfavorable binding events at a growing ubiquitin chain do exist.

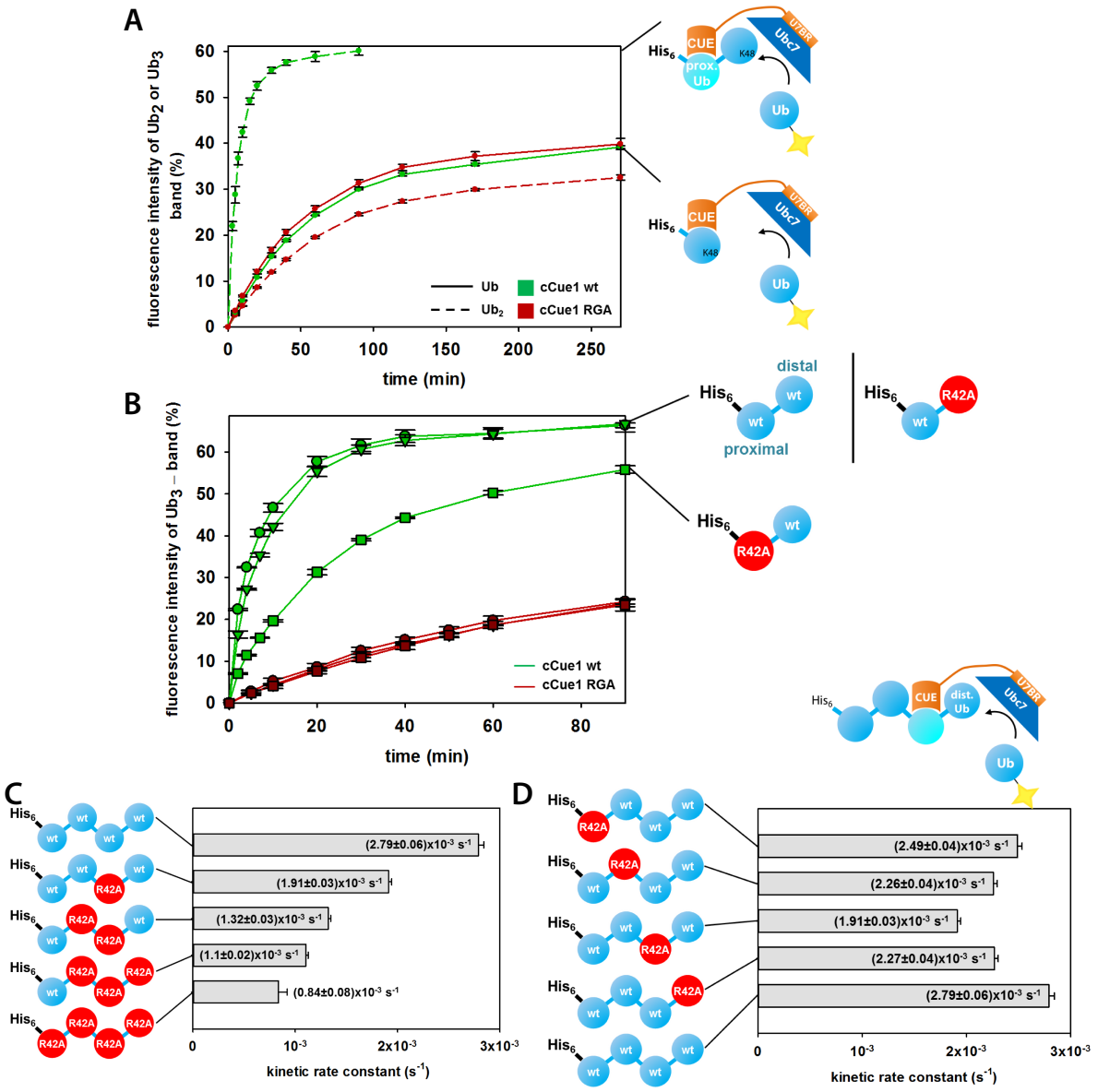

Figure 11: CUE domain binding to the ubiquitin directly adjacent to the distal end of a chain promotes chain elongation. (A) Time course measurements of monoubiquitin (solid lines) and K48-linked diubiquitin (dashed lines) elongation. Reactions were stopped after different time points and product formation analyzed by SDS PAGE and subsequent fluorescent scanning. Reactions contained E1, Ubc7 and Cue1 wt (green) or the unfolded RGA mutant (red) as a control to provide a baseline and separate UBD and U7BR contributions. (B) Wild type chains (circles), distally R42A mutated (inverted triangles) and proximally R42A mutated (squares) chain elongations reveal a CUE position dependence for acceleration. (C) Kinetic rate constants for elongations of K48-linked tetraubiquitin carrying an increasing number of R42 mutant ubiquitins. (D) Rate constants for elongations of K48-linked tetraubiquitin chains containing a single R42A mutation which specifically decreases CUE binding at this position. Elongation reactions were performed by Maximilian von Delbrück. The figure was adapted from von Delbrück et al. 2016.

CUE binding directly adjacent to the acceptor site for further ubiquitin conjugation promote elongation. The RGA mutant of Cue1 lead to elongations that where completely independent from mutations within the chain. Which further strengthens the model that this effect is CUE domain inherent and it can be viewed as independent from the U7BR-mediated activation mechanism.

Introducing multiple R42A mutations in a chain yielded decelerated elongations (Figure 11C) and show that CUE domain binding might involve multiple binding events within a chain before productive chain elongation occurs and that the local concentration of Ubc7 in proximity of the chain is another important factor for elongation. The interaction profile of Cue1 for stimulating elongations was analyzed in more detail by specifically introducing single R42A mutations in tetraubiquitin. Directly adjacent to the distal tip of a chain the negative effect was most pronounced (Figure 11D) with a ~30 % reduction in the rate constant for a single elongation step compared to the wild type chain. This data implies that the CUE domain binds adjacent to the distal end but can easily switch between ubiquitins during elongation which is supported by the weak affinity and high k_{on} and k_{off} rates of the binding reaction. Interactions were found to be in the fast exchange regime in NMR experiments.

Guided by the structural analysis using HADDOCK, two cysteine residues were identified for chemical crosslinking of the CUE domain to different ubiquitins within a chain (Figure 12A) to restricts its interaction profile und further support the data.

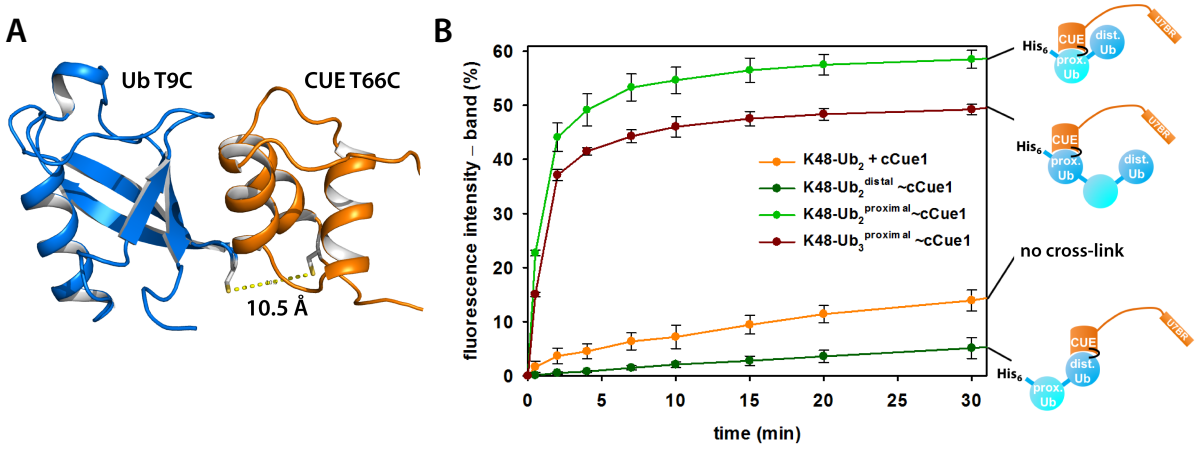

Figure 12: Crosslinking of the CUE domain to different positions in a ubiquitin chain. (A) HADDOCK model of the CUE-Ub complex showing the position of the crosslink. Ubiquitin T9C was crosslinked to Cue1 T66C using $BM(PEG)_2$, a homobifunctional maleimide crosslinker, for chain elongation experiments. (B) Chain elongation of proximally crosslinked Cue1 in diubiquitin (light green) and triubiquitin (red) was measured by time-course experiments. Data with distally crosslinked Cue1 is shown in dark green and significantly impairs elongation. Data containing no crosslink represent the control and is indicated in orange. HADDOCK modeling and planning of the cross-linking experiments was performed by me, while the elongation reaction was performed by Maximilian von Delbrück.

Crosslinking to the distal position inhibited the interaction, whereas crosslinking to proximal ubiquitins stimulated elongation compared to the reactions without crosslinking (Figure 12B). Again, positioning of CUE directly adjacent to the distal tip revealed the strongest effect (light green line in Figure 12B).

The CUE domain contributes with its proximal binding preference as well as with its position dependent accelerating effect on chain elongation to the formation of sufficiently long ubiquitin chains in ERAD to efficiently drive degradation of substrates. Specific binding events seem to dictate and coordinate the spatial arrangement of the E2 enzyme relative to the distal end of a chain for productive attack of the distal acceptor lysine at thioester linked donor ubiquitins on the E2 enzyme.

5.2. Chain assembly and disassembly processes differently affect the conformational space of ubiquitin chains

This project was a collaborative project with the group of Thomas Prisner of the Goethe-University Frankfurt and is published in Structure with Denise Schütz and me being co-first authors (Kniss et al., 2018). Sample preparations for PELDOR experiments and biochemical experiments were performed by me, while PELDOR data collection was done by Denise Schütz. The final computational modeling was performed by Sina Kazemi (Peter Güntert group, Goethe-University Frankfurt).

Ubiquitin chains have already been studied using a variety of different methodological approaches as described in detail earlier (chapter 1.1.4.). The currently hold opinion is that they adopt distinct conformations in solution, particularly in case of K48-linked diubiquitin and K48-linked tetraubiquitin that are characterized to predominantly adopt closed and compact conformational states in solution. However, the here presented PELDOR experiments and quantitative investigations provide new insights into the conformational landscape of ubiquitin chains by making use of long-range distance restraints, the small size of the attached labels (compared to FRET labels) and newly developed pulse sequences from the group of Thomas Prisner (Spindler et al., 2015).

5.2.1. Differently linked diubiquitins show distinct conformational flexibilities

PELDOR measurements detect the couplings of spatially distributed electron spins in a frozen sample and are thus dependent both on the internal spin label flexibility as well as on conformational flexibility of the studied protein system (Jeschke, 2013). In order to establish and validate that defined distance distributions can be obtained, monoubiquitin was doubly spin-labeled along its α-helix (Figure 13A). Well-defined distance distributions were obtained using Gaussian model fitting that resembled the simulated distribution obtained by *in silico* spin labeling of monoubiquitin (1UBQ). The detected small deviations are potentially due to the limitations in generating an appropriate rotamer library that does not take rearrangements of residues adjacent to the spin label into account (Figure 13A).

In order to get a first impression of the conformational flexibility and diversity of diubiquitin chains, the influence of the linkage type was tested using PELDOR spectroscopy. To this end, K11-, K48- and K63-linked diubiquitin chains were synthesized. These chains carried spin labels (MTSSL) at helical positions E24 and A28 in the proximal and distal ubiquitin, respectively, to gain insights into the spatial distributions of both ubiquitin moieties relative to each other (Figure 13B). Helical positions were chosen to reduce the contribution from internal spin label flexibility. Measurements yielded fast dampened oscillations revealing high conformational diversity and thus quantitative analysis yielded broad bimodal distance distributions. In this case, a two Gaussian model fit was used for simplicity reasons and because it resembled the Tikhonov regularization well. Comparison of all

three distributions show that they all reflect clearly distinguishable distributions of the attached spin labels and thus of the ubiquitin moieties. In particular, K48-linked chains showed a comparatively narrow distribution that corresponded to ~77% of the overall population with an underlying broader contribution. All fitting parameters are summarized in Table 10 of the appendix. Previous FRET experiments by Ye et al. (2012) have detected two distinct FRET populations for K48-linked diubiquitin with 90% populated in a conformation that resulted in high-FRET efficiencies. However, FRET experiments used Alexa Fluor 488 and Alexa Fluor 647 labels as a compatible fluorescent dye pair and involved labeling at N- and C-termini. Here, especially labeling at ubiquitin's highly mobile C-terminus (Lange et al., 2008) introduces additional flexibility. The employed fluorescent labels are 720 Da and 1250 Da in size, respectively, and are significantly larger than the MTSSL used in this study that only adds 184 Da to the mass of the protein of interest. In addition, a single long-range restraint is not sufficient to resolve distinct conformations in three-dimensional space. Detailed analysis of the adopted conformational space requires the measurement of several independent restraints to restrict the possibility of ambiguous conformational distributions that reflect the same inter-spin distance but correspond to different inter-ubiquitin arrangements.

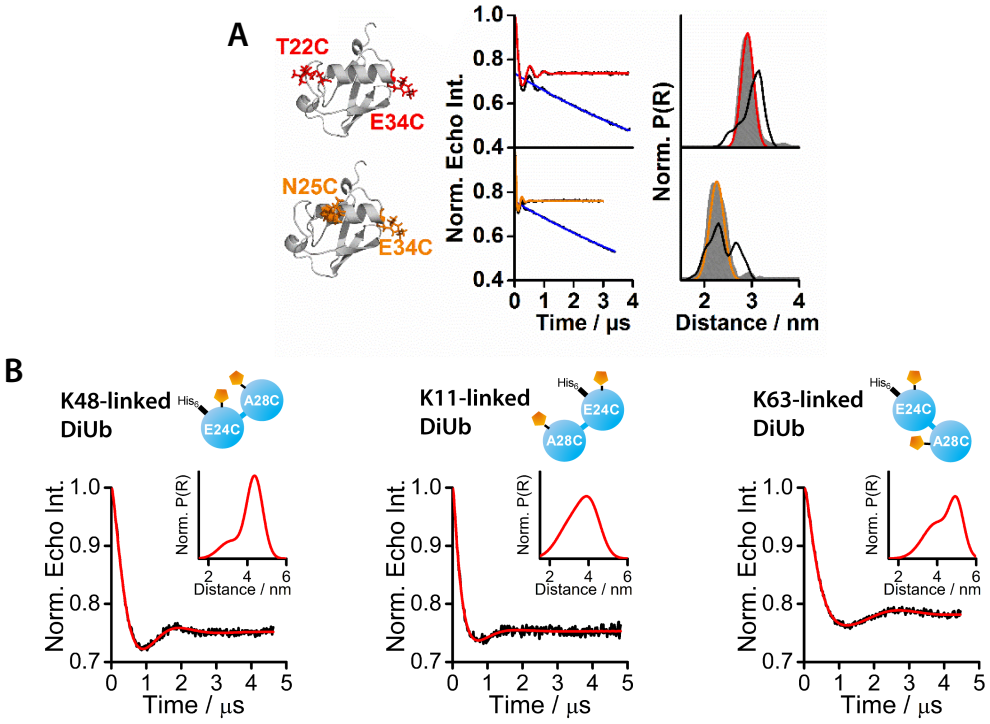

Figure 13: PELDOR experiments on ubiquitin and differently linked ubiquitin chains. (A) Monoubiquitin was labeled with MTSSL via site-directed spin labeling at T22C/E34C and N25C/E34C sites as a proof of principle and to test whether defined inter-spin distances can be deduced from PELDOR time traces. Primary and background-correcte, fitted four-pulse PELDOR data is shown as well as determined distance distributions. Distance distribution were determined by a single Gaussian model fit (red or orange, respectively) or by Tikhonov regularization (grey areas). For comparison, *in silico* determined distance distribution generated using the structure of ubiquitin (PDB code: 1UBQ) are shown in black. (B) PELDOR measurements on differently linked diubiquitins (K11-, K48- and K63-linked). Diubiquitins were spin-labeled at position E24C and A28C in each case but synthesized using different E2 enzymes of distinct linkage specificities. The background corrected PELDOR data was fitted assuming a two-Gaussian model and corresponding distance distributions calculated. The figure was adapted from Kniss et al. 2018.

5.2.2. Investigation of the conformational space of K48-linked ubiquitin chains

Five different spin-labeled K48-linked diubiquitin variants were synthesized. While three samples showed dipolar oscillations, the remaining two dampened comparably fast indicative of a broad distance distribution (Figure 14A).

To gain a better understanding of the conformational space that is accessible and populated in K48-linked diubiquitin 10^6 structural models were calculated using CYANA. These calculations and the generation of the structure ensembles were performed by Sina Kazemi from the Peter Güntert group (Goethe-University Frankfurt). Ubiquitin was treated as a rigid body while the linkage between the two moieties (C-terminal residues 72-76 of the distal ubiquitin) was kept flexible. The methodological approach of this modeling is detailed in Kniss et al. (2018) and also took spin label flexibility into account. Briefly, calculated structures were filtered by dropping structures with steric clashes, and filtering by models that fulfill the experimentally given restraints. This was achieved by calculating a normalized combined pseudo probability derived from the experimental data.

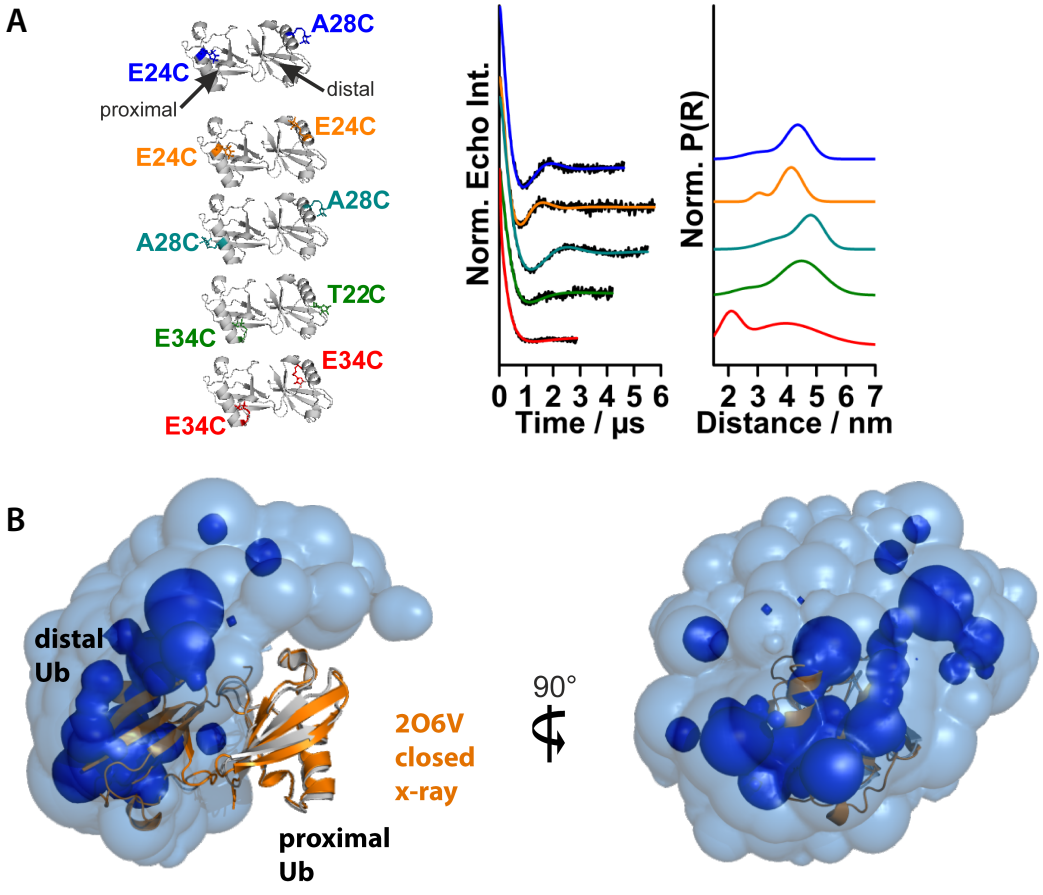

Figure 14: Analysis of the conformational space of K48-linked diubiquitin. (A) K48-linked diubiquitin was labeled at different positions in the proximal and distal ubiquitin moieties and studied by PELDOR spectroscopy. Obtained PELDOR time traces and distance distributions are shown (color coded). (B) Conformational ensemble of K48-linked diubiquitin. The accessible conformational space is shown as probability hyper-surfaces indicating the distribution of the distal relative to the proximal ubiquitin. Two surfaces are overlaid that represent combined probability cutoffs of 0.12 (light blue) and 0.4 (dark blue). Thus, spheres colored in dark blue show higher populated areas, whereas spheres colored in light blue show positions of the distal ubiquitin that are still accessible but less probable. Sample preparation was performed by me, measurements performed by Denise Schütz and modeling performed by Sina Kazemi. The figure was adapted from Kniss et al. 2018.

Results were visualized by probability hyper-surfaces that represent the position of the distal ubiquitin relative to the proximal ubiquitin as a sphere located in its center of mass. Sphere size (radius) corresponds to the combined probability of the distal ubiquitin at this respective position. Certain probability cutoffs were selected in PyMOL for representation using the isoslider plugin. That allowed to display only spheres that have a higher combined probability than the selected cutoff value. The obtained conformational space of K48-linked diubiquitin is shown in Figure 14B. Conformational variability is high; however, higher populated sub-spaces are found as well (dark blue).

In order to interpret this complex result, several known diubiquitin structures were compared both at the level of distance distributions (experimental and simulated distance distributions are compared in Figure 45 in the appendix) and structurally by superimposing the proximal ubiquitins of these structures onto the proximal ubiquitin of the determined structural ensemble (Figure 15).

Conformations where hydrophobic patch residues are found at the inter-domain interface, termed as closed conformations, are within or close to higher populated sub-spaces of the conformational space as seen by the overlay with the "closed" structures 2O6V (Figure 14B), 2BGF, 2PEA or 3M3J (Figure 15).

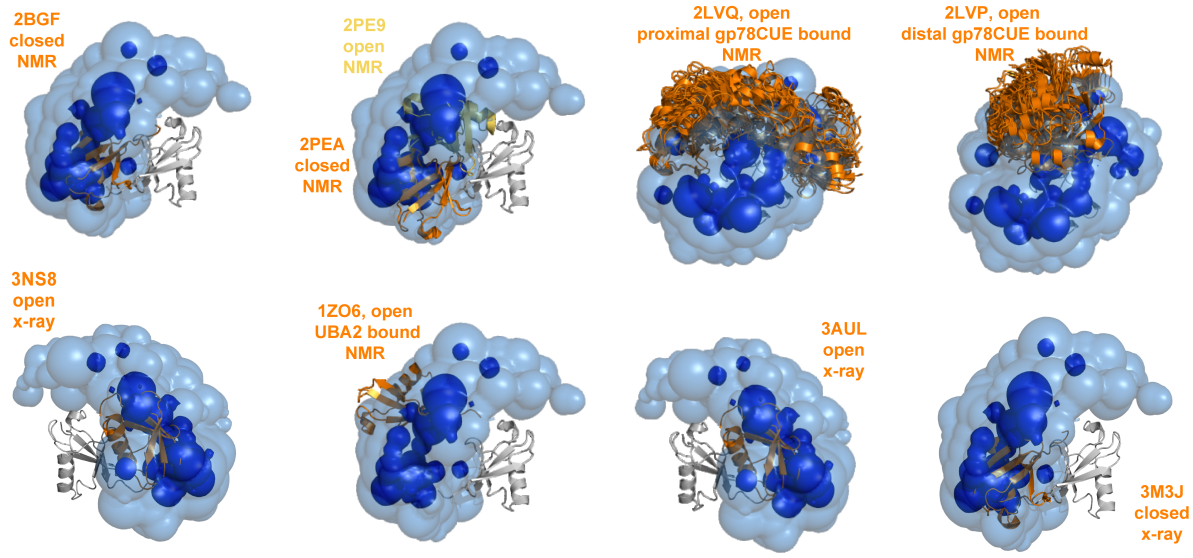

Figure 15: Comparison of the conformational ensemble with available structure of free and bound diubiquitin. Structural comparisons with available structures found in the PDB was achieved by superimposing proximal ubiquitins (grey) of both the determined ensemble by CYANA and different K48-linked diubiquitin structures. Distal ubiquitins of the respective X-ray or NMR structures are shown in orange. The analysis reveals that both open and closed conformations of K48-linked diubiquitin are in agreement with the determined ensemble. However, the "open" X-ray structures 3NS8 or 3AUL or the structure of a diubiquitin bound to the UBA2 of hHR23A (1ZO6) in a sandwich-like conformation are in less probable regions of the ensemble. The figure was adapted from Kniss et al. 2018.

An open conformation with freely accessible hydrophobic patches for noncovalent interactions (2PE9) is found in a different highly populated subspace of the conformational ensemble (Figure 15 and 16). The same applies for the NMR structure ensembles that were determined for complexes of

bound diubiquitin. 2LVP and 2LVQ are structures where gp78CUE is proximally or distally bound at the respective hydrophobic patches and must therefore feature accessible hydrophobic patches. These structures are highly populated in absence of interacting proteins, as seen by the calculated ensemble suggesting that ubiquitin recognition seems to be based on conformational selection out of a pool of diverse structures.

The sandwich-like complex of the UBA2 domain of the human Rad23 homologue with diubiquitin (1ZO6) is found to be less populated, but in close proximity to the subspace of highly populated open conformations. Being a shuttling proteasomal receptor this suggests that no huge structural rearrangements are necessary to allow the adoption of this conformation and thus binding.

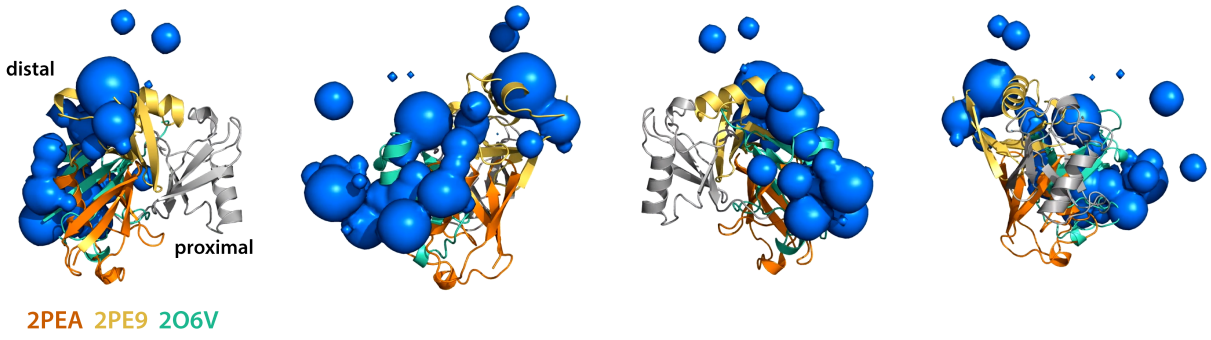

Figure 16: Comparison of high probability hyper-surfaces calculated for K48-linked diubiquitin with existing structures. Proximal ubiquitins are superimposed and the distributions of the distal ubiquitins compared. The figure was generated from frames of a 360° rotation found as a part of the supplemental video 1 that can be accessed online as supplemental material associated with the publication Kniss et al. (2018).

Thus far, our knowledge of chain conformations of chains longer than two ubiquitin units was predominantly based on X-ray crystallography data. Interestingly, efficient proteasomal targeting requires chains of four to six ubiquitins (Thrower, 2000). A previous study has suggested that tetraubiquitin predominantly adopts a compact conformation in solution, where two diubiquitin units in a closed conformation are stacked onto each other (Figure 17A). To address how chain conformations and flexibility are altered with increasing chain length, longer doubly spin-labeled ubiquitin chains were synthesized. The PELDOR samples are summarized in Figure 17A and were employed in PELDOR measurement using a recently developed seven-pulse CP PELDOR sequence to increase the time window for measurements (Spindler et al., 2015). Chain elongation to triubiquitin significantly increased the sampled conformational space and yielded even broader distributions compared to the previously obtained diubiquitin distributions (Figure 17B). The data was fitted assuming a single Gaussian model and yielded distance distributions with mean distances ranging from 3.0 to 4.9 nm (Figure 17B) depending on the selected labeling positions at both ends of the chain. Further chain elongation to tetraubiquitin added another layer of flexibility to the system and large discrepancies were observed especially when PELDOR time traces were compared with simulated dipolar evolution functions (Figure 17B, middle panel). Simulations were based on *in*

silico spin labeling of the compact structure of K48-linked tetraubiquitin (2O6V). Given these broad distributions it can be concluded that this compact arrangement of ubiquitin molecules is not the major conformation that is adopted in frozen liquid solution. This data was further strengthened by measuring spin-labeled diubiquitin incorporated into longer chains (Figure 17C-D) to rule out that further elongation has a stabilizing effect on a diubiquitin unit.

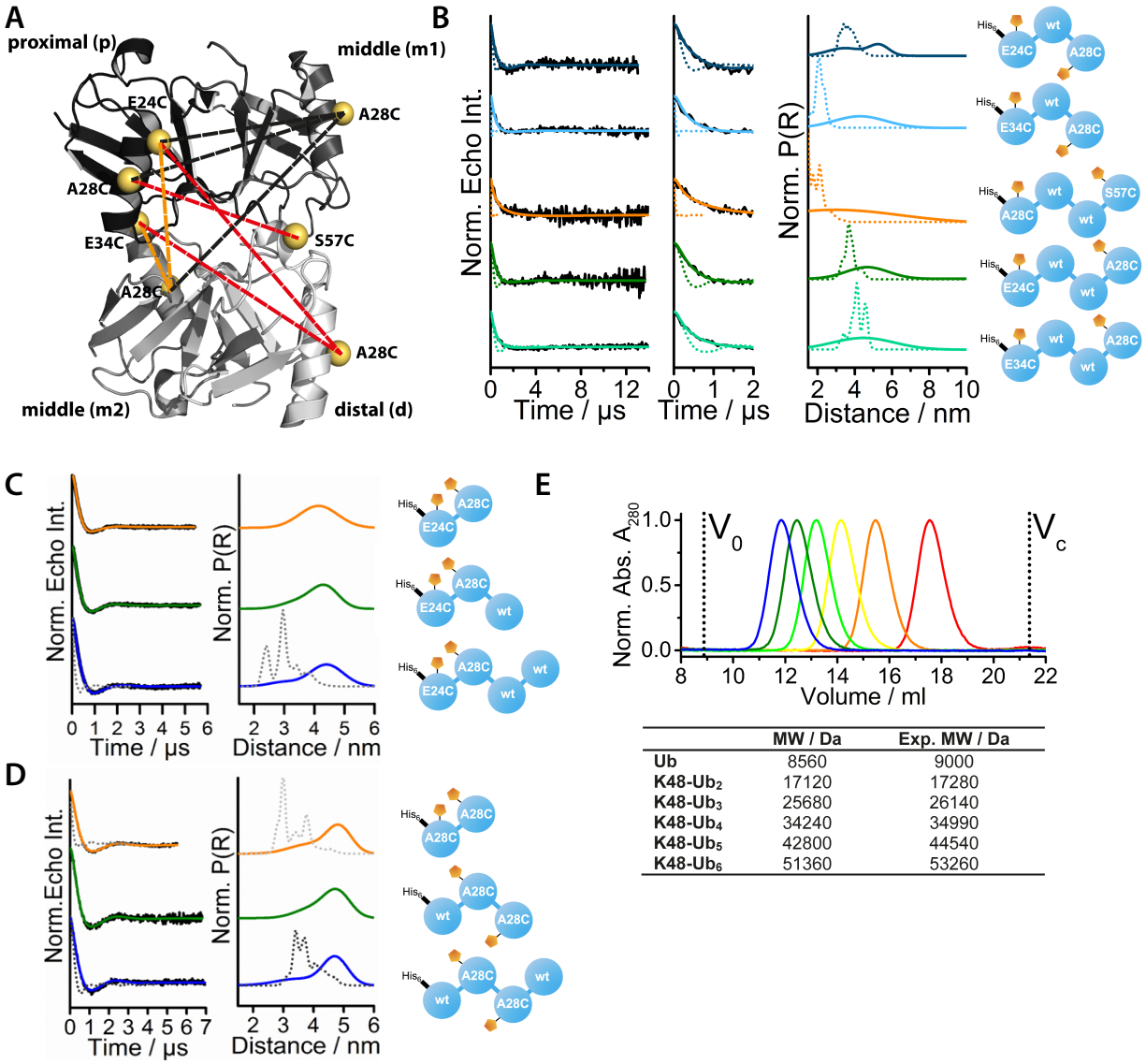

	MW / Da	Exp. MW / Da
Ub	8560	9000
K48-Ub$_2$	17120	17280
K48-Ub$_3$	25680	26140
K48-Ub$_4$	34240	34990
K48-Ub$_5$	42800	44540
K48-Ub$_6$	51360	53260

Figure 17: Conformational flexibility of K48-linked tri- and tetraubiquitin. (A) Spin labeling was performed on a variety of specifically assembled tri- and tetraubiquitin chains. Labeling sites are visualized on the compact X-ray structure of K48-linked tetraubiquitin (PDB code: 2O6V) as yellow spheres. Measured inter-ubiquitin distances covered directly adjacent ubiquitins (black lines), ubiquitins separated by a single ubiquitin (orange) and labeling at proximal and distal ends of a tetraubiquitin chain (red lines). (B) Seven-pulse CP PELDOR measurements on indicated tri- and tetraubiquitin chains showing background-corrected data (left), distance distributions (right), simulated dipolar evolution functions (dotted lines in the right and middle panels) and simulated distance distribution obtained from the crystal structure 2O6V (dotted lines in the right panel). (C) PELDOR data for spin-labeled diubiquitin that was further elongated to tri- or tetraubiquitin. (D) PELDOR data of spin-labeled diubiquitin incorporated into tri- or tetraubiquitin. (E) SEC experiments of a set of K48-linked chains assembled from wild type ubiquitin monomers. K48-linked ubiquitin chains were purified up to the length of hexaubiquitin and employed in analytical SEC experiments on a calibrated Superdex 75 10/300 GL column. V_o and V_C represent the void volme and the column volumn, respectively. Experimentally determined molecular weights from SEC experiments are indicated in the table below the SEC profiles. The figure was adapted from Kniss et al. 2018.

PELDOR traces and determined distance distributions resembled each other well suggesting that the already characterized conformational distribution found for diubiquitin might apply for every isopeptide linkage within a given chain. Long-range interactions seem to do not significantly contribute to shaping the conformational landscape of tri- or tetraubiquitin. Likewise, a completely elongated structure is due to the fitted mean distances also rather improbable. To support this idea wild type K48-linked ubiquitin chains up to the length of hexaubiquitin were synthesized and purified. Hydrodynamic volumes were determined by size exclusion chromatography (SEC) (Figure 17E). Calibration of a Superdex 75 10/300 GL column was performed using a set of globular reference proteins and allowed the calculation of apparent molecular weights by measuring the elution volumes of the ubiquitin chains (Figure 17E). These experiments revealed that K48-linked ubiquitin chains adopt a hydrodynamic volume that is only slightly larger than that of globular proteins of the same molecular weight. Thus, ubiquitin chains are not fully elongated as well as not compact, which would in addition be entropically unfavorable.

5.2.3. Ubiquitin chain elongation is impacted by the presence of binding proteins

My results from the previous study on the CUE domain on Cue1 raised the question how processes that modify chain length are affected by interacting proteins. Chain elongation is a spatially dynamic process which requires that defined chemical reactions take place at the distal tip of a nascent ubiquitin chain. The previous study has shown that Cue1 coordinates this process by the help of its CUE domain as well as its U7BR region. Thus, proximity of a growing chain and a ubiquitin charged Ubc7 is induced in a favorable way via binding adjacent to the acceptor site (von Delbruck et al., 2016). This chain recruitment was shown to be dependent on affinity. However, the actual conjugation reaction and the position dependence of CUE binding is dependent on how the adopted conformational space of the distal ubiquitin is modulated by CUE binding. Since the CUE domain is not directly binding and stabilizing the distal end of a chain, mechanism have to ensure that a fast and directed reaction of the acceptor lysine is possible. Certainly, Ubc7's acidic loop may be involved in aligning the K48 residue of the acceptor ubiquitin with the donor ubiquitin (Chong et al., 2014) as studied for the E2 enzyme Cdc34, but the CUE domain might also have an supporting function on this process.

In theory, closed conformations of ubiquitin chains that involve hydrophobic patch interactions might affect elongations, due to a lower accessibility of the K48 residue in theses conformations. In addition, a CUE domain with a too high affinity could impair the reaction by leading to disfavorable arrangements of the components at the distal tip of a chain when bound to the distal ubiquitin (remember the experiments were the CUE domain was crosslinked to the distal ubiquitin).

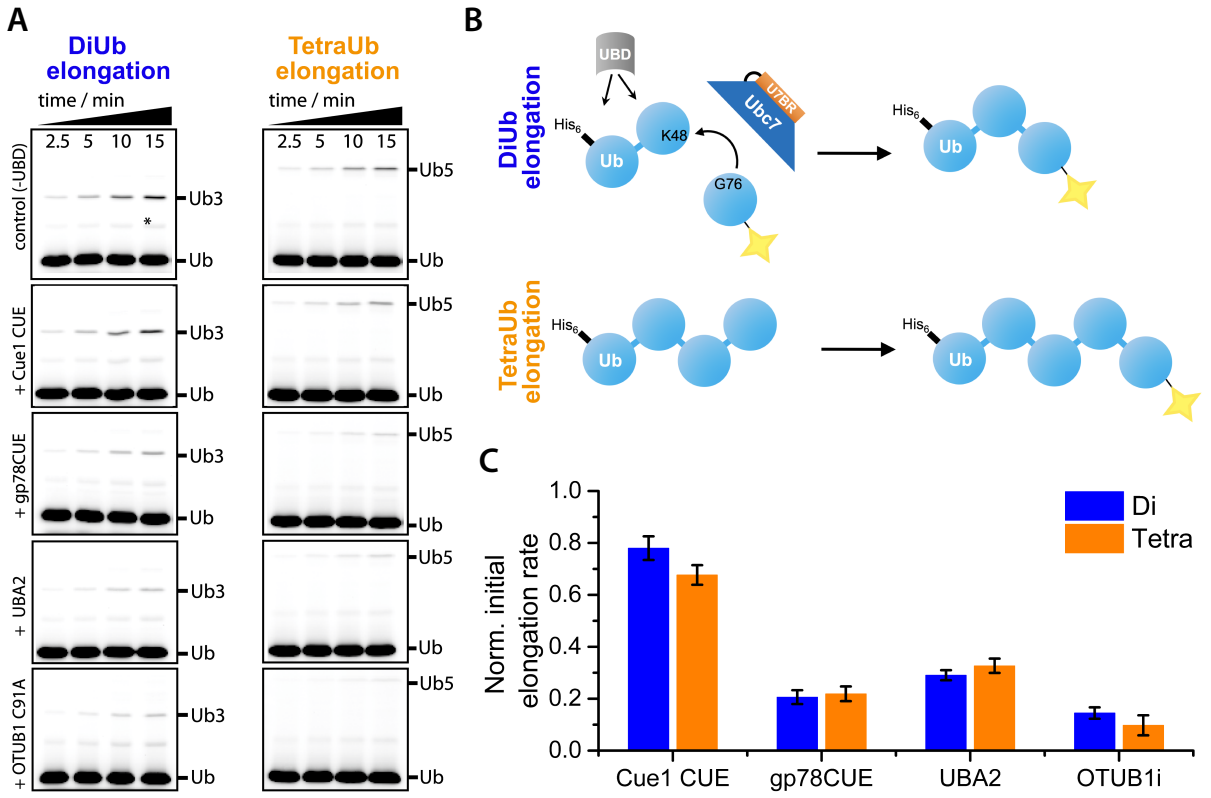

Figure 18: Impact of ubiquitin binding domains on ubiquitin chain elongation by the E2 enzyme Ubc7. (A) Time-course experiments of *in vitro* ubiquitin chain elongations in presence of different ubiquitin interacting proteins (UBDs). The reactions were stopped at the indicated time points and a fluorescence scan of the SDS-PAGE-separated chains was performed. (B) Components of the elongation assay. Reactions contained a single chain construct of Ubc7 and the U7BR of Cue1 to generate an active E2 enzyme and decouple the E2 enzyme from Cue1's inherent position dependent interaction arising from its relative to the U7BR in cis acting CUE domain (as described in the previous chapter). (C) Initial elongation rates were quantified from the data presented in A and performed in triplicates. Rates were normalized to the elongation rates of a control reaction in absence of further chain interacting proteins. The assay was performed together with Lukas Pluska in the lab of Thomas Sommer. The figure was adapted from Kniss et al. 2018.

To test these ideas a modified fluorescence-based chain elongation assay was employed. Reactions contained a single chain construct of Ubc7 and the U7BR of Cue1 to decouple E2 activation from the Cue1's inherent position dependent interaction via its CUE domain (Figure 18A-B). Single turnover elongation kinetics were analyzed in presence of various ubiquitin interacting proteins and in particular in the presence of the CUE domain of Cue1. The presence of the CUE domain of Cue1 resulted in only a slight reduction of the elongation rate compared to a control reaction without any binding partners (70-80% of the elongation rate). Other UBDs, like the CUE domain of the E3 ubiquitin ligase gp78 and the K48-linkage specific UBA2 domain of human Rad23 had strong inhibitory effects (Figure 18C) indicative of potentially disfavorable modulations of the conformational space of the ubiquitin chain or blocking of the acceptor ubiquitin. In conclusion the CUE domain of Cue1 seems to be optimally adapted for beneficially impacting the conformations of a diubiquitin chain so that its elongation site can be easily accessed even in CUE-bound states.

5.2.4. The CUE domain of Cue1 uses conformational selection to support the chain elongation process

PELDOR was used to gain detailed insights into ubiquitin conformations at the distal tip of a chain and define the conformational space of ubiquitin chains in a CUE domain complex (Figure 19A, C-D). The PELDOR time traces obtained in presence of the CUE domain showed marked oscillations indicative of a conformational stabilization and lower conformational flexibility (Figure 19A). Especially the calculated distance distributions for the E24C/A28C and E24C/E2C variants were significantly narrower compared to the free state. Modeling of the conformational space yielded a restricted ensemble, where highly populated states corresponded to open chain conformations. By comparison with free diubiquitin (Figure 19D) it can be concluded that Cue1 selects pre-existing open conformation out of the complex conformational distribution and stabilizes them. This might help positioning the distal acceptor ubiquitin for nucleophilic attack of its lysine at the thioester linked donor ubiquitin.

As control experiments R42A or V70A mutant ubiquitin were introduced both at proximal and distal positions. These mutants have previously been established to significantly reduce CUE binding (chapter 5.1.1). Additionally, these mutations are located at the inter-domain interface in closed conformations of K48-linked diubiquitin. They should therefore also affect conformational distributions in free diubiquitin in case noncovalent inter-ubiquitin interactions significantly contribute to the sampled conformational space as hypothesized by earlier research (summarized in chapter 1.1.4.). Interestingly, both mutations had a negligible effect on the PELDOR signals and calculated distributions for free diubiquitin (Figure 19E). In contrast, noncovalent interactions with the CUE domain were completely abrogated and resulted in the expected PELDOR time traces and distributions that resembled the free diubiquitin state. This yields to the conclusion that noncovalent interaction between adjacent ubiquitin moieties are not impacting the conformational space of diubiquitin, while the CUE effect could successfully be inhibited by appropriate mutations.

Conformational selection by the CUE domain is clearly visible on the level of diubiquitin. By introducing spin labels at the proximal and distal ends of tri- and tetraubiquitin and adding CUE, the influence on the overall arrangements of ubiquitin molecules was studied. Mean distances of the distributions are shifted towards longer distances (Figure 19B) and suggest a further unwinding of K48-linked ubiquitin chains. Altogether this data shows that the conformational selection effect by Cue1 is restricted to shape conformational distributions around a single isopeptide linkage. Since CUE was found to act on the ubiquitin unit directly adjacent to the distal end, this makes totally sense and underscores that the CUE domain is optimally suited to organize the elongation process.

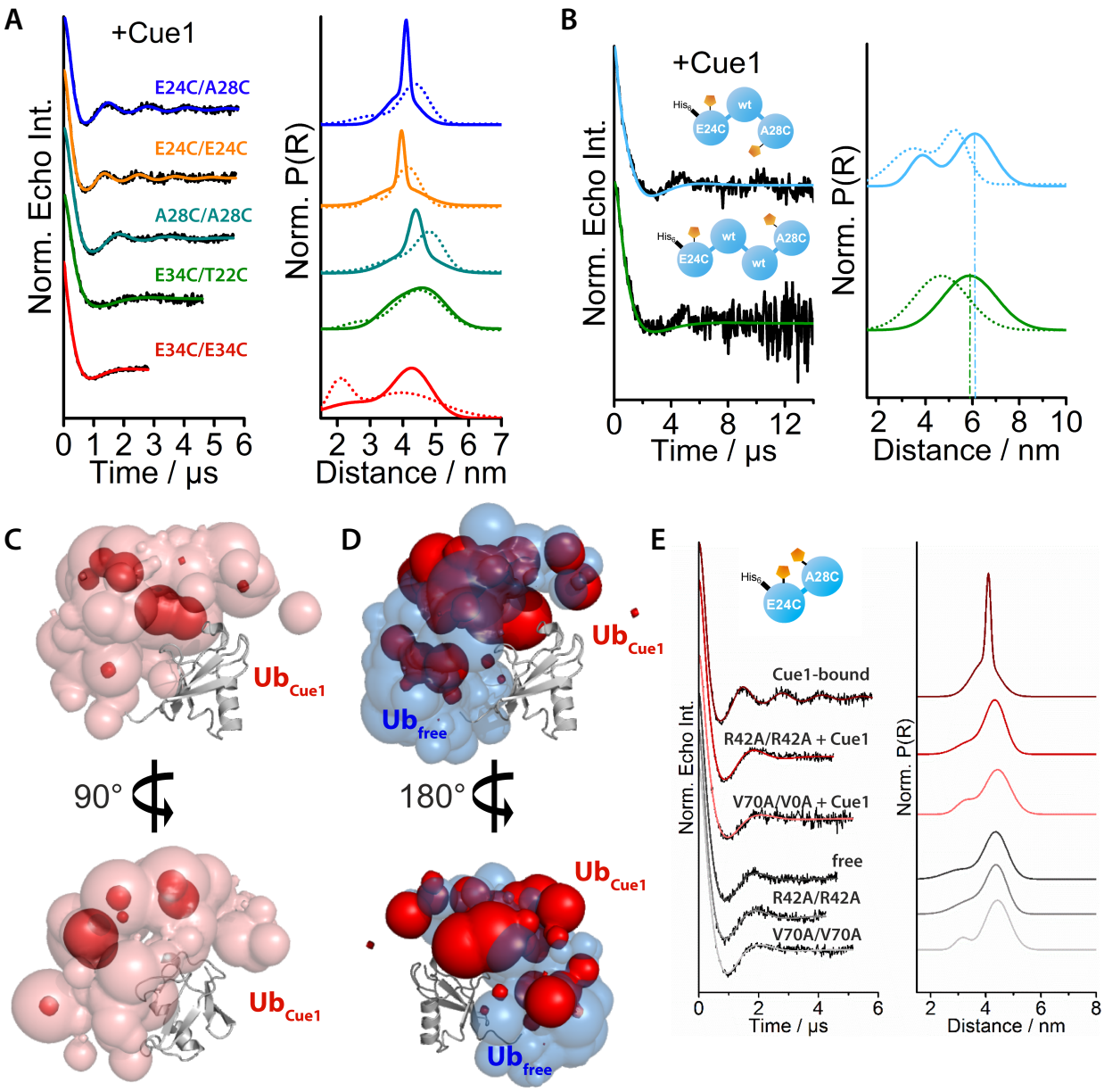

Figure 19: Cue1 uses conformational selection to bind K48-linked chains. (A) PELDOR time traces and obtained distance distributions of a set of five different doubly spin-labeled K48-linked diubiquitins complexed with the CUE domain of Cue1. Distributions in absence of Cue1 are given as dotted lines and indicate conformational changes in diubiquitin that are induced by Cue1. (B) Seven-pulse CP PELDOR time traces of indicated tri- and tetraubiquitin chains. Distance distribution also reflect conformational changes. Measurements in presence of Cue1 are given as solid lines, while dotted lines represent the corresponding experiments using free ubiquitin chains. (C) Probability hyper-surfaces showing the distribution of the distal ubiquitin relative to the proximal ubiquitin (grey) in a complex of K48-inked diubiquitin and Cue1. Regions of higher probability (corresponding to a probability cutoff of 0.4) are shown in red, less probable regions (cutoff value of 0.12) are shown in light red. (D) Comparison of the conformational ensemble of free (blue) diubiquitin and in complex with Cue1 (red) both at a probability cutoff of 0.2. Cue1 leads to a conformational selection of a subpopulation that is already sampled in the free state. (E) Hydrophobic patch mutations (V70A/V70A) or R42A/R42A ubiquitin variants were introduced in both moieties of K48-linked E24C/A28C diubiquitin and measured by PELDOR in absence and presence of Cue1. PELDOR traces and distance distributions are shown together with data of chains carrying no CUE binding mutations. The data shows that the populated ubiquitin chain conformations are not significantly affected by inter-ubiquitin interactions, while noncovalent interaction with CUE significantly shape the conformational landscape of diubiquitin. The figure was adapted from Kniss et al. 2018.

5.2.5. Chain recognition during hydrolysis requires remodeling of the conformational distribution

The action of deubiquitinating enzymes (DUB) necessitates accessibility to the isopeptide linkage for subsequent hydrolysis. Although recently a X-ray structure of a linkage specific DUB (OTUD7B) in complex with K11-linked diubiquitin has been reported (Mevissen et al., 2016) our knowledge about how chain conformations are altered during this process is limited. To address this issue the impact of two linkage specific DUBs on spin-labeled diubiquitin was investigated. Catalytically inactive mutants of OTUB1 (C91A) and OTUD7B (Cezanne) (C194S) were purified and added to their respective substrates: K48-linked diubiquitin or K11-linked diubiquitin. PELDOR analysis revealed a dramatic impact on PELDOR time traces and distance distributions for all measured doubly spin-labeled diubiquitin variants (Figure 20A). Depending on the specific labeling scheme shifts towards smaller or longer distances were observed. For instance, the mean distance for the E24C/E24C distribution shifted from ~4.0 nm in the free state to ~2.5 nm in the DUB bound state. E24C/A28C, E24C/E24C and E34C/E34C diubiquitin yielded significantly narrowed distributions indicative of conformational stabilization. Interestingly, distance distributions in the DUB complex reflected conformational states that were not or only populated to a low extent in free diubiquitin. For tetraubiquitin chains, DUB binding induced a conformational stabilization that yielded a narrower peak at 5.3 nm which corresponded to 40 % of the population (Figure 20B). An explanation for this observation might be multiple DUBs that were involved in interaction with this chain.

Calculation of the sampled conformational space in the OTUB1i-diubiquitin complex revealed conformational remodeling as the binding mechanism (Figure 20C-D). The conformational distribution of the distal ubiquitin relative to the proximal in the OTUB1i complex and in the free state are superimposed in Figure 20D. This underlines that the conformational space is strongly shifted towards conformations that were previously not populated.

As a second example the interaction of K11-linked diubiquitin and OTUD7Bi was investigated by means of a single PELDOR sample to prove that significant conformational stabilization and rearrangements are also detectable for this chain type (Figure 20E). Similar effects were detected suggesting that linkage specific recognition of DUBs at the isopeptide linkage might consistently involve conformational remodeling of the chain to allow subsequent chain hydrolysis.

The availability of X-ray structures of both free K11-linked diubiquitin (Bremm et al., 2010) and OTUD7B in complex with K11-linked diubiquitin (Mevissen et al., 2016) also enable to investigate how ubiquitin are rearranged relative to each other (Figure 20F). Aligning proximal ubiquitins illustrates that the conformation of free K11-linked diubiquitin (grey) is incompatible for DUB catalysis as distal ubiquitins in both structures are reoriented. This further supports the fact that intense rearrangement take place after DUB binding.

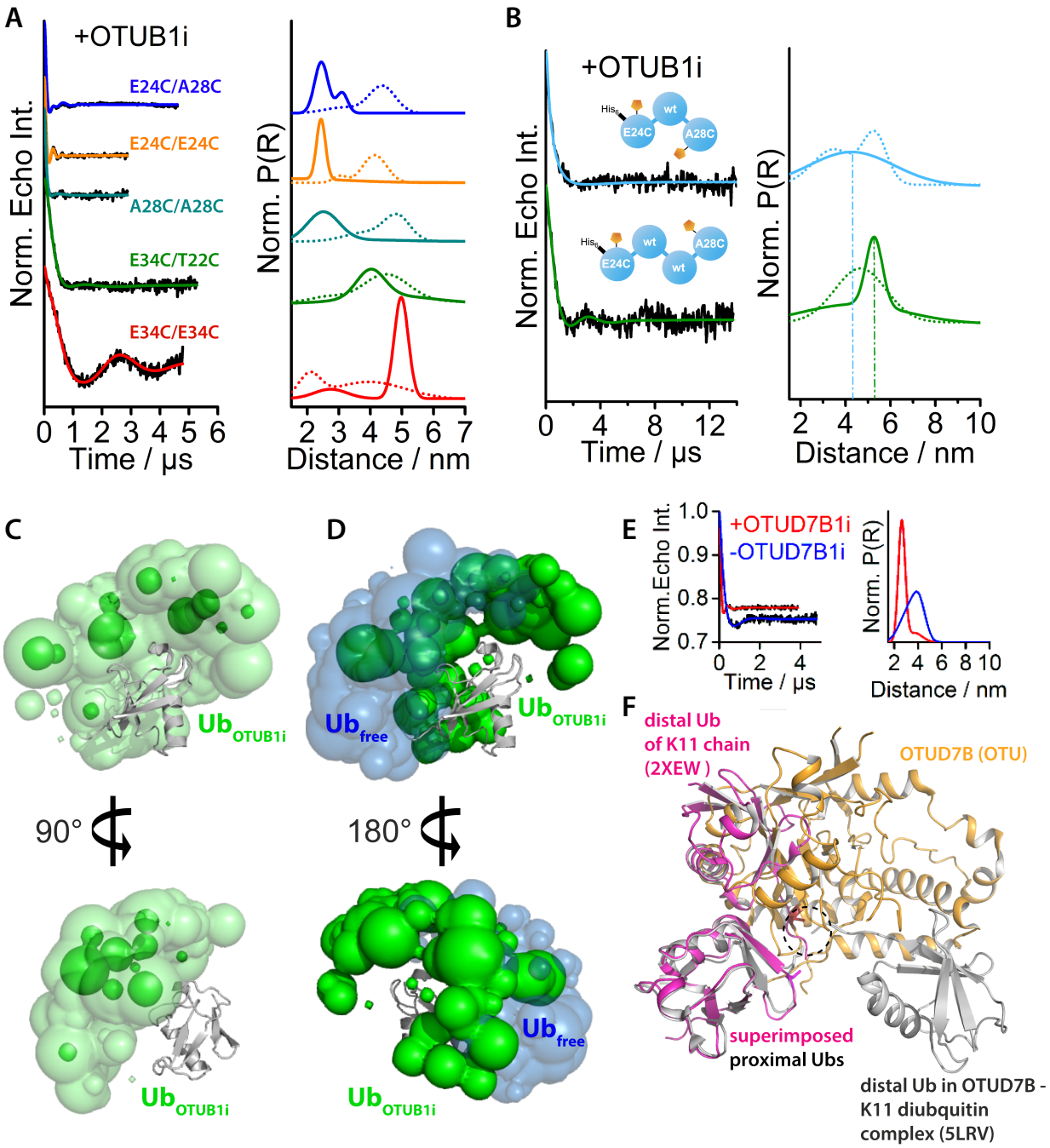

Figure 20: The effect of the DUB OTUB1 on the conformational flexibility of ubiquitin chains. (A) PELDOR time traces and obtained distance distributions of a set of five different doubly spin-labeled K48-linked chains in complex with the K48-linkage specific DUB OTUB1. Distance distributions in absence of OTUB1 are given as dotted lines. (B) Seven-pulse CP PELDOR time traces and distance distributions of indicated tri- and tetraubiquitin chains in absence (dotted) and presence of OTUB1 (solid). (C) Conformational ensemble of the distal relative to the proximal ubiquitin (grey) in a complex of K48-linked diubiquitin and OTUB1. Regions of higher probability (corresponding to a probability cutoff of 0.4) are shown in green, less probable regions (cutoff value of 0.12) are shown in light green. (D) Comparison of the conformational ensemble of free diubiquitin (blue) and in complex with OTUB1 (green) at a probability cutoff of 0.2. OTUB1 induces conformational remodeling of the sampled conformational space. (E) PELDOR time traces and determined distance distributions for K11-linked diubiquitin E24C/A28C in complex with the OTU domain of the K11-linkage specific DUB OTUD7B (Cezanne). Data measured for the complex is shown in red and data of free K11-chains is shown in blue. (F) The proximal ubiquitins in the X-ray structures of the OTUD7B-diubiquitin complex (PDB code: 5LRV) and K11-linked diubiquitin was superimposed to compare the relative orientation of the distal ubiquitin in the free and bound states. OTUD7B is colored yellow, the free form of K11-linked diubiquitin is magenta and DUB-bound diubiquitin is grey. The region where the catalytic residue OTUD7B and the K11 linkage is located is indicated by a circle. Parts of the figure were adapted from Kniss et al. 2018.

5.3. Analysis of interactions involving the E2 enzyme Ubc7

Having studied the ubiquitin chain elongation process mediated by the CUE domain of Cue1 and how the conformational space of ubiquitin chains is modulated therein, my next research project dealt with structural and function studies on the central ERAD E2 enzyme Ubc7. Gaining insights into the ubiquitination activity of Ubc7 and how it acts together with its cognate RING domains of the ERAD ubiquitin ligases Hrd1 and Doa10 is crucial to comprehensively understand the efficient ubiquitination machinery in the ERAD process.
A previous study has solved the structure of Ubc7 in complex with the U7BR of Cue1 by X-ray crystallography, however, protein stability issues precluded the NMR assignment of all residues of Ubc7 that is required for detailed NMR-based analyses (Metzger et al., 2013).

This project was a collaborative research project with the group of Thomas Sommer from the Max-Delbrück-Centrum in Berlin. I performed all structural analyses, whereas ubiquitination assays were conducted together with Lukas Pluska.

5.3.1. Optimization of Hrd1 and Ubc7 constructs for NMR studies

In order to study how the two cognate RING domains of Hrd1 and Doa10 interact with Ubc7 and compare their activity, I generated a variety of different Hrd1, Ubc7 and Doa10 constructs. The initial aim was to find RING domain constructs that retain activity but lack unstructured regions that would interfere with NMR studies and have a high long-term stability at 30°C.
Poor solubility and low stability of Ubc7 was circumvented by generating a single chain construct comprising full length Ubc7 followed by a diglycine linker and the U7BR of Cue1 (147-203, C147S). This construct was called Ubc7-U7BR. The U7BR is a unique E2-binding region that recognizes the back side of the E2 enzyme and dramatically increased the *in vitro* stability of Ubc7. Interestingly, in cell stability of Ubc7 also requires association with the U7BR (Ravid and Hochstrasser, 2007).
Initial trials to obtain a backbone assignment for this 26 kDa protein, using uniformly ^{13}C, ^{15}N labeled Ubc7-U7BR failed due to poor 3D spectra for sequential backbone assignment. Hence, Ubc7-U7BR was produced fully deuterated using ^{13}C, ^{2}H glucose and ^{15}N ammonium chloride as the sole carbon and nitrogen sources, respectively. Unfortunately, some backbone amide deuterons were protected from exchange to hydrogens resulting in a variety of weak and missing signals in the HSQC spectrum. Refolding from 6M urea solved the problem. Backbone assignment was subsequently performed using a standard set of TROSY-based 3D spectra.
Optimization of the Hrd1 RING domain was performed by screening a variety of different ^{15}N-labeled Hrd1 protein constructs using HSQC experiments (Figure 21). The aim was to reduce overlap by removing unstructured regions and finally obtain a relatively stable, minimal construct. I ended up

with Hrd1 (337-412) as the best NMR construct, although the highest solubility and stability was observed for Hrd1 (325-412).

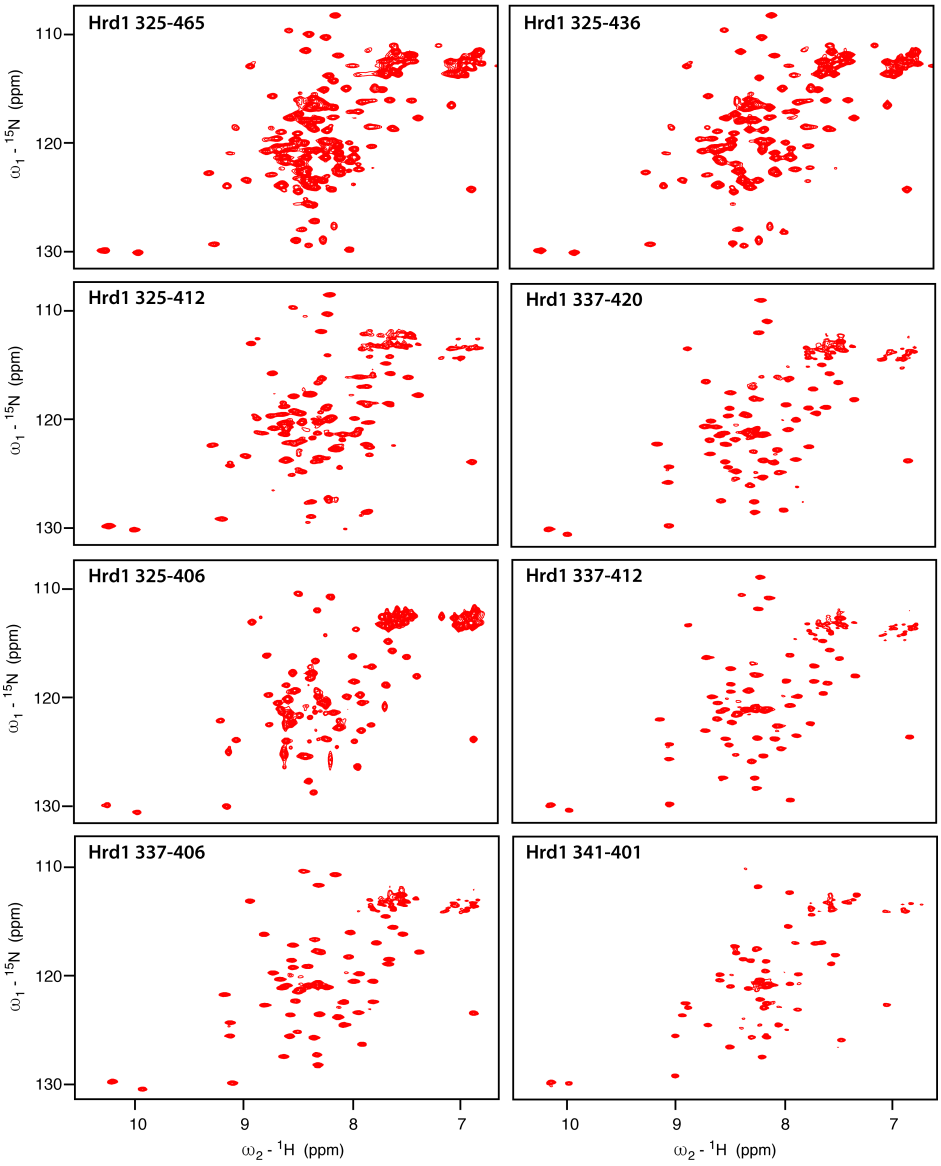

Figure 21: Construct optimization of the Hrd1 RING domain for NMR. ^{15}N,^{1}H HSQC spectra of a variety of different ^{15}N-labeled Hrd1 RING domain constructs that were generated in order to find an optimal NMR construct in terms of signal dispersion and long-term sample stability. For instance, Hrd1 (325-465) has a crowded HSQC spectrum with strong overlap in the central region of the spectrum indicative of a large extent of unstructured regions within this domain construct. Hrd1 (337-412) was selected for structural studies since it showed well dispersed signals and was relatively stable at the experimental conditions.

For the Doa10 RING domain, construct design was based on the previously determined structure by Lim and Son (2014; PDB code: 2M6M) and comprised residues 19 to 101.

Backbone assignments of both RING domains were performed using a standard set of TROSY-based 3D spectra under the same experimental conditions as established for Ubc7-U7BR.

5.3.2. Activity and structural differences between Hrd1 and Doa10 RING domains

Ubc7 and Cue1 are central components of the ubiquitination machinery of both membrane embedded HRD1 and DOA10 ERAD E3 ubiquitin ligase complexes. Regulative mechanisms that impact Ubc7 activity are essential for highly processive ubiquitin chain formation and for effective ERAD substrate turnover. Both E3 ligases target a discrete set of ERAD substrates with potential differential requirements to the ubiquitination machinery. A previous study has shown that a mutation in helix α2 of Ubc7 (K118R) results in differential activation by both RING domains. *In vivo* degradation of a Doa10-dependent substrate was affected, while no apparent effect was measured for Hrd1-dependent substrates suggesting that distinct regulatory mechanisms exist (Cohen et al., 2015).

In order to gain a better understanding of the formed E2-E3 complexes comparative NMR titration experiments were performed. A ^{2}H, ^{15}N-labeled Ubc7-U7BR single chain construct was both titrated with Hrd1 and Doa10 RING domains until complex saturation (Figure 22A-B). Both interactions showed a fast exchange behavior with high complex on- and off-rates indicative of weak interactions in the high µM range. Since a 20-fold molar excess of Doa10 was required to approach the saturation point, this interaction seemed to be significantly weaker. Analysis of the chemical shift perturbations (CSP) revealed that binding only affected a small set of distinct residues while many residues were completely unaffected. This suggests that the conformational movements of Ubc7 upon RING association are limited to a few regions (Figure 22C). However, surface mapping of all Ubc7-U7BR residues that undergo significant changes upon Hrd1 interaction revealed three distinct sites: Firstly, a surface involving the β3β4 loop and parts of the β4α2 connecting loop that represents the Hrd1 interaction site based on other known E2-E3 complexes (Das et al., 2013), secondly, a region adjacent to the catalytic cysteine that includes I92 and thirdly the Ubc7-U7BR interface (Figure 22D). Allosteric effects that occur between RING and U7BR binding sites have been previously observed (Das et al., 2013; Metzger et al., 2013) and may provide a rationale for shifts induced at the Ubc7-U7BR interface. The revealed binding surface of Doa10 is largely overlapping with the Hrd1 binding site, but still CSP analysis showed some uniquely affected residues for either interaction. For instance, Hrd1 caused shifts for backbone amides of also K62 and D63 (in the β3β4), while they remained completely unchanged for the Doa10 interaction. Conversely, the backbone amide of V116 (located at the N-terminal end of helix α2) was only affected by Doa10 and not by Hrd1.

Most importantly, differences between RING titrations occurred at a region adjacent to the catalytic cysteine (Figure 22C-E). In particular, I92, a residue in proximity to the catalytic cysteine C89, experienced an enormous shift upon titration with the Hrd1 RING domain and remained largely unchanged upon titration of Doa10 RING (Figure 23). This suggests that Hrd1 is able to induce additional conformational changes around the catalytic center, whereas Doa10 is unable to do so.

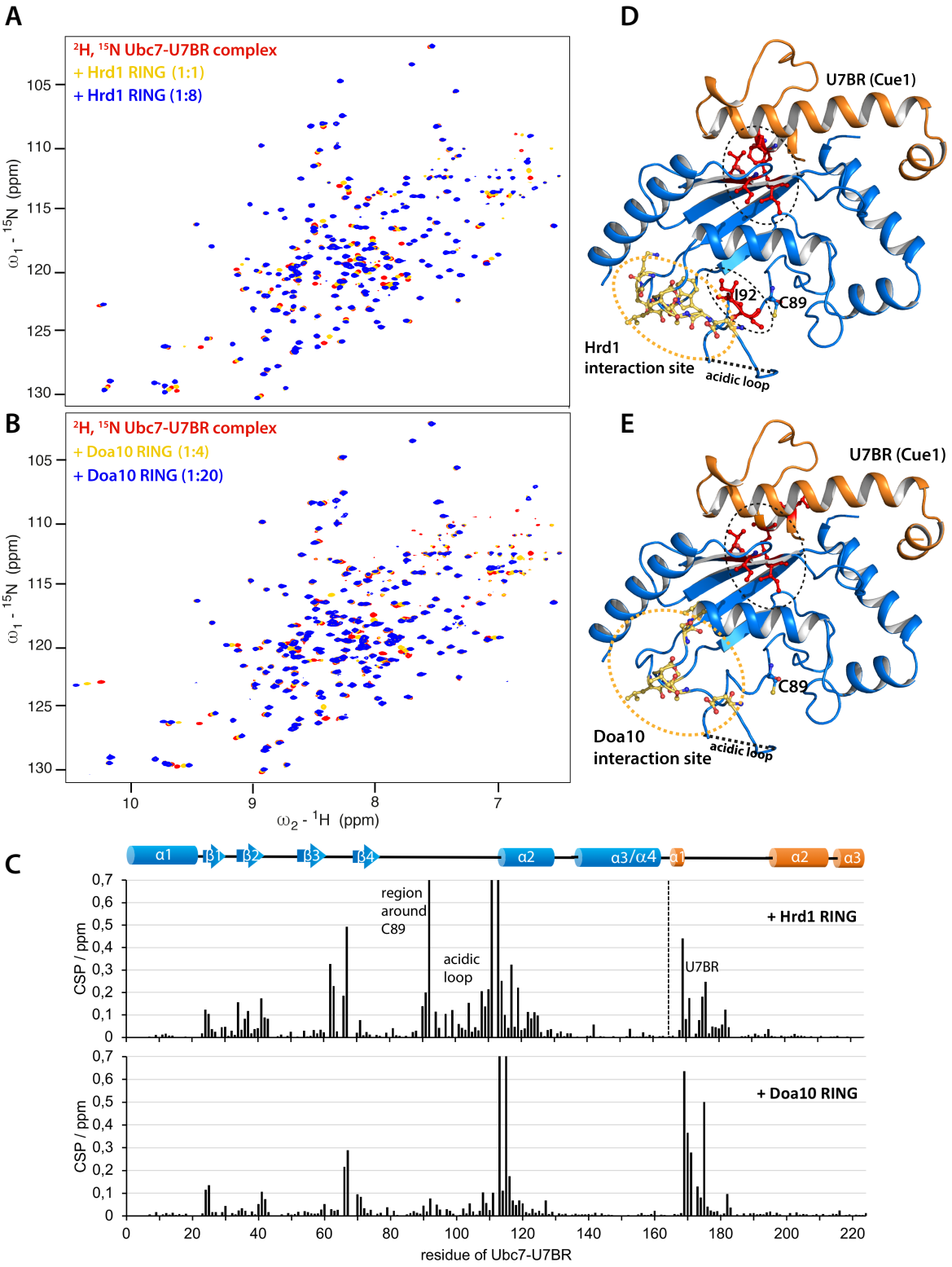

Figure 22: Comparison of NMR titrations of Ubc7-U7BR with Hrd1 and Doa10 RING domains. (A) NMR titration experiments of ^{2}H, ^{15}N-labeled Ubc7-U7BR single chain construct and Hrd1 RING domain. [^{15}N,^{1}H]-TROSY HSQC spectra in absence (red) and presence of the Hrd1 RING domain (325-412) are overlaid. The spectrum of the saturated complex (eight-fold molar excess) is shown in blue, while the spectrum at equimolar concentrations of both interaction partners is shown in yellow. (B) NMR titration experiments of ^{2}H, ^{15}N-labeled Ubc7-U7BR and the Doa10 RING domain (19-101). Color code is similar as in A. 20-fold molar excess of Doa10 RING domain was required to saturate Ubc7-U7BR. (C) Comparative chemical shift perturbation analysis of Ubc7-U7BR residues upon interaction with Hrd1 and Doa10 RING domains. (D) Mapping of the affected residues upon Hrd1 RING titration onto the crystal structure of the Ubc7-U7BR complex (PDB code: 4JQU). Residues form three distinct sites: a surface involving the β3β4 and β4α2 loops (yellow), a region adjacent to the catalytic cysteine (I92, red) and the Ubc7-U7BR interface (also shown in red). (E) Mapping of significantly affected residues upon Doa10 RING titration onto Ubc7-U7BR. Affected residues also locate at a surface involving the β3β4 and β4α2 loops (yellow) and at the Ubc7-U7BR interface (red) but do not include a region adjacent to the catalytic cysteine.

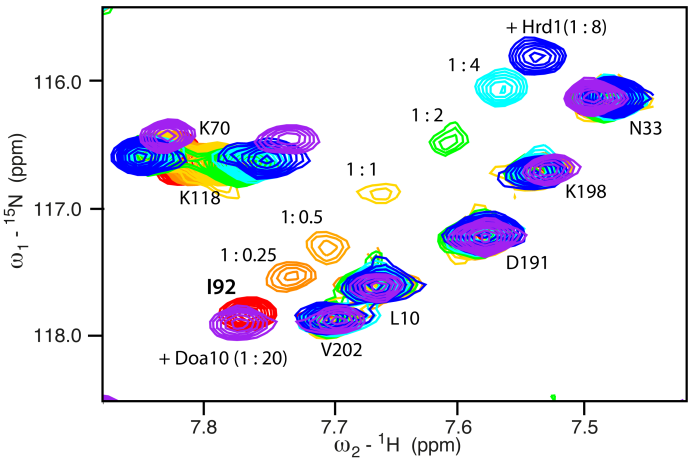

Figure 23: HSQC spectra of Ubc7-U7BR showing the titration behavior of I92. Overlay of sections from [^{15}N,^{1}H]-TROSY HSQC spectra of ^{2}H, ^{15}N-labeled Ubc7-U7BR (0.2 mM) showing the backbone amide resonance of I92. Spectra were recorded at indicated molar ratios of the Hrd1 RING domain. The reference spectrum is shown in red. For comparison the spectrum at 20-fold molar excess of Doa10 RING domain (4 mM) is additionally overlaid (purple) and reveals that I92 remains unaffected upon Doa10 interaction. I92 is located in close proximity to the catalytic cysteine C89.

Likewise, the acidic loop that was shown to be involved in aligning the K48 residue with the donor ubiquitin for the E2 Cdc34 (Chong et al., 2014), experienced more pronounced shifts for the Hrd1 interaction.

In order to shed more light into the structural and functional differences among these two RING domains I solved the NMR solution structure of a Hrd1 RING domain construct comprising residues 337 to 412 (Figure 24). To this end, the protein was expressed in ^{13}C,^{15}N-labeled form and all backbone and side chain resonances assigned manually by the help of a standard set of TROSY-based triple resonance experiments. In total 808 resonances were assigned. Distance restraints were derived from ^{15}N-edited as well as ^{13}C-edited NOESY HSQC spectra. The solution structure was calculated using CYANA (Guntert and Buchner, 2015; Guntert et al., 1997) based on 1440 assigned NOE distance restraints including a total of 447 long range ($|i-j| \geq 5$) restraints, 82 dihedral angle restraints (φ/ψ) derived from TALOS+ software (Shen et al., 2009) and 32 restraints for zinc coordination (Table 7 in the appendix). The structure ensemble of the Hrd1 RING domain shows a C3H1-type zinc finger protein. The first zinc ion is complexed by side chains of C349, C352, C385 and H382. The second zinc ion is hold in place by side chains of C377, H379, C396 and C399 (Figure 24A). Comparison to the Doa10 RING structure shows that the helix as well as the zinc coordinating residues are well conserved (Figure 24B). Unlike Doa10, Hrd1 contains a β-sheet region and completely different loop regions due to different sequence insertions as revealed by a multiple sequence alignment shown in Figure 24D. The RING domain of the mammalian E3 ligase gp78 is more similar to Hrd1 although the sequence insertion after the first two zinc coordinating cysteines also predetermines a different loop organization in Hrd1 (Figure 24C-D).

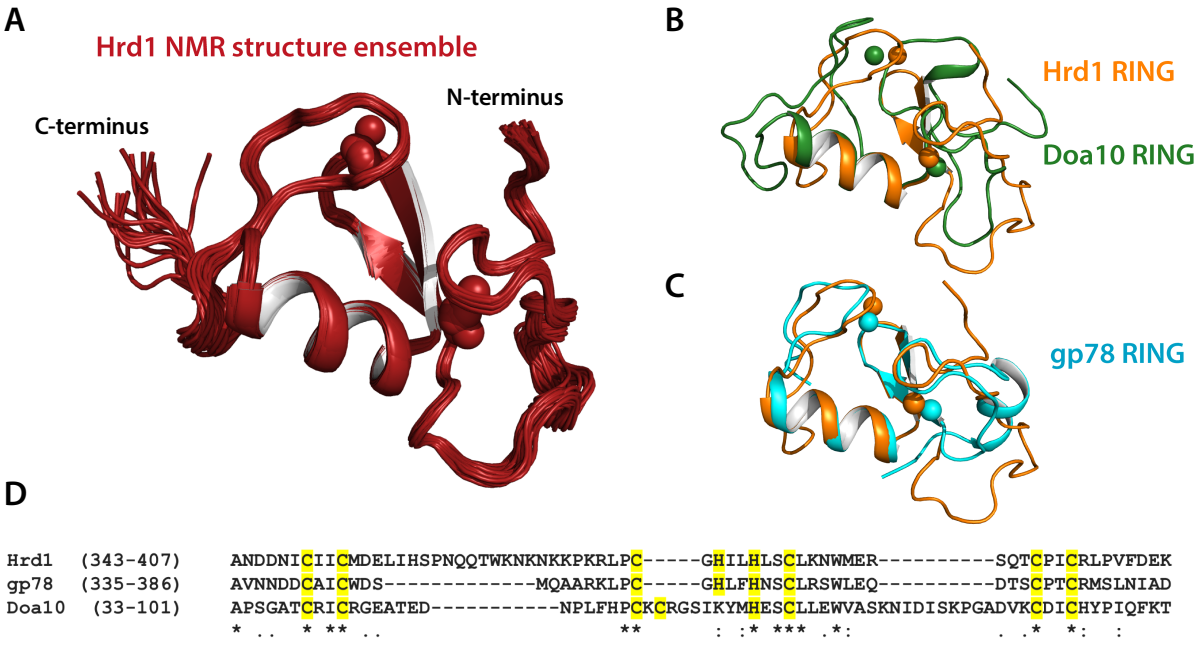

Figure 24: Solution NMR structure of the Hrd1 RING domain. (A) NMR structure ensemble of the Hrd1 RING domain. The NMR construct comprised residues 337-412. The cartoon representation includes residues 344-412, since the seven N-terminal residues were not defined in the structure bundle. Two zinc ions are bound per molecule by C3H1-motifs and shown as spheres. (B) Structural comparison of the Hrd1 (orange) and Doa10 RING domains (PDB code: 2M6M, green). Unlike the Hrd1 RING domain, Doa10 RING domain contains no β-sheet regions. (C) Structural comparison of the Hrd1 and the gp78 RING domain. The structures are largely similar regarding the zinc finger structure but differ in the loop regions. (D) Multiple sequence alignment of Hrd1, Doa10 and gp78 RING domains. Cysteine and histidine residues that are involved in complexing zinc are highlighted and well conserved. Hrd1 contains a unique insertion after the first two cysteines.

With this structure at hand I intended to analyze the impact of RING domains on ubiquitin chain elongation in more detail. In the employed fluorescence-based ubiquitin chain elongation assay preassembled diubiquitin served as acceptor for fluorescently labeled monoubiquitins (Figure 25A). The reaction mixtures additionally contained E1, ATP, Ubc7-U7BR and different RING domain constructs. A similar reaction has been previously established (von Delbrück et al., 2016). A control reaction lacking RING domains showed only slight accumulation of the desired triubiquitin elongation product (Figure 25B). As expected Doa10 RING and Hrd1 RING domains lead to a significant acceleration of this process with Hrd1 RING domain constructs being consistently more active (Figure 25 B-C). Notably, reactions employing the entire cytoplasmic fragment of Hrd1 directly following the last transmembrane region (Schoebel et al., 2017) also showed some RING auto-ubiquitination. Removal of amino acids 466-551 abolished RING autoubiquitination suggesting that at least in this *in vitro* assay auto-ubiquitination occurs at the c-terminal end of the protein and not within the RING domain which contains 7 lysine residues (366, 368, 370, 371, 373, 387, 407). Hrd1 autoubiquitination at the C-terminal tail (residues 511, 518, 539, 540, 546) of Hrd1 has been previously observed *in vitro*. In addition it has been shown that polyubiquitinated Hrd1 recruits the Cdc48 complex that is required for substrate extraction (Stein et al., 2014).

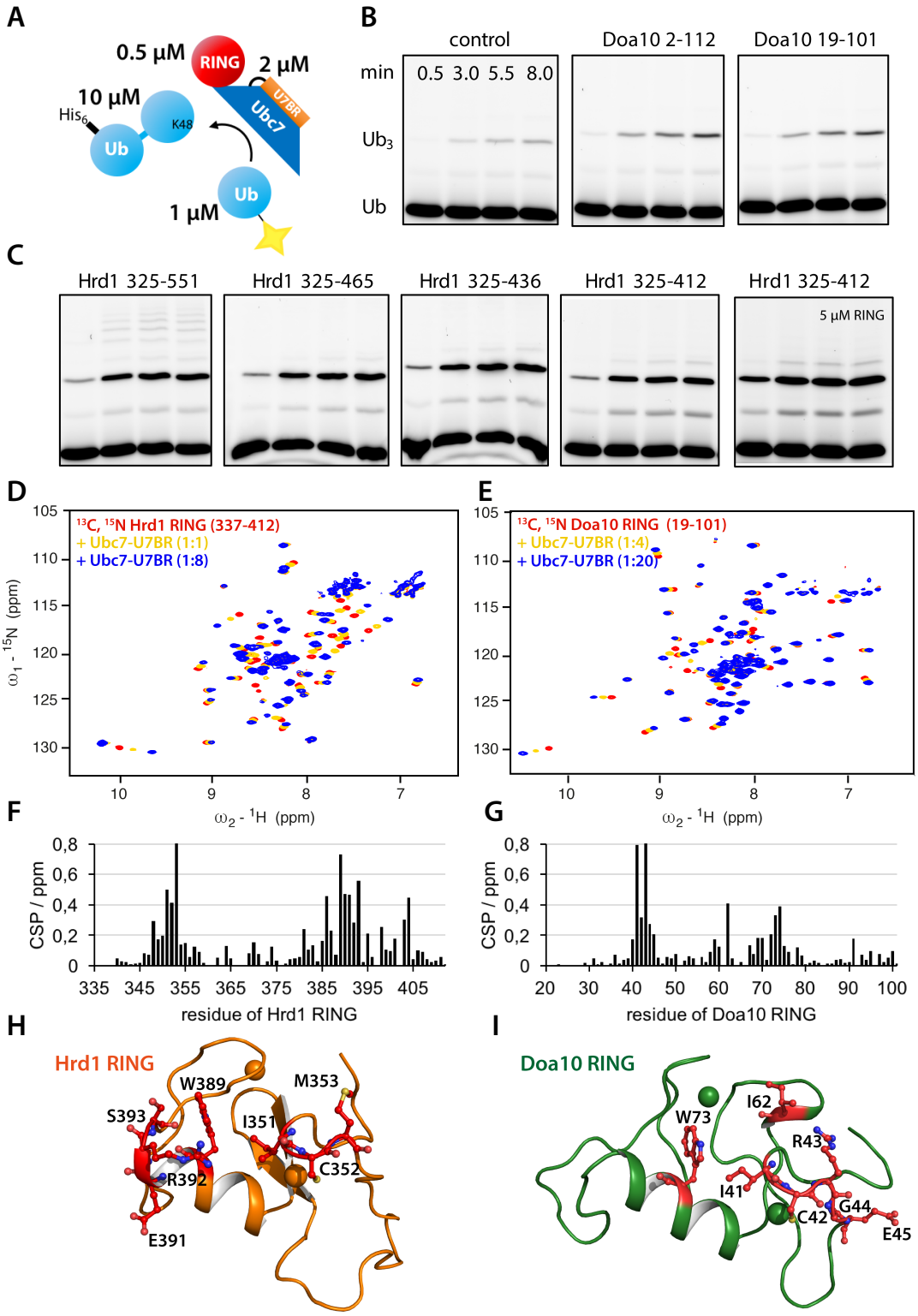

Figure 25: Activity and structural differences between Hrd1 and Doa10 RING domains. (A) Schematic depiction of the fluorescence-based ubiquitin chain elongation assay. Preassembled diubiquitin served as acceptor in single turnover elongation reactions using fluorescently labeled ubiquitin. The Ubc7-U7BR single chain construct was used as E2. The assay was performed together with Lukas Pluska. Concentrations of important reaction components are indicated. E1 concentration was 0.2 µM. (B) Fluorescence scan of SDS-PAGE separated reactions that were stopped at indicated time points. The control reaction as well as reactions in presence of two different Doa10 RING domain constructs are shown. (C) Fluorescence scans as in B, but for reactions employing Hrd1 RING domain constructs. The last reaction contained a higher RING concentration of 5 µM. (D) NMR titration experiment of ^{13}C,^{15}N-labeled Hrd1 RING (337-412) and Ubc7-U7BR. HSQC spectra were recorded at different molar ratios (1:0, 1:1 and 1:8). (E) NMR titration experiment of ^{13}C,^{15}N-labeled Doa10 RING (19-101) and Ubc7-U7BR. HSQC spectra were recorded at different molar ratios (1:0, 1:4 and 1:20). (F) CSP analysis of the residues of the Hrd1 RING domain upon Ubc7-U7BR interaction. (G) CSP analysis as in F, but for the Doa10 RING. (H) Mapping of the significantly affected, solvent exposed residues onto the Hrd1 NMR structure. (I) Mapping of the significantly affected, solvent exposed residues onto the NMR structure of the Doa10 RING domain (PDB code: 2M6M).

NMR titration experiments were performed to determine the interaction surface on the structure of both RING domains (Figure 25D-I). For both interactions a fast exchange regime was identified. Hrd1 contacts Ubc7 by using a mainly hydrophobic surface formed by I351, C352, M353, W389, R392, and S393 (Figure 25 F, H). Doa10 RING domain interacts with a patch that includes I41, C42, R43, G44, E45, I62 and W73. Again, the titration that involved the Doa10 RING domain and Ubc7-U7BR revealed the weaker interaction as a 20-fold excess of Ubc7-U7BR was required to approach saturation.
These different binding affinities correlate well with the observed activity difference observed in the fluorescence-based chain elongation assay (Figure 25 A-B). Quantification of RING domain enhanced reactions yielded a ~7-fold acceleration for the Doa10 RING and a ~28-fold acceleration for the Hrd1 RING domain in Ubc7-catalyzed diubiquitin elongation reactions (Figure 26).

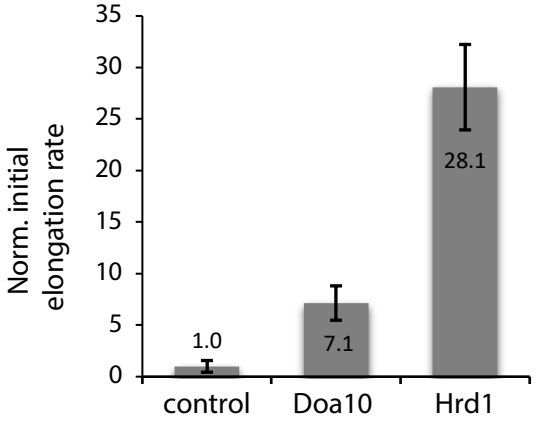

Figure 26: Quantification of elongation acceleration by Doa10 and Hrd1 RING domains. Doa10 19-101 (1 µM) and Hrd1 325-412 (1 µM) constructs were used to measure acceleration of chain elongation catalyzed by Ubc7-U7BR in a reaction setup similar to the assay in Figure 25A except for the indicated RING concentrations. Data was normalized to a reaction in absence of RING domains. The kinetic measurements were performed by Lukas Pluska.

5.3.3. HADDOCK model of the Ubc7-U7BR-Hrd1(RING) complex

To gain more detailed structural insights into the highly active Ubc7-U7BR-Hrd1(RING) complex I calculated a structural model using the HADDOCK software (de Vries et al., 2010; van Zundert et al., 2016) based on the NMR titration data (Figure 27). The RING domain occupies the conventional RING binding site similar to previously determined E2-E3 complexes (Das et al., 2013). An arginine residue on Hrd1 that is conserved among many RING domains (R400 in Hrd1, R379 in gp78RING) is contacting two glutamate residues (E107 and E108) on Ubc7 thereby providing a direct connection to this important loop region in proximity to the catalytic site. In addition the involvement of this arginine in forming contacts to also the donor ubiquitin has been shown for example for UbcH5A and RNF4 (Plechanovova et al., 2012) as well as for Ube2g2 and gp78 (Das et al., 2013). Interestingly, this arginine is absent in the Doa10 RING domain that features a histidine residue at this position (Figure 24D). This may provide a hint for the weaker effect in promoting Ubc7 activity.

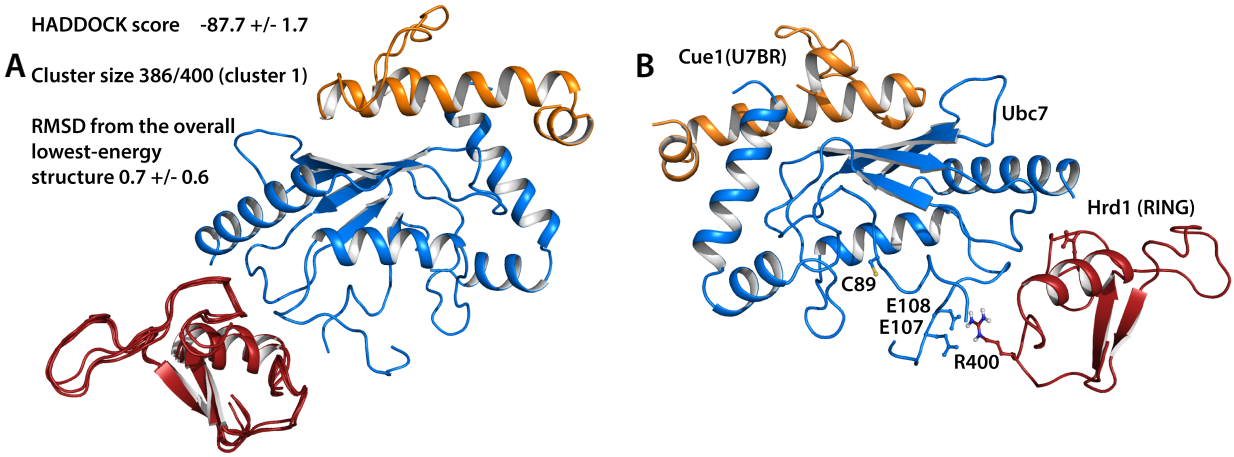

Figure 27: HADDOCK model of the Ubc7-U7BR-Hrd1(RING) complex. (A) Three representative structures of cluster 1 are aligned and reveal that the orientation of Hrd1 onto Ubc7 is well defined. (B) A conserved arginine residue (R400) in the Hrd1 RING domain is pointing towards two glutamate residues on Ubc7. This region is in proximity to the catalytic cysteine C89.

5.3.4. Investigation of the interaction between the donor ubiquitin and Ubc7

E2 enzymes mainly exist as E2~Ub thioester conjugates in the cell (Siepmann et al., 2003). Since this linkage is mediated by the flexible C-terminus of ubiquitin, the ubiquitin molecule can in principle sample a whole conformational space relative to the E2 enzyme. Solution studies have shown that open as well as closed conformations can be adopted and that they can differ significantly among different E2 enzymes (Pruneda et al., 2011). Closed conformations are allosterically promoted by RING domains and constitute the most active state of E2 enzymes towards a nucleophilic attack (Pruneda et al., 2012). Such a closed state has been captured in a previous study by Plechanovova et al. 2012, where the hydrophobic patch of ubiquitin interacts with the helix α2 of the E2 enzyme.

To test whether the donor ubiquitin adopts only open conformations or significantly interacts noncovalently with Ubc7 in absence of RING domains a stable Ubc7-Ub conjugate was synthesized. This was achieved by incubating a Ubc7-U7BR C89K mutant single chain construct with ATP, E1 enzyme and ubiquitin at a high pH of 10. The stable isopeptide linked ubiquitin conjugate was subsequently purified (Figure 28D). For NMR studies both ^{15}N-Ubc7-U7BR linked to unlabeled ubiquitin and unlabeled Ubc7-U7BR linked to ^{15}N-Ub conjugates were assembled. Comparison of HSQC spectra and chemical shifts relative to the non-conjugated ^{15}N-labeled proteins revealed significant chemical shift perturbations (Figure 28A, B, E) both on Ubc7-U7BR and ubiquitin. CSPs on Ubc7-U7BR were observed at distinct sites and not equally distributed around the conjugation site as would have been expected for a freely tumbling ubiquitin without any favored conformational states. Affected residues located on two adjacent sites: a region involving the α2α3 loop and helix α3, which is completely non-overlapping with the RING domain interacting surface and a region adjacent to the catalytic cysteine that also includes the acidic loop (Figure 28C).

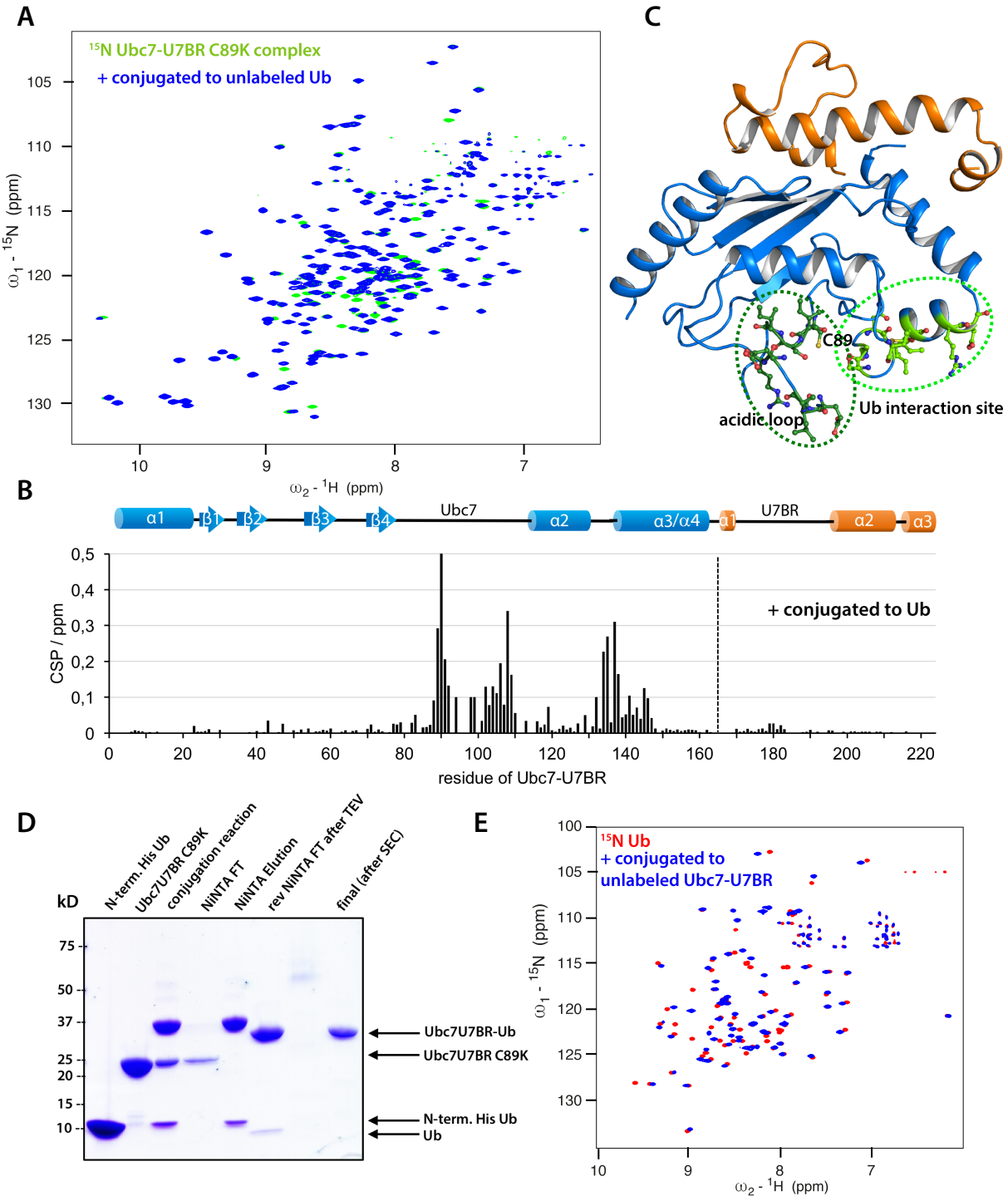

Figure 28: Interactions within the stably charged Ubc7-U7BR complex. (A) Overlay of [^{15}N,^{1}H]-TROSY HSQC spectra of ^{15}N-labeled Ubc7-U7BR C89K (green) and ^{15}N-labeled Ubc7-U7BR C89K-Ub (blue). Unlabeled ubiquitin was conjugated to the lysine residue via a stable isopeptide bond to investigate the interaction between Ubc7 and the donor ubiquitin. (B) CSP analysis of Ubc7-U7BR residues upon interaction with the donor ubiquitin. The interaction occurs on a site distinct from the RING domain interaction surface. (C) Mapping of the affected residues upon ubiquitin interaction onto the crystal structure of the Ubc7-U7BR complex (PDB code: 4JQU). Affected residues locate on two adjacent sites: a region involving the α2α3 loop and helix α3 (light green) and a region adjacent to the catalytic cysteine that also includes the acidic loop (dark green). (D) SDS-PAGE of the synthesis of a stable Ubc7-U7BR-Ub conjugate as used for NMR experiments shown in A or E. (E) Overlay of [^{15}N,^{1}H]-TROSY HSQC spectra of ^{15}N-labeled Ub (red) and Ubc7-U7BR C89K-(^{15}N-Ub) (blue). ^{15}N-labeled ubiquitin was conjugated to the lysine residue of an unlabeled Ubc7-U7BR complex.

Interestingly, no significant shifts were detected for residues in the helix α2 (Figure 28B). This suggest that this state might only be populated in presence of RING domains. In summary it can be stated that Ubc7 populates, at least to some extent, closed conformations in absence of RING domains that are distinct from the closed state that has been previously observed for RING domain complexes.

5.3.5. Ubc7 catalyzes ubiquitin dimer formation in absence of the CUE domain

It has been reported earlier that Ubc7 is also capable of forming active site linked ubiquitin chains (C89-linked chains) (Bazirgan and Hampton, 2008; Ravid and Hochstrasser, 2007). The mechanism is not known, but definitely requires a second active site in proximity in order to achieve chain formation. A possible mechanism would involve dimerization of Ubc7. Yeast two-hybrid data for Ubc7 already suggested dimerization *in vivo* (Chen et al., 1993), however, so far no *in vitro* association was detected between Ubc7 molecules. Metzger et al. (2013) proposed that potentially thioester-linked Ubc7 is required for dimerization. By contrast, dimerization of the human homologue Ube2g2 has already been reported and studied (Liu et al., 2014).

Together with Lukas Pluska I reinvestigated ubiquitin chain elongations by Ubc7-U7BR, but now employing lower E2 concentrations to increase the pool of charged E2 enzymes. Since the assay used preassembled diubiquitin as acceptor in 10-fold excess over fluorescently labeled monoubiquitin the main reaction product was triubiquitin. Strikingly lowering the E2 concentration from 2 µM to 0.3 µM resulted in an unexpected shift of the main product towards diubiquitin formation (Figure 29A). To exclude that this effect is limited to the Ubc7-U7BR single chain construct and does not occur with wild type Ubc7, the reaction was repeated using separately purified Ubc7 and the cytosolic fragment of Cue1 (Figure 29B). In absence of the U7BR ubiquitin chain formation is strongly impeded which can be attributed to the missing allosteric activation. With Cue1 RGA that contains a dysfunctional CUE domain both diubiquitin and triubiquitin formation were observed. This resembled the situation that was observed with the single chain construct Ubc7-U7BR. Addition of Cue1 bearing a functional CUE domain shifted the main product towards triubiquitin due to its positioning effect in promoting distal elongation via binding directly adjacent to it (von Delbrück et al., 2016). This fast diubiquitin formation that occurs despite a large excess of already preformed diubiquitin as acceptor, suggests a direct interaction between charged Ubc7 molecules. This provides the first *in vitro* evidence for Ubc7 dimerization. Interestingly, Ubc7 self-association seems to involve electrostatic interactions as increasing the salt concentration during ubiquitination had a significant impact on diubiquitin formation (Figure 29C). Albeit, triubiquitin formation was also slightly impaired which is most likely due to the fact that many interactions during chain formations, both for elongation of chains and formation of diubiquitin are dependent on electrostatic interactions of the various components that are involved.

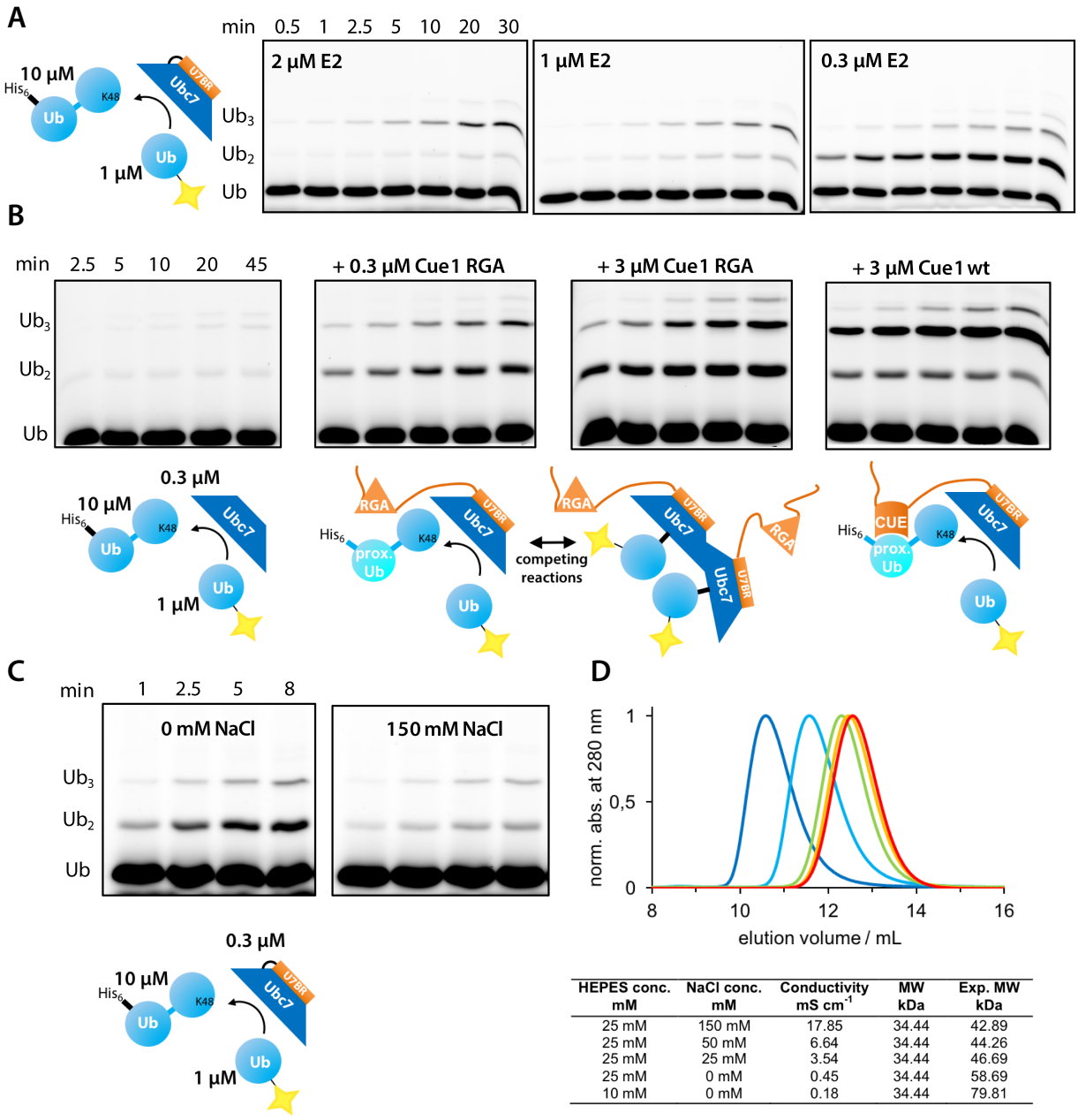

HEPES conc. mM	NaCl conc. mM	Conductivity mS cm^{-1}	MW kDa	Exp. MW kDa
25 mM	150 mM	17.85	34.44	42.89
25 mM	50 mM	6.64	34.44	44.26
25 mM	25 mM	3.54	34.44	46.69
25 mM	0 mM	0.45	34.44	58.69
10 mM	0 mM	0.18	34.44	79.81

Figure 29: Ubc7 preferentially catalyzes diubiquitin formation in absence of an active CUE domain. (A) Fluorescence based ubiquitin chain elongation assay with different E2 concentrations. Reactions contained 0.2 µM E1 and preassembled diubqiutin as acceptor in 10-fold excess over fluorescently labeled monoubiquitin. At high E2 (Ubc7-U7BR) concentration of 1 to 2 µM triubiquitin is the main product, while a lower E2 concentration (0.3 µM) stimulate the formation of a diubiquitin product. (B) Impact of Cue1 domains, CUE and U7BR, on ubiquitin chain elongation reactions. A schematic depiction of the reactions is given below each fluorescence scan. Ubc7 activity is only low in absence of the U7BR, while addition of Cue1 RGA (contains an unfolded CUE domain) results in dimer and trimer formation. Including also an active CUE domain (reaction on the right) yields primarily to the elongation product (triubiquitin). (C) Elongation reactions employing Ubc7-U7BR at high and low salt concentrations. Efficiency is lower at high salt concentrations but has more pronounced effects on the formation of the diubiquitin product suggesting E2 association based on electrostatic interactions. Ubiquitin chain elongation assays were performed together with Lukas Pluska. (D) Analytical SEC experiments of purified, stably "charged" Ubc7-U7BR (Ubc7-U7BR C89K-Ub) in buffer with different ionic strength. SEC experiments were performed on a calibrated Superdex 75 10/300 GL column. Experimentally determined molecular weights from SEC experiments are indicated in the table below the SEC profiles. Ubc7 elutes earlier with decreasing ionic strength indicative of a transient self-association based on electrostatic interactions.

Furthermore, stably charged Ubc7-U7BR-Ub exhibited a salt-dependent behavior on an analytical size exclusion chromatography column. The elution peak shifted towards lower elution volumes and thus higher molecular weights with lower ionic strength of the buffer (Figure 29D). This is indicative of the formation of transient dimers on the column.

The initial intention was now to define a Ubc7 mutant that specifically abolishes diubiquitin formation, while leaving triubiquitin formation and thus the chain elongation activity unaffected. In total 22 different mutations were introduced on solvent exposed, charged residues and tested using the fluorescence-based ubiquitination assay. Unfortunately, no convincing dimerization mutant was obtained. However, activity abolishing mutants were observed for mutations in the acidic loop (D98, D99, E103, E107, E108) as well as mutations of R109 and R145 (Figure 30). This indicates that all these residues together with the catalytic cysteine C89 are crucial for Ubc7 activity. R109 has previously been shown to contribute to K48-linkage specificity in Ube2g2 (Liu et al., 2014) by interacting with the incoming acceptor ubiquitin. The mutational analysis additionally revealed a hyper-activated mutant (D146R) that promoted both diubiquitin as well as triubiquitin formation. Notably, this residue is located close to the site were chemical shift perturbation were detected for the Ubc7-U7BR-Ub complex suggesting that donor ubiquitin interaction might be modulated by this mutation. A possible but yet unproven mechanism would be through stabilization of a distinct closed donor ubiquitin conformation with helix α3.

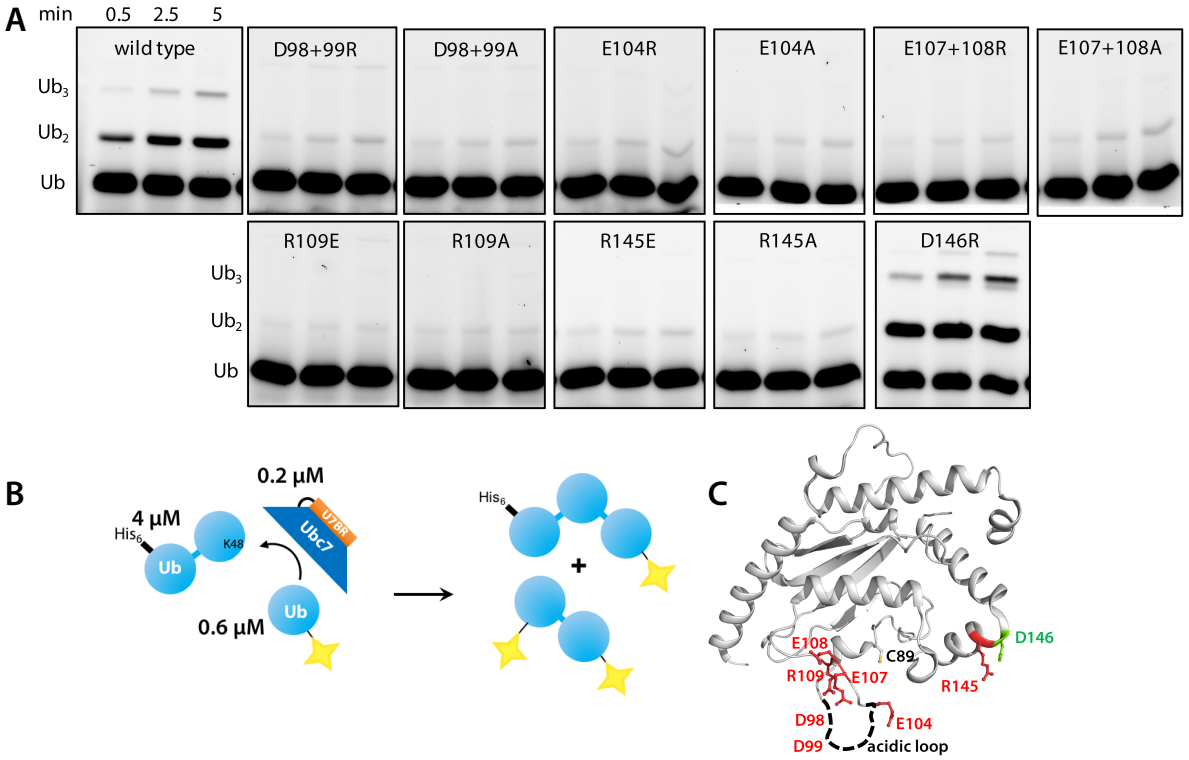

Figure 30 Mutational analysis of Ubc7-U7BR. (A) Fluorescence-based ubiquitin chain elongation assay using different Ubc7-U7BR mutants for catalysis. Mutations in the acidic loop (D98, D99, E104, E107, E108) as well as mutation of R109 and R145 result in strongly impaired reactions. The D146R mutant is hyper-activated in promoting both diubiquitin formation and diubiquitin elongation to triubiquitin. (B) Schematic overview of the assay in A. The assay was performed by Lukas Pluska using Ubc7-U7BR mutants purified by me. (C) Mapping of residues affecting ubiquitination activity of Ubc7 onto the structure of the Ubc7-U7BR complex (PDB code: 4JQU). Residues that are crucial for E2 activity are displayed in red. D146 is shown in green and can increase activity when mutated to R (charge inversion).

5.3.6. Ubc7 transiently dimerizes *in vitro*

The preferential formation of a ubiquitin dimer by Ubc7 necessitates the formation of a Ubc7 dimer during catalysis. To further characterize and prove that this dimer can transiently form *in vitro* intermolecular paramagnetic relaxation enhancement (PRE) experiments were performed. PRE-analysis offers an excellent tool to study transient low-populated intermediates in macromolecular interactions (Clore et al., 2007). States in fast exchanging systems (time scale of less than ~250-500 µs) with populations as low as 0.5–5 % can be detected (Tang et al., 2008).

Here, I used intermolecular PRE-experiments to characterize the weak transient dimerization of Ubc7. To this end I introduced spin labels at four different faces of Ubc7-U7BR to probe the interaction with ^{15}N-labeled Ubc7-U7BR. The positions S30, A106, S128 and S158 were selected (Figure 31A). In case Ubc7-U7BR self-associates signal attenuations are induced on the ^{15}N-labeled component of the dimer. PRE-experiments were conducted on samples containing 0.2 mM ^{15}N-labeled Ubc7-U7BR and a two-fold excess of a NMR invisible MTSL labeled Ubc7-U7BR variant and show that indeed transient dimeric states are populated (Figure 31B). Changing the position of the MTSL label had distinct effects on enhancing relaxation of backbone amide resonances on ^{15}N-Ubc7-U7BR (Figure 31B). Interestingly, PRE-effects were observed for the MTSL labeled S30C, A106C, and S128C mutants, whereas the S158C conjugated MTSL label showed no signal attenuation as illustrated by the overlay of BEST-[^{15}N,^{1}H]-TROSY spectra of the respective diamagnetic and paramagnetic samples. The S158C conjugated spin label was either not in proximity to the ^{15}N-labeled component in a transient dimeric complex or completely abolished dimerization. In the second scenario S158 would constitute an important part of the dimer interface. Insufficient spin labeling can be excluded since all samples were checked for successful labeling by the help of CW-EPR spectroscopy.

Residue-specific intermolecular PRE relaxation rates Γ were quantified according to Iwahara et al. (2007) and are summarized in Figure 32A. To further prove that this dimerization is mainly driven by electrostatic interactions, as previous experiments have already suggested, experiments were repeated at a lower salt concentration of 50 mM (compared to 150 mM). Quantification of both experimental sets reveal consistently higher PRE rates at lower salt concentration (Figure 32B). This proves that Ubc7 self-association is based on electrostatic contacts between both molecules.

In conclusion it was shown that Ubc7 can initiate chain formation by forming diubiquitin via a dimeric Ubc7 intermediate and can subsequently switch to processive CUE domain dependent chain elongation. Functional aspects were shown by fluorescence-based ubiquitination assays, while PRE-studies further showed transient but functionally important dimerization of Ubc7 molecules.

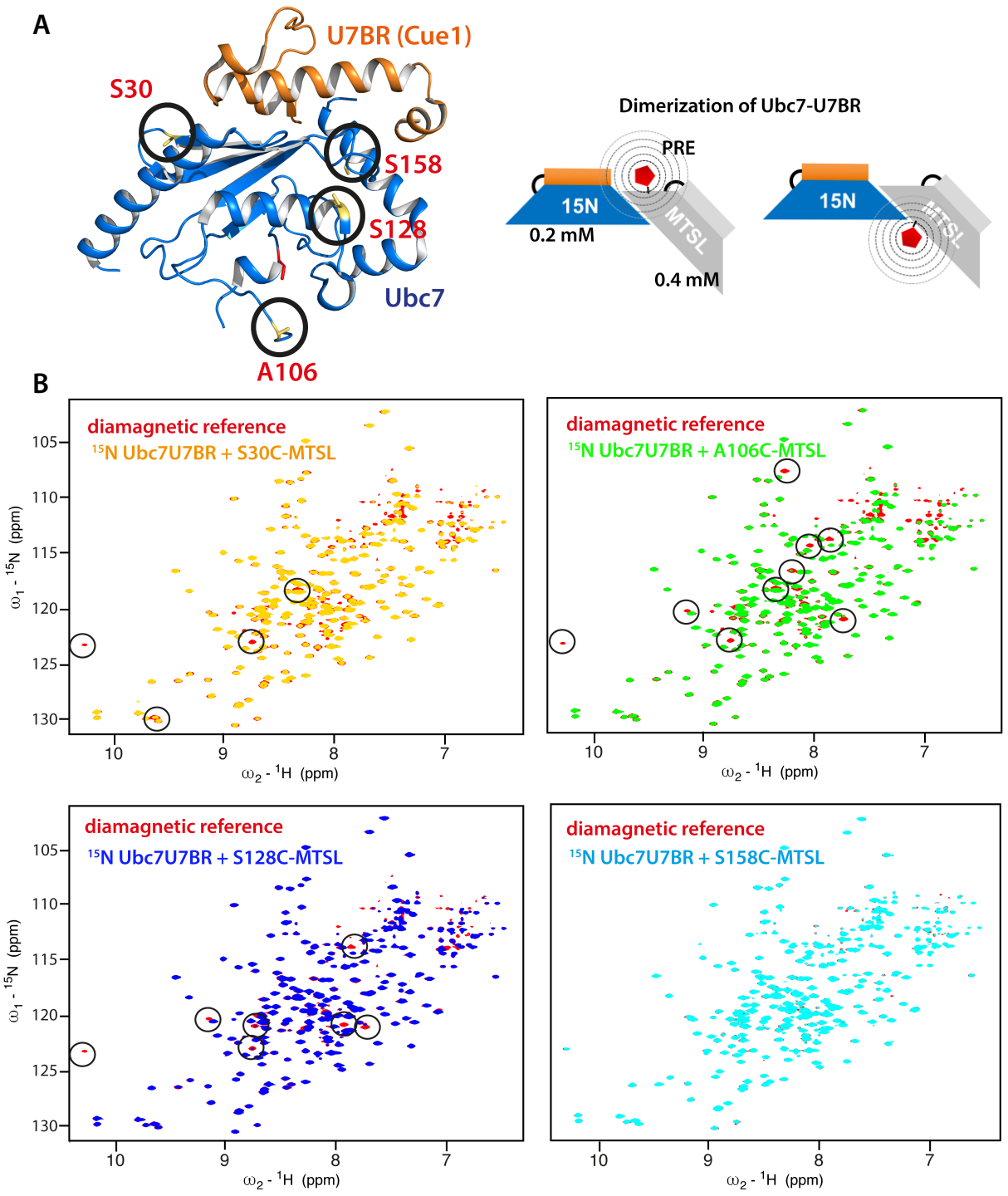

Figure 31: PRE-experiments reveal transient dimerization of Ubc7-U7BR molecules. (A) Left: Overview of the four different sites that were selected for MTSL labeling (S30, A106, S128, S158) on the structure of Ubc7-U7BR (PDB code: 4JQU). Right: Schematic depiction of the sample composition for intermolecular PRE-experiments. The paramagnetic samples included 0.2 mM ^{15}N-labeled Ubc7-U7BR and 0.4 mM MTSL labeled ^{14}N-Ubc7-U7BR. Different positions of the MTSL label should have distinct effects on enhancing relaxation of backbone amide resonances on ^{15}N Ubc7-U7BR as illustrated. (B) Overlay of BEST-[^{15}N,^{1}H]-TROSY spectra with additional spin-echo (Δ=8ms) during INEPT for a diamagnetic reference sample and different paramagnetic samples of Ubc7-U7BR. The samples were measured at a salt concentration of 150 mM. The diamagnetic reference sample contained 0.2 mM ^{15}N-labeled Ubc7-U7BR and 0.4 mM unlabeled Ubc7-U7BR. Intermolecular PRE-effects are observed for the MTSL labeled S30C, A106C and S128C mutants, whereas the S158C conjugated MTSL label is not in proximity to the second ^{15}N-labeled molecule in a transient dimeric complex or abolishes dimerization.

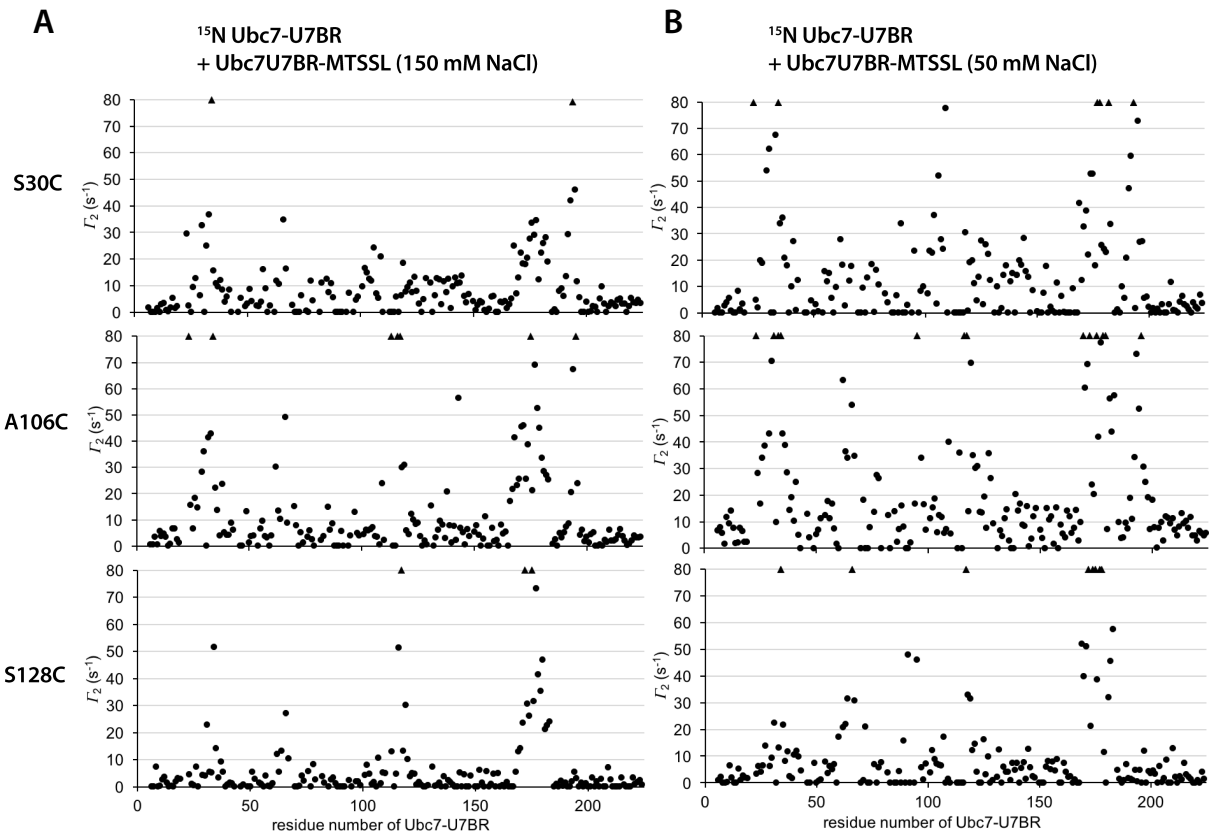

Figure 32: Quantitative analysis of the PRE-experiments on Ubc7-U7BR. (A) Residue-specific intermolecular PRE-rates (Γ_2) on the ^{15}N-labeled Ubc7-U7BR complex induced by proximity of different MTSL labeled Ubc7-U7BR mutants (circles). Measurements were performed in presence of 150 mM NaCl. Cysteines were introduced at indicated positions. Rates for peaks that completely disappeared in the spectrum of the paramagnetic samples are shown as triangles and have an arbitrary value of 80 s^{-1}. (B) Residue-specific intermolecular PRE-rates (Γ_2) as in A, but measured at a lower NaCl concentration of 50 mM. Decreasing the salt concentration enhances the observed PRE-effects.

5.4. Structural analysis of glycan recognition by the MRH domain of Yos9 within ERAD

The lectin Yos9 locates in the lumen of the ER and is involved in recognition of terminally misfolded proteins in the ERAD process. It contains a mannose 6-phoshate receptor homology (MRH) domain that mediates carbohydrate binding as well as a dimerization domain (DD), followed by a largely unstructured region. In a previous study it was shown that Hrd3 binding was mediated by a Yos9 MRH fragment (Hanna et al., 2012). A different study has also suggested that Yos9 is additionally involved in binding to unfolded protein species independent of a glycan structure (Smith et al., 2014). However, Yos9 formed insoluble aggregates during NMR titration experiments using a labeled unfolded model protein in this study.

This project was a collaborative research project with Thomas Sommer and Ernst Jarosch from the Max-Delbrück-Centrum in Berlin. In this context, I established and performed structural and interaction studies on the MRH domain of Yos9 by NMR.

5.4.1. Optimization of Yos9 MRH domain constructs for structural studies

So far, structural studies of Yos9 were limited to the dimerization domain of Yos9. I started by establishing and optimizing the protein expression and purification protocol for the production of mg quantities of the correctly folded disulfide bond containing MRH domain of Yos9. Different constructs encompassing the predicted MRH domain were cloned and subsequently expressed and purified as His6-GB1-, His6-MBP- and His10-Ub-tagged versions and the final compared of TEV-cleaved pure proteins. Although soluble expression was possible using SHuffle® T7 Express Competent *E. coli,* it only yielded poor results compared to insoluble expression and refolding using an oxidative *in vitro* refolding protocol to allow correct disulfide bond formation.
Correct sequence boundaries of the Yos9 MRH domain and thus the optimal NMR construct was determined by screening a variety of different ^{15}N-labeled Yos9 protein constructs by HSQC experiments. Guided by a sequence alignment with the MRH domain of its human homologue OS-9, which was solved by X-ray crystallography, a construct comprising residues 115 to 240 should have been sufficient. Notably, secondary structure predictions were indicative of an additional helical region directly preceding the MRH domain of Yos9. Thus, a set of different N- and C-terminally elongated version of the core MRH domain was investigated by NMR (Figure 33). This revealed Yos9 (90-249) as the minimal MRH domain construct, since further N- or C-terminally shortened versions affected a significant number of chemical shifts indicating that these regions additionally interact with the core β-sheet structure. The region between residues 249 and 262 is dispensable, since the removal of these 13 amino acids induces no chemical shift perturbations in the MRH domain. A construct encompassing also the region that is N-terminal of the predicted MRH domain Yos9 (32-

249) added only peaks with low chemical shift dispersion to the spectrum of Yos9 (90-249) thereby suggesting that this region is largely unstructured and not interacting with the MRH core structure (Figure 34). The domain organization of Yos9 is also summarized in the same figure including the already known structure of the Yos9 DD domain.

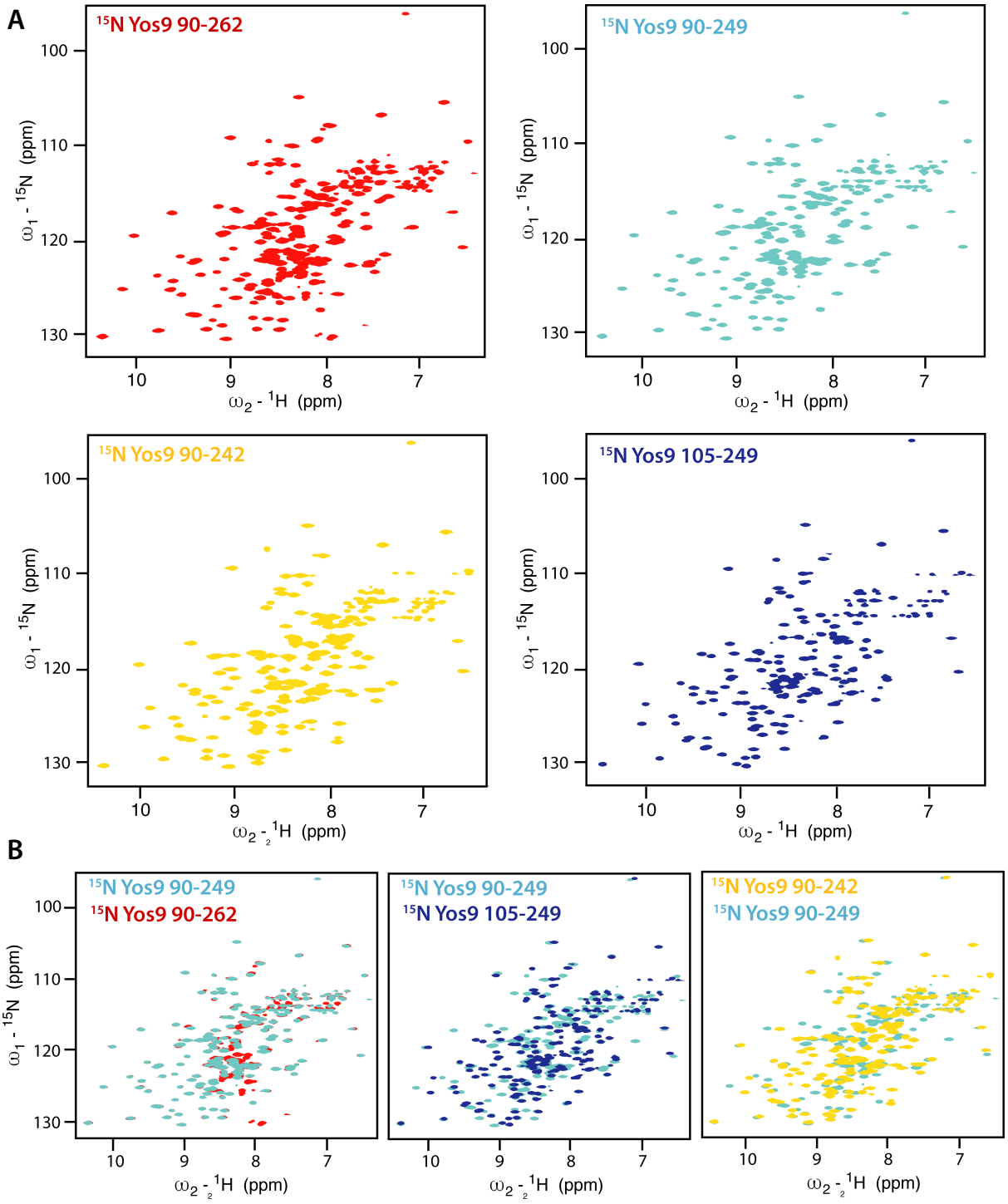

Figure 33: Construct optimization of the Yos9 MRH domain for NMR. (A) [^{15}N,^{1}H]-TROSY HSQC spectra of ^{15}N-labeled Yos9 MRH domain constructs 90-262, 90-249, 90-242 and 105-249. The spectra show well dispersed signals except for the construct 90-262 which has significant overlap in the central region of the spectrum. Yos9 (90-249) was identified as the optimal NMR construct (B) Pairwise superimposition of HSQC spectra of different Yos9 constructs with the spectrum of the optimal Yos9 (90-249) construct. Removal of residues 250-262 results in no detectable chemical shift perturbations (left), whereas removal of residues 90-104 or residues 243-249 induced significant chemical shift perturbations in the entire MRH domain. This shows that these regions are folded and associated with the MRH core structure.

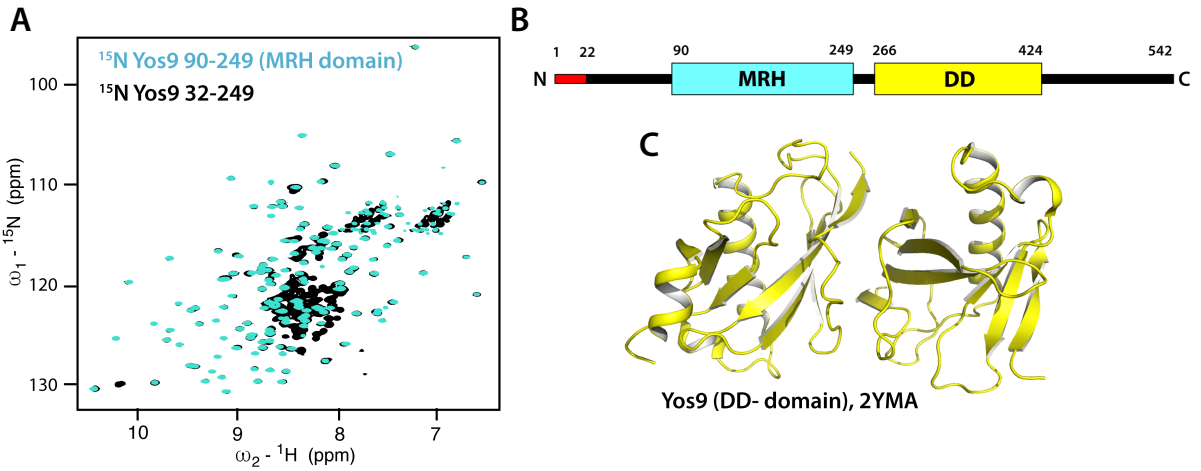

Figure 34: HSQC spectrum of Yos9 (32-249) and domain organization of Yos9. (A) Overlay of HSQC spectra of Yos9 (32-249) and Yos9 (90-249). (B) Domain organization of full-length Yos9. The signal sequence for ER import is shown in red. This region is followed by an unstructured N-terminal region, the MRH domain, a short linker, the DD domain and a largely unstructured C-terminal domain. (C) Structure of the Yos9 dimerization domain (DD). PDB code: 2YMA (Hanna et al., 2012).

5.4.2. Glycan binding to the MRH domain of Yos9 results in structural rearrangements of the β-barrel structure

Subsequently, the optimized Yos9 (90-249) construct was expressed in ^{13}C,^{15}N-labeled form and all backbone and side chain resonances assigned manually by the help of a standard set of TROSY-based triple resonance experiments. In total 1626 resonances were assigned. Distance restraints were derived from ^{15}N-edited as well as ^{13}C-edited NOESY HSQC spectra. The solution structure of the free MRH domain was calculated using CYANA (Guntert and Buchner, 2015; Guntert et al., 1997). The calculation was based on 3610 assigned NOE distance restraints including a total of 1368 long range ($|i-j| \geq 5$) restraints and 250 dihedral angle restraints (φ/ψ) derived from TALOS+ software (Shen et al., 2009) (Table 8 in the appendix). Interestingly, addition of a glycan mimicking carbohydrate (3α, 6α-mannopentaose), which exposes a terminal α1,6-linked mannose residue resulted in significant shifts of almost all backbone amide resonances. In the following, I also determined the structure of Yos9 in a saturated complex by NMR to define the structural rearrangements in Yos9 upon glycan binding. The structure of the bound conformation of the Yos9 MRH domain was based on 3885 NOE distance restraints (1549 long range restraints) and 248 dihedral angle restraints (Table 9 in the appendix). Both structure ensembles are superimposed in Figure 35 A and B and are well-defined and tight except for the β3β4 loop region (residues 141-155). However, they represent distinct states with reoriented loops (Figure 35B). The Yos9 MRH domain features a β-barrel structure similar to its human homologue OS-9, however contains two helical regions that frame and stabilize the core β-barrel (Figure 35C). In particular, the N-terminally located helix α1 is 22 amino acids long and lies directly on one face of the β-barrel thereby restricting the arrangement of the nine β-strands. Regarding the β-barrel, the most significant structural difference is the completely different

arrangement of β5 and β6 (Figure 35E). However, the glycan interaction surface on one opening of the β-barrel is largely conserved in sequence and structure between Yos9 and OS-9 (Figure 35D). The largest difference in Yos9 in proximity to the glycan binding site is its elongated β3β4 loop.

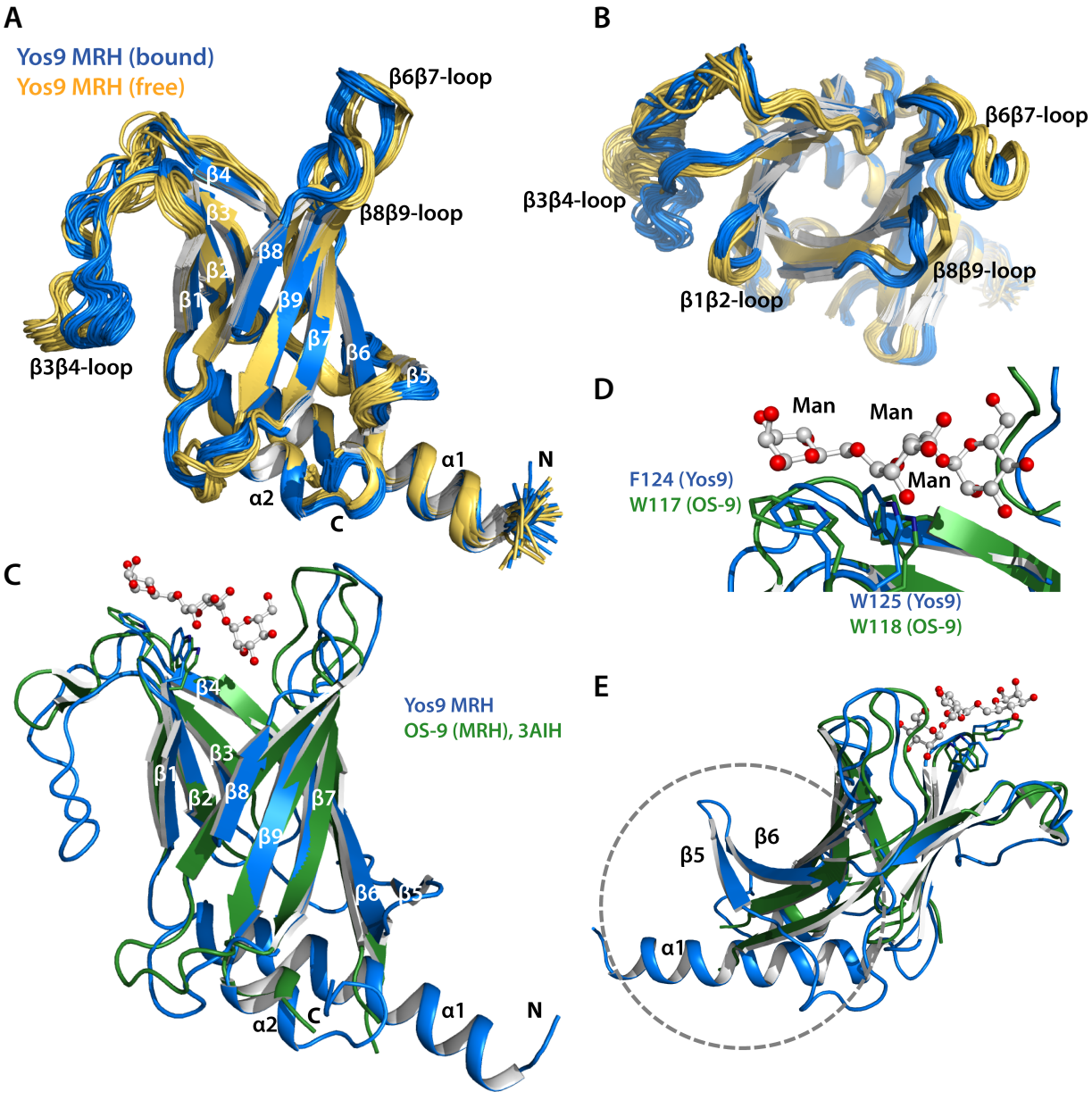

Figure 35: Glycan binding results in a conformational change of Yos9 and comparison of Yos9 and OS-9 MRH domains. (A) Superimposition of the NMR solution structure ensemble for Yos9 (20 structures) in its two conformational states, free (yellow) and bound to 3α, 6α-mannopentaose (blue). (B) Top view of the glycan recognition site at one opening of the β-barrel. β1β2, β6β7 and β8β9 loop regions are reoriented in the sugar bound form and well-defined in both conformational states. The distance between the β1β2 and β6β7 loops is significantly decreased in the bound form suggesting that these loops wrap around the sugar. The β8β9 loop is additionally closing the binding pocket. (C) Structural comparison of the X-ray structure of OS-9 MRH (PDB code: 3AIH) and the structure with the lowest target function of the structure ensemble of Yos9 MRH. The sugar which was co-crystallized with the OS-9 MRH domain is also shown and binds to one opening of the β-barrel. Structural differences include, the additional helix α1, a longer β3β4 loop and the completely different arrangement of β-strand 5 and 6. (D) Comparison of the double WW motif of OS-9 and the FW motif involved in mannose binding. Side chain orientations of these aromatic residues are well conserved among both proteins. (E) Comparison of Yos9 and OS-9 as in C but in a different view to highlight the different arrangement of β-strand 5 and 6 in both β-barrel structures.

Both NMR structures provide insights into the structural rearrangements that the protein experiences upon binding of the sugar. The two structures also explain why the addition of 3α, 6α-mannopentaose resulted in chemical shift perturbation of not only residues close to or at the glycan binding site, but significantly affected also backbone amides of the β1 and β3 strands or at the C-terminal end of the N-terminal helix (Figure 36 A-B). To prove that the carbohydrate only binds to the known site as in OS-9 and show that chemical shift perturbations also occur distant from the binding site filtered NOESY experiments were performed. These experiments allowed to unambiguously identify key residues on Yos9 that are in direct contact to the sugar. These residues form a contiguous surface and are shown in Figure 36C. The surface resembles the site found by superimposing the OS-9 sugar complex and the Yos9 structure (Figure 35C).

Chemical shift perturbation at distant sites can be explained by significant conformational movements upon glycan binding that are transmitted through the β-barrel even to the opposite face of the MRH domain where the helix is located. In more detail, β1β2, β6β7 and β8β9 loops that are among other residues involved in glycan binding are reoriented in the bound complex compared to the free form (Figure 35B). Interestingly, the distance between the β1β2 and β6β7 loops is significantly decreased in the bound form suggesting that these loops wrap around a binding sugar. The β8β9 loop seems to additionally close the binding pocket. By contrast, OS-9 was only solved in complex with its sugar thereby revealing no information about these motions. It is tempting to speculate that these rearrangements might define an additional signal that is transmitted to nearby components in the HRD1 ligase complex. This signal might be required to hand over a misfolded client protein that was successfully scanned for the correct glycan structure to membrane components that are responsible for translocation.

Previous analyses have shown that OS-9 recognizes the glycan structure using a double tryptophan motif. In Yos9 the same binding mode is achieved by a FW-motif that is stabilized by an CH-π interaction (Figure 35D). The previously described loop orientations might be the determinants of specificity for the correct glycan structure. Yos9 recognizes the C-branch of glycans that were processed by Htm1 to expose a terminal α1,6-linked mannose residue. Figure 36D summarizes the glycan processing in the ER and highlights the Yos9 recognition motif as well as the sugar that was experimentally used (Figure 36D). I also tested whether Yos9 bears an intrinsic sugar binding propensity that does not require the correct linkage. To this end, the MRH domain of Yos9 was titrated with increasing amounts of 2α-mannobiose that contains a single α1,2-linkage between two mannose moieties (Figure 36D). A weak interaction in the fast exchange regime was observed (Figure 36E). However even at a 100-fold molar excess of the sugar binding was not saturated. Interestingly, this sugar was not able to induce the same chemical shift perturbations that were previously observed for 3α, 6α-mannopentaose. This suggests that the glycan binding site might be composed of a region that is pre-formed for binding to mannose independent from the type of

glycosidic bond that connects the mannose residues as well as a region that senses the terminal α1,6-linked mannose at the C-arm of the glycan via conformational motion of the β6β7 and β8β9 loops. This might represent a scanning like mechanism where the MRH domain is capable of binding mannose residue independent from their linkages. However, in case the correct signal is recognized a conformational transition enables higher affinity interactions.

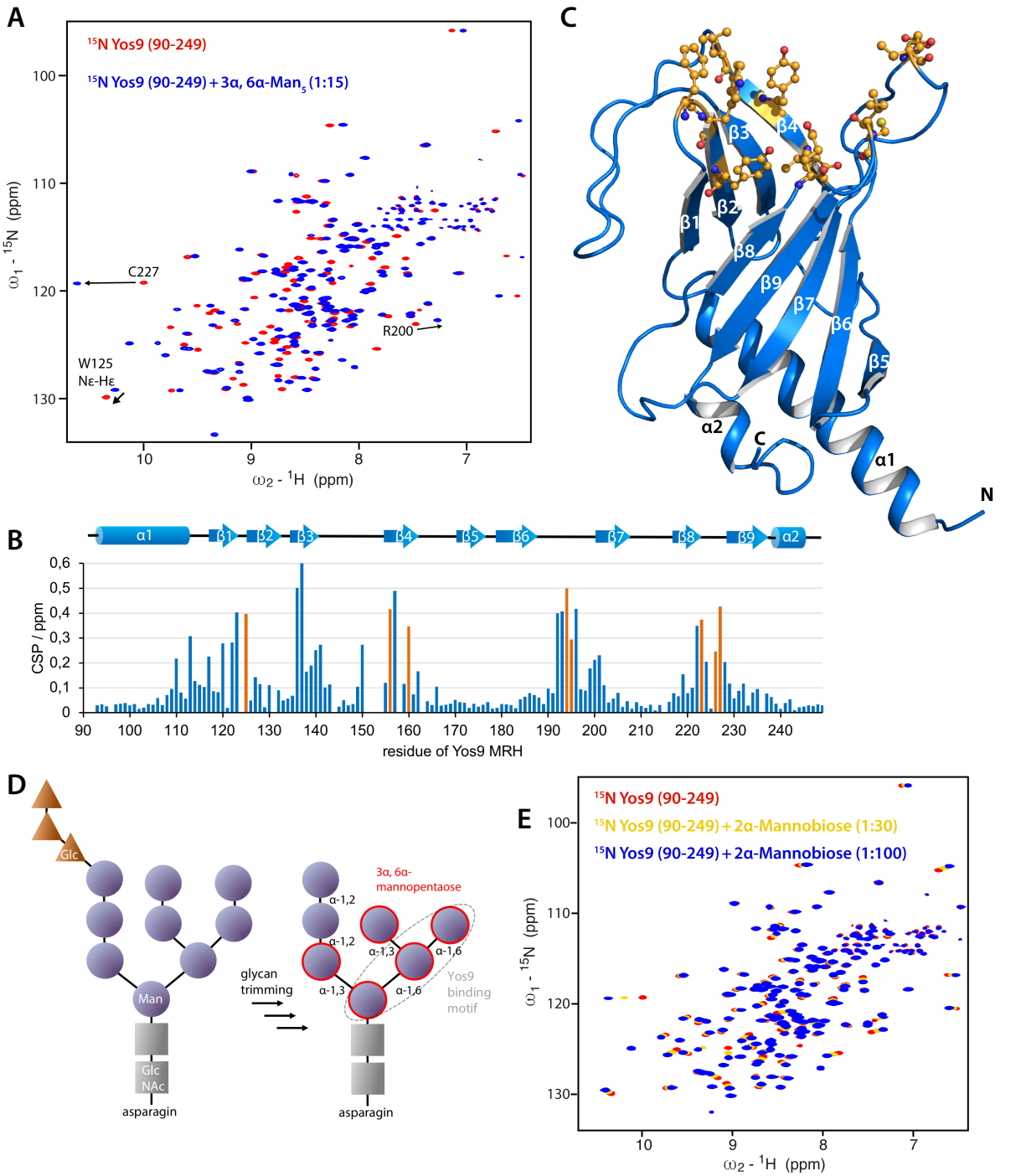

Figure 36: NMR titration experiments showing carbohydrate binding activity and specificity of Yos9 MRH domain for terminally exposed α-1,6 mannose. (A) Overlay of ^{15}N,^{1}H HSQC spectra of Yos9 (90-249) in absence (red) and presence of 3α, 6α-mannopentaose (15-fold molar excess). Large regions of Yos9 are affected. (B) CSP analysis of Yos9 residues upon interaction with the sugar. Residue for which specific intermolecular NOEs have been detected are displayed in orange. This reveals that many shifts arise from conformational changes. (C) Mapping of residues on the Yos9 MRH structure that are in contact (NOEs were detected) with the sugar. (D) Schematic overview of the N-linked glycan trimming by ER glucosidases and mannosidases. The sugar used in NMR experiments is highlighted in red, the Yos9 binding motif is circled in grey. (E) NMR titration experiment of Yos9 and 2α-mannobiose.

In conclusion it was shown that the Yos9 MRH domain contains a β-barrel structure that is similar to its human homologue OS-9 but has additional structural elements like a long N-terminal helix that closes one opening of the barrel. Significant conformational differences were detected upon binding of a correct glycan structure and were not restricted to the binding region. These conformational changes might be important for substrate selection by Yos9/Hrd3 and may represent a signal for having detected the correctly trimmed glycan that targets terminally misfolded protein for ERAD.
In addition to this analysis it was also tested to observe binding of unfolded peptides to the MRH domain. To this end several peptide fragments derived from the ERAD model substrate CPY* were titrated up to a 20-fold molar excess, but without detecting significant binding. However, it cannot be excluded that very weak, transient interactions might be present. In the cellular context already bound glycan structures would facilitate potential binding of adjacent peptide regions simply by induced proximity and increased local concentration effects. Yos9 recognition of unfolded peptide structures requires further analysis.

5.5. Characterization of high affinity SUMO-based Ubc9 inhibitors by ITC and NMR

This project was a part of a research project from Andreas Ernst (Institute of Biochemistry II, Goethe-University Frankfurt) and is published in The Journal of Biological Chemistry (Wiechmann et al., 2017). My contribution to this research project was the characterization of high affinity SUMO2 variants by ITC and NMR.

5.5.1. ITC experiments of the SUMO2–Ubc9 interaction

The conducted screen of a SUMO2 library to find binders to the SUMO E2 enzyme Ub9 using phage display by Wiechmann et al. (2017) yielded 45 unique SUMO2 variants that selectively bind Ubc9. Out of this pool two variants were selected along with the wild type protein for further characterization of their interaction with Ubc9.

For protein yield optimization reasons Ubc9 was cloned as N-terminal His10-tagged-ubiquitin fusion protein with a TEV protease cleavage site (Rogov et al., 2012). This significantly increased soluble expression in *E. coli*. In line with previous studies SUMO2 interacted with Ubc9 only with a low change in binding enthalpy (Knipscheer et al., 2007) in initial isothermal titration experiments performed at 25°C. This lead only to inaccurate fits of the binding constants (data not shown). To increase the directly measurable enthalpy contribution of the binding reaction, the following experiments were conducted at 37°.

The noncovalent back side interaction of Ubc9 with wild type SUMO2 yielded a K_D of 2.44 µM. Binding was mainly driven by a large change in entropy ($-T\Delta S = -5.15$ kcal mol^{-1}) but also showed a negative enthalpy contribution ($\Delta H = -2.80$ kcal mol^{-1}) that both added up to yield a free binding enthalpy ΔG of −7.95 kcal mol^{-1} (Figure 37A and Table 5). Investigation of the SUMO2 A09 variant revealed different enthalpy and entropy contributions (Figure 37B). The binding isotherm and thermodynamic analysis of the interaction driving forces indicated a stronger interaction with a three-fold higher binding enthalpy of −8.49 kcal mol^{-1} due to potentially establishing new noncovalent contacts to Ubc9. The determined K_D was 42-fold higher (58 nM).

Fitting of the data for the SUMO2 E08 was unfortunately not accurately possible at the given experimental conditions since the strong interaction resulted in a rectangular shaped binding isotherm as soon as a ligand to protein molar ratio of 1 was reached (Figure 37C). To resolve this issue, I measured the K_D by using a competition assay by displacing SUMO2 wt from the binding site on Ubc9 (Figure 37D). To this end 20 µM Ubc9 was presaturated with SUMO2 wt (160 µM) and displaced by titrating a 300 µM solution of SUMO2 E08 into the solution of the complex. Analysis using a competitive binding model and taking the thermodynamic parameters of the wild type interaction into account yielded a K_D for the high affinity interaction with SUMO2 E08 of 16 nM. This corresponds to a 150-fold increase in affinity. Interestingly, this interaction was almost solely driven

by the large enthalpy change of −11.33 kcal mol^{-1}. In addition, successful competing for a single binding site supports the idea that SUMO variants retain back side binding. In conclusion a change from the entropy driven wild type interaction towards enthalpy driven interactions with the variants is observed (Table 5).

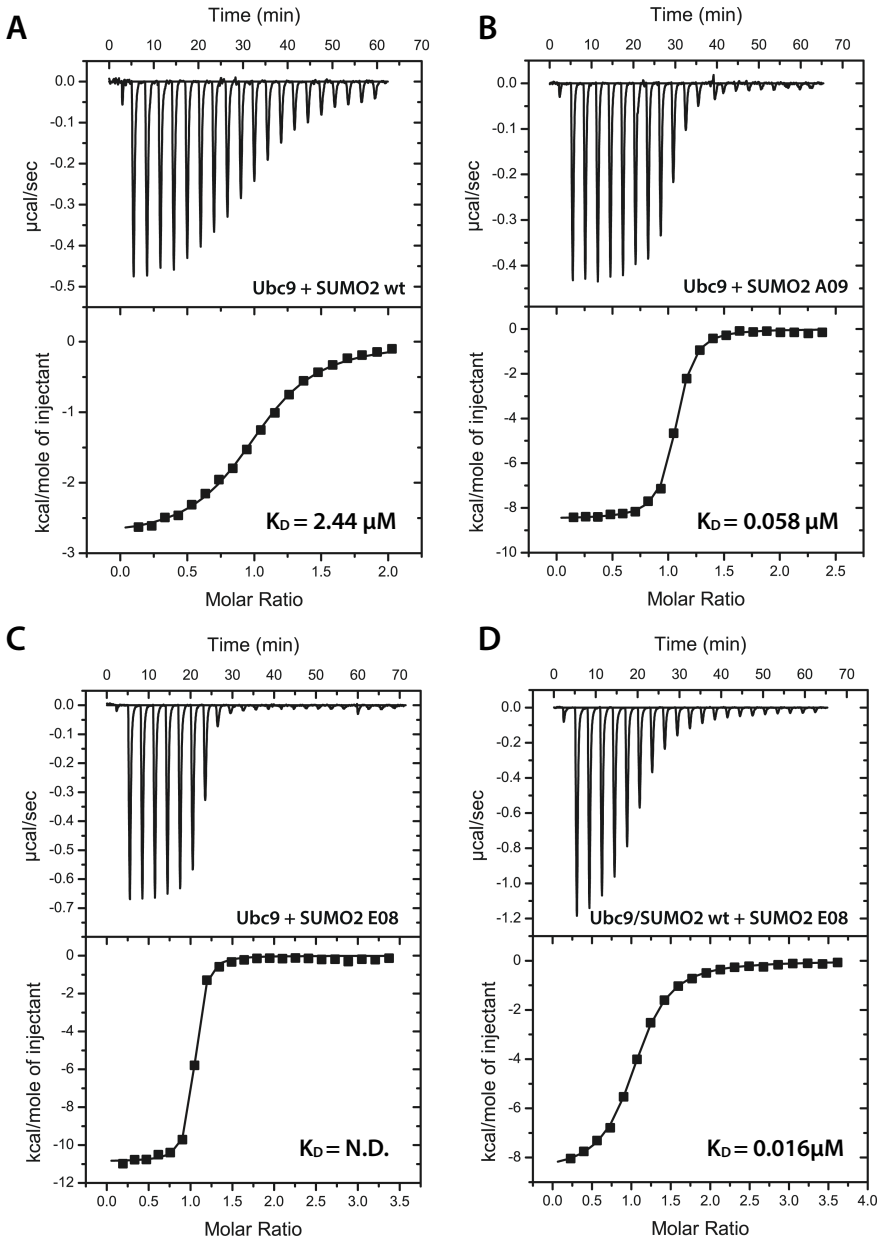

Figure 37: ITC experiments of Ubc9 and SUMO2 variants. Experiments were performed at 37°C by titrating SUMO2 wild type or variants into Ubc9. The thermodynamic parameters of the SUMO2 E08 interaction were determined by competing for the binding site on Ubc9 with SUMO2 wt. N.D. = not determined.

Table 5: Thermodynamic parameters of the Ubc9-SUMO2 interactions determined by ITC at 37°C. The experiments were performed at near physiological conditions in buffer containing 25 mM HEPES (pH 7.0), 150 NaCl. K_a is the association constant, K_d is the dissociation constant and N is the experimentally determined number of binding sites.

Ubc9	ΔH (kcal/mol)	ΔS (cal/mol/K)	−T·ΔS (kcal/mol)	ΔG (kcal/mol)	K_a (M^{-1})	K_d (µM)	N
+ SUMO2 wt	−2.80 ± 0.03	+16.60	−5.15	−7.95	$4.09 \pm 0.23 \cdot 10^5$	2.44	1.01 ± 0.01
+ SUMO2 A09	−8.49 ± 0.04	+5.74	−1.78	−10.27	$1.72 \pm 0.13 \cdot 10^7$	0.058	1.02 ± 0.01
+ SUMO2 E08	−11.33 ± 0.05	−0.87	+0.27	−11.06	$6.29 \pm 0.23 \cdot 10^7$	0.016	1.02 ± 0.01

5.5.2. SUMO2-variants bind to the back side of Ubc9

ITC experiments were indicative of at least overlapping binding sites. To further characterize the exact contact residues on Ubc9, NMR titration experiments were performed. Ubc9 was expressed and purified in ^{15}N-labeled form and titrated in a stepwise manner with unlabeled SUMO2 variants and HSQC spectra recorded after each titration step. An overlay of the free form of Ubc9 and in a saturated complex with SUMO2 wt is given in Figure 38A. Backbone amide resonance assignments required for the analysis of residue specific chemical shift perturbations were adapted from Liu et al. (1999). CSP analysis revealed that binding of SUMO2 mainly affects and involves residues at the C-terminal end of helix α1, the connecting $\alpha1\beta1$ loop and the N-terminal region of helix α3. Comparison of all three performed NMR titration experiments showed that largely the same residues undergo changes upon SUMO2 interaction (Figure 38B-C). However, for some residues differences in the directions and chemical shift perturbation values were noticed that are most likely due to specific changes of the chemical environment of Ubc9 residues at the binding interface that are interacting with mutated residues on the SUMO2 variants.

The SUMO2 wt interaction showed an intermediate exchange behavior, while the interactions with the high affinity variants were in slow exchange mode relative to the NMR time scale (Figure 38D). At molar ratios below one, two distinct peaks were observed for some largely affected backbone resonances like K18 during the SUMO2 E08 titration (Figure 38D, lower panel). This indicates that the on- and off-rates for complex formation are slow enough to separately see resonances in their two states during titration, free and interacting with the SUMO2 variant.

The identified interaction site (Figure 38B) involves residues K14, R17, K18, D19, H20 and F22 and corresponds to the previously determined back side binding site on E2 enzymes. This distinct interaction site is at the opposite site of the catalytically active cysteine residue (Figure 38E). As described in the introduction, interactions mediated via the back side of E2 enzymes are crucial for cofactors like Cue1 (for Ubc7), ubiquitin or like in this case SUMO2 in order to modulate for example the processivity of chain formation.

Further analysis of the high affinity SUMO2 variants were conducted in the lab of Andreas Ernst (Institute of Biochemistry II, Goethe-University Frankfurt) and showed that the herein characterized SUMO2 E08 variant limited SUMO chain formation *in vitro* as well as *in vivo* (Wiechmann et al., 2017). For instance, it was shown that this high-affinity variant was also able to almost completely abolish polySUMOylation-mediated arsenic-induced degradation of PML (Wiechmann et al., 2017) in HeLa cells. Interestingly, mono-SUMO modified PML was only moderately affected by the presence of the SUMO2 variant. In conclusion, inhibition of the back side interaction successfully impairs polySUMO chain formation which further underscores the importance of those noncovalent interactions.

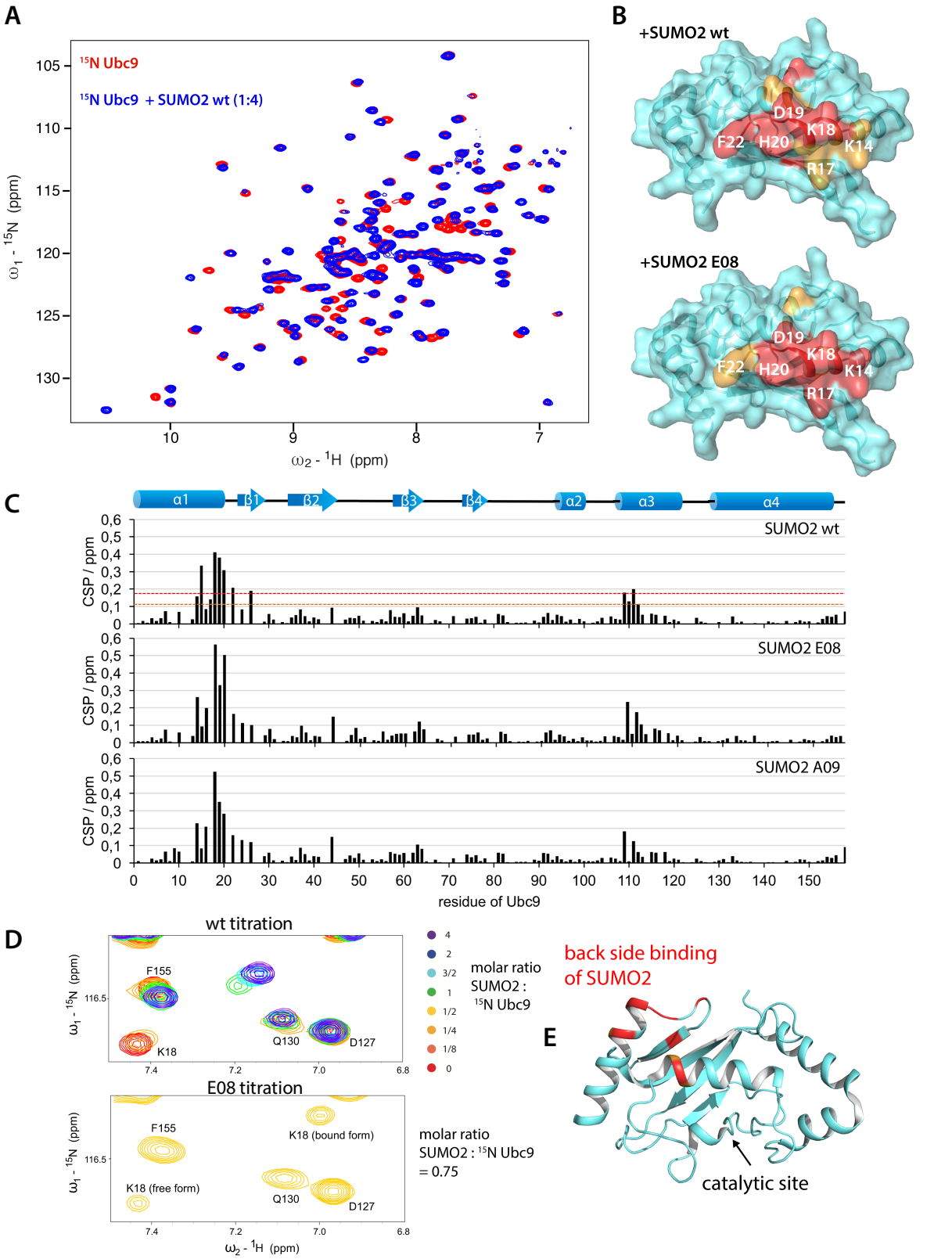

Figure 38: SUMO2 wt and variants bind to the back side of Ubc9. (A) Overlay of ^{15}N, ^{1}H HSQC spectra of Ubc9 (0.2 mM) in absence (red) and presence (blue) of SUMO2 wt (four-fold molar excess). (B) Mapping of the interacting residues on a surface representation of Ubc9. Residues with a CSP larger than 1x standard deviation (S.D) (orange) and 2x S.D. (red) from the mean are mapped onto Ubc9 (PDB code: 5D2M) for the SUMO2 wt interaction (upper panel) and for the SUMO2 E08 interaction (lower panel). (C) Comparative CSP analysis of Ubc9 residues upon interaction with SUMO2 wt, SUMO2 E08 and SUMO2 A09. The CSP value corresponding to the mean + 1x S.D. is shown as a dashed line in orange, while the CSP value that indicates large shifts (mean + 2x S.D.) is shown as a red dashed line for the SUMO2 wt interaction. (D) Upper: Overlay of HSQC spectra showing the behavior of the backbone amide resonance of K18 of Ubc9 during titration of SUMO2 wt. Lower: Single section of the HSQC spectrum (0.2 mM Ubc9 and 0.15 mM SUMO2 E08) showing that this resonance is in slow exchange indicating the free and bound Ubc9 states. (E) Cartoon representation of the back side binding site and the catalytic site of Ubc9.

6. Discussion

ERAD ensures quality control of newly synthesized soluble and membrane proteins of the secretory pathway. Proteins failing to fold into their native structure are processed in a multistep process and finally ubiquitinated and degraded by the proteasome in the cytosol. My thesis covered structural as well as functional studies of various protein components that constitute the protein complexes that are responsible for this process in order to protect the cell from proteotoxic stress.

Figure 39 summarizes all proteins and protein complexes that were structurally investigated. In addition, mechanistic insights into the ubiquitination process itself were obtained that explain how Ubc7 and Cue1 act together to achieve optimal ubiquitin chain formation to efficiently mark substrates for proteasomal degradation. Below all projects are discussed in separate chapters.

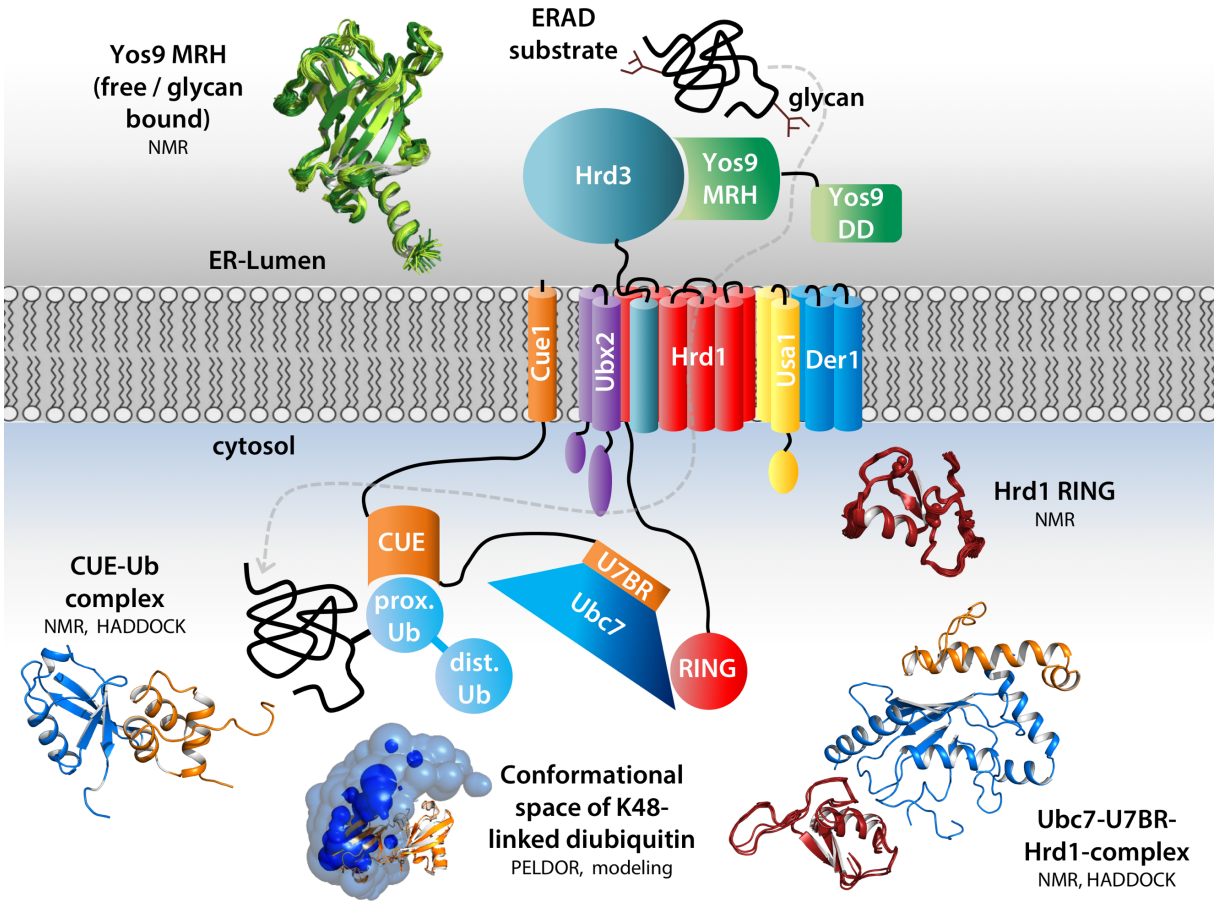

Figure 39: Overview of the ERAD pathway and summary of studied proteins and macromolecular complexes.
The most important proteins involved in ERAD and the HRD1 complex are shown. In this thesis, structural investigations covered the MRH domain of the lectin Yos9, the interaction between Yos9 MRH and the glycan, interactions between the CUE domain of Cue1 and ubiquitin chains, the RING domain of the E3 ubiquitin ligase Hrd1, the interactions between the E2 enzyme Ubc7 and Hrd1 RING and a comprehensive analysis of the conformational space of K48-linked diubiquitin. Structures of the Yos9 MRH domain in free form and complexed to the glycan were solved by solution NMR. The Hrd1 RING domain was also solved by NMR. HADDOCK modeling was employed to generate CUE-Ub and Ubc7-U7BR-RING complexes and PELDOR restraints were used to calculate the conformational space of K48-linked diubiquitin. In addition, the CUE domain assisted mechanism of ubiquitin chain elongation is shown. CUE binds to the ubiquitin moiety directly adjacent to the conjugation site thereby spatially organizing the distal tip of the ubiquitin chain in the elongation complex. The studied transient dimerization of Ubc7 molecules which stimulates formation of diubiquitin is not shown.

6.1. The CUE domain of Cue1 accelerates the ubiquitin chain elongation process in ERAD

Processive ubiquitin chain formation poses a steric problem to the participating enzymatic components because the elongation site must be constantly repositioned to provide an optimal arrangement of acceptor and donor ubiquitins for isopeptide bond formation. Thus, several mechanisms have evolved to organize this process that rely on noncovalent ubiquitin binding events occurring in proximity to the active site of the E2 enzyme. It has been shown that this can involve interaction with the back side of the E2 enzyme (Brzovic et al., 2006) or can include inherent ubiquitin binding activity of RING domains (Brown et al., 2014; Buetow et al., 2015; Wright et al., 2016). In this work it was shown that also ubiquitin binding domains have regulatory functions in ubiquitin chain assembly. The CUE domain of Cue1 which is in cis to its Ubc7 activating region (U7BR) accelerates the ubiquitin chain elongation process by coordinating the spatial arrangement of the distal ubiquitin of a chain and the E2 enzyme by binding directly adjacent to the distal tip of a chain (Figure 40).

Preferential binding to ubiquitin units within a chain that bear K48-linked ubiquitins (e.g. the proximal ubiquitin in diubiquitin) is achieved by a slightly enlarged surface due to additional interactions with the C-terminus of the conjugated ubiquitin. Although the binding preference and ubiquitin binding affinity were rather low and exhibited only a two-fold preference for the proximal ubiquitin in diubiquitin, these weak interactions ensure that the process remains dynamic. Interestingly this was enough to accelerate chain elongation of tetraubiquitin by a factor of five for a single elongation step. Kinetic analyses also suggested that multiple interactions between CUE and the ubiquitin chain are required for optimal chain elongation which is pointing to a CUE domain that can easily switch between adjacent binding sites on a chain. This was shown by introducing R42A mutations. Hence, induced proximity and local concentration effects also play an important role.

The inability of the CUE domain to promote monoubiquitin elongation, specific mutant ubiquitin incorporated at distinct sites within a chain and cross-linking experiments show that CUE binding at the second ubiquitin counted from the distal end enhanced elongation the most. This is most likely due to an optimal steric arrangement of both acceptor (the distal end of a chain) and donor (thioester-linked) ubiquitins.

Ubiquitin chain formation by APC/C in cell cycle control has been shown to involve tracking of the distal end of a chain by a RING-E3 dependent increasing of the affinity of the E2 enzyme for the distal ubiquitin (Kelly et al., 2014). However, chain elongation was shown to become less likely with increasing chain length, so that this mechanism limits the length of a synthesized ubiquitin chain (Kelly et al., 2014; Meyer and Rape, 2014; Wickliffe et al., 2011). In contrast the Cue1 system accelerates the process due to increased CUE domain binding to longer chains and provides guidance via binding adjacent to the distal acceptor. Fast K48-linked chain assembly may be

important to ensure fast extraction of polyubiquitinated substrates from the membrane in the ERAD process and additionally ensure that K48-linked ubiquitin chain are long enough to efficiently signal proteasomal degradation. This is underlined by the fact that reducing the ubiquitin affinity of the CUE domain delayed the degradation of the ERAD model substrate Ubc6 *in vivo*.

The model of UBD assisted chain elongation is summarized in Figure 40.

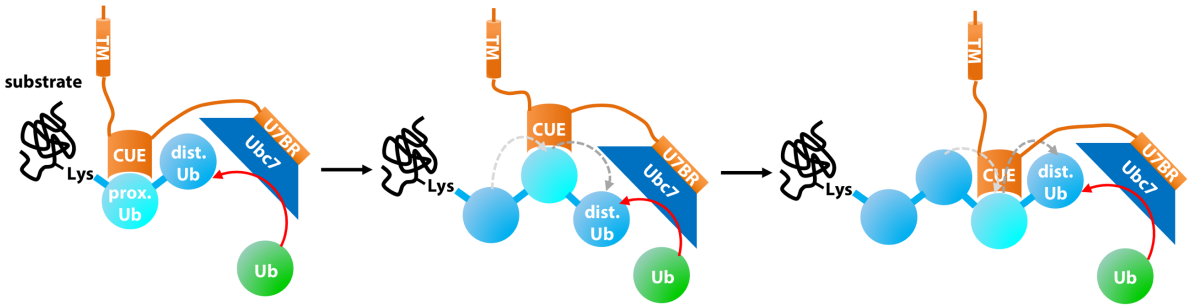

Figure 40: Model of CUE domain assisted ubiquitin chain elongation. The CUE domain needs a substrate primed with diubiquitin to promote chain elongation via binding next to the distal ubiquitin (highlighted in light blue). Longer chains provide further interaction site that lead to a progressively accelerated process.

The CUE domain necessitates a substrate primed with diubiquitin for highly processive elongation. How this priming event is catalyzed is unclear to present, but first experimental evidences are provided in chapter 5.3 and 6.3 and suggest a mechanism that involves Ubc7 dimerization.

The distal ubiquitin is kept accessible throughout the whole process which involves dynamic switching of the CUE domain. The high on- and off-rates of the CUE-Ub complex are significantly faster than the kinetic rates of the enzymatic reaction and ensure sampling of different interactions within a growing chain. This accelerates the chain formation with increasing chain length by proving more interaction possibilities. In this process CUE binding adjacent to the distal end ensures optimal orientation of the E2 enzyme, donor and acceptor ubiquitins.

6.2. Chain assembly and disassembly processes differently affect the conformational space of ubiquitin chains

Ubiquitin signals are encoded both by the linkage and length of ubiquitin chains. The conformation of ubiquitin chain has been the subject of intensive research over the last decade and has revealed a variety of different conformations, but also lead to inconsistent views on the conformation of certain ubiquitin chains (Castañeda et al., 2013). In addition, the numerous structures provide only snapshots of specific conformations that were either crystallized, supported by short-range restraints or based on insufficient long-range restraints. In addition, how ubiquitin binding domains and deubiquitinating enzymes impact the conformational space of ubiquitin chains still remained elusive.

This study employed PELDOR spectroscopy to define the conformational space of K48-linked ubiquitin chains. K48-linked diubiquitin adopts a large conformational space as has been shown by measuring five long-range inter-ubiquitin restraints and subsequent modeling of the conformational space. This structural ensemble unifies previously reported NMR and X-ray structures which are part of the structural ensemble but extends the conformational diversity and also shows how different conformations are populated. The PELDOR based conformational distribution contains highly populated subspaces and indicates that free K48-linked diubiquitin also samples open conformation to a high extent. Those conformations can be bound by interacting proteins that recognize the I44 or I36 centered hydrophobic patches on ubiquitin.

As ubiquitin chain formation requires access to the acceptor lysine of the distal ubiquitin on a chain closed conformations that impair this access would hinder a highly processive process. The CUE domain of the Cue1 uses conformational selection of pre-populated open conformations to support elongation. Cue1 seems to be the optimal scaffold for promoting chain elongation as was shown by measuring chain elongation in presence of ubiquitin interacting proteins.

Similar conformational requirements exist for chain disassembly by deubiquitinating enzymes. Prerequisite for hydrolysis is the access to the isopeptide linkage. PELDOR measurements revealed that in presence of a catalytically inactive K48-linkage specific deubiquitinating enzyme (OTUB1i) the conformational ensemble is shifted towards weakly or even non-populated conformations. This is indicative of a conformational remodeling mechanism. Such binding mechanisms in macromolecular recognitions have been previously reported (Boehr et al., 2009; Ye et al., 2012).

Both distinct recognition mechanisms by Cue1 and OTUB1 are summarized in Figure 41.

Previous models have suggested that chain elongation to tetraubiquitin would have an stabilizing effect as it was proposed that K48-linked tetraubiquitin predominantly adopts a closed conformation in solution (Eddins et al., 2007; Ye et al., 2012). Here, it is shown that chain elongation leads to more conformational flexibility and significantly increases the sampled conformational space. So it seems that no major structural rearrangements (Zhang et al., 2016) are required for

simultaneous binding to the proteasomal receptors Rpn10 and Rpn13. Cryo-EM studies have located those stably to the 19S regulatory particles associated receptors approximately 10 nm apart (Sakata et al., 2012).

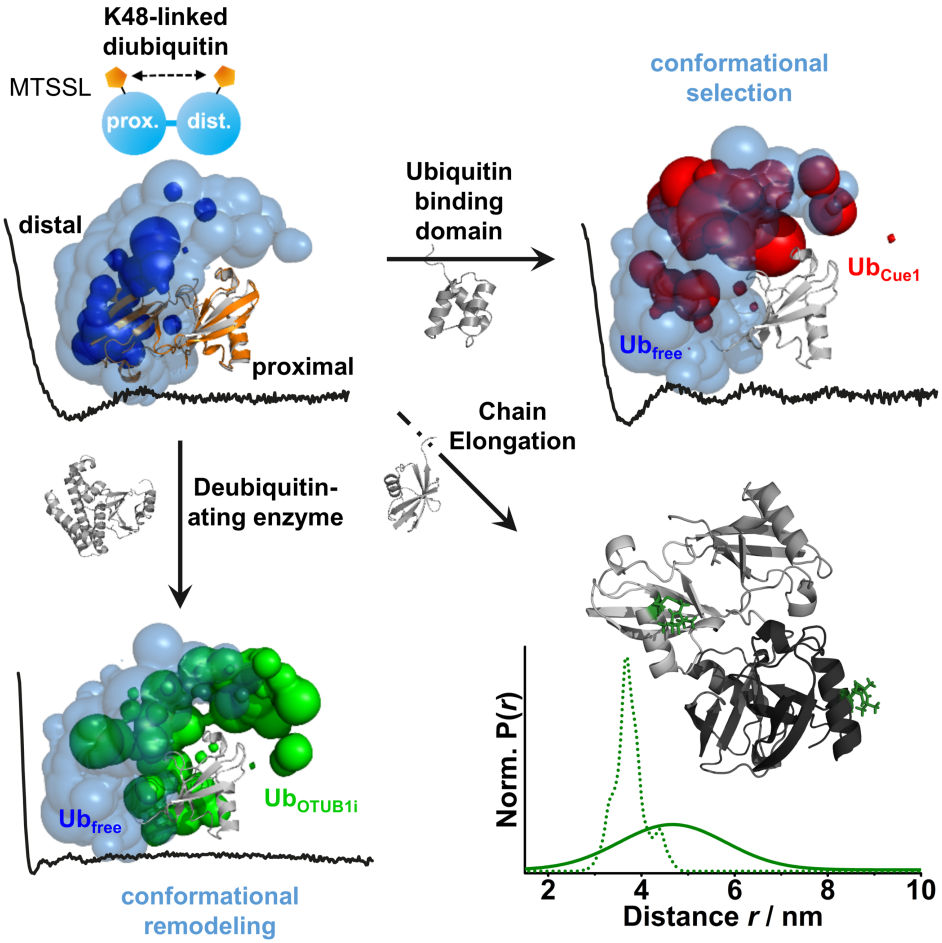

Figure 41: Summary of PELDOR studies on K48-linked ubiquitin chains. K48-linked diubiquitin samples a broad conformational space that can be restricted by ubiquitin binding domains (CUE of Cue1) via conformational selection, remodeled by interacting deubiquitinating enzymes (OTUB1i), or increased by further chain elongation. The figure was adapted from Kniss et al., 2018.

It seems that the increased conformational flexibility that is found with chain elongation to tri- or tetraubiquitin allows efficient association with the proteasome. Further measurements of spin-labeled diubiquitin variants in presence of Rpn13 support this idea, because Rpn13 induced an even broader conformational distribution (Figure 42A). The PELDOR data on spin-labeled diubiquitin incorporated into longer chains additionally implies that each isopeptide linkage contribute equally to the enormous conformational space that is sampled by for example tetraubiquitin (Figure 42B). Conformational sampling in ubiquitin chains seems to be largely independent from long-range inter-ubiquitin interactions as mutations in the hydrophobic patch had no significant impact on PELDOR time traces and determined distributions at least in case of the E24C/A28C diubiquitin variant. By contrast, noncovalent interactions with a weakly binding CUE domain significantly modulated the conformational space.

The interpretation that tetraubiquitin does not provide a structurally discrete degradation signal is supported by recent work that monoubiquitin can also suffice to function as a degradation signal (Braten et al., 2016). Despite, the conformation of K48-linked chains is still different from K63-linked chains (Figure 42C) since the K48-linkage does not allow a completely elongated molecule. These characteristics might still be important for more efficient binding and processing of the chains at the proteasome.

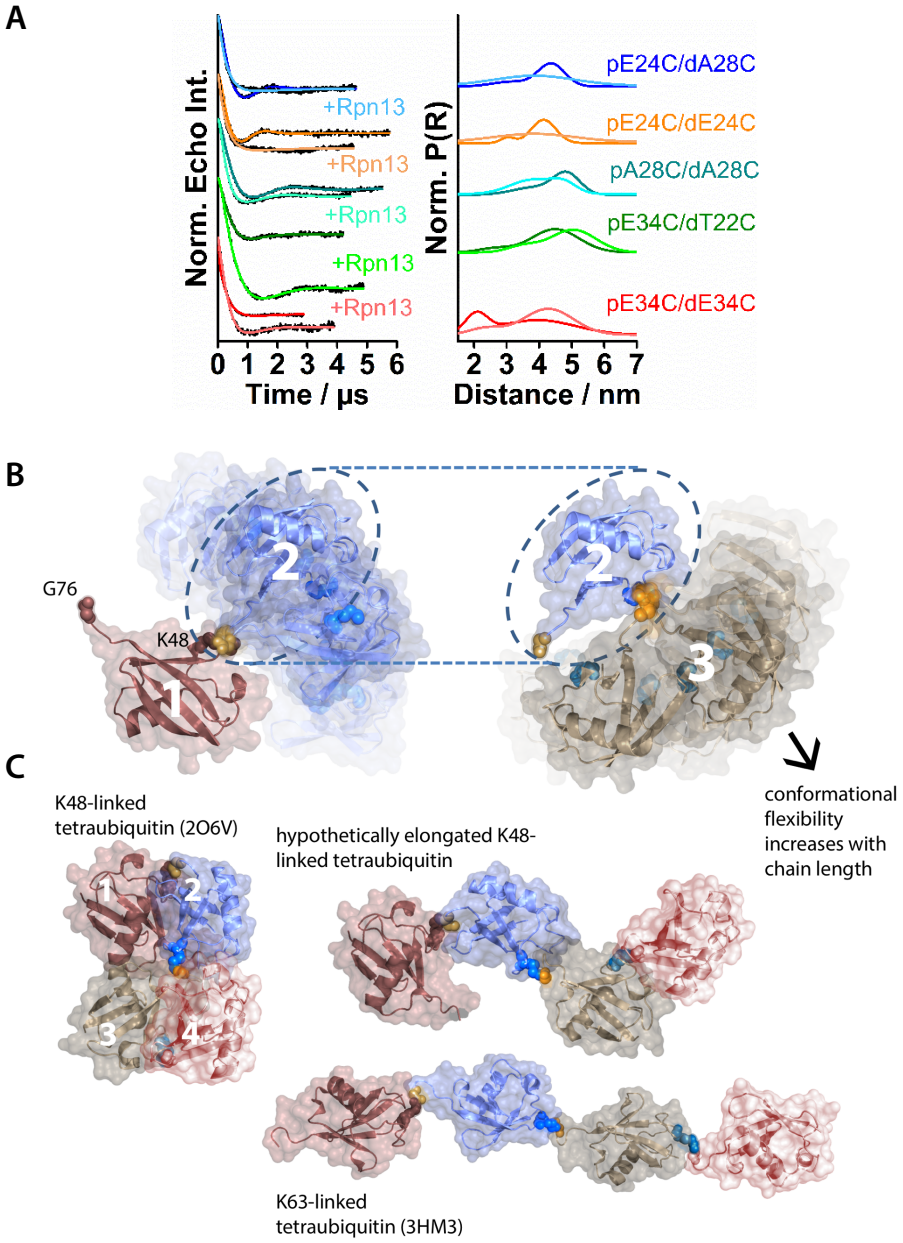

Figure 42: Interaction of the proteasomal ubiquitin receptor Rpn13 with diubiquitin and model of the conformational distribution of K48-linked tetraubiquitin. (A) Comparison of PELDOR time traces and determined distance distributions of a set of differently spin-labeled K48-linked diubiquitin variants measured in absence and presence of Rpn13. Rpn13 induces an even broader distribution in K48-linked diubiquitin. (B) Schematic representation of the conformational space of K48-linked diubiquitin. Ubiquitins are not equally distributed, but sample distinct sub-spaces. This conformational sampling seems to be independent from long-range inter-ubiquitin interactions between ubiquitin molecules. Every isopeptide linkage seems to add a similar conformational variety to the overall distribution as visualized by the elongation of a hypothetical diubiquitin to triubiquitin. (C) The compact crystal structure of K48-linked tetraubiquitin (PDB code: 2O6V) is shown together with a hypothetically elongated form of K48-linked tetraubiquitin and a crystal structure of K63-linked tetraubiquitin (PDB code: 3HM3). The figure was adapted from Kniss et al., 2018.

6.3. Analysis of interactions involving the E2 enzyme Ubc7

Ubc7 is the central E2 enzyme of the HRD1 and DOA10 ligase complexes involved in ERAD as well as involved in quality control of the inner nuclear membrane by the Asi complexes (Foresti et al., 2014; Khmelinskii et al., 2014). Ubc7 activity is modulated by its cofactor Cue1 as well as by the RING domains of its cognate E3 ubiquitin ligases. Here, I explored the differential activation caused by Hrd1 and Doa10 RING domains as well as how Ubc7 dimerization drives rapid diubiquitin formation as a potential mechanism for ubiquitin chain initiation in ERAD. Previous work has already elucidated that ubiquitin chain assembly involving the Cue1-Ubc7 complex necessitates a substrate primed with diubiquitin for highly processive ubiquitin chain elongation that is dependent on additional nonconvalent ubiquitin binding events by a CUE domain.

My investigations show that Hrd1 and Doa10 RING domains contact Ubc7 via largely overlapping binding sites that correspond to the canonical RING binding region (Deshaies and Joazeiro, 2009). The associations are weak and affinities for the Hrd1 RING have already been reported to be in the range of 13-107 µM depending on the presence of the U7BR (Metzger et al., 2013). However, a correlation between E3 ligase activity and the affinity for E2 enzymes is often not observed (Christensen et al., 2007; Lorick et al., 1999). The Hrd1 RING domain was able to induce significant allosteric changes around the catalytic cysteine as proven by NMR titration experiments, while this region remained largely unaffected by Doa10 interaction. This might represent a mechanism to further promote ubiquitin discharge, since the U7BR of Cue1 promotes Ubc7 discharge also via inducing changes around the active center (Metzger et al., 2013). In line with this observation, Hrd1 was able to accelerate ubiquitin chain elongation by factor of ~28 compared to a ~7-fold stimulation with Doa10. This is quite remarkable for interactions in the high µM range and underscores that fast ubiquitination can rely on weak associations (von Delbruck et al., 2016). The higher activity of Hrd1 compared to Doa10 might also be attributed to the otherwise conserved R400 residue that is missing in Doa10. This residue has been described to be the “allosteric linchpin” for other RING E3 ligases (Pruneda et al., 2012) and is involved in interactions that shift the conformational ensemble of active site linked ubiquitin towards closed conformations. Interestingly, my studies show that the active site linked ubiquitin on Ubc7 is already significantly sampling closed conformations in absence of RING domains. The determined site at the α2α3loop and helix α3 is non-overlapping with the RING interaction site. The ubiquitin is here at least contacting this region that is distinct from the proposed helix α2 mediated closed state which is adopted in presence of RING domains (Plechanovova et al., 2012). The existence of additional distinct closed conformations may provide an explanation for the high ubiquitination activity that is already seen with U7BR-activated Ubc7 in absence of RING domains.

Several previous studies have already proposed a direct interaction between Ubc7 molecules (Chen et al., 1993; Metzger et al., 2013; Ravid and Hochstrasser, 2007).

Here, I show that Ubc7 preferentially catalyzes diubiquitin formation via Ubc7 dimerization, particularly in absence of a CUE domain, which in turn promotes diubiquitin elongation. With a functional CUE domain Ubc7 is able to rapidly catalyze both: initial diubiquitin assembly and processive elongation of those preassembled chains. Mechanistically this is achieved by dimerization of charged Ubc7 molecules via mainly electrostatic interactions and the formation of a cysteine-linked diubiquitin chain. Such active site linked chain have been previously observed for Ubc7 (Bazirgan and Hampton, 2008; Ravid and Hochstrasser, 2007). This diubiquitin is simply discharged in the fluorescence-based assay but might likely be conjugated to an acceptor lysine residue on ERAD substrates. Paramagnetic relaxation enhancement experiments further supports the model of Ubc7 self-association. The observed intermolecular PRE-effects occur on specific regions and differ among the differently spin-labeled Ubc7 molecules.

Based on these results I would like to propose the following model for both Ubc7 catalyzed substrate polyubiquitination as well as for Ubc7 catalyzed autoubiquitination (Figure 43):

E2 enzymes like Ubc7 mainly exist as activated E2~Ub conjugates in the cell (Siepmann et al., 2003). In a first scenario (Figure 43A) where cellular concentrations of Cue1 and Ubc7 are equal, the enzyme is bound to Cue1 and correctly localized at the ER membrane in proximity to the HRD1 and DOA10 E3 ligase complexes. It should be noted that the E3 ligase Hrd1 is also dimeric. Here, charged Ubc7 molecules dimerize and the K48 residue of one ubiquitin attacks the thioester on the other molecule of the dimeric complex which results in the formation of thioester linked diubiquitin. Discharge of this cysteine-linked diubiquitin might serve as the priming event in substrate conjugated ubiquitin chain formation (chain initiation). This can be promoted by E3 ubiquitin ligases that additionally bring E2 enzyme and substrate together. As soon as the substrate is primed with diubiquitin the system switches to processive chain elongation catalyzed by a CUE domain assisted mechanism (von Delbrück et al., 2016).

In a second scenario (Figure 43B) where cellular concentrations of Ubc7 exceed those of its cofactor Cue1, Ubc7 dimerization provides a mechanistic explanation for the formation of K48-linked polyubiquitin chains onto the catalytic cysteine C89 (autoubiquitination). In absence of Cue1 Ubc7 is less prone to discharge which allows to form longer chains compared to the situation when primarily Ubc7-Cue1 complexes exist. Dimerization also provides here the required proximity of a K48 side chain and the thioester bond to form diubiquitin. Multiple rounds of association with further charged Ubc7 molecules lead to the assembly of chains that finally target the mislocalized Ubc7 molecules for proteasomal degradation via a Ufd4 dependent pathway (Ravid and Hochstrasser, 2007). Interestingly these cysteine chains cannot be transferred to a nearby lysine as has been show for other E2 enzymes (Lin et al., 2002; Machida et al., 2006). A sequence alignment of

yeast E2 enzymes (Figure 44) shows that Ubc7 features a histidine residue at the corresponding position.

In conclusion Ubc7 dimerization seems to be an important mechanism that further activates this E2 enzyme by induced proximity of acceptor and donor ubiquitins that both reside at the active site of the E2 enzyme.

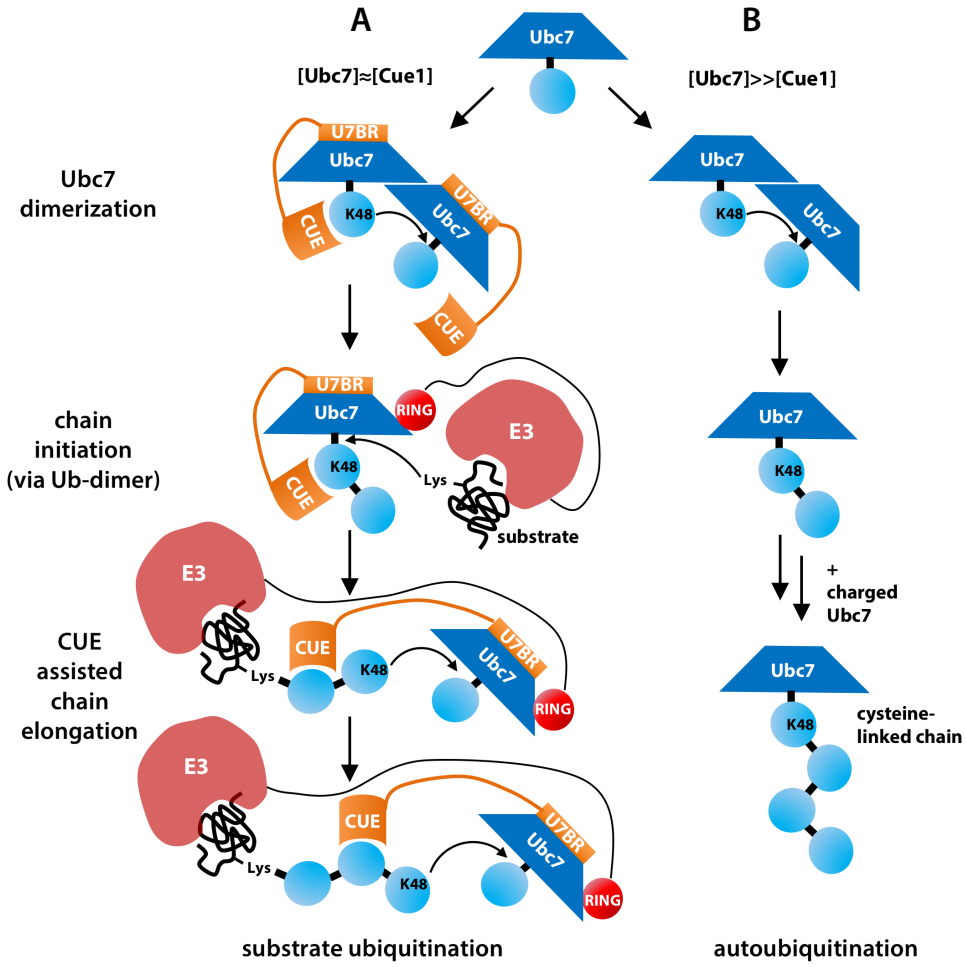

Figure 43: Hypothetical model of Ubc7-dimerization mediated ubiquitin chain initiation on a ERAD substrate and autoubiquitination via cysteine linked polyubiquitin chain formation. (A) In case of balanced cellular concentrations of Cue1 and Ubc7, the enzyme is bound to Cue1 and tethered to the ER membrane to function as an important ERAD E2 enzyme. Here, two charged Ubc7 molecules dimerize. Since the CUE domain is in cis to the U7BR it might also stabilize the thioester-linked ubiquitin. The K48 residue of one ubiquitin attacks the thioester on the other molecule of the dimeric complex which results in the formation of thioester linked diubiquitin. Discharge of this cysteine-linked diubiquitin might serve as the priming event in substrate conjugated chain formation (chain initiation). This can be promoted by E3 ubiquitin ligases that additionally bring E2 enzyme and substrate together. As soon as the substrate is primed with diubiquitin the system switches to processive chain elongation catalyzed by a CUE domain assisted mechanism. This involves CUE binding directly adjacent to the distal end of a chain thereby providing the optimal orientation of acceptor, donor ubiquitin and E2 enzyme. (B) In another scenario where cellular concentrations of Ubc7 exceed those of its cofactor Cue1, Ubc7 dimerization provides a mechanistic explanation for the formation of K48-linked polyubiquitin chains on the catalytic cysteine C89 (autoubiquitination). In absence of Cue1 Ubc7 is less prone to discharge which allows to form longer chains compared to the scenario described in A. Multiple rounds of association with charged Ubc7 molecules lead to the assembly of chains that finally target the mislocalized Ubc7 molecules for proteasomal degradation via a Ufd4 dependent pathway.

```
Ubc1    78 PNISSVTGAICLDILK-------------NAWSPVITLKSAL 105
Ubc2    79 PNVYA-NGEICLDILQ-------------NRWTPTYDVASIL 105
Ubc3    86 PNVYR-DGRLCISILHQSGD-PMTDEPDAETWSPVQTVESVL 124
Ubc4    77 PNINA-NGNICLDILK-------------DQWSPALTLSKVL 103
Ubc5    77 PNINS-SGNICLDILK-------------DQWSPALTLSKVL 103
Ubc6    82 P-----NTRLCLSMSD----------YHPDTWNPGWSVSTIL 107
Ubc7    80 PNIYP-NGEVCISILHSPGDDPNMYELAEERWSPVQSVEKIL 119
Ubc8    75 PNIDIASGSICLDVIN-------------STWSPLYDLINIV 103
Ubc9    84 PNVYP-SGTICLSILNE-----------DQDWRPAITLKQIV 112
Ubc10  105 CNVKSATGEICLNILK------------PEEWTPVWDLLHCV 133
Ubc11   84 PNVDK-SGNICLDILK-------------EKWSAVYNVETIL 110
Ubc12  106 PNIDL-KGNVCLNILR-------------EDWSPALDLQSII 132
Ubc13   78 PNIDR-LGRICLDVLK-------------TNWSPALQIRTVL 104
                  :*:.:                 *     :   :
```

Figure 44: Multiple sequence alignment of yeast E2 enzymes. The sequence region surrounding the catalytic cysteine of 13 different yeast E2 enzymes is shown. Six out of 13 E2 enzymes have a lysine residue in proximity to the catalytic cysteine that might serve as a potential acceptor site for autoubiquitination.

6.4. Structural analysis of glycan recognition by the MRH domain of Yos9 within ERAD

Yos9 is a lectin in the ERAD pathway that contains a mannose-6-phosphate receptor homology (MRH) domain. MRH domains are a common feature in many proteins involved in the secretory pathway as the β subunit of ER glucosidase II or the γ subunit of Golgi GlcNAc-phosphotransferase (D'Alessio and M. Dahms, 2015). Yos9 glycan recognition is crucial for determining whether a protein retains in the ER or is retrotranslocated by the HRD1 complex for cytosolic degradation.

Here, I solved the structure of the Yos9 MRH domain by solution NMR in two distinct conformational states: in a free form and bound to the minimal mannosyl oligosaccharide structure that is also exposed on ERAD substrates.

The MRH domain of Yos9 shares only a ~25 % sequence similarity to its human homologue and has a distinct structure. The Yos9 MRH domain is composed of a central β-barrel that has been previously observed in homologous structures (Satoh et al., 2010). However, the β-barrel is additionally closed on one opening by a unique ~20 amino acids long α helix. Such a helical element within MRH domains has not yet been observed. The existence of this additional structural element significantly restricts the arrangement of the nine β-strands of the MRH and results in a completely different arrangement of for example strands β5 and β6 that would otherwise collide with the helix.

Comparison of both NMR structures revealed insights into glycan recognition by Yos9. Significant backbone reorientations were detected that were not restricted to the binding region of the ligand. In particular the distances between loops β1β2, β6β7 and β8β9 are decreased in the bound form compared to the free form. This suggest a gripping movement of those regions upon glycan binding. The MRH domain of the β subunit of glucosidase II has also been solved in a free and bound form (complexed with mannose). But unlike Yos9 only repositioning of side chains were observed without any major differences in the protein backbone (Olson et al., 2013, 2015). The fact that Yos9 exhibits those rearrangements and other MRH domains not might suggest that this constitutes an additional signal that is required to hand over misfolded client proteins to nearby components of HRD1 ligase complex. Yos9 has the difficult task to select only the correctly processed glycan structures on the C-arm that expose a terminal α1,6-linked mannose. By contrast, glucosidase II performs initial trimming of glucose on the A-branch of the N-linked glycans (Stigliano et al., 2009) and its MRH domain recognizes mannose residues either localized on the B and/or C-arm of the glycan (Hu et al., 2009; Stigliano et al., 2011).

Glycan binding of Yos9 involves an FW motif that superimposes well with the WW-motif on OS-9 in a structural alignment. This indicates that the sugar binding pocket to recognize the trimmed C-arm is well conserved. Since also binding of Yos9 to α1,2-linked mannose was observed by NMR, the glycan site might be composed of a region that has an inherent affinity for mannose and a region that senses the terminal α1,6-linked mannose via conformational motion of the β6β7 and β8β9

loops. This would represent a scanning like mechanism that ensures that only correctly processed glycans induce the conformational changes in the Yos9 MRH domain.

Previous studies have suggested that the peptide surrounding in which a glycan is presented impacts Yos9 recognition. Unfortunately, I was unable to detect binding of unfolded peptide fragments derived from the ERAD model substrate CPY* although a cooperation partner has detected an aggregation prevention activity within the MRH domain. The structural understanding of this activity still remains unclear. One option would be that transient interactions occur with unfolded peptides that were not detectable by NMR titration experiments. A second question that is still not clear is how Hrd3 and Yos9 interact. A previous study has suggested that the Hrd3 binding site lies within the herein structurally determined MRH domain of Yos9 (Hanna et al., 2012). Further studies have to focus on the Hrd3-Yos9 interaction.

6.5. Characterization of high affinity SUMO-based Ubc9 inhibitors by ITC and NMR

SUMO-chains have been identified to form as a stress response mechanism for degradation or as a reaction to DNA damage (Nie and Boddy, 2016). A famous example of poly-SUMO-dependent ubiquitination of substrate proteins is the degradation of promyelocytic leukemia (PML) protein (Lallemand-Breitenbach et al., 2008) by RNF4 which is induced by arsenic trioxide treatment in acute promyelocytic leukemia (Tatham et al., 2008). The SUMO specific E2 enzyme Ubc9 can interact with SUMO covalently via thioester bond formation as well as via noncovalent binding to the back side of the E2 enzyme (Knipscheer et al., 2007) which is critical for poly-SUMO chain formation by SUMO-E3 ligases (Eisenhardt et al., 2015).

Here, high affinity SUMO2-based Ubc9 inhibitors were characterized by ITC and NMR. These studies show that the inhibitors selectively block the back side binding site of the E2 enzyme. ITC data demonstrated that the SUMO2 variant E08 binds with a 150-fold increased affinity to Ubc9 compared to the interaction with the wild type protein. From a thermodynamic perspective, this SUMO2 variant exhibited a solely enthalpy driven binding reaction, while wild type SUMO2 had a significant entropy contribution. This can be explained by newly established interactions between mutated residues on the SUMO2 variant and the interacting amino acids on Ubc9.

Cellular implications of this noncovalent inhibition mechanism were studied by Svenja Wiechmann and Anne Gärtner in their publication (Wiechmann et al. 2017). They showed that this inhibition caused an overall reduction of poly-SUMO chain formation in cells and that mono-SUMOylation was unaffected. This indicates that only the transfer of a second SUMO2 moiety was impaired. Similarly, another study has revealed that mutations on the back side binding site have similar effects on poly-SUMO chain formation (Capili and Lima, 2007).

In conclusion this inhibition mechanism is now well characterized and provides some important advantages when compared to for example RNA interference-based knockdowns of Ubc9 that would both affect mono-SUMO and poly-SUMO dependent cellular processes.

.

7. References

Abdul Rehman, S.A., Kristariyanto, Y.A., Choi, S.-Y., Nkosi, P.J., Weidlich, S., Labib, K., Hofmann, K., and Kulathu, Y. (2016). MINDY-1 Is a Member of an Evolutionarily Conserved and Structurally Distinct New Family of Deubiquitinating Enzymes. Mol. Cell *63*, 146–155.

Alfano, C., Faggiano, S., and Pastore, A. (2016). The Ball and Chain of Polyubiquitin Structures. Trends Biochem. Sci. *41*, 371–385.

Andrews, P. (1970). Estimation of molecular size and molecular weights of biological compounds by gel filtration. Methods Biochem Anal *18*, 1–53.

Bagola, K., von Delbruck, M., Dittmar, G., Scheffner, M., Ziv, I., Glickman, M.H., Ciechanover, A., and Sommer, T. (2013). Ubiquitin binding by a CUE domain regulates ubiquitin chain formation by ERAD E3 ligases. Mol Cell *50*, 528–539.

Bassermann, F., Eichner, R., and Pagano, M. (2014). The ubiquitin proteasome system - implications for cell cycle control and the targeted treatment of cancer. Biochim. Biophys. Acta *1843*, 150–162.

Bax, A., Clore, G.M., and Gronenborn, A.M. (1990). 1H 1H correlation via isotropic mixing of 13C magnetization, a new three-dimensional approach for assigning 1H and 13C spectra of 13C-enriched proteins. J. Magn. Reson. 1969 *88*, 425–431.

Bays, N.W., Gardner, R.G., Seelig, L.P., Joazeiro, C.A., and Hampton, R.Y. (2001). Hrd1p/Der3p is a membrane-anchored ubiquitin ligase required for ER-associated degradation. Nat. Cell Biol. *3*, 24–29.

Bazirgan, O.A., and Hampton, R.Y. (2008). Cue1p Is an Activator of Ubc7p E2 Activity *in Vitro* and *in Vivo*. J. Biol. Chem. *283*, 12797–12810.

Becker, T., Bhushan, S., Jarasch, A., Armache, J.-P., Funes, S., Jossinet, F., Gumbart, J., Mielke, T., Berninghausen, O., Schulten, K., et al. (2009). Structure of Monomeric Yeast and Mammalian Sec61 Complexes Interacting with the Translating Ribosome. Science *326*, 1369–1373.

Berndsen, C.E., and Wolberger, C. (2011). A spectrophotometric assay for conjugation of ubiquitin and ubiquitin-like proteins. Anal Biochem *418*, 102–110.

Biederer, T., Volkwein, C., and Sommer, T. (1997). Role of Cue1p in ubiquitination and degradation at the ER surface. Science *278*, 1806–1809.

Boehr, D.D., Nussinov, R., and Wright, P.E. (2009). The role of dynamic conformational ensembles in biomolecular recognition. Nat. Chem. Biol. *5*, 789–796.

Braten, O., Livneh, I., Ziv, T., Admon, A., Kehat, I., Caspi, L.H., Gonen, H., Bercovich, B., Godzik, A., Jahandideh, S., et al. (2016). Numerous proteins with unique characteristics are degraded by the 26S proteasome following monoubiquitination. Proc. Natl. Acad. Sci. *113*, E4639–E4647.

Bremm, A., Freund, S.M., and Komander, D. (2010). Lys11-linked ubiquitin chains adopt compact conformations and are preferentially hydrolyzed by the deubiquitinase Cezanne. Nat Struct Mol Biol *17*, 939–947.

Brown, N.G., Watson, E.R., Weissmann, F., Jarvis, M.A., VanderLinden, R., Grace, C.R.R., Frye, J.J., Qiao, R., Dube, P., Petzold, G., et al. (2014). Mechanism of Polyubiquitination by Human Anaphase-Promoting Complex: RING Repurposing for Ubiquitin Chain Assembly. Mol. Cell *56*, 246–260.

Brzovic, P.S., Lissounov, A., Christensen, D.E., Hoyt, D.W., and Klevit, R.E. (2006). A UbcH5/Ubiquitin Noncovalent Complex Is Required for Processive BRCA1-Directed Ubiquitination. Mol. Cell *21*, 873–880.

Buetow, L., Gabrielsen, M., Anthony, N.G., Dou, H., Patel, A., Aitkenhead, H., Sibbet, G.J., Smith, B.O., and Huang, D.T. (2015). Activation of a Primed RING E3-E2–Ubiquitin Complex by Non-Covalent Ubiquitin. Mol. Cell *58*, 297–310.

Camirand, A., Heysen, A., Grondin, B., and Herscovics, A. (1991). Glycoprotein biosynthesis in Saccharomyces cerevisiae. Isolation and characterization of the gene encoding a specific processing alpha-mannosidase. J. Biol. Chem. *266*, 15120–15127.

Capili, A.D., and Lima, C.D. (2007). Structure and Analysis of a Complex between SUMO and Ubc9 Illustrates Features of a Conserved E2-Ubl Interaction. J. Mol. Biol. *369*, 608–618.

Carvalho, P., Goder, V., and Rapoport, T.A. (2006). Distinct Ubiquitin-Ligase Complexes Define Convergent Pathways for the Degradation of ER Proteins. Cell *126*, 361–373.

Castañeda, C.A., Kashyap, T.R., Nakasone, M.A., Krueger, S., and Fushman, D. (2013). Unique Structural, Dynamical, and Functional Properties of K11-Linked Polyubiquitin Chains. Structure *21*, 1168–1181.

Chau, V., Tobias, J.W., Bachmair, A., Marriott, D., Ecker, D.J., Gonda, D.K., and Varshavsky, A. (1989). A multiubiquitin chain is confined to specific lysine in a targeted short-lived protein. Science *243*, 1576–1583.

Chen, Z.J. (2005). Ubiquitin signalling in the NF-κB pathway. Nat. Cell Biol. *7*, 758–765.

Chen, P., Johnson, P., Sommer, T., Jentsch, S., and Hochstrasser, M. (1993). Multiple ubiquitin-conjugating enzymes participate in the in vivo degradation of the yeast MAT alpha 2 repressor. Cell *74*, 357–369.

Chiti, F., and Dobson, C.M. (2017). Protein Misfolding, Amyloid Formation, and Human Disease: A Summary of Progress Over the Last Decade. Annu. Rev. Biochem. *86*, 27–68.

Choi, Y.-S., Wu, K., Jeong, K., Lee, D., Jeon, Y.H., Choi, B.-S., Pan, Z.-Q., Ryu, K.-S., and Cheong, C. (2010). The Human Cdc34 Carboxyl Terminus Contains a Non-covalent Ubiquitin Binding Activity That Contributes to SCF-dependent Ubiquitination. J. Biol. Chem. *285*, 17754–17762.

Chong, R.A., Wu, K., Spratt, D.E., Yang, Y., Lee, C., Nayak, J., Xu, M., Elkholi, R., Tappin, I., Li, J., et al. (2014). Pivotal role for the ubiquitin Y59-E51 loop in lysine 48 polyubiquitination. Proc. Natl. Acad. Sci. *111*, 8434–8439.

Christensen, D.E., Brzovic, P.S., and Klevit, R.E. (2007). E2–BRCA1 RING interactions dictate synthesis of mono- or specific polyubiquitin chain linkages. Nat. Struct. Mol. Biol. *14*, 941–948.

Clerc, S., Hirsch, C., Oggier, D.M., Deprez, P., Jakob, C., Sommer, T., and Aebi, M. (2009). Htm1 protein generates the N-glycan signal for glycoprotein degradation in the endoplasmic reticulum. J. Cell Biol. *184*, 159–172.

Clore, G.M., Tang, C., and Iwahara, J. (2007). Elucidating transient macromolecular interactions using paramagnetic relaxation enhancement. Curr. Opin. Struct. Biol. *17*, 603–616.

Cohen, I., Wiener, R., Reiss, Y., and Ravid, T. (2015). Distinct activation of an E2 ubiquitin-conjugating enzyme by its cognate E3 ligases. Proc. Natl. Acad. Sci. *112*, E625–E632.

Conaway, R.C. (2002). Emerging Roles of Ubiquitin in Transcription Regulation. Science *296*, 1254–1258.

Cook, W.J., Jeffrey, L.C., Carson, M., Chen, Z., and Pickart, C.M. (1992). Structure of a diubiquitin conjugate and a model for interaction with ubiquitin conjugating enzyme (E2). J Biol Chem *267*, 16467–16471.

Cook, W.J., Jeffrey, L.C., Kasperek, E., and Pickart, C.M. (1994). Structure of Tetraubiquitin Shows How Multiubiquitin Chains Can Be Formed. J. Mol. Biol. *236*, 601–609.

D'Alessio, C., and M. Dahms, N. (2015). Glucosidase II and MRH-Domain Containing Proteins in the Secretory Pathway. Curr. Protein Pept. Sci. *16*, 31–48.

Daniels, R., Kurowski, B., Johnson, A.E., and Hebert, D.N. (2003). N-linked glycans direct the cotranslational folding pathway of influenza hemagglutinin. Mol. Cell *11*, 79–90.

Das, R., Liang, Y.-H., Mariano, J., Li, J., Huang, T., King, A., Tarasov, S.G., Weissman, A.M., Ji, X., and Byrd, R.A. (2013). Allosteric regulation of E2:E3 interactions promote a processive ubiquitination machine. EMBO J. *32*, 2504–2516.

Datta, A.B., Hura, G.L., and Wolberger, C. (2009). The Structure and Conformation of Lys63-Linked Tetraubiquitin. J. Mol. Biol. *392*, 1117–1124.

von Delbruck, M., Kniss, A., Rogov, V.V., Pluska, L., Bagola, K., Lohr, F., Guntert, P., Sommer, T., and Dotsch, V. (2016). The CUE Domain of Cue1 Aligns Growing Ubiquitin Chains with Ubc7 for Rapid Elongation. Mol Cell *62*, 918–928.

Deshaies, R.J., and Joazeiro, C.A.P. (2009). RING domain E3 ubiquitin ligases. Annu. Rev. Biochem. *78*, 399–434.

van Dijk, A.D.J., Fushman, D., and Bonvin, A.M.J.J. (2005). Various strategies of using residual dipolar couplings in NMR-driven protein docking: Application to Lys48-linked di-ubiquitin and validation against 15N-relaxation data. Proteins Struct. Funct. Bioinforma. *60*, 367–381.

Dikic, I., Wakatsuki, S., and Walters, K.J. (2009). Ubiquitin-binding domains — from structures to functions. Nat. Rev. Mol. Cell Biol. *10*, 659–671.

Dong, K.C., Helgason, E., Yu, C., Phu, L., Arnott, D.P., Bosanac, I., Compaan, D.M., Huang, O.W., Fedorova, A.V., Kirkpatrick, D.S., et al. (2011). Preparation of distinct ubiquitin chain reagents of high purity and yield. Structure *19*, 1053–1063.

Eddins, M.J., Carlile, C.M., Gomez, K.M., Pickart, C.M., and Wolberger, C. (2006). Mms2–Ubc13 covalently bound to ubiquitin reveals the structural basis of linkage-specific polyubiquitin chain formation. Nat. Struct. Mol. Biol. *13*, 915–920.

Eddins, M.J., Varadan, R., Fushman, D., Pickart, C.M., and Wolberger, C. (2007). Crystal Structure and Solution NMR Studies of Lys48-linked Tetraubiquitin at Neutral pH. J. Mol. Biol. *367*, 204–211.

Edelmann, M.J., Iphöfer, A., Akutsu, M., Altun, M., di Gleria, K., Kramer, H.B., Fiebiger, E., Dhe-Paganon, S., and Kessler, B.M. (2009). Structural basis and specificity of human otubain 1-mediated deubiquitination. Biochem. J. *418*, 379–390.

Eisenhardt, N., Chaugule, V.K., Koidl, S., Droescher, M., Dogan, E., Rettich, J., Sutinen, P., Imanishi, S.Y., Hofmann, K., Palvimo, J.J., et al. (2015). A new vertebrate SUMO enzyme family reveals insights into SUMO-chain assembly. Nat. Struct. Mol. Biol. *22*, 959–967.

Eletr, Z.M., Huang, D.T., Duda, D.M., Schulman, B.A., and Kuhlman, B. (2005). E2 conjugating enzymes must disengage from their E1 enzymes before E3-dependent ubiquitin and ubiquitin-like transfer. Nat. Struct. Mol. Biol. *12*, 933–934.

Elsasser, S., Chandler-Militello, D., Müller, B., Hanna, J., and Finley, D. (2004). Rad23 and Rpn10 Serve as Alternative Ubiquitin Receptors for the Proteasome. J. Biol. Chem. *279*, 26817–26822.

van den Ent, F., and Lowe, J. (2006). RF cloning: a restriction-free method for inserting target genes into plasmids. J Biochem Biophys Methods *67*, 67–74.

Fielding, L. (2003). NMR methods for the determination of protein-ligand dissociation constants. Curr Top Med Chem *3*, 39–53.

Finley, D. (2009). Recognition and Processing of Ubiquitin-Protein Conjugates by the Proteasome. Annu. Rev. Biochem. *78*, 477–513.

Finley, D., Ulrich, H.D., Sommer, T., and Kaiser, P. (2012). The Ubiquitin-Proteasome System of Saccharomyces cerevisiae. Genetics *192*, 319–360.

Flotho, A., and Melchior, F. (2013). Sumoylation: a regulatory protein modification in health and disease. Annu. Rev. Biochem. *82*, 357–385.

Foresti, O., Rodriguez-Vaello, V., Funaya, C., and Carvalho, P. (2014). Quality control of inner nuclear membrane proteins by the Asi complex. Science *346*, 751–755.

Fushman, D., and Walker, O. (2010). Exploring the Linkage Dependence of Polyubiquitin Conformations Using Molecular Modeling. J. Mol. Biol. *395*, 803–814.

Galanty, Y., Belotserkovskaya, R., Coates, J., and Jackson, S.P. (2012). RNF4, a SUMO-targeted ubiquitin E3 ligase, promotes DNA double-strand break repair. Genes Dev. *26*, 1179–1195.

Gao, S., Pan, M., Zheng, Y., Huang, Y., Zheng, Q., Sun, D., Lu, L., Tan, X., Tan, X., Lan, H., et al. (2016). Monomer/Oligomer Quasi-Racemic Protein Crystallography. J. Am. Chem. Soc. *138*, 14497–14502.

Gareau, J.R., and Lima, C.D. (2010). The SUMO pathway: emerging mechanisms that shape specificity, conjugation and recognition. Nat. Rev. Mol. Cell Biol. *11*, 861–871.

Gauss, R., Jarosch, E., Sommer, T., and Hirsch, C. (2006). A complex of Yos9p and the HRD ligase integrates endoplasmic reticulum quality control into the degradation machinery. Nat. Cell Biol. *8*, 849–854.

Gill, S.C., and von Hippel, P.H. (1989). Calculation of protein extinction coefficients from amino acid sequence data. Anal Biochem *182*, 319–326.

Goto, E., Yamanaka, Y., Ishikawa, A., Aoki-Kawasumi, M., Mito-Yoshida, M., Ohmura-Hoshino, M., Matsuki, Y., Kajikawa, M., Hirano, H., and Ishido, S. (2010). Contribution of Lysine 11-linked Ubiquitination to MIR2-mediated Major Histocompatibility Complex Class I Internalization. J. Biol. Chem. *285*, 35311–35319.

Grzesiek, S., Anglister, J., and Bax, A. (1993). Correlation of Backbone Amide and Aliphatic Side-Chain Resonances in 13C/15N-Enriched Proteins by Isotropic Mixing of 13C Magnetization. J. Magn. Reson. B *101*, 114–119.

Guntert, P., and Buchner, L. (2015). Combined automated NOE assignment and structure calculation with CYANA. J Biomol NMR *62*, 453–471.

Guntert, P., Mumenthaler, C., and Wuthrich, K. (1997). Torsion angle dynamics for NMR structure calculation with the new program DYANA. J Mol Biol *273*, 283–298.

Habeck, G., Ebner, F.A., Shimada-Kreft, H., and Kreft, S.G. (2015). The yeast ERAD-C ubiquitin ligase Doa10 recognizes an intramembrane degron. J. Cell Biol. *209*, 261–273.

Haglund, K., and Dikic, I. (2012). The role of ubiquitylation in receptor endocytosis and endosomal sorting. J. Cell Sci. *125*, 265–275.

Haglund, K., Sigismund, S., Polo, S., Szymkiewicz, I., Di Fiore, P.P., and Dikic, I. (2003). Multiple monoubiquitination of RTKs is sufficient for their endocytosis and degradation. Nat. Cell Biol. *5*, 461–466.

Hanna, J., Schütz, A., Zimmermann, F., Behlke, J., Sommer, T., and Heinemann, U. (2012). Structural and Biochemical Basis of Yos9 Protein Dimerization and Possible Contribution to Self-association of 3-Hydroxy-3-methylglutaryl-Coenzyme A Reductase Degradation Ubiquitin-Ligase Complex. J. Biol. Chem. *287*, 8633–8640.

Hebert, D.N., Foellmer, B., and Helenius, A. (1995). Glucose trimming and reglucosylation determine glycoprotein association with calnexin in the endoplasmic reticulum. Cell *81*, 425–433.

Hershko, A., and Ciechanover, A. (1998). THE UBIQUITIN SYSTEM. Annu. Rev. Biochem. *67*, 425–479.

Hershko, A., Ciechanover, A., Heller, H., Haas, A.L., and Rose, I.A. (1980). Proposed role of ATP in protein breakdown: conjugation of protein with multiple chains of the polypeptide of ATP-dependent proteolysis. Proc. Natl. Acad. Sci. U. S. A. *77*, 1783–1786.

Hirano, T., Serve, O., Yagi-Utsumi, M., Takemoto, E., Hiromoto, T., Satoh, T., Mizushima, T., and Kato, K. (2011). Conformational Dynamics of Wild-type Lys-48-linked Diubiquitin in Solution. J. Biol. Chem. *286*, 37496–37502.

Hirsch, C., Gauss, R., Horn, S.C., Neuber, O., and Sommer, T. (2009). The ubiquitylation machinery of the endoplasmic reticulum. Nature *458*, 453–460.

Hornbeck, P.V., Zhang, B., Murray, B., Kornhauser, J.M., Latham, V., and Skrzypek, E. (2015). PhosphoSitePlus, 2014: mutations, PTMs and recalibrations. Nucleic Acids Res. *43*, D512-520.

Hu, D., Kamiya, Y., Totani, K., Kamiya, D., Kawasaki, N., Yamaguchi, D., Matsuo, I., Matsumoto, N., Ito, Y., Kato, K., et al. (2009). Sugar-binding activity of the MRH domain in the ER -glucosidase II subunit is important for efficient glucose trimming. Glycobiology *19*, 1127–1135.

Hu, H., Brittain, G.C., Chang, J.-H., Puebla-Osorio, N., Jin, J., Zal, A., Xiao, Y., Cheng, X., Chang, M., Fu, Y.-X., et al. (2013). OTUD7B controls non-canonical NF-κB activation through deubiquitination of TRAF3. Nature *494*, 371–374.

Hu, M., Li, P., Song, L., Jeffrey, P.D., Chenova, T.A., Wilkinson, K.D., Cohen, R.E., and Shi, Y. (2005). Structure and mechanisms of the proteasome-associated deubiquitinating enzyme USP14. EMBO J. *24*, 3747–3756.

Huang, T.T., and D'Andrea, A.D. (2006). Regulation of DNA repair by ubiquitylation. Nat. Rev. Mol. Cell Biol. *7*, 323–334.

Hurley, J.H., Lee, S., and Prag, G. (2006). Ubiquitin-binding domains. Biochem. J. *399*, 361–372.
Husnjak, K., and Dikic, I. (2012). Ubiquitin-Binding Proteins: Decoders of Ubiquitin-Mediated Cellular Functions. Annu. Rev. Biochem. *81*, 291–322.

Husnjak, K., Elsasser, S., Zhang, N., Chen, X., Randles, L., Shi, Y., Hofmann, K., Walters, K.J., Finley, D., and Dikic, I. (2008). Proteasome subunit Rpn13 is a novel ubiquitin receptor. Nature *453*, 481–488.

Ikeda, F., Deribe, Y.L., Skånland, S.S., Stieglitz, B., Grabbe, C., Franz-Wachtel, M., van Wijk, S.J.L., Goswami, P., Nagy, V., Terzic, J., et al. (2011). SHARPIN forms a linear ubiquitin ligase complex regulating NF-κB activity and apoptosis. Nature *471*, 637–641.

Iwahara, J., Tang, C., and Marius Clore, G. (2007). Practical aspects of 1H transverse paramagnetic relaxation enhancement measurements on macromolecules. J. Magn. Reson. *184*, 185–195.

Jeschke, G. (2012). DEER distance measurements on proteins. Annu Rev Phys Chem *63*, 419–446.

Jeschke, G. (2013). Conformational dynamics and distribution of nitroxide spin labels. Prog. Nucl. Magn. Reson. Spectrosc. *72*, 42–60.

Jin, L., Williamson, A., Banerjee, S., Philipp, I., and Rape, M. (2008). Mechanism of Ubiquitin-Chain Formation by the Human Anaphase-Promoting Complex. Cell *133*, 653–665.

Kamadurai, H.B., Souphron, J., Scott, D.C., Duda, D.M., Miller, D.J., Stringer, D., Piper, R.C., and Schulman, B.A. (2009). Insights into Ubiquitin Transfer Cascades from a Structure of a UbcH5B∼Ubiquitin-HECTNEDD4L Complex. Mol. Cell *36*, 1095–1102.

Kang, R.S., Daniels, C.M., Francis, S.A., Shih, S.C., Salerno, W.J., Hicke, L., and Radhakrishnan, I. (2003). Solution structure of a CUE-ubiquitin complex reveals a conserved mode of ubiquitin binding. Cell *113*, 621–630.

Kelly, A., Wickliffe, K.E., Song, L., Fedrigo, I., and Rape, M. (2014). Ubiquitin Chain Elongation Requires E3-Dependent Tracking of the Emerging Conjugate. Mol. Cell *56*, 232–245.

Khmelinskii, A., Blaszczak, E., Pantazopoulou, M., Fischer, B., Omnus, D.J., Le Dez, G., Brossard, A., Gunnarsson, A., Barry, J.D., Meurer, M., et al. (2014). Protein quality control at the inner nuclear membrane. Nature *516*, 410–413.

Knipscheer, P., van Dijk, W.J., Olsen, J.V., Mann, M., and Sixma, T.K. (2007). Noncovalent interaction between Ubc9 and SUMO promotes SUMO chain formation. EMBO J. *26*, 2797–2807.

Kniss, A., Schuetz, D., Kazemi, S., Pluska, L., Spindler, P.E., Rogov, V.V., Husnjak, K., Dikic, I., Güntert, P., Sommer, T., et al. (2018). Chain Assembly and Disassembly Processes Differently Affect the Conformational Space of Ubiquitin Chains. Structure.

Knop, M., Finger, A., Braun, T., Hellmuth, K., and Wolf, D.H. (1996). Der1, a novel protein specifically required for endoplasmic reticulum degradation in yeast. EMBO J. *15*, 753–763.

Koegl, M., Hoppe, T., Schlenker, S., Ulrich, H.D., Mayer, T.U., and Jentsch, S. (1999). A novel ubiquitination factor, E4, is involved in multiubiquitin chain assembly. Cell *96*, 635–644.

Komander, D., and Rape, M. (2012). The Ubiquitin Code. Annu. Rev. Biochem. *81*, 203–229.

Komander, D., Reyes-Turcu, F., Licchesi, J.D.F., Odenwaelder, P., Wilkinson, K.D., and Barford, D. (2009a). Molecular discrimination of structurally equivalent Lys 63-linked and linear polyubiquitin chains. EMBO Rep. *10*, 466–473.

Komander, D., Clague, M.J., and Urbé, S. (2009b). Breaking the chains: structure and function of the deubiquitinases. Nat. Rev. Mol. Cell Biol. *10*, 550–563.

Koradi, R., Billeter, M., and Güntert, P. (2000). Point-centered domain decomposition for parallel molecular dynamics simulation. Comput. Phys. Commun. *124*, 139–147.

Kostova, Z., Mariano, J., Scholz, S., Koenig, C., and Weissman, A.M. (2009). A Ubc7p-binding domain in Cue1p activates ER-associated protein degradation. J. Cell Sci. *122*, 1374–1381.

Kreft, S.G., and Hochstrasser, M. (2011). An Unusual Transmembrane Helix in the Endoplasmic Reticulum Ubiquitin Ligase Doa10 Modulates Degradation of Its Cognate E2 Enzyme. J. Biol. Chem. *286*, 20163–20174.

Kreft, S.G., Wang, L., and Hochstrasser, M. (2006). Membrane Topology of the Yeast Endoplasmic Reticulum-localized Ubiquitin Ligase Doa10 and Comparison with Its Human Ortholog TEB4 (MARCH-VI). J. Biol. Chem. *281*, 4646–4653.

Kristariyanto, Y.A., Abdul Rehman, S.A., Campbell, D.G., Morrice, N.A., Johnson, C., Toth, R., and Kulathu, Y. (2015a). K29-Selective Ubiquitin Binding Domain Reveals Structural Basis of Specificity and Heterotypic Nature of K29 Polyubiquitin. Mol. Cell *58*, 83–94.

Kristariyanto, Y.A., Choi, S.-Y., Rehman, S.A.A., Ritorto, M.S., Campbell, D.G., Morrice, N.A., Toth, R., and Kulathu, Y. (2015b). Assembly and structure of Lys33-linked polyubiquitin reveals distinct conformations. Biochem. J. *467*, 345–352.

Laemmli, U.K. (1970). Cleavage of structural proteins during the assembly of the head of bacteriophage T4. Nature *227*, 680–685.

Lai, M.-Y., Zhang, D., LaRonde-LeBlanc, N., and Fushman, D. (2012). Structural and biochemical studies of the open state of Lys48-linked diubiquitin. Biochim. Biophys. Acta BBA - Mol. Cell Res. *1823*, 2046–2056.

Lallemand-Breitenbach, V., Jeanne, M., Benhenda, S., Nasr, R., Lei, M., Peres, L., Zhou, J., Zhu, J., Raught, B., and de Thé, H. (2008). Arsenic degrades PML or PML–RARα through a SUMO-triggered RNF4/ubiquitin-mediated pathway. Nat. Cell Biol. *10*, 547–555.

Lander, E.S., Linton, L.M., Birren, B., Nusbaum, C., Zody, M.C., Baldwin, J., Devon, K., Dewar, K., Doyle, M., FitzHugh, W., et al. (2001). Initial sequencing and analysis of the human genome. Nature *409*, 860–921.

Lange, O.F., Lakomek, N.-A., Fares, C., Schroder, G.F., Walter, K.F.A., Becker, S., Meiler, J., Grubmuller, H., Griesinger, C., and de Groot, B.L. (2008). Recognition Dynamics Up to Microseconds Revealed from an RDC-Derived Ubiquitin Ensemble in Solution. Science *320*, 1471–1475.

Lee, I., and Schindelin, H. (2008). Structural Insights into E1-Catalyzed Ubiquitin Activation and Transfer to Conjugating Enzymes. Cell *134*, 268–278.

Lee, W., Tonelli, M., and Markley, J.L. (2015). NMRFAM-SPARKY: enhanced software for biomolecular NMR spectroscopy. Bioinformatics *31*, 1325–1327.

Lin, Y., Hwang, W.C., and Basavappa, R. (2002). Structural and Functional Analysis of the Human Mitotic-specific Ubiquitin-conjugating Enzyme, UbcH10. J. Biol. Chem. *277*, 21913–21921.

Liu, Q., Shen, B., Chen, D.J., and Chen, Y. (1999). Backbone resonance assignments of human UBC9. J Biomol NMR *13*, 89–90.

Liu, S., Chen, Y., Li, J., Huang, T., Tarasov, S., King, A., Weissman, A.M., Byrd, R.A., and Das, R. (2012). Promiscuous Interactions of gp78 E3 Ligase CUE Domain with Polyubiquitin Chains. Structure *20*, 2138–2150.

Liu, W., Shang, Y., Zeng, Y., Liu, C., Li, Y., Zhai, L., Wang, P., Lou, J., Xu, P., Ye, Y., et al. (2014). Dimeric Ube2g2 simultaneously engages donor and acceptor ubiquitins to form Lys48-linked ubiquitin chains. EMBO J. *33*, 46–61.

Lohr, F., Hansel, R., Rogov, V.V., and Dotsch, V. (2007). Improved pulse sequences for sequence specific assignment of aromatic proton resonances in proteins. J Biomol NMR *37*, 205–224.

Lorick, K.L., Jensen, J.P., Fang, S., Ong, A.M., Hatakeyama, S., and Weissman, A.M. (1999). RING fingers mediate ubiquitin-conjugating enzyme (E2)-dependent ubiquitination. Proc. Natl. Acad. Sci. U. S. A. *96*, 11364–11369.

Machida, Y.J., Machida, Y., Chen, Y., Gurtan, A.M., Kupfer, G.M., D'Andrea, A.D., and Dutta, A. (2006). UBE2T Is the E2 in the Fanconi Anemia Pathway and Undergoes Negative Autoregulation. Mol. Cell *23*, 589–596.

Marion, D., Driscoll, P.C., Kay, L.E., Wingfield, P.T., Bax, A., Gronenborn, A.M., and Clore, G.M. (2002). Overcoming the overlap problem in the assignment of proton NMR spectra of larger proteins by use of three-dimensional heteronuclear proton-nitrogen-15 Hartmann-Hahn-multiple quantum coherence and nuclear Overhauser-multiple quantum coherence spectroscopy: application to interleukin 1.beta. Biochemistry (Mosc.) *28*, 6150–6156.

Matic, I., van Hagen, M., Schimmel, J., Macek, B., Ogg, S.C., Tatham, M.H., Hay, R.T., Lamond, A.I., Mann, M., and Vertegaal, A.C.O. (2008). *In Vivo* Identification of Human Small Ubiquitin-like Modifier Polymerization Sites by High Accuracy Mass Spectrometry and an *in Vitro* to *in Vivo* Strategy. Mol. Cell. Proteomics *7*, 132–144.

Matlack, K.E., Mothes, W., and Rapoport, T.A. (1998). Protein translocation: tunnel vision. Cell *92*, 381–390.

Matsumoto, M.L., Wickliffe, K.E., Dong, K.C., Yu, C., Bosanac, I., Bustos, D., Phu, L., Kirkpatrick, D.S., Hymowitz, S.G., Rape, M., et al. (2010). K11-Linked Polyubiquitination in Cell Cycle Control Revealed by a K11 Linkage-Specific Antibody. Mol. Cell *39*, 477–484.

Medicherla, B., Kostova, Z., Schaefer, A., and Wolf, D.H. (2004). A genomic screen identifies Dsk2p and Rad23p as essential components of ER-associated degradation. EMBO Rep. *5*, 692–697.

Mehnert, M., Sommer, T., and Jarosch, E. (2014). Der1 promotes movement of misfolded proteins through the endoplasmic reticulum membrane. Nat. Cell Biol. *16*, 77–86.

Metzger, M.B., Liang, Y.-H., Das, R., Mariano, J., Li, S., Li, J., Kostova, Z., Byrd, R.A., Ji, X., and Weissman, A.M. (2013). A Structurally Unique E2-Binding Domain Activates Ubiquitination by the ERAD E2, Ubc7p, through Multiple Mechanisms. Mol. Cell *50*, 516–527.

Mevissen, T.E.T., Hospenthal, M.K., Geurink, P.P., Elliott, P.R., Akutsu, M., Arnaudo, N., Ekkebus, R., Kulathu, Y., Wauer, T., El Oualid, F., et al. (2013). OTU deubiquitinases reveal mechanisms of linkage specificity and enable ubiquitin chain restriction analysis. Cell *154*, 169–184.

Mevissen, T.E.T., Kulathu, Y., Mulder, M.P.C., Geurink, P.P., Maslen, S.L., Gersch, M., Elliott, P.R., Burke, J.E., van Tol, B.D.M., Akutsu, M., et al. (2016). Molecular basis of Lys11-polyubiquitin specificity in the deubiquitinase Cezanne. Nature *538*, 402–405.

Meyer, H.-J., and Rape, M. (2014). Enhanced Protein Degradation by Branched Ubiquitin Chains. Cell *157*, 910–921.

Michel, M.A., Elliott, P.R., Swatek, K.N., Simicek, M., Pruneda, J.N., Wagstaff, J.L., Freund, S.M.V., and Komander, D. (2015). Assembly and Specific Recognition of K29- and K33-Linked Polyubiquitin. Mol. Cell *58*, 95–109.

Montelione, G.T., Lyons, B.A., Emerson, S.D., and Tashiro, M. (1992). An efficient triple resonance experiment using carbon-13 isotropic mixing for determining sequence-specific resonance assignments of isotopically-enriched proteins. J. Am. Chem. Soc. *114*, 10974–10975.

Nakada, S., Tai, I., Panier, S., Al-Hakim, A., Iemura, S.-I., Juang, Y.-C., O'Donnell, L., Kumakubo, A., Munro, M., Sicheri, F., et al. (2010). Non-canonical inhibition of DNA damage-dependent ubiquitination by OTUB1. Nature *466*, 941–946.

Nakasone, M.A., Livnat-Levanon, N., Glickman, M.H., Cohen, R.E., and Fushman, D. (2013). Mixed-Linkage Ubiquitin Chains Send Mixed Messages. Structure *21*, 727–740.

Nakatsukasa, K., Huyer, G., Michaelis, S., and Brodsky, J.L. (2008). Dissecting the ER-Associated Degradation of a Misfolded Polytopic Membrane Protein. Cell *132*, 101–112.

Neuber, O., Jarosch, E., Volkwein, C., Walter, J., and Sommer, T. (2005). Ubx2 links the Cdc48 complex to ER-associated protein degradation. Nat. Cell Biol. *7*, 993–998.

Nie, M., and Boddy, M. (2016). Cooperativity of the SUMO and Ubiquitin Pathways in Genome Stability. Biomolecules *6*, 14.

Ohtake, F., Saeki, Y., Ishido, S., Kanno, J., and Tanaka, K. (2016). The K48-K63 Branched Ubiquitin Chain Regulates NF-κB Signaling. Mol. Cell *64*, 251–266.

Olson, L.J., Orsi, R., Alculumbre, S.G., Peterson, F.C., Stigliano, I.D., Parodi, A.J., D'Alessio, C., and Dahms, N.M. (2013). Structure of the Lectin Mannose 6-Phosphate Receptor Homology (MRH) Domain of Glucosidase II, an Enzyme That Regulates Glycoprotein Folding Quality Control in the Endoplasmic Reticulum. J. Biol. Chem. *288*, 16460–16475.

Olson, L.J., Orsi, R., Peterson, F.C., Parodi, A.J., Kim, J.-J.P., D'Alessio, C., and Dahms, N.M. (2015). Crystal Structure and Functional Analyses of the Lectin Domain of Glucosidase II: Insights into Oligomannose Recognition. Biochemistry (Mosc.) *54*, 4097–4111.

Page, R.C., Pruneda, J.N., Amick, J., Klevit, R.E., and Misra, S. (2012). Structural Insights into the Conformation and Oligomerization of E2∼Ubiquitin Conjugates. Biochemistry (Mosc.) *51*, 4175–4187.

Pannier, M., Veit, S., Godt, A., Jeschke, G., and Spiess, H.W. (2000). Dead-time free measurement of dipole-dipole interactions between electron spins. J Magn Reson *142*, 331–340.

Peng, J., Schwartz, D., Elias, J.E., Thoreen, C.C., Cheng, D., Marsischky, G., Roelofs, J., Finley, D., and Gygi, S.P. (2003). A proteomics approach to understanding protein ubiquitination. Nat. Biotechnol. *21*, 921–926.

Petrucelli, L., and Dawson, T.M. (2004). Mechanism of neurodegenerative disease: role of the ubiquitin proteasome system. Ann. Med. *36*, 315–320.

Phillips, C.L., Thrower, J., Pickart, C.M., and Hill, C.P. (2001). Structure of a new crystal form of tetraubiquitin. Acta Crystallogr Biol Crystallogr *57*, 341–344.

Plechanovova, A., Jaffray, E.G., Tatham, M.H., Naismith, J.H., and Hay, R.T. (2012). Structure of a RING E3 ligase and ubiquitin-loaded E2 primed for catalysis. Nature *489*, 115–120.

Polyhach, Y., Bordignon, E., and Jeschke, G. (2011). Rotamer libraries of spin labelled cysteines for protein studies. Phys Chem Chem Phys *13*, 2356–2366.

Ponder, J.W., and Case, D.A. (2003). Force fields for protein simulations. Adv Protein Chem *66*, 27–85.

Pruneda, J.N., Stoll, K.E., Bolton, L.J., Brzovic, P.S., and Klevit, R.E. (2011). Ubiquitin in Motion: Structural Studies of the Ubiquitin-Conjugating Enzyme∼Ubiquitin Conjugate. Biochemistry (Mosc.) *50*, 1624–1633.

Pruneda, J.N., Littlefield, P.J., Soss, S.E., Nordquist, K.A., Chazin, W.J., Brzovic, P.S., and Klevit, R.E. (2012). Structure of an E3:E2∼Ub Complex Reveals an Allosteric Mechanism Shared among RING/U-box Ligases. Mol. Cell *47*, 933–942.

Quan, E.M., Kamiya, Y., Kamiya, D., Denic, V., Weibezahn, J., Kato, K., and Weissman, J.S. (2008). Defining the glycan destruction signal for endoplasmic reticulum-associated degradation. Mol. Cell *32*, 870–877.

Raasi, S., and Pickart, C.M. (2005). Ubiquitin chain synthesis. Methods Mol Biol *301*, 47–55.
Raman, N., Nayak, A., and Muller, S. (2013). The SUMO system: a master organizer of nuclear protein assemblies. Chromosoma *122*, 475–485.

Ravid, T., and Hochstrasser, M. (2007). Autoregulation of an E2 enzyme by ubiquitin-chain assembly on its catalytic residue. Nat. Cell Biol. *9*, 422–427.

Rodriguez, M.S., Dargemont, C., and Hay, R.T. (2001). SUMO-1 Conjugation *in Vivo* Requires Both a Consensus Modification Motif and Nuclear Targeting. J. Biol. Chem. *276*, 12654–12659.

Rogov, V.V., Rozenknop, A., Rogova, N.Y., Lohr, F., Tikole, S., Jaravine, V., Guntert, P., Dikic, I., and Dotsch, V. (2012). A universal expression tag for structural and functional studies of proteins. Chembiochem *13*, 959–963.

Rohaim, A., Kawasaki, M., Kato, R., Dikic, I., and Wakatsuki, S. (2012). Structure of a compact conformation of linear diubiquitin. Acta Crystallogr. D Biol. Crystallogr. *68*, 102–108.

Ryabov, Y., and Fushman, D. (2006). Interdomain mobility in di-ubiquitin revealed by NMR. Proteins Struct. Funct. Bioinforma. *63*, 787–796.

Ryabov, Y., and Fushman, D. (2007). Structural Assembly of Multidomain Proteins and Protein Complexes Guided by the Overall Rotational Diffusion Tensor. J. Am. Chem. Soc. *129*, 7894–7902.

Sakata, E., Satoh, T., Yamamoto, S., Yamaguchi, Y., Yagi-Utsumi, M., Kurimoto, E., Tanaka, K., Wakatsuki, S., and Kato, K. (2010). Crystal Structure of UbcH5b~Ubiquitin Intermediate: Insight into the Formation of the Self-Assembled E2~Ub Conjugates. Structure *18*, 138–147.

Sakata, E., Bohn, S., Mihalache, O., Kiss, P., Beck, F., Nagy, I., Nickell, S., Tanaka, K., Saeki, Y., Forster, F., et al. (2012). Localization of the proteasomal ubiquitin receptors Rpn10 and Rpn13 by electron cryomicroscopy. Proc. Natl. Acad. Sci. *109*, 1479–1484.

Salzmann, M., Pervushin, K., Wider, G., Senn, H., and Wuthrich, K. (1998). TROSY in triple-resonance experiments: new perspectives for sequential NMR assignment of large proteins. Proc Natl Acad Sci U A *95*, 13585–13590.

Salzmann, M., Wider, G., Pervushin, K., Senn, H., and Wüthrich, K. (1999). TROSY-type Triple-Resonance Experiments for Sequential NMR Assignments of Large Proteins. J. Am. Chem. Soc. *121*, 844–848.

Schauber, C., Chen, L., Tongaonkar, P., Vega, I., Lambertson, D., Potts, W., and Madura, K. (1998). Rad23 links DNA repair to the ubiquitin/proteasome pathway. Nature *391*, 715–718.

Scheffner, M., Nuber, U., and Huibregtse, J.M. (1995). Protein ubiquitination involving an E1–E2–E3 enzyme ubiquitin thioester cascade. Nature *373*, 81–83.

Schoebel, S., Mi, W., Stein, A., Ovchinnikov, S., Pavlovicz, R., DiMaio, F., Baker, D., Chambers, M.G., Su, H., Li, D., et al. (2017). Cryo-EM structure of the protein-conducting ERAD channel Hrd1 in complex with Hrd3. Nature *548*, 352–355.

Schubert, U., Antón, L.C., Gibbs, J., Norbury, C.C., Yewdell, J.W., and Bennink, J.R. (2000). Rapid degradation of a large fraction of newly synthesized proteins by proteasomes. Nature *404*, 770–774.

Schuberth, C., and Buchberger, A. (2005). Membrane-bound Ubx2 recruits Cdc48 to ubiquitin ligases and their substrates to ensure efficient ER-associated protein degradation. Nat. Cell Biol. *7*, 999–1006.

Schulman, B.A., and Harper, J.W. (2009). Ubiquitin-like protein activation by E1 enzymes: the apex for downstream signalling pathways. Nat. Rev. Mol. Cell Biol. *10*, 319–331.

Shen, Y., Delaglio, F., Cornilescu, G., and Bax, A. (2009). TALOS+: a hybrid method for predicting protein backbone torsion angles from NMR chemical shifts. J Biomol NMR *44*, 213–223.

Siepmann, T.J., Bohnsack, R.N., Tokgöz, Z., Baboshina, O.V., and Haas, A.L. (2003). Protein Interactions within the N-end Rule Ubiquitin Ligation Pathway. J. Biol. Chem. *278*, 9448–9457.

Sims, J.J., and Cohen, R.E. (2009). Linkage-Specific Avidity Defines the Lysine 63-Linked Polyubiquitin-Binding Preference of Rap80. Mol. Cell *33*, 775–783.

Sloper-Mould, K.E., Jemc, J.C., Pickart, C.M., and Hicke, L. (2001). Distinct Functional Surface Regions on Ubiquitin. J. Biol. Chem. *276*, 30483–30489.

Smith, M.H., Rodriguez, E.H., and Weissman, J.S. (2014). Misfolded Proteins Induce Aggregation of the Lectin Yos9. J. Biol. Chem. *289*, 25670–25677.

Spindler, P.E., Waclawska, I., Endeward, B., Plackmeyer, J., Ziegler, C., and Prisner, T.F. (2015). Carr-Purcell Pulsed Electron Double Resonance with Shaped Inversion Pulses. J Phys Chem Lett *6*, 4331–4335.

Sriramachandran, A.M., and Dohmen, R.J. (2014). SUMO-targeted ubiquitin ligases. Biochim. Biophys. Acta BBA - Mol. Cell Res. *1843*, 75–85.

Stein, A., Ruggiano, A., Carvalho, P., and Rapoport, T.A. (2014). Key Steps in ERAD of Luminal ER Proteins Reconstituted with Purified Components. Cell *158*, 1375–1388.

Stigliano, I.D., Caramelo, J.J., Labriola, C.A., Parodi, A.J., and D'Alessio, C. (2009). Glucosidase II Subunit Modulates N-Glycan Trimming in Fission Yeasts and Mammals. Mol. Biol. Cell *20*, 3974–3984.

Stigliano, I.D., Alculumbre, S.G., Labriola, C.A., Parodi, A.J., and D'Alessio, C. (2011). Glucosidase II and N-glycan mannose content regulate the half-lives of monoglucosylated species in vivo. Mol. Biol. Cell *22*, 1810–1823.

Streich, F.C., and Lima, C.D. (2014). Structural and functional insights to ubiquitin-like protein conjugation. Annu. Rev. Biophys. *43*, 357–379.

Tang, C., Ghirlando, R., and Clore, G.M. (2008). Visualization of Transient Ultra-Weak Protein Self-Association in Solution Using Paramagnetic Relaxation Enhancement. J. Am. Chem. Soc. *130*, 4048–4056.

Tatham, M.H., Geoffroy, M.-C., Shen, L., Plechanovova, A., Hattersley, N., Jaffray, E.G., Palvimo, J.J., and Hay, R.T. (2008). RNF4 is a poly-SUMO-specific E3 ubiquitin ligase required for arsenic-induced PML degradation. Nat. Cell Biol. *10*, 538–546.

Tenno, T., Fujiwara, K., Tochio, H., Iwai, K., Morita, E.H., Hayashi, H., Murata, S., Hiroaki, H., Sato, M., Tanaka, K., et al. (2004). Structural basis for distinct roles of Lys63- and Lys48-linked polyubiquitin chains. Genes Cells *9*, 865–875.

Thrower, J.S. (2000). Recognition of the polyubiquitin proteolytic signal. EMBO J. *19*, 94–102.

Trempe, J.-F., Brown, N.R., Noble, M.E.M., and Endicott, J.A. (2010). A new crystal form of Lys48-linked diubiquitin. Acta Crystallograph. Sect. F Struct. Biol. Cryst. Commun. *66*, 994–998.

Varadan, R., Walker, O., Pickart, C., and Fushman, D. (2002). Structural Properties of Polyubiquitin Chains in Solution. J. Mol. Biol. *324*, 637–647.

Varadan, R., Assfalg, M., Raasi, S., Pickart, C., and Fushman, D. (2005). Structural Determinants for Selective Recognition of a Lys48-Linked Polyubiquitin Chain by a UBA Domain. Mol. Cell *18*, 687–698.

van der Veen, A.G., and Ploegh, H.L. (2012). Ubiquitin-Like Proteins. Annu. Rev. Biochem. *81*, 323–357.

Velazquez-Campoy, A., and Freire, E. (2006). Isothermal titration calorimetry to determine association constants for high-affinity ligands. Nat Protoc *1*, 186–191.

Vijay-Kumar, S., Bugg, C.E., and Cook, W.J. (1987). Structure of ubiquitin refined at 1.8 A resolution. J. Mol. Biol. *194*, 531–544.

Virdee, S., Ye, Y., Nguyen, D.P., Komander, D., and Chin, J.W. (2010). Engineered diubiquitin synthesis reveals Lys29-isopeptide specificity of an OTU deubiquitinase. Nat. Chem. Biol. *6*, 750–757.

Voges, D., Zwickl, P., and Baumeister, W. (1999). The 26S proteasome: a molecular machine designed for controlled proteolysis. Annu. Rev. Biochem. *68*, 1015–1068.

de Vries, S.J., van Dijk, M., and Bonvin, A.M. (2010). The HADDOCK web server for data-driven biomolecular docking. Nat Protoc *5*, 883–897.

Wang, Z.X., and Jiang, R.F. (1996). A novel two-site binding equation presented in terms of the total ligand concentration. FEBS Lett *392*, 245–249.

Wang, X., Herr, R.A., Chua, W.-J., Lybarger, L., Wiertz, E.J.H.J., and Hansen, T.H. (2007). Ubiquitination of serine, threonine, or lysine residues on the cytoplasmic tail can induce ERAD of MHC-I by viral E3 ligase mK3. J. Cell Biol. *177*, 613–624.

Weeks, S.D., Grasty, K.C., Hernandez-Cuebas, L., and Loll, P.J. (2009). Crystal structures of Lys-63-linked tri- and di-ubiquitin reveal a highly extended chain architecture. Proteins Struct. Funct. Bioinforma. *77*, 753–759.

Werner, E.D., Brodsky, J.L., and McCracken, A.A. (1996). Proteasome-dependent endoplasmic reticulum-associated protein degradation: an unconventional route to a familiar fate. Proc. Natl. Acad. Sci. U. S. A. *93*, 13797–13801.

Wiborg, O., Pedersen, M.S., Wind, A., Berglund, L.E., Marcker, K.A., and Vuust, J. (1985). The human ubiquitin multigene family: some genes contain multiple directly repeated ubiquitin coding sequences. EMBO J. *4*, 755–759.

Wickliffe, K.E., Lorenz, S., Wemmer, D.E., Kuriyan, J., and Rape, M. (2011). The Mechanism of Linkage-Specific Ubiquitin Chain Elongation by a Single-Subunit E2. Cell *144*, 769–781.

Wiechmann, S., Gartner, A., Kniss, A., Stengl, A., Behrends, C., Rogov, V.V., Rodriguez, M.S., Dotsch, V., Muller, S., and Ernst, A. (2017). Site-specific inhibition of the small ubiquitin-like modifier (SUMO)-conjugating enzyme Ubc9 selectively impairs SUMO chain formation. J Biol Chem *292*, 15340–15351.

Williamson, M.P. (2013). Using chemical shift perturbation to characterise ligand binding. Prog. Nucl. Magn. Reson. Spectrosc. *73*, 1–16.

Wright, J.D., Mace, P.D., and Day, C.L. (2016). Secondary ubiquitin-RING docking enhances Arkadia and Ark2C E3 ligase activity. Nat. Struct. Mol. Biol. *23*, 45–52.

Xu, C., and Ng, D.T.W. (2015). Glycosylation-directed quality control of protein folding. Nat. Rev. Mol. Cell Biol. *16*, 742–752.

Xu, P., Duong, D.M., Seyfried, N.T., Cheng, D., Xie, Y., Robert, J., Rush, J., Hochstrasser, M., Finley, D., and Peng, J. (2009). Quantitative Proteomics Reveals the Function of Unconventional Ubiquitin Chains in Proteasomal Degradation. Cell *137*, 133–145.

Yamazaki, T., Forman-Kay, J.D., and Kay, L.E. (1993). Two-dimensional NMR experiments for correlating carbon-13.beta. and proton.delta./.epsilon. chemical shifts of aromatic residues in 13C-labeled proteins via scalar couplings. J. Am. Chem. Soc. *115*, 11054–11055.

Ye, Y., and Rape, M. (2009). Building ubiquitin chains: E2 enzymes at work. Nat. Rev. Mol. Cell Biol. *10*, 755–764.

Ye, Y., Meyer, H.H., and Rapoport, T.A. (2001). The AAA ATPase Cdc48/p97 and its partners transport proteins from the ER into the cytosol. Nature *414*, 652–656.

Ye, Y., Blaser, G., Horrocks, M.H., Ruedas-Rama, M.J., Ibrahim, S., Zhukov, A.A., Orte, A., Klenerman, D., Jackson, S.E., and Komander, D. (2012). Ubiquitin chain conformation regulates recognition and activity of interacting proteins. Nature *492*, 266–270.

Zhang, Y., Vuković, L., Rudack, T., Han, W., and Schulten, K. (2016). Recognition of Poly-Ubiquitins by the Proteasome through Protein Refolding Guided by Electrostatic and Hydrophobic Interactions. J. Phys. Chem. B *120*, 8137–8146.

Ziemba, A., Hill, S., Sandoval, D., Webb, K., Bennett, E.J., and Kleiger, G. (2013). Multimodal Mechanism of Action for the Cdc34 Acidic Loop: A CASE STUDY FOR WHY UBIQUITIN-CONJUGATING ENZYMES HAVE LOOPS AND TAILS. J. Biol. Chem. *288*, 34882–34896.

Zuiderweg, E.R. (2002). Mapping protein-protein interactions in solution by NMR spectroscopy. Biochemistry (Mosc.) *41*, 1–7.

van Zundert, G.C.P., Rodrigues, J., Trellet, M., Schmitz, C., Kastritis, P.L., Karaca, E., Melquiond, A.S.J., van Dijk, M., de Vries, S.J., and Bonvin, A. (2016). The HADDOCK2.2 Web Server: User-Friendly Integrative Modeling of Biomolecular Complexes. J Mol Biol *428*, 720–725.

8. Appendix

The following list contains all constructs that were successfully expressed and purified in this work (Table 6). Integrity and purity of all purified proteins was checked by SDS PAGE and analytical SEC and in some cases by mass spectrometry.

Table 6: Overview of expressed constructs

Insert	affinity tag and cleavage site	vector	source
Ubc7(FL)-GG-Cue1(147-203, C147S) abbreviated to Ubc7-U7BR	Ub19 (His10) – TEV (N-term.)	pET39b(+)	(Kniss et al., 2018)
Ubc7-U7BR D46R	Ub19 (His10) – TEV (N-term.)	pET39b(+)	this study
Ubc7-U7BR D46A	Ub19 (His10) – TEV (N-term.)	pET39b(+)	this study
Ubc7-U7BR C89K	Ub19 (His10) – TEV (N-term.)	pET39b(+)	this study
Ubc7-U7BR D98R, D99R	Ub19 (His10) – TEV (N-term.)	pET39b(+)	this study
Ubc7-U7BR D98A, D99A	Ub19 (His10) – TEV (N-term.)	pET39b(+)	this study
Ubc7-U7BR E104R	Ub19 (His10) – TEV (N-term.)	pET39b(+)	this study
Ubc7-U7BR E104A	Ub19 (His10) – TEV (N-term.)	pET39b(+)	this study
Ubc7-U7BR E107R, E108R	Ub19 (His10) – TEV (N-term.)	pET39b(+)	this study
Ubc7-U7BR E107A, E108A	Ub19 (His10) – TEV (N-term.)	pET39b(+)	this study
Ubc7-U7BR R109E	Ub19 (His10) – TEV (N-term.)	pET39b(+)	this study
Ubc7-U7BR R109A	Ub19 (His10) – TEV (N-term.)	pET39b(+)	this study
Ubc7-U7BR E129R	Ub19 (His10) – TEV (N-term.)	pET39b(+)	this study
Ubc7-U7BR E129A	Ub19 (His10) – TEV (N-term.)	pET39b(+)	this study
Ubc7-U7BR E133R	Ub19 (His10) – TEV (N-term.)	pET39b(+)	this study
Ubc7-U7BR E133A	Ub19 (His10) – TEV (N-term.)	pET39b(+)	this study
Ubc7-U7BR R145E	Ub19 (His10) – TEV (N-term.)	pET39b(+)	this study
Ubc7-U7BR R145A	Ub19 (His10) – TEV (N-term.)	pET39b(+)	this study
Ubc7-U7BR D146R	Ub19 (His10) – TEV (N-term.)	pET39b(+)	this study
Ubc7-U7BR D146A	Ub19 (His10) – TEV (N-term.)	pET39b(+)	this study
Ubc7-U7BR R148E	Ub19 (His10) – TEV (N-term.)	pET39b(+)	this study
Ubc7-U7BR R148A	Ub19 (His10) – TEV (N-term.)	pET39b(+)	this study
Ubc7-U7BR E152R	Ub19 (His10) – TEV (N-term.)	pET39b(+)	this study
Ubc7-U7BR E152A	Ub19 (His10) – TEV (N-term.)	pET39b(+)	this study
Ubc7-U7BR E129R	Ub19 (His10) – TEV (N-term.)	pET39b(+)	this study
Ubc7-U7BR E129A	Ub19 (His10) – TEV (N-term.)	pET39b(+)	this study
Ubc7-U7BR E133R	Ub19 (His10) – TEV (N-term.)	pET39b(+)	this study
Ubc7-U7BR S30C, C39S, C89K, C141S	Ub19 (His10) – TEV (N-term.)	pET39b(+)	this study
Ubc7-U7BR C39S, C89K, A106C, C141S	Ub19 (His10) – TEV (N-term.)	pET39b(+)	this study
Ubc7-U7BR C39S, C89K, S128C, C141S	Ub19 (His10) – TEV (N-term.)	pET39b(+)	this study
Ubc7-U7BR C39S, C89K, C141S, S158C	Ub19 (His10) – TEV (N-term.)	pET39b(+)	this study
Ub wt (human sequence)	no tag	pETM-60	gift from V. Rogov
Ub 6His	His6 (C-term.)	pETM-60	(von Delbruck et al., 2016)
Ub 6His A28C	His6 (C-term.)	pETM-60	(Kniss et al., 2018)
Ub 6His E24C	His6 (C-term.)	pETM-60	(Kniss et al., 2018)
Ub 6His E34C	His6 (C-term.)	pETM-60	(Kniss et al., 2018)
Ub 6His K48R	His6 (C-term.)	pETM-60	(von Delbruck et al., 2016)
Ub 6His E24C, K63R	His6 (C-term.)	pETM-60	(Kniss et al., 2018)
Ub 6His N25C, E34C	His6 (C-term.)	pETM-60	(Kniss et al., 2018)
Ub 6His T22C, E34C	His6 (C-term.)	pETM-60	(Kniss et al., 2018)
Ub 6His T9C	His6 (C-term.)	pETM-60	(von Delbruck et al., 2016)
Ub A28C	no tag	pETM-60	(Kniss et al., 2018)
Ub A28C, K48R	no tag	pETM-60	(Kniss et al., 2018)
Ub A28C, K63R	no tag	pETM-60	(Kniss et al., 2018)
Ub E24C	no tag	pETM-60	(Kniss et al., 2018)
Ub E34C	no tag	pETM-60	(Kniss et al., 2018)
Ub K48R	no tag	pETM-60	(von Delbruck et al., 2016)
Ub K63R	no tag	pETM-60	(von Delbruck et al., 2016)

Ub S20C	no tag	pETM-60	(von Delbruck et al., 2016)
Ub S57C, K48R	no tag	pETM-60	(Kniss et al., 2018)
Ub T22C	no tag	pETM-60	(Kniss et al., 2018)
Ub T9C	no tag	pETM-60	(von Delbruck et al., 2016)
Ub 6His E24C, R42A	His6 (C-term.)	pETM-60	(Kniss et al., 2018)
Ub 6His E24C, V70A	His6 (C-term.)	pETM-60	(Kniss et al., 2018)
Ub A28C, R42A	no tag	pETM-60	(Kniss et al., 2018)
Ub A28C, K48R, V70A	no tag	pETM-60	(Kniss et al., 2018)
Cue1 24-203 T66C, C147S	GST – 3C (N-term.)	pGEX6p1	(von Delbruck et al., 2016)
Cue1 (25-203, C147S)	Ub19 – TEV (N-term.) and His6 (C-term.)	pET39b(+)	(von Delbruck et al., 2016)
Cue1 CUE (45-115)	Ub19 (His10) – TEV (N-term.)	pET39b(+)	my diploma thesis
Cue1 (59-115) with N-term biotinylation site	Ub19 (His10) – TEV (N-term.)	pET39b(+)	(von Delbruck et al., 2016)
gp78CUE (453-503)	Ub19 (His10) – TEV (N-term.)	pET39b(+)	(Kniss et al., 2018)
Cue2 CUE1(6-54)	Ub19 (His10) – TEV (N-term.)	pET39b(+)	(Kniss et al., 2018)
hHR23A UBA2 (315-363)	Ub19 (His10) – TEV (N-term.)	pET39b(+)	this study
OTUB1 (FL, 1-271)	His6 – GST – 3C (N-term.)	pOPINK	addgene plasmid #61420
Cezanne (OTUD7B, 53-446)	His6 – GST – 3C (N-term.)	pOPINK	addgene plasmid #61581
OTUB1 (FL, 1-271) C91A	His6 – GST – 3C (N-term.)	pOPINK	(Kniss et al., 2018)
Cezanne (OTUD7B, 53-446) C194S	His6 – GST – 3C (N-term.)	pOPINK	(Kniss et al., 2018)
mouse Rpn13 (1-150)	His6 – 3C (N-term.)	pRSET	(Husnjak et al., 2008)
Ubc7 (2-165)	Ub19 (His10) – TEV (N-term.)	pET39b(+)	this study
Hrd1 (325-551)	Ub19 (His10) – TEV (N-term.)	pET39b(+)	this study
Hrd1 (337-412)	His6 – MBP (N. term.)	pETMBP	this study
Hrd1 (325-465)	Ub19 (His10) – TEV (N-term.)	pET39b(+)	this study
Hrd1 (325-436)	Ub19 (His10) – TEV (N-term.)	pET39b(+)	this study
Hrd1 (341-401)	Ub19 (His10) – TEV (N-term.)	pET39b(+)	this study
Hrd1 (337-406)	Ub19 (His10) – TEV (N-term.)	pET39b(+)	this study
Hrd1 (325-412)	Ub19 (His10) – TEV (N-term.)	pET39b(+)	this study
Doa10 (2-112)	Ub19 (His10) – TEV (N-term.)	pET39b(+)	this study
Doa10 (19-101)	Ub19 (His10) – TEV (N-term.)	pET39b(+)	this study
Cdc34	GST – 3C (N-term.)	pGEX6p1	(von Delbruck et al., 2016)
Ubc13	GST – 3C (N-term.)	pGEX6p1	(von Delbruck et al., 2016)
Uev1a	GST – 3C (N-term.)	pGEX6p1	(von Delbruck et al., 2016)
Ube2SΔC (1-156)	TEV – 6His (C-term.)	pET	(Kniss et al., 2018)
Ube1 (human E1)	His6 (N-term.)	pET21d	(Berndsen and Wolberger, 2011)
Yos9 (90-262)	His6 – GB1 (N. term.)	pETGB1	this study
Yos9 (90-249)	His6 – GB1 (N. term.)	pETGB1	this study
Yos9 (90-242)	His6 – GB1 (N. term.)	pETGB1	this study
Yos9 (105-249)	His6 – GB1 (N. term.)	pETGB1	this study
Yos9 (32-249)	His6 – GB1 (N. term.)	pETGB1	this study
Ubc9	Ub19 (His10) – TEV (N-term.)	pET39b(+)	(Wiechmann et al., 2017)
SUMO2-wtΔGG (also called S2.wtΔGG)	His6 – TEV (N-term.)	pET53-TEV	(Wiechmann et al., 2017)
SUMO2-E08 (also called S2v.E2.34)	His6 – TEV (N-term.)	pET53-TEV	(Wiechmann et al., 2017)
SUMO2-A09ΔGG (also called S2v.E2.15)	His6 – TEV (N-term.)	pET53-TEV	(Wiechmann et al., 2017)
N-term His-Ub	His6 – TEV (N-term.)	pET39b(+)	this study

Structural statistics of Hrd1 RING (337-412)

Table 7: Structural statistics of the solution NMR structure calculation of the Hrd1 RING domain. The table was prepared by Sina Kazemi.

NOE assignment (a)	**CYANA result**	**energy minimized** (b)
^{15}N-resolved NOESY cross peaks	852	
^{13}C-resolved NOESY cross peaks	2314	
^{13}C-resolved aromatic NOESY cross peaks	269	
Total number of NOESY cross peaks	3435 (100%)	
Assigned cross peaks (d)	3192 (92.9%)	
Unassigned cross peaks (d)	243 (7.1%)	
Structural restraints		
Assigned NOE distance restraints (e)	1440 (100%)	
Short range |i-j|≤1	743 (51.6%)	
Medium range 1<|i-j|<5	250 (17.4%)	
Long range |i-j|≥5	447 (31.0%)	
Dihedral angle restraints (φ/ψ)	82	
Restraints for zinc coordination (upl/lol)	32	
Structure statistics		
Average CYANA target function value (Å^2)	1.11 ± 0.03	2.79 ± 0.58
Average AMBER Energies (kcal/mol)	-1604.64 ± 70.79	-2298.39 ± 59.47
Average AMBER Energies (kJ/mol)	-6713.81 ± 296.19	-9616.46 ± 248.82
Restraint violations (c)		
Max. distance restraint violation (Å)	0.18	0.12
Number of violated distance restraints > 0.2 Å	0	0
Max. dihedral angle restraint violations (°)	6.34	5.00
Number of violated dihedral angle constraints > 5°	1	0
Ramachandran plot		
Residues in most favored regions	70.9%	72.0%
Residues in additionally allowed regions	29.1%	27.2%
Residues in generously allowed regions	0.0%	0.7%
Residues in disallowed regions	0.0%	0.0%
RMSD (residues 345-358, 369-404)		
Average backbone RMSD to mean (Å)	0.10 ± 0.02	0.22 ± 0.03
Average heavy atom RMSD to mean (Å)	0.51 ± 0.06	0.59 ± 0.06

(a) using automated NOE assignment and structure calculation functionalities of CYANA
(b) after restrained energy minimization with OPALp
(c) after energy minimization, calculated with CYANA
(d) in parenthesis the percentage of the total cross peaks
(e) in parenthesis the percentage of the total distance restraints from the peak assignment

Structural statistics of Yos9 MRH (90-249)

Table 8: Structural statistics of the solution NMR structure calculation of the Yos9 MRH domain. The table was prepared by Sina Kazemi.

NOE assignment (a)	**CYANA result**	**energy minimized** (b)
^{15}N-resolved NOESY cross peaks	2160	
^{13}C-resolved NOESY cross peaks	5039	
^{13}C-resolved aromatic NOESY cross peaks	661	
Total number of NOESY cross peaks	7860 (100%)	
Assigned cross peaks (d)	6642 (84.5%)	
Unassigned cross peaks (d)	1218 (15.5%)	
Structural restraints		
Assigned NOE distance restraints (e)	3610 (100%)	
Short range |i-j|≤1	1705 (47.2%)	
Medium range 1<|i-j|<5	537 (14.9%)	
Long range |i-j|≥5	1368 (37.9%)	
Dihedral angle restraints (φ/ψ)	250	
Structure statistics		
Average CYANA target function value (Å^2)	1.94 ± 0.09	3.60 ± 0.50
Average AMBER Energies (kcal/mol)	-5004.46 ± 144.38	-6419.61 ± 128.60
Average AMBER Energies (kJ/mol)	-20938.66 ± 604.09	-26859.65 ± 538.06
Restraint violations (c)		
Max. distance restraint violation (Å)	0.45	0.13
Number of violated distance restraints > 0.2 Å	0	0
Max. dihedral angle restraint violations (°)	8.29	6.67
Number of violated dihedral angle constraints > 5°	2	1
Ramachandran plot		
Residues in most favored regions	82.6%	85.6%
Residues in additionally allowed regions	17.2%	13.9%
Residues in generously allowed regions	0.2%	0.5%
Residues in disallowed regions	0.0%	0.0%
RMSD (residues 94..140, 156..209, 215..246)		
Average backbone RMSD to mean (Å)	0.27 ± 0.05	0.33 ± 0.05
Average heavy atom RMSD to mean (Å)	0.59 ± 0.06	0.65 ± 0.05

(a) using automated NOE assignment and structure calculation functionalities of CYANA
(b) after restrained energy minimization with OPALp
(c) after energy minimization, calculated with CYANA
(d) in parenthesis the percentage of the total cross peaks
(e) in parenthesis the percentage of the total distance restraints from the peak assignment

Structural statistics of Yos9 MRH (90-249) bound to 3α, 6α-mannopentaose

Table 9: Structural statistics of the solution NMR structure calculation of the Yos9 MRH domain (bound to 3α, 6α-Mannopentaose. The table was prepared by Sina Kazemi.

NOE assignment (a)	**CYANA result**	**energy minimized** (b)
^{15}N-resolved NOESY cross peaks	1986	
^{13}C-resolved NOESY cross peaks	5684	
^{13}C-resolved aromatic NOESY cross peaks	532	
Total number of NOESY cross peaks	8202 (100%)	
Assigned cross peaks (d)	6716 (81.9%)	
Unassigned cross peaks (d)	1486 (18.1%)	
Structural restraints		
Assigned NOE distance restraints (e)	3885 (100%)	
Short range |i-j|≤1	1773 (45.6%)	
Medium range 1<|i-j|<5	563 (14.5%)	
Long range |i-j|≥5	1549 (39.9%)	
Dihedral angle restraints (φ/ψ)	248	
Structure statistics		
Average CYANA target function value (Å^2)	1.33 ± 0.10	3.46 ± 0.52
Average AMBER Energies (kcal/mol)	-5045.07 ± 125.14	-6444.60 ± 110.82
Average AMBER Energies (kJ/mol)	-21108.57 ± 125.14	-26964.21 ± 463.67
Restraint violations (c)		
Max. distance restraint violation (Å)	0.38	0.12
Number of violated distance restraints > 0.2 Å	1	0
Max. dihedral angle restraint violations (°)	6.55	7.29
Number of violated dihedral angle constraints > 5°	2	1
Ramachandran plot		
Residues in most favored regions	77.7%	83.0%
Residues in additionally allowed regions	22.3%	16.7%
Residues in generously allowed regions	0.0%	0.2%
Residues in disallowed regions	0.0%	0.0%
RMSD (residues 94..140, 156..209, 215..246)		
Average backbone RMSD to mean (Å)	0.24 ± 0.03	0.30 ± 0.03
Average heavy atom RMSD to mean (Å)	0.57 ± 0.04	0.63 ± 0.04

(a) using automated NOE assignment and structure calculation functionalities of CYANA
(b) after restrained energy minimization with OPALp
(c) after energy minimization, calculated with CYANA
(d) in parenthesis the percentage of the total cross peaks
(e) in parenthesis the percentage of the total distance restraints from the peak assignment

Distance Determination by PELDOR

Table 10: Fitting parameters for PELDOR data analysis. Data listed are as mean of a single Gaussian (R1 and R2) with the standard deviations σ1 and σ2, respectively. The population of each Gaussian distribution is given by P1 and P2, respectively. The mean distance of the entire distribution is given by <R> and the corresponding standard deviation by σ. The data was provided by Denise Schütz and is published (Kniss et al. 2018).

Mutant	Addition	R1 / nm	σ1 / nm	P1 / %	R2 / nm	σ2 / nm	P2 / %	<R>[a] / nm	σ[a] / nm
Ubiquitin T22C/E34C (100µM)		2.91	0.19	100	-	-	-	2.91	0.13
Ubiquitin N25C/E34C (100µM)		2.26	0.22	100	-	-	-	2.26	0.15
K48-linked									
Diubiquitin (100µM)									
pE24C/dA28C		3.12	0.82	22.5	4.38	0.59	77.5	4.09	0.69
pE24C/dA28C	Low pH (pH=4.5)	2.57	0.49	13.6	4.24	0.57	86.4	4.02	0.70
pE24C/dA28C	+Cue1 (50 µM)							4.10*	0.64*
pE24C/dA28C	+Cue1 (150 µM)	3.98	0.68	69.4	4.10	0.12	30.6	4.02	0.40
pE24C/dA28C	+Cue1 (600 µM)							3.95*	0.63*
pE24C/dA28C	+gp78CUE (150 µM)	3.45	0.95	40	4.60	0.73	60	4.14	0.81
pE24C/dA28C	+Cue2 (600 µM)	3.39	0.97	34.3	4.46	0.64	65.7	4.10	0.74
pE24C/dA28C	+UBA2 (120 µM)	3.90	0.77	21.2	4.60	0.51	78.8	4.45	0.50
pE24C/dA28C	+OTUB1i (150 µM)	2.45	0.31	75.4	3.11	0.25	24.6	2.61	0.35
pE24C/dA28C	+Rpn13 (150 µM)	3.73	1.46	100	-	-	-	3.77	0.98
pE24C,R42A/dA28C,R42A		3.52	0.86	34	4.41	0.52	66	4.11	0.63
pE24C,R42A/dA28C,R42A	+Cue1 (150 µM)	3.40	0.66	22	4.35	0.52	78	4.14	0.56
pE24C,V70A/dA28C,V70A		3.15	0.36	12	4.43	0.62	88	4.27	0.59
pE24C,V70A/dA28C,V70A	+Cue1 (150 µM)	3.26	0.46	17	4.43	0.66	83	4.24	0.62
pE24C/dE24C		3.03	0.31	12.2	4.14	0.53	87.8	4.00	0.51
pE24C/dE24C	+Cue1 (150 µM)	3.96	0.13	28.7	3.93	0.96	71.3	3.94	0.57
pE24C/dE24C	+OTUB1i (150 µM)	1.5	2.39	28.6	2.44	0.20	71.5	2.55	0.59
pE24C/dE24C	+Rpn13	3.86	1.78	100	-	-	-	3.94	1.17
pA28C/dA28C		3.86	0.96	37.5	4.85	0.58	62.5	4.48	0.71
pA28C/dA28C	+Cue1(150 µM)	4.39	0.26	33.9	4.30	1.01	66.1	4.33	0.59
pA28C/dA28C	+OTUB1i (150 µM)	2.51	0.71	88.5	3.77	1.79-	11.5-	2.96	0.73
pA28C/dA28C	+Rpn13	3.80	0.98	73.5	4.76	0.55	26.5	4.05	0.76
pE34C/dT22C		2.62	0.69	10.2	4.49	1.03	89.8	4.30	0.90
pE34C/dT22C	+Cue1 (150 µM)	3.96	0.71	26.8	4.71	0.88	73.2	4.44	0.75
pE34C/dT22C	+OTUB1i (150 µM)	4.01	0.63	54.4	4.66	1.88	45.6	4.32	0.99
pE34C/dT22C	+Rpn13	3.50	0.68	16.0	5.04	0.99	84.0	4.80	0.88
pE34C/dE34C		2.07	0.48	26.8	3.95	1.65	73.2	3.49	1.28
pE34C/dE34C	+Cue1 (150 µM)	2.57	1.37	32.9	4.31	0.81	67.1	3.82	0.96
pE34C/dE34C	+OTUB1i (150 µM)	2.74	0.74	17.7	4.98	0.32	82.3	4.58	0.90
pE34C/dE34C	+Rpn13	2.34	0.70	13.4	4.28	1.1	86.6	4.03	0.98
Triubiquitin (50 µM)									
pE24C/dA28C		3.47	1.33	56.2	5.31	0.75	43.8	4.30	1.17
pE24C/dA28C	+Cue1 (112.5 µM)	3.84	0.75	27.1	6.11	1.15	72.9	5.49	1.26
pE24C/dA28C	+gp78CUE (112.5 µM)	5.36	2.47	100	-	-	-	5.40	1.65
pE24C/dA28C	+OTUB1i (150 µM)	4.27	2.68	100	-	-	-	4.54	1.64
pE24C/mA28C		3.57	0.83	34.6	4.37	0.63	65.4	4.09	0.63
mA28C/dA28C								4.52*	0.61*
Tetraubiquitin									
pE24C/dA28C (50 µM)		4.93	1.5	100	-	-	-	4.93	1.04
pE24C/dA28C (50 µM)	Low pH (pH=4.5)	4.73	1.94	100	-	-	-	4.76	1.33
pE24C/dA28C (50 µM)	+Cue1 (150 µM)	5.78	1.18	100	-	-	-	5.88	1.14
pE24C/dA28C (100 µM)	+Cue1 (300 µM)	-	-	-	-	-	-	5.94*	1.68*
pE24C/dA28C (100 µM)	+Cue1 (1200 µM)	-	-	-	-	-	-	6.38*	2.02*
pE24C/dA28C (50 µM)	+gp78CUE (150 µM)	6.96	4.28	100	-	-	-	6.35	2.11
pE24C/dA28C (50 µM)	+OTUB1i (225 µM)	4.39	3.92	61.6	5.28	0.52	38.4	4.99	1.50
pE24C/m1A28C (100 µM)		4.14	0.91	100	-	-	-	4.14	0.64
pE24C/dS57C (50 µM)		2.95	5	100	-	-	-	4.68	2.10
m1A28C/m2A28C								4.83*	0.74*
pE24C/m2A28C		2.69	1.67	73.4	5.3	0.91	26.6	3.61	1.31
K11-linked Diubiquitin (100µM)									
pE24C/dA28C		3.20	1.05	55.1	4.11	0.76	49.9	3.62	0.78
pE24C/dA28C	+OTUD7Bi (150µM)	2.64	0.40	85.2	3.73	0.93	14.8	2.80	0.53
K63-linked Diubiquitin (100µM)									
pE24C/dA28C		3.99	1.03	59.5	5.00	0.52	40.5	4.40	0.78

[a] Obtained from Approximate pake transformation

* Distance distribution from Tikhonov Regularization

Comparison of experimental and calculated inter-ubiquitin distances

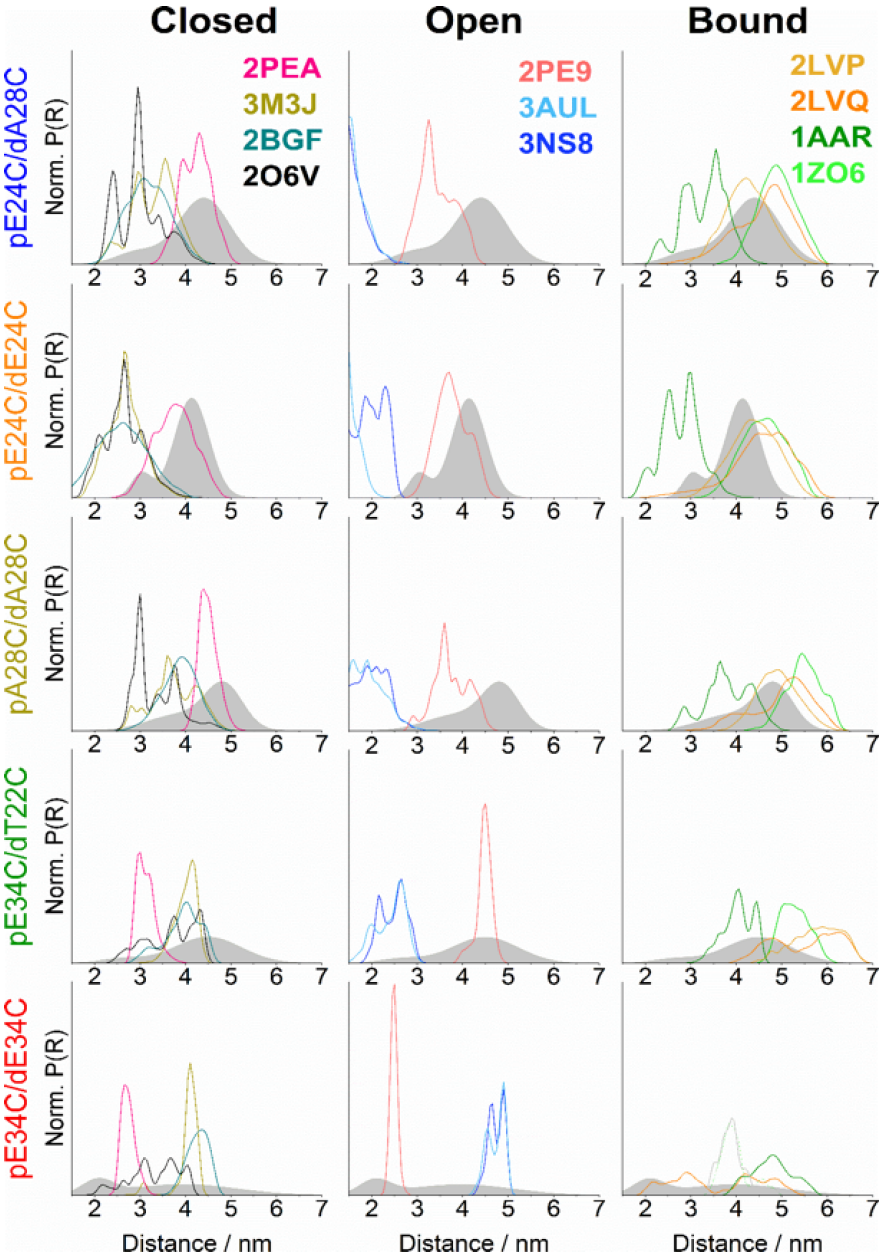

Figure 45: Comparison of experimental and calculated inter-ubiquitin distances. Distance distributions were measured for various diubiquitin variants. For comparison distance distributions of different ubiquitin chain structures found in the PDB were generated by *in silico* spin labeling in MMM2015.2 (Polyhach et al., 2011). The experimental distributions are shown as grey areas. The PDB structures are classified in closed (2PEA, 3M3J, 2BGF, 2O6V), open (2PE9, 3AUL, 3NS8) and bound (2LVP, LVQ, 1AAR, 1OZ6) conformations. The figure was adapted from Kniss et al. 2018.